Part 1 Design, Synthesis and Bioactivity of a Phosphorylated Prodrug for the Inhibition of Pin1

Part 2 Conformational Specificity of Cdc25c Substrate for Cdc2 Kinase using LC-MS/MS

by

Song Zhao

Dissertation submitted to the faculty of the
Virginia Polytechnic Institute and State University
In the partial fulfillment of the requirement for the degree of

Doctor of Philosophy
In Chemistry

Dr. Felicia A. Etzkorn
Dr. Paul R. Carlier
Dr. Neal Castagnoli
Dr. David G. I. Kingston
Dr. Larry T. Taylor

December 17, 2007
Blacksburg, Virginia

Keywords: conformation, Cdc25, Cdc2, cell cycle, inhibition, isosteres, Pin1, Ser-*cis*-Pro, Ser-*trans*-Pro, peptidomimetics, assay, LC-MS/MS, phosphorylation, kinase

Abstract

The phosphorylation-dependent PPIase (peptidyl prolyl isomerase), Pin1 (Protein interacting with NIMA#1), has been found to regulate cell cycle through a simple conformational change, the cis-trans isomerization of phospho-Ser/Thr-Pro amide bonds. A variety of key cell cycle regulatory phosphoproteins, including Cdc25 phosphatase,Cdc27, p53 oncogene, c-Myc oncogene, Wee1 kinase, Myt1 kinase, and NIMA kinas, have been confirmed as substrates of Pin1. Pin1 was also observed to be overexpressed in a variety of cancer cell lines, and the inhibitors of Pin1 showed antiproliferative activities towards these cancer cells. These results implied that Pin1 might serve as a potential anti-cancer drug target. Besides, Pin1 has an important neuroprotective function and represents a potential new therapeutic agent for Alzheimer's disease.

In order to understand the interaction between Pin1 and Cdc25c and the role of Pin1 in the mechanism for the regulation of mitosis, two amide isosteres, Ser-Ψ[(*Z*)CH=C]-Pro-OH and Ser-Ψ[(*E*)CH=C]-Pro-OH were incorporated into two peptidomimetics derived from human Cdc25c. Phosphorylation of these two peptidomimetics by the incubation with Cdc2 was studied using LC-MS/MS technique. It was found that Cdc2 kinase was conformationally specific to its Cdc25c substrate. Only the trans conformer of Cdc25c at its Ser168-Pro position can be recognized and phosphorylated by Cdc2 kinase, thereby creating the binding site for Pin1.

In an effort to improve the cell permeability of the charged inhibitors of Pin1, bisPOM (pivaloyloxymethyl) prodrug moiety was introduced to mask the phosphate group of

Fmoc-pSer-Ψ[(*Z*)CH=C]-Pro-(2)-*N*-(3)-ethylaminoindole, which is one inhibitor of Pin1. Fmoc-pSer-Ψ[(*Z*)CH=C]-Pro-(2)-*N*-(3)-ethylaminoindole and its bisPOM prodrug were synthesized efficiently starting with Boc-Ser-Ψ[(*Z*)CH=C]-Pro-OH in 24% and 12% yields respectively. The charged inhibitor showed a moderate inhibition towards Pin1 (IC_{50} = 28.3 μM). Its antiproliferative activity towards A2780 ovarian cancer cells (IC_{50} = 46.2 μM) was significantly improved by its bisPOM prodrug (IC_{50} = 26.9 μM), which is comparable to the IC_{50} of the charged inhibitor towards Pin1 enzymatic activity. These results not only established the bisPOM strategy as an efficient prodrug choice for Pin1 inhibitors, but also added additional evidence for Pin1 as a potential anticancer drug target.

Dedicated to my parents, my wife and my brothers and sister

ACKNOWLEDGEMENTS

I would like to express my sincere gratitude to my supervisor, Dr. Felicia A. Etzkorn. I am so fortunate to join her research group and have the opportunity to carry out this challengeable and wonderful project. During the course for the completion of this research, she not only provided intellectual guidance and support, but also has improved me as a research chemist. I also would like to give my sincere appreciation to my committee members, Dr. Paul R. Carlier, Dr. Neal Castagnoli, Dr. David G. I. Kingston and Dr. Larry T. Taylor for their help and excellent teaching through my graduate studies at Virginia Tech.

I also want to thank many former and current group members, Dr. Xiaodong Wang, Dr. Tao Liu, Dr. Bailing Xu, Mr. Nan Dai, Mr. Xingguo Chen, Mr. Matthew Shoulders, Mr. Keith Leung, Ms. Guoyan Xu, Ms. Ashley Mullins, Ms. Ana Mercedes and Mr. Boobalan Pachaiyappan for their help in the lab and valuable discussion about various scientific topics.

I reserve my utmost thanks to my wife, Ms. Jianxiong Bao, who always supports me and encourages me during the past five years. No word can express how grateful I feel to her. Finally, but the most important, my parents, Zeyin Zhao and Xuzhi Jiang, they provide me everything. Without their solid support and consistent encourage through the past five years, it would be much difficult for me to complete my graduate studies.

Financial support from Virginia Tech and NIH are also appreciated.

Table of Contents

Chapter 1. Introduction and Background……..1

1.1. Biology of the Peptidyl Prolyl Isomerase Pin1……1

1.1.1. The cis prolyl amide bond……1

1.1.2. Peptidyl prolyl isomerases (PPIases)……...3

1.1.3. Pin1……..6

1.2. Protein Phosphorylation and Ser/Thr-Pro specific Protein Kinases……13

1.2.1. Protein phosphorylation……13

1.2.2. Classification of protein kinases and their functions in cell cycle regulation……15

1.2.3. Structural features of protein kinases……19

1.2.4. Regulation of the activity of protein kinases……19

1.2.5. The chemical mechanism of phosphorylation……21

1.3. Conclusion……...35

Chapter 2. Scaled-up Synthese of the Fmoc-Ser-*cis*-Pro-OH and Fmoc-Ser-*trans*-Pro-OH Isosteres……...36

2.1. Design of Ser-Pro isosteres……36

2.2. Scaled-up Synthesis of Fmoc-Ser-Ψ[(*E*)CH=C]-Pro-OH……...38

2.3. Scaled-up Synthesis of Fmoc-Ser-Ψ[(Z)CH=C]-Pro-OH……45

2.4. Conclusions……..51

Experimental……...52

Chapter 3. Synthesis of a Phosphorylated Prodrug for the Inhibition of Pin1……69

3.1. Prodrug Strategies for Phosphorylated Compounds……....69

3.1.1. Prodrugs of phosphates, phosphonates and phosphinates……..69

3.1.2. Simple and substituted alkyl and aryl Ester……...72

3.1.3. Acyoxyalkyl phosphate ester……74

3.1.4. Phospholipid prodrugs……76

3.1.5. SATE and DTE prodrug strategy……...77

3.1.6. Cyclic prodrugs……..77

3.1.7. Carbohydrate prodrugs……...78

3.1.8. Miscellaneous prodrug strategies……...78

3.2. Bis-pivaloyloxymethyl (POM) Prodrugs……79

3.3. Strategies for the Synthesis of bisPOM Prodrugs……81

3.4. Design of Phosphorylated Substrate-Analogue Inhibitors of Pin1……..86

3.5. Synthesis of Fmoc BisPOM-pSer-Ψ[(*Z*)CH=C]-Pro-(2)-*N*-(3)- ethylaminoindole **34**

……90

3.6. Synthesis of Fmoc-pSer-Ψ[(*Z*)CH=C]-Pro-(2)-*N*-(3)-ethylaminoindole **33**……..103

3.7. Pin1 Inhibition Studies of Inhibitor **33**……...107

3.8. Antiproliferative Activity of A2780 Studies of **33** and **34**……110

3.9. Conclusions……...112

Experimental……112

Chapter 4. Study of the Substrate Conformational Specificity of the Upstream Kinase of Pin1……130

4.1. Substrate Conformational Specificity of Proline-directed Kinases and Phosphatases

…….130

4.2. Interaction Between Pin1 and its Protein Substrate Cdc25 in Cell Cycle Regulation

……..131

4.2.1. Regulation of cell cycle by Cdc25 and Pin1……...131

4.2.2. Regulation of phosphatase activity of Cdc25c……....133

4.2.3. Interaction between Pin1 and Cdc25……...135

4.2.4. Possible positions of pCdc25c phosphatase for the interaction with Pin1 PPIase domain……..139

4.2.5. Possible upstream kinases of Pin1 for interaction with Cdc25c……..140

4.3. The Conformational Specificity of Upstream Kinases for the Interaction between Cdc25c and Pin1……...140

4.4. Techniques for Detecting Phosphopeptides and Phosphoproteins…….141

4.4.1. Enrichment of phosphopeptides and phosphoproteins…….143

4.4.2. Detection of phosphopeptides and phosphoproteins……146

4.4.3. Quantitative analysis of phosphopeptides and phosphoproteins……..150

4.4.4. Determination of the phosphorylation position in the phosphopeptides and phosphoproteins…….152

4.4.5. Fragment ions in mass spectrometry……153

4.5. Optimization of the Peptide Substrates Derived from the Sequence Around Ser^{168}-Pro in Cdc25c for Cdc2 Kinase……...156

4.5.1. Synthesis of eight peptides containing Ser^{168}-Pro moiety of Cdc25c by solid phase peptide synthesis……..156

4.5.2. Purification of the crude peptides by RP-HPLC and characterization of these peptides……159

4.5.3. Synthesis and purification of four phosphopeptide standards……160

4.5.4. Phosphorylation of the eight peptide substrates using mitotic extract…..162

4.5.5. Phosphorylation of peptide substrates using pure Cdc2/cyclin B……167

4.5.5.1. Phosphorylation of control peptide substrate in Cdc2 kinase reaction……..167

4.5.5.2. Method development for the quantitative analysis of target phosphorylated peptide substrates by LC-MS/MS……..169

4.5.5.3. Optimization of peptide substrates derived from Cdc25c at Ser^{168} in Cdc2 kinase reactions……..173

4.6. Synthesis of Peptidomimetics Containing Alkene Ser-Pro Isotsteres……177

4.7. The Conformational Specificity of Cdc25c at Ser^{168}-Pro for Cdc2 Kinase Using Peptidomimetics **71** and **72**……...185

4.8. Discussion……..191

4.9. Conclusions……192

Experimental……193

References……..206

List of Figures

Figure 1.1 Stabilization of trans amide conformation via electronic effect……..1

Figure 1.2 Prolyl cis/trans isomerization as a conformational molecular switch…….....3

Figure 1.3 Energy diagram for prolyl cis-trans isomerization……..5

Figure 1.4 Nucleophilic mechanism proposed for PPIase activity……...6

Figure 1.5 X-ray crystal structure of Pin1……9

Figure 1.6 The cell cycle……10

Figure 1.7 Phosphorylation and dephosphorylation of proteins…….14

Figure 1.8 Regulation of Cdc2/cyclin B complex by phosphorylation and dephosphorylation…….17

Figure 1.9 Key residue interactions in the kinase domain of cAPK……..22

Figure 1.10 Dissociative and associative transition states for phosphoryl transfer……..26

Figure 1.11 Proposed proton transfer mechanism……29

Figure 1.12 The roles of Asp-166 and Mg^{2+} ion in the catalytic domain of cAPK……..31

Figure 2.1 Design of Ser-*cis*-Pro and Ser-*trans*-Pro isosteres……37

Figure 2.2 Fmoc protected (*Z*) and (*E*) alkene Ser-Pro isotere synthetic targets……37

Figure 3.1 Structures of phosphate, phosphonate and phosphinate drugs……..69

Figure 3.2 Permeation of prodrugs and their trapping inside target cells……...71

Figure 3.3 Alkyl prodrugs of AZT H-phosphonate analogue…….72

Figure 3.4 Alkyl ester prodrugs of araCMP……...73

Figure 3.5 Haloalkyl diester prodrugs of an AZT analogue and a ddCD analog……...74

Figure 3.6 Various acyoxyalkyl ester prodrugs of PMEA……..76

Figure 3.7 General structure of phospholipid prodrugs……..76

Figure 3.8 A mannopyranoside prodrug of AZTMP……..78

Figure 3.9 BisPOM prodrug of Tryptamine-phosphopantetheine……..80

Figure 3.10 Two pentapeptide analogues inhibitors of Pin1 containing cis- and trans- amide alkene isosteres……..88

Figure 3.11 Designed phosphorylated Pin1 inhibitors without (**33**) and with (**34**) bis-POM prodrug masking group…….90

Figure 3.12 ^{31}P-NMR study of the phosphorylation step…….93

Figure 3.13 Retrosynthetic analysis of compound **34**……..95

Figure 3.14 Dose response curve. Blue: inhibition against Pin1……109

Figure 3.15 Dose Response curve. Blue: inhibition of antiproliferative activity against A2780 ovarian cancer cells…….110

Figure 3.16 Dose response curve for inhibition of Pin1 by compound **33**…….126

Figure 3.17 Dose response curve for the inhibition of A2780 ovarian cancer cells proliferation activity of **33**……...128

Figure 3.18 Dose response curve for the inhibition of A2780 ovarian cancer cells proliferation activity of **34**……...129

Figure 4.1 Regulation of G2/M transition by the activation of Cdc2/Cyclin B complex……...132

Figure 4.2 Interaction of Pin1 and Cdc25C phosphatase……..136

Figure 4.3 Two steps mechanism for the interaction between Pin1 and Cdc25 phosphatase…….138

Figure 4.4 Alkene isoteres as the conformationally locked surrogates for *cis* and *trans* Ser-Pro amide bonds in Cdc25c……..141

Figure 4.5 Chemical structures of phosphor-amino acid residues formed biologically ..142

Figure 4.6 Chemical modification of phosphate group to enrich the phosphopeptide….145

Figure 4.7 Cleavage of phosphate group at different scan modes in mass spectrometry.148

Figure 4.8 Quantitation of phosphorylation by ICAT coupled with MS……..151

Figure 4.9 Nomenclature of fragment ions from mass spectrometry……...154

Figure 4.10 Formation of b and y type ions in CID through oxazolone pathway……..155

Figure 4.11 Formation of b and y type ions through the cleavage of amide bond from doubly charged parent ions…….156

Figure 4.12 Phosphorylation of peptide substrates by mitotic extract……...163

Figure 4.13 Q1 full scan LC-MS analysis of the incubation of AcMKYLG**SP**ITTVNH_2 with mitotic extract……..164

Figure 4.14 SIM scan LC-MS analysis of the incubation of AcMKYLG**SP**ITTVNH_2 with mitotic extract…….165

Figure 4.15 Neutral loss scan for the incubation of AcMKYLG**SP**ITTVNH_2 with mitotic extract…….166

Figure 4.16 Procedure for Cdc2 kinase reaction……168

Figure 4.17 SIM scan for 1135 ($[M+H]^+$) in control experiment with Ac-pSPGRRRRK-NH2, a histone H1 peptide for Cdc2 kinase…..……...169

Figure 4.18 Chromatograms for the MRM experiment (1330.4 → 1232.8) for AcMKYLGpSPITTVNH$_2$ at concentrations: 15, 10, 5 and 2 μM……..172

Figure 4.19 Chromatogram for SIM scan experiment for Cdc2 kinase reaction with AcMKYLGSPITTVNH$_2$ peptide substrate…….173

Figure 4.20 Chromatogram for MRM experiment (1330.4 → 1232.8) for the incubation of AcMKYLGSPITTVNH$_2$ peptide substrate with ATP and Cdc2 kinase……..174

Figure 4.21 Chromatogram for MRM experiment (1330.2 → 578.1, 1330.2 →801.0, 1330.2 → 1015.0) for the incubation of the AcMKYLGSPITTVNH$_2$ peptide substrate with ATP and Cdc2 kinase……..175

Figure 4.22 MRM experiments for the incubation of shorter peptide substrates with ATP and Cdc2 kinase……...177

Figure 4.23 Chromatogram obtained for MRM experiment to detect the phosphorylation of the trans peptidomimetic substrate **72** with Cdc2 kinase or without Cdc2 kinase……..187

Figure 4.24 Chromatogram obtained for MRM experiment to detect the phosphorylation of the cis peptidomimetic substrate **71** with Cdc2 kinase or without Cdc2 kinase……..…….189

Figure 4.25 MRM experiments for determining the phosphorylation position of the trans peptidomimetic substrate **72** in Cdc2 kinase reaction…….190

Figure 4.26 Mechanism for the interaction between Pin1 and Cdc25 phosphatase……...191

List of Schemes

Scheme 2.1 Transition states of the Ireland-Claisen rearrangement……..39

Scheme 2.2 Chelation controlled Luche reduction……39

Scheme 2.3 Synthesis of allylic ester precursor for Ireland-Claisen Rearrangement…...40

Scheme 2.4 Lithium chelated tetrahedral intermediate for the synthesis of **4**……..41

Scheme 2.5 Synthesis of reagent cyclopentenyl iodide **8**……41

Scheme 2.6 Synthesis of reagent *tert*-butyldimethylsilyloxyacetyl chloride **11**……...42

Scheme 2.7 Synthesis of Fmoc-Ser-Ψ[(*E*)CH=C]-Pro-OH **2**……...43

Scheme 2.8 Two possible transition states and the products for the Still-Wittig rearrangement……45

Scheme 2.9 Felkin-Ahn transition state for the reduction with $LiAlH_4$……47

Scheme 2.10 Synthesis of the allylic ether precursor **21**.....47

Scheme 2.11 Synthesis of iodomethyltributyltin reagent **23**……...48

Scheme 2.12 Still-Wittig rearrangement……49

Scheme 2.13 Synthesis of Fmoc-Ser-Ψ[(*Z*)CH=C]-Pro-OH **1**……...50

Scheme 3.1 Degradation of acyloxyalkyl prodrug by esterases……...75

Scheme 3.2 Degradation mechanism of SATE or DTE prodrugs of nucleoside monophosphate……..77

Scheme 3.3 Degradation of phosphoramidate prodrug……79

Scheme 3.4 Phosphoramidite method for the synthesis of bisPOM prodrugs……..82

Scheme 3.5 The second method for the synthesis of a bisPOM prodrug……83

Scheme 3.6 Preparation of bisPOM ester of N_3dUMP via its stannyl intermediate…….84

Scheme 3.7 The synthesis of silver bisPOM phosphate and bisPOM phosphoric acid…….84

Scheme 3.8 The direct phosphorylation of the hydroxyl compound with bisPOM phosphate diester or bisPOM phosphoric acid……..85

Scheme 3.9 Synthesis of bisPOM phosphoryl chloride……85

Scheme 3.10 Synthesis of bisPOM prodrug using bisPOM phosphoryl chloride……...86

Scheme 3.11 Synthesis of bisPOM phosphate……92

Scheme 3.12 Synthesis of bisPOM phosphoryl chloride **38**……...92

Scheme 3.13 Model reaction for the coupling with tryptamine……..96

Scheme 3.14 Formation of 7-member ring lactone **41**……96

Scheme 3.15 Synthesis of Fmoc-Ser(TBS)Ψ[(*Z*)CH=C]-Pro-OH **42**…….97

Scheme 3.16 Synthesis of Fmoc-Ser(bisPOM)-OH without protecting group……...97

Scheme 3.17 Synthesis of Fmoc-Ser(bisPOM)-OH **43** with TBS as temporary protecting group……..98

Scheme 3.18 Synthesis of Fmoc-Ser(bisPOM)Ψ[(*Z*)CH=C]-Pro-OH **45**……...98

Scheme 3.19 Hydrolysis of lactone **41**……99

Scheme 3.20 Synthesis of Boc-Ser(TBS)-Ψ[(*Z*)CH=C]-Pro-OH **46**……..99

Scheme 3.21 Synthesis of the key intermediate **39**……...100

Scheme 3.22 Phosphorylation using bisPOM phosphate **37**…….101

Scheme 3.23 Synthesis of **34** using Et_3N……..101

Scheme 3.24 Synthesis of bisPOM prodrug **34** usinga large excess of pyridine……..102

Scheme 3.25 Synthesis of bisPOM protected Fmoc-Ser-tryptamine **52** and hydrolysis of bisPOM Fmoc-Ser-tryptamine **52**……103

Scheme 3.26 Synthesis of **33**……104

Scheme 3.27 Alternative route for the synthesis of **33**……..105

Scheme 3.28 Pin1 PPIase inhibition assay……108

Scheme 4.1 Solid phase peptide synthesis of peptide AcMKYLGSPITTVNH_2…….158

Scheme 4.2 Synthesis of AcMKYLGpSPITTVNH_2 **12**……..161

Scheme 4.3 Synthesis of Fmoc-Ser(TBS)-OH **70**……...178

Scheme 4.4 Synthesis of the TBS protected trans (top) and cis isostere (bottom).....179

Scheme 4.5 Model peptide synthesis using Fmoc-Ser(OH)-OH and Fmoc-Ser(TBS)-OH **70**……..180

Scheme 4.6 Solid phase peptide synthesis of two target peptidomimetics **71** and **72**…….181

Scheme 4.7 Synthesis of phosphorylation reagent **75**…….182

Scheme 4.8 Synthesis of phosphorylated building blocks **76** and **77**……..183

Scheme 4.9 **Scheme 4.10.** Solid phase peptide synthesis of two phosphopeptidomimetics**73** and **74**……..184

List of Tables

Table 1.1 Effect of phosphorylation on kinetic constants of cis/trans isomerization of peptide-4-nitroanilide at pH 7.8…….....7

Table 1.2 Specific consensus sequences for several protein kinases……..24

Table 3.1 Yields for the phosphorylation step of **39** using different bases…….....102

Table 3.2 Inhibition of Pin1 PPIase enzymatic activity and antiproliferative activity towards A2780 ovarian cancer cells for compounds **33** and **34**……111

Table 4.1 Comparison of techniques for the detection of phosphopeptides and phosphoproteins…….....147

Table 4.2 Scan modes for the detection of phosphopeptides in tandem MS…….149

Table 4.3 Summary for the techniques used for the detection of phosphopeptides and phosphoproteins in mass spectrometry…….....150

Table 4.4 Amounts, percent yields of eight peptides after purification by RP-HPLC …….....159

Table 4.5 Molecular weights and determined masses of eight peptides…….....160

Table 4.6 Amounts and percent yields for the synthesis of phosphopeptides….....162

Table 4.7 Calculated and experimental $[M+H]^+$ values for phosphopeptide standards……162

Table 4.8 Compound dependent parameters of Qtrap 3200 in an MRM experiment for AcMKYLGpSPITTVNH_2…….204

Table 4.9 Compound dependent parameters of Qtrap 3200 for the MRM experiment to

detect **73** and **74**…….205

Table 4.10 Compound dependent parameters of Qtrap 3200 in the MRM experiment to detect the phosphorylation position of **72** in Cdc2 kinase reaction.....205

List of Abbreviations

1. Amino acids

Ala, A	Alanine
Asn, N	Asparagine
Asp, D	Aspartic acid
Arg, R	Arginine
Cys, C	Cysteine
Gln, Q	Glutamine
Gly, G	Glycine
His, H	Histidine
Ile, I	Isoleucine
Leu, L	Leucine
Lys, L	Lysine
Met, M	Methionine
Phe, F	Phenyalanine
Pro, P	Proline
Ser, S	Serine
Thr, T	Threonine
Trp, W	Tryptophan
Tyr, Y	Tyrosine
Val, V	Valine
p	Phosphor-

pSer-Pro	phosphoSer-Pro
pThr-Pro	phosphoThr-Pro

2. Enzymes

APP	amyloid precursor protein
CaK1p	cyclin-dependent kinase-activating kinase
Cdks	cyclin-dependent kinases
CsA	cyclosporine A
Cyp	cyclophilin
EGFR	epidermal growth factor receptor
ERK2	Mitogen-activated protein kinase 1
FKBPs	FK-506 binding proteins
HIV	human immunodeficiency virus
MPM-2	mitotic phosphoprotein monoclonal-2
MAP	mitogen activated protein kinase
MAPKK	mitogen-activated protein (MAP)-kinase kinase
MPF	the mitosis-promoting factor
NIMA	never in mitosis A kinase
Par	parvulins
Pin1	protein interacting with NIMA#1
PKA	cyclic nucleotide-dependent protein kinases
Plk1	Polo-like kinase
PP2A	phosphatase 2A

PPIases	Peptidyl Prolyl Isomerases
protein kinase C	phospholipids-dependent protein kinases
PTPA	phosphatase 2A (PP2A) activator
RAR	retinoic acid receptor
RSK	ribosomal S6 protein kinases
SAPK/JNK	stress-activated protein kinase
WW domain	WW stands for two tryptophans

3. Phase of mitosis

G1	preparation for chromosome replication
G2	preparation for mitosis
M	mitosis
S	DNA replication

4. Synthesis

Ac	acetyl
AMP	cyclic adenosine monophosphate
ATP	adenosine triphosphate
AZT	3'-azido-2', 3'-dideoxythymidine
BisPOM	bis-pivaloyoxymethyl
Bn	benzyl
Boc	*tert*-butoxycarbonyl
CKIs	cyclin-dependent kinase inhibitors
CoA	tryptamine-phosphopantetheine

DCC	*N, N*-dicyclohexylcarbodiimide
DCU	*N,N*-dicyclohexyl urea
ddUMP	2',3'-dideoxyuridine 5'-monophosphate
DET	dithiodiethanol
DIC	diisopropylcarbodiimide
DIPEA	*N*-ethyl-di-isopropylamine
DMAP	4-(dimethylamino)pyridine
DMF	*N, N'*-dimethylformamide
DMSO	dimethyl sulfoxide
DTT	Dithiothreitol
EDC	1-[3-(dimethylammino)propyl]-3-ethylcarbodiimide hydrochloride
EGTA	Ethylenediaminetetraacetic acid
fdUMP	5-fluoro-2'-deoxyuridylic acid monophosphate
Fmoc	Fluorenylmethoxycarbonyl
HATU	*O*-(7-azabenzotriazol-1-yl)-*N,N,N',N'*-tetramethyluronium hexafluorophosphate
HBTU	*O*-(benzotriazol-1-yl)-*N,N,N',N'*-tetramethyluronium hexafluorophosphate
HEPES	4-(2-hydroxyethyl)-1-piperazineethanesulfonic acid
HOAt	1-hydroxy-7-azabenzotriazole
HOBt	1-hydroxybenzotriazole
LDA	lithium diisopropylamide
MCPBA	meta-chloroperbenzoic acid
N_3dUMP	5-azido-2'-deoxyuridine 5'-triphosphate

NMM	*N*-methyl morpholine
N_3UMP	2'-azido-2'-deoxyuridine 5'-mono-phosphate
PMA	Phosphomolybdic acid
PMEA	9-(2-phosphonomethoxyethyl)adenine
SATE	*S*-acetylthioethanol
TBAF	tetrabutylammonium fluoride
TBS	*tert*-butyldimethylsilyl
THF	tetrahydrofuran
TIS	triisopropyl silane
TMSCl	chlorotrimethylsilane
TLC	thin layer chromatography
Tris	2-amino-2-hydroxymethyl-1,3-propanediol

5. Spectrometry

CEP	collision cell entrance potential
CXP	collision cell exit potential
CE	collision energies
CID	collision induced dissociation
DP	declustering potential
ECD	electron capture dissociation
ESI	electrospray ionization
FTICR-MS	Fourier transform ion cyclotron resonance
GS1	sheath gas pressure

GS2	auxillary gas pressure
IS	ionization spray voltage
HPLC	high performance liquid chromatography
HMQC	heteronuclear multiple quantum correlation
IMAC	Immobilized metal affinity chromatography
LC-MS/MS	HPLC coupled with tandem mass spectrometer
MALDI	Matrix assisted laser desorption ionization
MRM	multiple reaction monitoring
MS/MS	tandem mass spectrometer
NOESY	nuclear overhauser and exchange spectroscope
Q1	quadrupole 1
Q2	collision cell
Q3	quadrupole 3
SIM	single ion monitor

6. Terms

IC_{50}	the concentration required for 50% inhibition in determination of receptor
k_{cat}	catalyzed rate constant
K_m	michaelis constant
SDS-PAGE	sodium dodecyl sulfate-polyacryamide gel electrophoresis
k_{cat}/K_m	enzyme efficiency
QM/MM	hybrid quantum mechanical/molecular mechanical

Chapter 1. Introduction and Background

1.1 Biology of the Peptidyl Prolyl Isomerase Pin1.

1.1.1 The cis Prolyl Amide Bond

Amide bonds in proteins and peptides are planar structures due to the partial double bond character of the C-N bond.[1] For this reason, amide bonds exist discretely in cis and trans conformations. Specifically, if the α-carbons are on the same side of the partial C=N bond, the amide bond is considered to be in the cis conformation; if the α-carbons are on the opposite side of the partial C=N bond, the amide bond is considered to be in the trans conformation. The energy barrier for the interconversion between the cis amide and trans amide conformations is between 18 kcal/mol to 21 kcal/mol at room temperature.[2] Secondary amide bonds exist exclusively in the trans conformation due to the steric interaction of the two extended side chains.[3] In addition to the steric advantage, trans amide bonds are also observed to be stabilized by an electronic effect (Figure 1.1).[4] An $n \rightarrow \pi^*$ interaction between the oxygen of the peptide bond and the subsequent carbonyl carbon in the polypeptide chain also contributes to this preference.[4] Therefore, over 99.99 % of secondary amide bonds assume the trans conformation.[3]

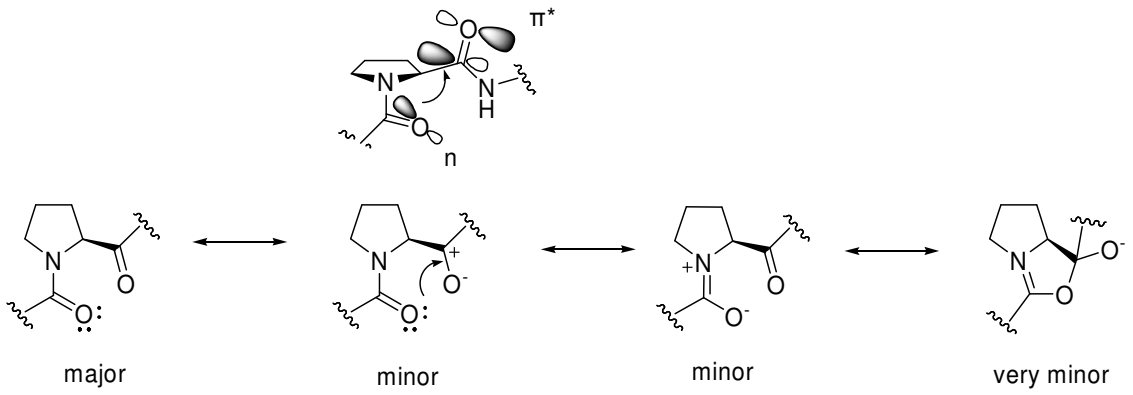

Figure 1.1 Stabilization of trans amide conformation via electronic effect[4]

However, the prolyl amide bond, which immediately precedes the proline residue, is unique because it is the only tertiary amide bond among the 20 naturally occurring amino acids. About 10-30 % of prolyl amides exist in the cis conformation, which is proportionally much higher compared to secondary amide bonds.[5] The reason for this high percentage of cis prolyl amide is due to the reduced steric advantage of the trans prolyl amide, which is associated with the *N*-alkylation of the proline residue. Therefore, prolyl isomerization occurs, which refers to the cis/trans isomerization of the imidic bond preceding the proline residue. In theory, there are 2^n conformers for a polypeptide containing n proline residues. Due to the restricted torsional angle Φ imposed by the fixed *N*-alkyl bond in the five-membered ring, proline plays a very important role in the secondary structures of proteins and polypeptides. Since the interconversion dynamics are generally slow, as shown by NMR at room temperature, rotamer formation is often observed for polypeptides containing proline.

In kinetic terms, cis/trans prolyl amide isomerization is a very slow process (1 to 7 min for model peptides) compared with protein folding (millisecond time scale) and other biological processes.[6] The occurrence of prolines in the proteins may impede the protein folding process by trapping one or more of the prolines in nonnative isomers, especially when native proteins require the cis isomer. This is likely because proline residues are exclusively synthesized in the trans form on the ribosome.[6-9] Prolines, therefore, play a key role in the folding and unfolding transitions of globular proteins.[6-8] It should also be noted that proteins containing proline residues are often observed to have a mixture of fast and slow folding molecules, which was first reported for ribonuclease.[6, 10] Proline residues in fast folding molecules have the same conformations as those in the native forms of proteins, while proline

residues in slow folding molecules are exclusively in non-native conformations.[7-9, 11] For protein folding to occur, the slow folding molecules must convert into the fast folding molecules through the cis/trans prolyl isomerization of specific proline residues.[7] Therefore, the presence of proline residues can significantly impact the activity of proteins. Proline may act as a conformational switch to turn on or turn off various protein functions (Figure 1.2). In fact, it was recently reported that cis/trans prolyl amide isomerization could open the core for a neurotransmitter-gated ion channel.[12] The cis/trans isomerization of prolyl amides can also be used in an enzyme-regulated manner to control the timing of biological events such as cell cycle regulation, cell signaling and protein-protein interactions.[13]

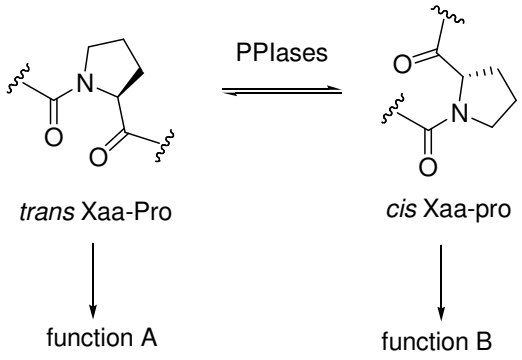

Figure 1.2 Prolyl cis/trans isomerization as a conformational molecular switch

1.1.2. Peptidyl Prolyl Isomerases (PPIases)

Since thermal cis/trans prolyl isomerization is a relatively slow process (usually measured in minutes) compared to other biological processes, peptidyl prolyl isomerases (PPIases) have evolved to accelerate this process.[11, 14] PPIases are inactive toward both nonproline *N*-alkyl amino acid moieties and secondary amides, but are highly active toward various proline-containing oligopeptides.[15] To date, PPIases represent the only example of

enzymes that are able to catalyze conformational interconversions.[3, 14] Four categories of PPIases have been reported: 1) cyclophilins (Cyp), 2) FK-506 binding proteins (FKBPs), 3) parvulins (Par), and 4) a recently discovered protein known as Ser/Thr phosphatase 2A (PP2A) activator (PTPA).[13, 16-19] These PPIase varieties have unrelated amino acid sequences, as well as distinct substrate specificities.[16, 17, 19] They exist ubiquitously in all organisms including bacteria, fungi, plants and animals, and are highly abundant in most tissues and cells, which indicates the universal functionality of PPIases in protein folding and many other biological processes.[3, 15, 20-24]

Cyclophilins comprise an entire class of PPIases that bind the immunosuppressant drug cyclosporine A (CsA).[25] FKBPs represent the PPIases that are capable of tight binding to the immunosuppressant drugs, FK-506 and rapamycin.[25] The binding of immunosuppressant drugs to their respective receptors can inhibit their PPIase activity to varying degrees. Cyclophilins and FKBPs are of interest in drug development because they are associated with anti-infective activities (CsA and FK-506),[26, 27] imunosuppression (CyP and FKBP),[27] chaperone activities (CyP),[28] and in suppressing HIV (the human immunodeficiency virus) infection (CyP).[29] Parvulins represent another family of PPIases that are unrelated to immunophilins (CyP and FKBPs) in protein sequence and they do not bind immunosuppressant drugs.[3, 16, 17, 30] Unlike the cyclophilins, FKBPs, and parvulins, which all have a central β-sheet and function as monomers in their catalytic domains, the catalytic domain of PTPA is an all α-helix fold with the active site located at the interface of a substrate-induced dimmer.[13, 18]

The cis/trans isomerization rates of prolyl amides can be accelerated by several

orders of magnitude by PPIases (from minute scale to millisecond scale), which is closer to dynamic biological processes. PPIases are remarkably special enzymes since cis and trans conformers of the proline-related peptide substrate can each act as either the substrate or the product in PPIase-catalyzed reactions. Moreover, the activation barrier for the prolyl isomerization reaction can be decreased by PPIases, either by lowering the energy of the transition state (transition state stabilization) or by raising the energy of the bound substrate (substrate activation).[13, 14] A twisted (90°) syn transition state for the interconversion process was proposed by Linus Pauling.[1, 31, 32] An energy diagram for the prolyl cis/trans isomerization process is shown in Figure 1.3.[13]

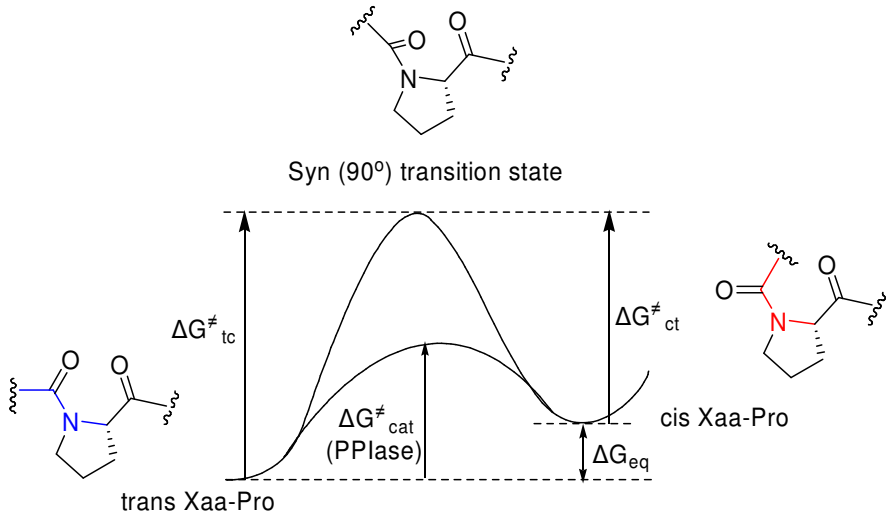

Figure 1.3. Energy diagram for prolyl cis-trans isomerization[13]

In order to determine how PPIases overcome the energy barrier (20 kcal/mol) associated with prolyl isomerization, several mechanisms have been proposed. These include substrate desolvation, substrate autocatalysis, preferential transition-state binding and nucleophilic catalysis, although the process is still not fully understood yet.[25] The present experimental data do not support a common mechanism for all PPIases. A substrate

desolvation mechanism was proposed based on the fact that the energy of a bound substrate in the active site of an enzyme (more hydrophobic) is typically higher than the substrate in a polar solvent such as water.[3, 33, 34] The partially charged species in the peptide backbone destabilize the substrate in a hydrophobic environment, thus increasing the energy of the substrate and lowering the activation barrier for the reaction.[33, 34] In the substrate autocatalysis mechanism, the H-bond between the imide nitrogen lone pair and the NH of the amino acid following the proline in the substrate may somewhat stabilize the transition state.[3, 35, 36] In the preferred transition-state binding mechanism, binding between the twisted transition state and the active sites of PPIases is favored, which is associated with the electrophilic stabilization of the nitrogen lone pair through H-bond with water.[16] In the nucleophilic catalysis mechanism, nucleophilic attack on the prolyl carbonyl carbon by an activated enzyme group, such as a cysteine side chain, forms a tetrahedral intermediate.[3, 13, 37] Since resonance is eliminated in the tetrahedral intermediate, the energy barrier can be greatly reduced (Figure 1.4).[3, 13, 37]

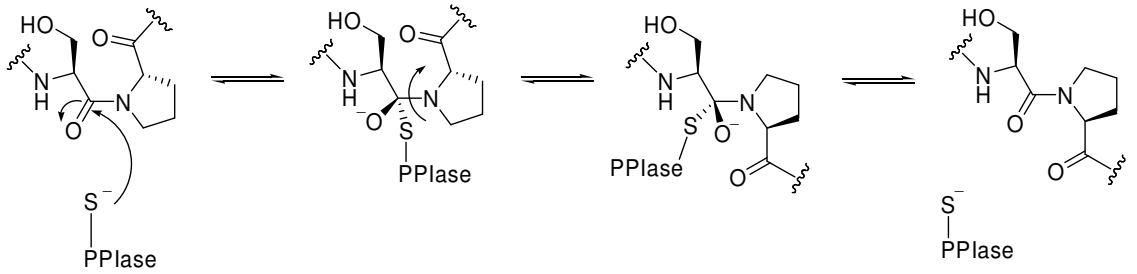

Figure 1.4 Nucleophilic mechanism proposed for PPIase activity

1.1.3. Pin1

Pin1 (protein interacting with NIMA#1) was originally identified in 1996 by its ability

to interact with NIMA (never in mitosis A kinase), which is a mitotic kinase phosphorylated on multiple Ser/Thr-Pro motifs during mitosis.[38] Pin1 is a highly conserved PPIase belonging to the parvulin family. Unlike all other known PPIases, Pin1 selectively binds to and isomerizes specifically the phosphoSer-Pro or phosphoThr-Pro motifs in certain proteins.[37, 39-41] Phosphorylation of Ser-Pro and Thr-Pro motifs has been shown to be a critical regulatory event for many proteins.[42] Indeed, the biological significance of these phosphorylated motifs has been greatly enhanced by the discovery of Pin1.[13, 43] Specifically, phosphorylation on Ser/Thr residues immediately preceding a proline not only slows down the thermal prolyl cis/trans isomerization rate, but also creates binding sites for Pin1 (Table 1.1).[44] With the exception of Pin1, other known PPIases cannot catalyze proline isomerization after the phosphorylation of Ser or Thr residues preceding a proline. The selectivity of Pin1 for pSer/Thr-Pro motifs over non-phosphorylated Ser/Thr-Pro motifs has been shown to be more than 1300-fold.[39]

Table 1.1 Effect of phosphorylation on kinetic constants of cis/trans isomerization of peptide-4-nitroanilide at pH 7.8.[44]

Peptide derivatives	Cis content (%)	$k_{\text{cis to trans}} \times 10^3$ (s^{-1})	$\Delta G^{\ddagger}$ 25°C (kJ/mol)
Ala-Ala-Thr-Pro-Phe-NH-Np	10.2 ± 0.3	13.1 ± 0.8	79.5
Ala-Ala-Thr(PO_3H_2)-Pro-Phe-NH-Np	5.7 ± 0.4	1.7 ± 0.3	84.1
Ala-Ala-Ser-Pro-Phe-NH-Np	12.5 ± 0.2	9.7 ± 0.1	80.4
Ala-Ala-Ser(PO_3H_2)-Pro-Phe-NH-Np	17.5 ± 0.3	4.2 ± 0.2	82.1

Pin1 uses substrate Ser/Thr phosphorylation as an additional level of cell cycle regulation.[13] The isomerization of the pSer/Thr-Pro motifs is especially important because some proline-directed kinases and phosphatases are conformation-specific, acting only on the trans conformation.[44-48] For instance, one MAP kinase (Mitogen activated protein kinase), ERK2 (Mitogen-activated protein kinase 1), was found to only recognize and phosphorylate trans Ser/Thr-Pro amides in its substrates.[45, 47] Another example is the phosphatase PP2A, which dephosphorylates trans pCdc25 and inactivates Cdc25.[46, 48] Pin1 is required for the efficient restoration of the equilibrium between the cis and trans conformers for a variety of phosphoproteins involved in mitosis.[13]

In addition to the high selectivity of most phosphorylated species, arginine at the +1 position and aromatic residues at positions -1 through -3 around the pSer/Thr-Pro core are also favored in the substrates of Pin1.[39]

The X-ray crystal structure of Pin1 has been obtained with the dipeptide Ala-Pro bound to its catalytic domain in the presence of sulfate ion (Figure 1.5).[37]

In Figure 1.5, two domains of Pin1 can be easily identified: the *N*-terminal WW-domain (residues 1-39), which contains a three-stranded anti-parallel β sheet, and the *C*-terminal PPIase domain (residues 40-163).[37] The WW domain is a small protein-protein interaction domain that has been observed in a variety of cell signaling proteins. One hypothesis is that this domain is required for the function of Pin1 by targeting the catalytic PPIase domain to its phosphoSer/Thr-Pro substrates.[49] The *C*-terminal catalytic PPIase domain of Pin1, which consists of four α-helices and a four-stranded anti-parallel β-sheet, shares little similarity with either the cyclophilins or the FKBPs.[37] Important residues in the

active sites of Pin1 catalytic domain include His59, His157, Cys113, Arg68 and Arg69.[37] In particular, the highly conserved residues Lys63, Arg68 and Arg69 form a basic cluster at the entrance of the active site binding the sulfate ions, indicating the strong preference of Pin1 for a negatively charged residue immediately preceding a proline in its substrates (Figure 1.5).[37]

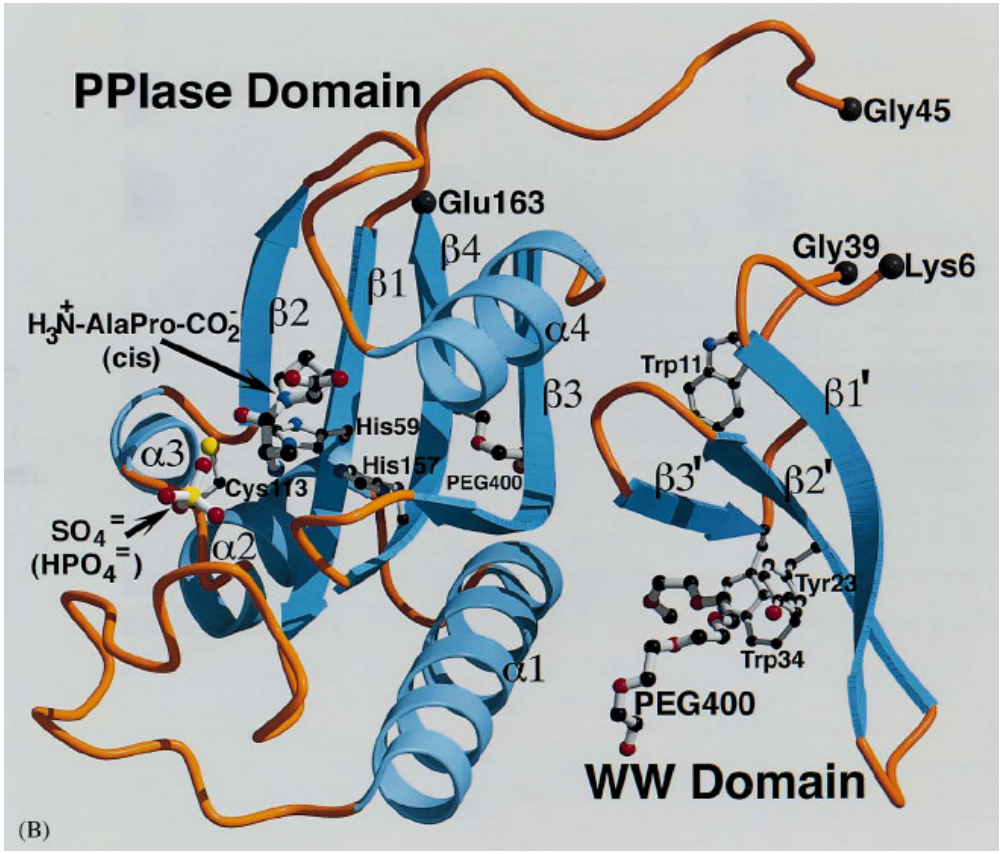

Figure 1.5 X-ray crystal structure of Pin1[37]

Ranganathan, R.; Lu, K. P.; Hunter, T.; Noel, J. P. *Cell* **1997,** *89*, (*6*), 875-886. Copyright [1997] Elsevier Limited.

Pin1 is the only PPIase found to be essential for regulating cell cycle.[38-40] It is particularly important for the transition from G2 to mitosis.[39-41] Typically, the cycle of a cell is defined by four stages: preparation for DNA replication (G1), DNA replication (S),

preparation for mitosis (G2) and mitosis (M). Cell division occurs during the mitosis stage (Figure 1.6).

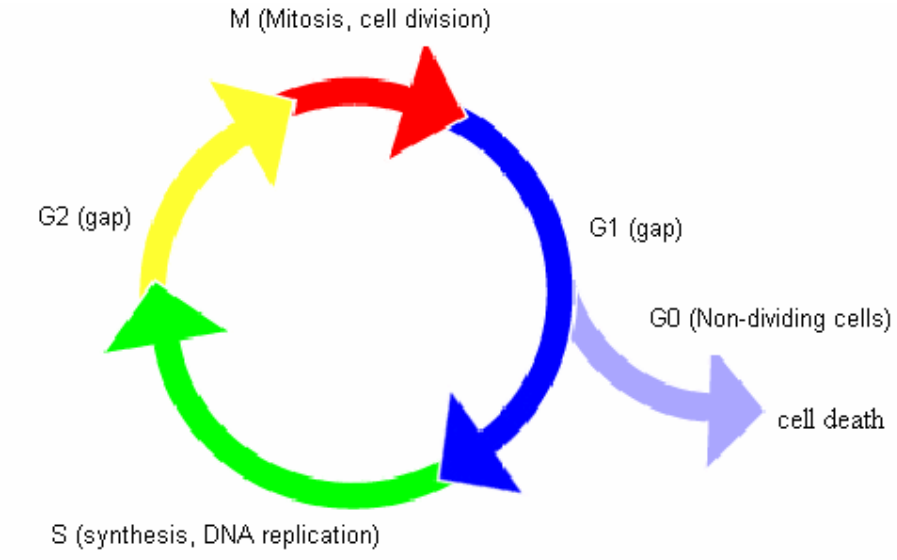

Figure 1.6. The cell cycle

Progression through the different stages of the cell cycle is regulated by the timely activation and inactivation of different proline-directed cyclin-dependent kinases (Cdks) and phosphatases.[50-52] The activation of these Cdks and phosphatases induce the appropriately timed structural modification of a large number of proteins through the process of phosphorylation/dephosphorylation.[51-53] For instance, during the transition from G2 to mitosis, several hundred proteins are phosphorylated by Cdc2 kinase, a key regulator of the cell cycle.[53] However, it is still not entirely clear how these phosphorylated proteins are coordinated to induce a series of cell cycle events. With the discovery of the phosphorylation-dependent PPIase, Pin1, Pin1-catalyzed prolyl isomerization might be an important mechanism in the cell cycle regulatory process.

HeLa cells depleted of Pin1 were characterized by mitotic arrest and nuclear

fragmentation, while the overexpression of Pin1 induces G2 arrest and inhibits entry into mitosis.[39-41] Pin1 acts as a negative regulator of the G2 to mitosis transition, preventing lethal premature entry into mitosis.[38] Pin1 has also been shown to be necessary for mitotic progression.[39-41] In addition, Pin1 was found to play an important role in the transition between the G0/G1 and S phases, as well as to affect the DNA-replication-mediated mitotic checkpoint.[13]

Pin1 binds and regulates a highly conserved subset of proteins that undergo mitosis-specific phosphorylation.[39] Furthermore, Pin1 specifically binds and effectively catalyzes the prolyl isomerization of phosphorylated Ser/Thr-Pro motifs present in these mitosis-specific phosphoproteins involved in cell cycle regulation, which are also recognized by the phosphospecific mitosis marker MPM-2 (mitotic phosphoprotein monoclonal-2) monoclonal antibody.[39, 40, 54] The interactions between Pin1 and these mitosis-specific phosphoproteins were cell-cycle-regulated, although Pin1 levels are constant (about 0.5 μM) through the cell cycle.[40] Pin1-binding activity was low during G1 and S, increased in G2/M, and was highest when cells were arrested in mitosis.[40] The numbers of these phosphoproteins discovered that interact with Pin1 are still increasing, the most important ones include: NIMA kinases, Cdc25 phosphatase, Plk kinase ((Polo-like kinase)), Wee1 kinase, Myt1 kinase, tau protein, Cdc27, p53 oncogen,[55-57] the c-Myc oncogen,[58] and retinoic acid receptor (RAR).[59] Pin1-catalyzed post-phosphorylation regulation of these proteins are believed to be a possible mechanism for the function of Pin1 in cell cycle regulation.

A number of studies have revealed the critical role of prolyl cis/trans isomerization catalyzed by Pin1 in determining the timing and duration of several signaling pathways

involved in cell proliferation and transformation. One of the most well-recognized examples is the critical function of Pin1 in amplifying the Neu-Raf-Ras-MAP kinase pathway at multiple levels.[13, 60] Pin1 interacts directly with several intermediates (such as c-Jun, c-fos and Cyclin D1) of this cascade to turn on the positive feedback loop and interacts with Raf to turn off the negative feedback loop.[61-65] The overexpression of Pin1 was found to enhance the ability of both Ras and Neu to transform cells, while the inhibition of Pin1 prevented Ras or Neu from inducing cell transformation and cancer development.[13, 60, 66]

Pin1-catalyzed phosphorylation-dependent prolyl isomeration has been shown to bind and regulate the function of many transcription factors, including altering the activity of c-Jun, c-fos, and destabilizing the β-catenin and c-Myc—or both—for p53 and p73.[13, 61, 67] Pin1 was also found to regulate the RNA processing machinery.[13]

Overexpression of Pin1 was observed in most common cancers such as prostate, breast, brain, lung and colon, therefore the detection of Pin1's concentration may provide an efficient way to distinguish cancer cells from normal cells.[68] Other researchers have shown that overexpression of Pin1 is linked to cell transformation, centrosome amplification, genomic instability and tumor development.[54, 67, 69] Overexpression of Pin1 has also been correlated with elevated cyclin D1 levels in many cancer cell types.[61] Cyclin D1 is a cell cycle protein that plays a key role in the development of many cancers.[69, 70] Pin1 may activate c-Jun, or bind directly to phosphorylated cyclin D1 and stabilize it in the nucleus, thereby elevating cyclin D1 gene expression.[61, 62] In studies involving mice, deletion of the Pin1 gene resulted in a reduction of cyclin D1 levels.[61, 62] In addition, Pin1 elimination in mice prevented certain oncogenes from inducing tumors.[71, 72] The inhibition or depletion of Pin1 in cancer cells

can induce apoptosis and suppress their transformed phenotypes and tumorigenicity in mice.[69, 71, 72] In summary, increasing evidence suggests that Pin1 acts as a pivotal catalyst in multiple oncogenic pathways.[69] Therefore, designing highly specific and potent inhibitors of Pin1 may have potential in the development of anti-cancer drugs.

Phosphorylation-dependent prolyl isomerization catalyzed by Pin1 has also been shown to play a key role in protecting against age-dependent neurodegenerative disorders, such as Alzheimer's disease.[73] In Alzheimer's disease, Pin1 is overexpressed and exists at high levels in most neurons. Specifically, Pin1's role in inhibiting Alzheimer's disease can be understood by the fact that Pin1 facilitates tau dephosphorylation via the conformation specific phosphatase PP2A,[48, 74] as well as by regulating the degradation of the amyloid precursor protein (APP).[30, 75] Therefore, Pin1 has an important neuroprotective function and represents a potential new therapeutic agent for Alzheimer's disease.[30, 75]

The functions of Pin1 in the regulation of the cell cycle, cell signaling transduction, gene expression, neuron function, and immune response are all thought to occur as a result of interactions with its phosphoprotein substrates via prolyl isomerization at specific pSer/pThr-Pro motifs in its substrates.

1.2. Protein Phosphorylation and Ser/Thr-Pro specific Protein Kinases

1.2.1 Protein Phosphorylation

In 1955, Krebs and Fischer first identified a mechanism for regulating enzyme activity through the reversible addition of a phosphate group.[76] Over fifty years later, the reversible phosphorylation of proteins is now considered the most important posttranslational modification that occurs in a cell. It has been shown to be essential for regulating many

cellular signaling pathways and metabolic functions.[77] In essence, the reversible phosphorylation of proteins is a highly versatile and efficient mechanism for intermolecular communication.[78]

The enzymes involved in this reversible covalent modification are protein kinases and protein phosphatases. Protein kinases are enzymes that phosphorylate Ser, Thr and Tyr residues in proteins by transferring the γ phosphoryl group from adenosine triphosphate (ATP), as shown in Figure 1.7.

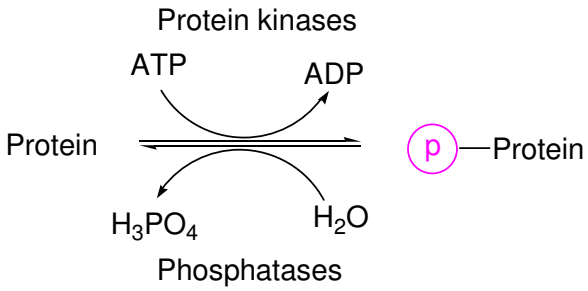

Figure 1.7. Phosphorylation and dephosphorylation of proteins.

In 1955, the first kinase to be discovered was glycogen phosphorylase.[76, 79] Over the next few years, protein phosphorylation on serine residues was thought to exist only in the glycogen mechanisms that control the activities of phosphorylase and glycogen synthase.[77] This notion began to change after the discovery in 1968 of cyclic adenosine monophosphate (c-AMP) dependent protein kinase (c-APK), with its broad substrate specificity and capability for both serine and threonine phosphorylation. In 1980, a tyrosine kinase was discovered in the product of the Rous sarcoma virus *Src* gene.[77] After that, the discovery of protein kinases began to grow exponentially. Kinases are involved in carbohydrate and lipid metabolism, membrane transport, neurotransmitter biosynthesis, cell motility, cell growth, cell division, learning and memory.[77, 80] So important were these discoveries that protein

phosphorylation became recognized as "the major general mechanism by which intracellular events in mammalian tissues are controlled by external physiological stimuli."[81]

The eukaryotic protein kinases comprise one of the largest protein families, since about 2 % of eukaryotic genes may code for them.[82] It is estimated that there may be as many as 2000 protein kinases to carry out a wide range of processes in the vertebrate genome.[82] They range from the large growth factor receptor kinases to the small cell-division kinases.[83-85]

While some kinases only recognize a few specific molecules, others are less particular and can catalyze the phosphorylation of multiple targets upon activation. Although these kinases may differ in subunit structure, subcellular localization, size and mechanism of regulation,[83] they share a common catalytic core of about 270 amino acids[86] and probably evolved from a common precursor.[87] Interestingly, phosphatases that catalyze dephosphorylation are more abundant than kinases and appear to function by several different catalytic mechanisms.[88, 89]

1.2.2 Classification of Protein Kinases and Their Functions in Cell Cycle Regulation

Based on substrate specificity, the eukaryotic protein kinases are divided into two classes: Ser/Thr-specific kinases and Tyr-specific kinases. It should be noted, however, that several kinases are able to phosphorylate both classes.[78, 90-92] For example, the mitogen-activated protein (MAP)-kinase kinase (MAPKK) is a dual-specific kinase.[93, 94] Another kinase, Wee1, plays an important role in cell cycle by catalyzing the inhibitory phosphorylation of Cdc2 kinase, which appears to be a dual-specific enzyme *in vitro*.[91]

Located near the more conserved catalytic domains of the eukaryotic protein kinases

are the highly variable regulatory domains, which contain binding sites for accessory regulatory proteins.[78, 95] These specific sequence differences in regulatory domains are responsible for the variety of ways that protein kinases can respond to many different extracellular signals.

Based on their particular structural and functional features, eukaryotic protein kinases can be classified into many subgroups. The Ser/Thr-specific kinase family includes: cyclic nucleotide-dependent protein kinases (c-APK or PKA), phospholipid-dependent protein kinases (protein kinase C), cyclin-dependent kinases (CDK), mitogen-activated kinases (MAP kinases), Ca^{2+}/calmodulin-regulated protein kinases, Raf kinases, casein kinase CK1 and CK2, ribosomal S6 protein kinases (RSK), Casein kinase CK2 and glycogen synthase kinase 3, transmembrane receptor-Ser/Thr-kinases, serpentine receptor kinases, and DNA-dependent kinases.[90] For the Tyr-specific kinases, two major subgroups exist: transmembrane receptor Tyr-kinases, and cytoplasmic tyrosine kinases including: Src, Csk, Syk, Btk, JAK, FAK, Abl, etc.[78, 96]

Different kinases are involved in regulating the four periods of a cell's cycle: preparation for chromosome replication (G1), DNA replication (S), preparation for mitosis (G2) and mitosis (M). To be specific, regulation of the cell cycle is achieved by the timed structural modification of proteins through both phosphorylation/dephosphorylation processes and ubiquitin-mediated protein degradation.[51, 52] Among them, cyclin-dependent kinases (CDKs) play a central role in the regulation of the cell cycle.[51, 52] CDKs are defined as one family of Ser/Thr kinases that totally rely on binding a cyclin partner for regulating their kinase activity.[50-52, 83] Their molecular weights range from 30 to 60 kDa.[50-52, 78]

Sequences of different CDKs have been shown to be ≥ 50 % identical.[52, 97]

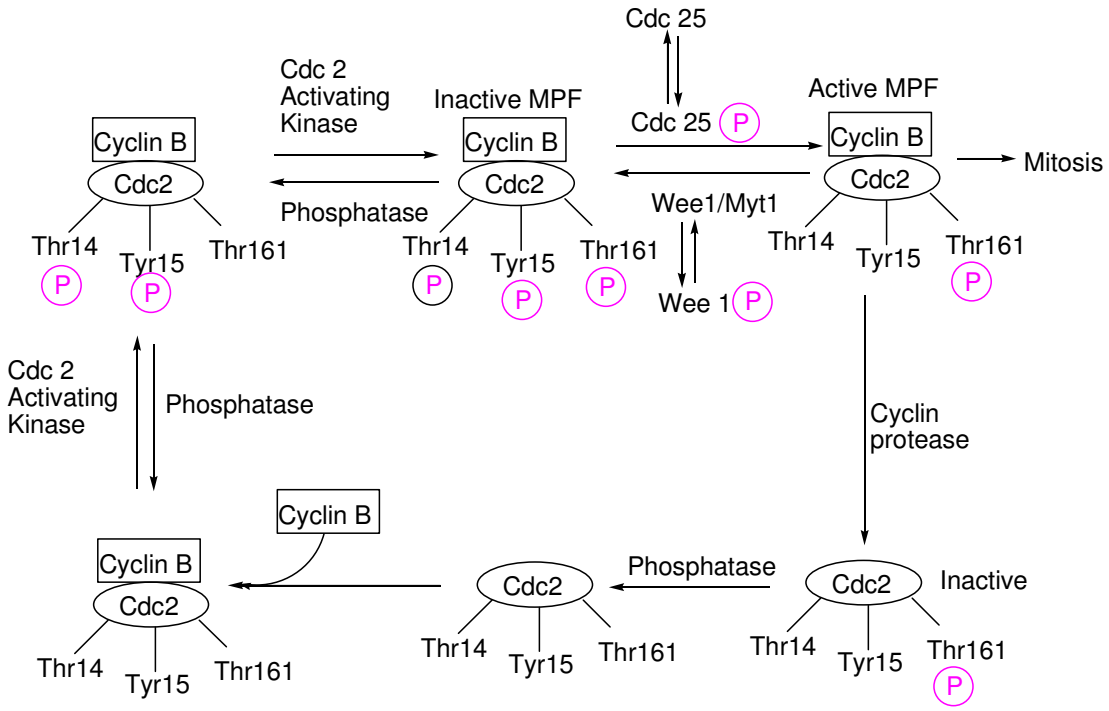

Figure 1.8. Regulation of the Cdc2/cyclin B complex by phosphorylation/dephosphorylation.[53]

Cdc2 was the first CDK discovered.[51] Researchers determined that the activation of the mitosis-promoting factor (MPF), which is a complex of Cdc2 and cyclin B, can trigger entry into mitosis from the G2 phase; while the inactivation of the MPF by proteolysis of cyclin B results in the termination of mitosis.[51, 52] Moreover, at different stages of cell cycle, different cyclin-CDK complexes were found. Understanding the roles of these cyclin-CDK complexes and their regulatory activity at the different cell cycle stages has become an important and intriguing challenge for biochemists.

Related research has confirmed that the timely regulation of the activities of cyclin-CDK complexes is critical to the cell cycle (Figure 1.8).[51-53] While there are several

mechanisms for achieving this, the simplest method is by regulating the amount of cyclin.[51, 52] Another control mechanism involves the phosphorylation/dephosphorylation of the CDK subunits.[51, 52] The third level of control is through the cyclin-dependent kinase inhibitors (CKIs), which bind and inactivate the related cyclin-CDK complexes.[51, 52] Cdc2/cyclin B kinase is activated and inactivated at the G2/M transition by phosphorylation and dephosphorylation and by cyclin B abundance (Figure 1.8). As shown, Thr161 has to be phosphorylated to turn on the kinase activity, while phosphorylation of both Thr14 and Tyr15 keeps the complex in an inactive form.[53] Therefore, the activity of Cdc2/cyclin B is positively regulated via the dephosphorylation of Thr14 and Tyr15 by the Cdc25 phosphatase,[52] while it is negatively regulated via phosphorylation by Wee1 (a Ser/Thr kinase) and Myt1 (a Tyr kinase).[50] Moreover, Cdc25 phosphatase activity is turned on upon phosphorylation, while Wee1 kinase activity is inhibited by phosphorylation.[52-54] Additional research has showed that Cdc25 is also regulated by the isomerization of prolyl amides by Pin1.[98]

In recent years, mounting evidence has suggested that other kinds of protein kinases also participate in cell cycle regulation, apart from the cyclin-dependent kinases.[99, 100] For example, MPF is not the only inducer for mitosis. Research has shown that NIMA-related kinases are required for entry into mitosis in the filamentous fungi, *Aspergillus nidulans*.[100] How the CDKs and NIMA act in concert to trigger cell cycle transitions is still unknown. In *Aspergillus,* entry into mitosis also requires activation of a Ca^{2+}-calmodulin-dependent protein kinase.[99]

Protein kinase C (PKC) also operates as a regulator of the cell cycle during chromosome replication (G1), as well as during the G2 to M transition.[101] The activation of

PKC in various cell systems leads to reduced activity of Cdc2.[101] Moreover, the cAMP-dependent protein kinase plays a role in the *Xenopus* oocyte system.[101] In meiotic frog oocytes, MAP kinases are activated by the Mos protein kinase as cells enter meiosis.[52, 102] Since the Raf kinases and MAPKK are the upstream kinases of the MAP kinases, these two kinds of kinases also participate in cell cycle regulation.[94] All of these protein kinases form cascades or complex signal transduction networks to regulate cell cycle.

1.2.3. Structural Features of Protein Kinases

The X-ray structure of the C-subunit of cAPK was elucidated in 1991,[103, 104] which represents the first three-dimensional structure of a protein kinase. Every member of the protein kinase family shares a conserved region of catalytic domain (kinase domain), which contains 200-250 amino acids and confers kinase activity.[86, 105] The kinase domain is responsible for ATP binding, peptide substrate binding, and phosphoryl group transfer. In contrast, there are various activation segments in different kinases that show little sequence conservation.[52, 83] The activation loop, which is critical for the regulation of different kinases, ranges in size from 19 to 32 residues.[77]

1.2.4. Regulation of Protein Kinases Activity

The activities of protein kinases are highly regulated by activating signals, such as second messengers,[106, 107] subcellular localization,[108-110] fatty acid acylation,[108, 109] and isoprenylation.[110, 111] Without input from these signals, protein kinases remain inactive. Many kinases are activated by a mechanism known as "intrasteric control",[78, 112] in which the kinases are activated by a pseudosubstrate domain.[78, 112, 113] A pseudosubstrate domain is a peptide sequence that encompasses all of the phosphorylation consensus sequence of a

substrate, with the exception of the amino acid to be phosphorylated.[78] A pseudosubstrate domain may be a separate subunit (in the case of the cAMP-dependent protein kinases) or reside in the catalytic domain (in the case of protein kinase C).[112, 113] When kinases are inactive, the pseudosubstrate domain interacts with the catalytic center, blocking binding of the substrate or ATP. Upon activation, the pseudosubstrate moves away and allows access of the substrate or ATP to the catalytic center.[112, 113]

Phosphorylation of kinases is another important way of regulating their activities. For example, in cAPK, phosphorylation of Thr-197 is essential for the activity of the kinase.[81, 117, 118] Many kinases are activated through phosphorylation of the activation loop, which can improve substrate binding and increase the rate of phosphoryl transfer.[78, 80] Activation loop phosphorylation generally increases the rate of phosphoryl transfer by 2-4 orders of magnitude.[78, 80] While some phosphorylation mechanisms can positively regulate the activities of kinases, others can be negative. As an example, Src kinases become inactive when the *C*-terminal phosphotyrosyl residue, a type of product inhibition, interacts with the SH2 domain.[114] These kinases, therefore, require dephosphorylation for activation. Interestingly, to regulate the Cdc2 kinases, both phosphorylation and dephosphorylation are required.[78, 80]

Different kinases require different specific activation mechanisms. In some kinases, for instance, the loop will move away and make the catalytic center free to attack by the substrate. In some cases, conformational changes occur in the loop of kinases upon phosphorylation. For example, the inactive conformation of CDK2 has a closed conformation in which the activation loop blocks the substrate binding site, resulting in the displacement of

the C-helix in the *N*-terminal lobe. The active conformation of CDK2 can occur as a result of the phosphorylation of Thr-160 and subsequent binding with cyclin A, resulting in profound conformational changes. It should be noted, however, that there is little sequence conservation within these loops. Some activation loops need only single phosphorylation, as is the case with the kinases cAPK and Cdc2, while others may need multiple phosphorylations (e.g., ERK2). For PhK, no phosphorylation is required.[80, 115]

1.2.5. The Chemical Mechanism of Phosphorylation

ATP Recognition

X-ray structures of the active ternary complexes of kinases, such as cAPK, PhK, with ATP or ATP analogues and their peptide substrates, give direct evidence that the ATP binding sites for catalysis are similar in these complexes.[77, 116, 117] Several conserved residues near the phosphoryl transfer site play important catalytic roles in ATP recognition. The chelation of two Mg^{2+} ions with the phosphates of the ATP, along with the conserved residues of the kinase, is essential for catalytic activation of protein kinases.

Figure 1.9 shows a good example of the positions of ATP binding in the catalytic domain in cAPK, as well as some of the key interactions between the conserved residues, Mg^{2+} and ATP.[80] In general, there are three major interactions that determine the location of ATP, the first of which requires two metal ions. Specifically, Mg1 chelates with the β-, γ-phosphates of ATP and two carbonyl oxygens of Asp-184 (Asp-167 in PhK), while Mg2 is coordinated with the α- and γ- phosphate of ATP, one carbonyl oxygen of Asp-184, and the amide oxygen of the Asn-171 (Asn-154 in PhK).[80] Mg1 may help position the γ phosphate of ATP for direct transfer to the hydroxyl acceptor. Lys-72 (Lys-48 in PhK) of the *N*-terminal

lobe interacts with the oxygen atoms of α- and β- phosphates of ATP, and simultaneously with Glu-91 (Glu-73 in PhK) of the *C* terminal lobe.[77, 117] The third interaction involves the coordination of Lys-168 (Lys-151 in PhK) with the γ- phosphate of ATP in cAPK.[80] This interaction, however, is not typical in other protein kinases.[118-122]

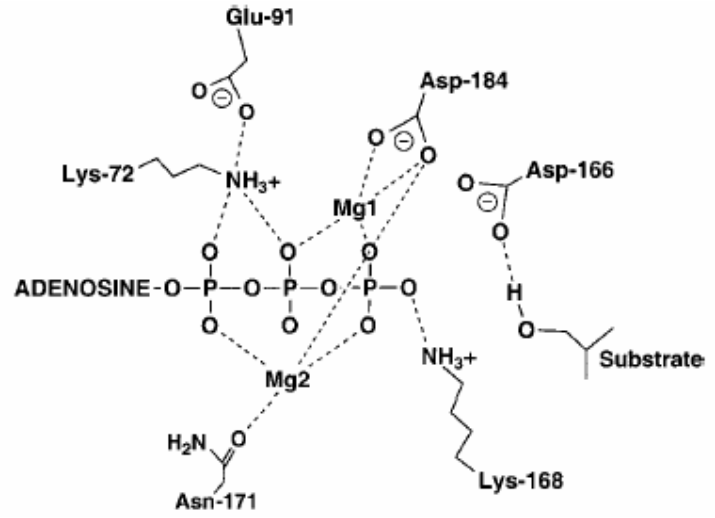

Figure 1.9. Key residue interactions in the kinase domain of cAPK.[80]

Adams, J. A. *Chem. Rev.* **2001,** *101*, (*8*), 2271-2290. Copyright [2001] American Chemical Society.

In the inactive conformations of these complexes, there are many differences between ATP binding sites. Therefore, a correction of the ATP binding position occurs upon activation of these kinases. In addition, the presence of a substrate can help further orient the ATP.

Substrate Recognition

Whether or not a Ser, Thr or Tyr residue in a peptide or protein substrate is phosphorylated by a kinase is strictly dependent on the local amino acid sequence around this residue. In terms of nomenclature, if the phosphorylation site is known as the P-site, then the residues *N*-terminal to these sites are numbered P–1, P–2, P–3, etc., and the residues

C-terminal to these sites are numbered P+1, P+2, P+3, etc. For example, one or more basic residues, such as Lys or Arg near the P-site, are necessary for substrate recognition in most Ser/Thr kinases, while the Tyr kinases favor acidic residues such as Glu or Asp. These local amino acid sequences are referred to as the consensus sequence for substrate phosphorylation. Specific consensus sequences for many types of protein kinases have been determined (Table 1.2). While some are very simple sequences, others are considerably more complex, such as –D-D-E-A-S/T*-V-S-K-T-E-T-S-E-V-A-P in the case of the rhodopsin kinase.[78] Consequently, the specificity of protein kinases varies widely.

Kemptide (LRRASLG), a standard peptide substrate for cAPK based on its specific consensus sequence, has been used widely to investigate the structure and mechanism of the cAPK kinase.[80] For Cdc2 and ERK2, a proline residue is essential for substrate recognition at the P+1 position after the Ser/Thr residue.[80, 116, 123] Hence, Cdc2 and ERK2 are commonly referred to as proline-directed kinases.[80, 116, 123] Substrate recognition can be achieved based on a combination of factors, including shape, hydropathy and electrostatic potential between the kinase and its specific consensus sequence of substrate. In cAPK, a hydrogen bond was observed between Asp-166 (Asp-149 in Src) and the hydroxyl group of the substrate, which may direct the hydroxyl group to the γ- phosphate of ATP.[80] This interaction is common in other kinases, such as in the ternary complexes for PhK and IRK.[80, 121] Thus Asp-166 is also a critical residue for substrate recognition.

For natural peptide substrates, there are additional binding determinants which are not located near the P-site. For example, p38, one member of the MAP kinase family, appears to use regions outside the consensus sequence for substrate recognition.[124] These regions are

called distal recognition regions, which are important for effective phosphorylation.[124] Therefore, the binding sites of substrates include both the consensus sequence and distal regions outside the active core.

Table 1.2. Specific consensus sequences for several protein kinases.[80]

Name	Consensus sequence
cAPK	-R-R-X-S/T*-Hyd
PhK	-R-X-X-S/T*-F-F
Cdc2	-S/T*-P-X-R/K
ERK2	-P-X-S/T*-P
Src	-E-E-I-Y*-E/G-X-F
Csk	-I-Y*-M-F-F-F
InRK	-Y*-M-M-M
EGFR	-L-E-D-A-E-Y*-A-A-R-R-R-G

Reaction Order

Since kinases need to bind ATP and substrates to form a ternary complex for phosphoryl transfer, a bisubstrate kinetic mechanism is necessary. If kinases sequentially bind one substrate before the other, the mechanism is considered to be ordered; if substrate binding does not occur in succession, the process is considered to be random. Steady-state kinetic experiments involving protein kinases in the presence of inhibitors have revealed that most of the kinases adopt a random mechanism.[105, 125] For example, cAPK was observed to show a marked random kinetic mechanism. However, results from thermodynamic calculations have revealed that binding ATP prior to substrate binding could be favored.[126-128] This conclusion was confirmed independently through two kinetic studies. First, in pulse-chase experiments,

radiolabeled phosphokemptide was generated from tritiated kemptide that was preequilibrated with cAPK prior to a cold chase, which indicated that the peptide substrate binds prior to the ATP.[127] Second, noncompetitive inhibition patterns were observed using either ADP in conjunction with kemptide, or using a serine peptide analogue, guanethidine, in conjunction with ATP.[128] Both results revealed that Kemptide and ATP can both bind cAPK independently through a strictly random kinetic mechanism.[126] For a few kinases, an ordered mechanism was observed. For example, the epidermal growth factor receptor (EGFR) kinase binds its peptide substrate, LEDAEYAARRRG, prior to ATP.[125] Substrate binding also helps orient the position of ATP in the active site of p38, which indicates that substrate binding preceeds ATP binding.[105] Therefore, reaction order can be influenced by the characteristics of the substrates. Larger substrates may prevent ATP from binding sterically, and instead induce conformational changes that favor ATP binding subsequent to substrate binding.

Mechanism of Phosphoryl Transfer

In the active core of protein kinases, there are different and specific binding sites for ATP and protein substrates. Once the ternary complex of the protein kinase ATP and its substrate is formed, the direct transfer of the γ- phosphoryl group from the ATP to the protein substrate can occur. No covalent intermediate has been observed over the course of the reaction, as evidenced by the fact that an inversion of the configuration of the substrate was noted after phosphorylation catalyzed by cAPK.[129] This indicates that in phosphorylation, the hydroxyl group of the substrate directly replaces the ADP in a single step, which is similar to an S_N2 mechanism.

Although there is clear evidence that nonenzymatic monophosphoryl transfer reactions proceed through a dissociative transition state, researchers have not generally agreed on how enzymatic phosphoryl transfer occurs.[80, 121] Two possible transition states, dissociative transition states and associative transition state, have been proposed for the phosphoryl transfer catalyzed by kinases (Figure 1.10).[80, 121, 130, 131] A dissociative transition state is defined as less than 50 % bond formation between the attacking nucleophile (hydroxyl groups of Ser, Thr or Tyr) and the γ- phosphate of ATP before the bond between the leaving group (ADP) and the γ- phosphate of ATP is at least 50% broken.[80] In the dissociative transition state, old bond breakage is more advanced than new bond formation, and thus nucleophilic participation is minimal. In an associative transition state, there is little bond breakage between the ADP (leaving group) and γ- phosphate of ATP, and a considerable amount of bond formation between the hydroxyl group (nucleophile) and the γ- phosphate of ATP. [80, 130, 131]

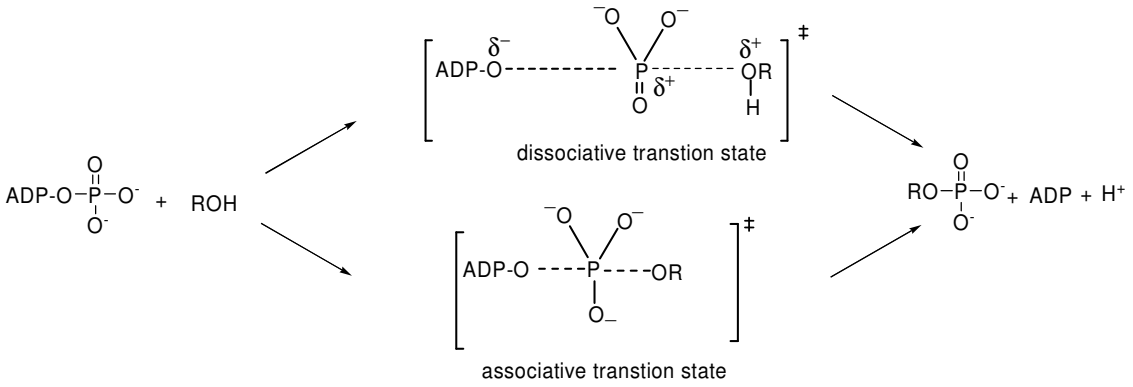

Figure 1.10. Dissociative and associative transition states for phosphoryl transfer.[80]

The dissociative mechanism is analogous to an S_N1 reaction, during which the nucleophilicity of the hydroxyl group is not critical (Figure 1.10). However, in the associative transition state, since more than 50 % of bond formation occurs between the nucleophilic

hydroxyl group and the γ phosphate of ATP, the participation of the nucleophile is clearly larger. Kinetic thio effect measurements, kinetic isotope effect measurements, and linear free energy plots have all been used to distinguish these two mechanisms involving key protein kinases.[132] The majority of protein kinases catalyze the phosphoryl transfer through a dissociative mechanism, although there were some paradoxical results. The first evidence is associated with measurements of the Bronsted nucleophile coefficient (β_{nuc}), which is a measure of the participation of the nucleophile in the transition state.[133, 134] In nonenzymatic phosphoryl transfer reactions, the β_{nuc} value is generally between 0-0.3 for a dissociative transition state, but is larger than 0.5 for an associative transition state.[133, 134] When β_{nuc} studies were conducted on the Csk kinase, resulting small values strongly suggested a dissociative mechanism.[131] Since the catalytic cores of the protein Ser/Thr and Tyr kinases are highly conserved, the dissociative mechanism revealed for Csk may be relevant to all other protein kinases.

In a study involving Tyr-specific kinase-catalyzed reactions, Parang et al. used the chemically more reactive phenoxide anion as the substrate instead of the neutral phenol in natural substrate.[132] For their experiment, a series of fluorotyrosine-containing peptides were used as substrates for Csk kinase. By comparing the reaction rates at pH 7.4 and pH 6.6 for these peptides, it was revealed that there was no increase in enzymatic reactivity with the phenoxide anion.[132] Surprisingly, they also observed that the neutral phenol was even more reactive than the phenoxide anion.[131, 132] These results implicitly support the presence of a dissociative transition state, since for this study and several others, the nucleophilic reagent was less important in phosphoryl transfer.[80, 131, 132] Moreover, additional research revealed

that the repulsion between the negatively charged phenoxide anion and other negative charges in the active site of the kinase might make it difficult to orient the γ- phosphorus for nucleophilic attack.[132, 133]

The third evidence for dissociative transition states involves the measurement of reaction coordinate distances. Based on experimental results from nonenzymatic monophosphoryl transfer reactions, Mildvan[135] proposed that a reaction coordinate distance larger than 4.9 Å between the entering hydroxyl group and the ATP γ- phosphoryl group is required for a dissociative transition state. Correspondingly, he asserted that a reaction coordinate distance smaller than 3.3 Å would represent an associative mechanism. Therefore, the reaction coordinate distance of 5.2 Å as determined by NMR in studies involving the cAPK active site strongly suggests a dissociative mechanism.[130, 136] Measurements of $\beta_{leaving\ group}$ provide additional details about the transition states in phosphoryl transfer. Specifically, a large negative $\beta_{leaving\ group}$ (ca. –1) for a nonenzymatic phosphoryl transfer reaction via the dissociative mechanism at neutral pH has been observed, indicating a large negative charge buildup on the leaving group and significant bond cleavage between the γ- phosphate of ATP and the leaving group ADP. However, a smaller $\beta_{leaving\ group}$ (ca. –0.27) has been observed via the dissociative mechanism in an acidic environment, indicating that protonation of the leaving group by acid can facilitate its departure.[130, 137] Similarly, a low $\beta_{leaving\ group}$ value (–0.33) was observed in Csk catalyzed phosphoryl transfer,[130] indicating a dissociative mechanism.

Despite these results, Huber argued that, unlike nonenzymatic catalyzed phosphoryl transfer reactions, kinase catalyzed phosphoryl transfer might become more associative by

surrounding the phosphate with groups with positive charges, thereby making it a better electrophile by neutralizing its negative charges.[138] A short reaction coordinate distance (2.7-3.1Å) between the hydroxyl group on Ser and the γ- phosphorus of ATP was observed in X-ray crystallography studies of ATP-bound cAPK.[138] As noted earlier, this result is paradoxical since a longer reaction coordinate distance (5.2 Å) for cAPK was observed by NMR.[136] This discrepancy could be due to the use of inactive ATP analogues.

Florian proposed a different mechanism, whereby proton transfer from a nucleophilic hydroxyl group to a phosphate occurs before the formation of the nucleophilic O-P bond (Figure 1.11).[139] Consequently, the associative pathway can be linked to this mechanism. This proton transfer mechanism also explains why the neutral phenol form of a substrate is favored over the more chemically reactive phenoxide anion.[139]

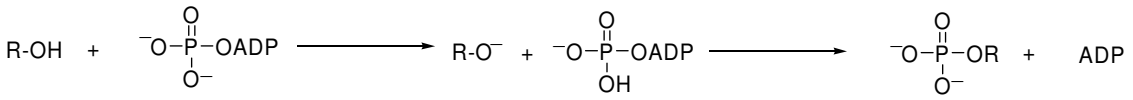

Figure 1.11. Proposed proton transfer mechanism.

Probably, neither the dissociative nor the associative mechanism represents the actual transition state in kinase-catalyzed phosphoryl transfer.[80] The two mechanisms, in fact, can be thought to represent the two extremes on a transition state continuum. Structural studies of the ternary complexes for cAPK by X-ray, NMR spectroscopy, and related calculations have shown that the transition state for phosphoryl transfer in cAPK is 8.4 % associative and 91.6% dissociative.[80] Despite the differences described above, the dissociative transition state is generally accepted for most of the protein kinases.

Catalytic Functions of Metal Ions in Kinases-Catalyzed Phosphorylation

Divalent metal ions, such as Mg^{2+} and Mn^{2+}, are essential for the catalysis of protein kinases.[5] These metal ions chelate ATP to form Mg-ATP complexes (Figure 1.9). These interactions have also been observed in the X-ray structures of most other protein kinases crystallized with ATP or its analogues. Since Mg1 can be observed even at low concentrations, Mg1 is known as the primary metal or activating metal. Mg2 is visible only at higher concentrations of Mg^{2+}, so it commonly referred to as the secondary or inhibitory metal ion. The dissociation constant of the secondary Mg^{2+} is twice that of the primary Mg^{2+}, implying that the secondary metal site is only partially occupied under physiological concentrations of Mg^{2+} ion. Therefore, it is believed that the Mg-ATP complex is necessary for the activation of all protein kinases.[126, 140]

Although all protein kinases seem to bind two divalent metal ions in their active conformations, the various functions of these metal ions are not consistent. For most protein kinases, the presence of just the primary magnesium ion is sufficient for activation.[80] In Csk, however, both the primary and secondary magnesium ions are required for activation.[141] Steady state kinetic experiments of several protein kinases revealed that the secondary Mg^{2+} may influence ATP affinity as well as substrate binding and related selectivities.[140, 141] For example, in v-Fps, the secondary Mg^{2+} increases ATP affinity by 80-fold,[80] while in other kinases, the secondary Mg^{2+} has no effect on ATP affinity.[80] The effects of secondary metal ions in the active sites of protein kinases on mechanisms are not conserved throughout the entire enzyme family.

Other divalent metal ions, such as Mn^{2+}, Co^{2+}, Cd^{2+}, can also be used as protein

kinase activators.[80] However, their catalytic activities are much lower when compared with Mg^{2+}.[142, 143] Moreover, compared with those metal ions, Mg^{2+} is more concentrated in the cell.[80] Thus, the Mg^{2+} ion is considered to be the true physiological activator of protein kinases. It should be noted, however, that for some of the tyrosine kinases, the Mn^{2+} ion was observed as the real activator with activities higher in comparison to Mg^{2+}.[80] The mechanism is not yet well understood.

General Acid/Base Catalyst

To date, there are many debates on the likelihood of a general base catalyst associated with phosphorylation catalyzed by protein kinases. The idea of a general base catalyst was initially proposed based on the following observations: 1) k_{cat}/K_m is sensitive to pH values in the phosphorylation of Kemptide by cAPK,[142] and 2) there exists a hydrogen bond between the hydroxyl groups of substrates and the carboxyl oxygen atoms of conserved Asp-166 in cAPK.[105, 121] The carboxyl group of the Asp-166 was thought to be a general base catalyst by abstracting the hydroxyl group proton of the substrate (Figure 1.12A).

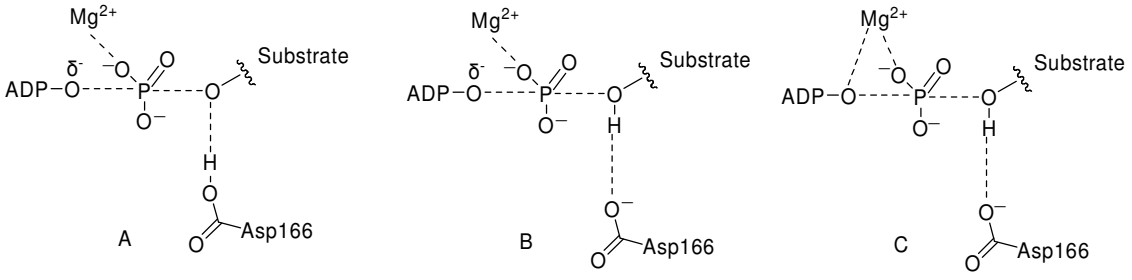

Figure 1.12. The roles of Asp-166 and Mg^{2+} ion in the catalytic domain of cAPK.[80]

In theory, if Asp-166 were to serve as the general base catalyst in phosphorylation,

then greater ionization of the carboxyl group would increase substrate binding. Consequently, protonation of the residue would also increase the activity of the kinase.[128] However, related experimental results have revealed that substrate affinity was not affected by ionization of Asp-166; nor was the rate of phosphoryl transfer in cAPK sensitive to pH in the expected range of 6 to 9.[128] In addition, the ionized substrate would be expected to be more reactive than the uncharged form in a general-base-catalyzed mechanism. However, it has been observed that the neutral form of phenol is more active for Tyr kinase substrates, while the better nucleophile, phenoxide ion at high pH value was shown to be less reactive for the Tyr kinases.[130] The higher activity associated with a neutral phenol substrate does not support a general-base-catalyzed process for the Tyr kinases.

Computational methods using hybrid quantum mechanical/molecular mechanical (QM/MM) calculations confirmed that protonation of Asp-166 leads to low energy transition states in the cAPK protein kinases. There is a mounting body of evidence that contradicts the likelihood of a general base catalyst role for Asp-166. The repulsion between the negative charge on the hydroxyl group and the γ- phosphoryl group would inhibit the reaction if such a hydrogen bond actually existed.[130]

Based on the analysis described above, two other possible modes of interaction were proposed, which are depicted in Figures 1.12 (B) and 1.12 (C). In Figure 1.12 (B), the carboxyl group in Asp-166 helps position the hydroxyl group of the substrate for attack on the γ- phosphoryl group of ATP. In this way, the hydroxyl group is frozen as one rotamer, which represents the appropriate geometry for attack.[121] Asp-166 also can accelerate the dissociation of a phosphoprotein product. In a dissociative pathway, negative charges would

accumulate on the oxygen atom in the leaving group (ADP). In Figure 1.12 (C), one of the Mg^{2+} ions chelates this oxygen atom and stabilizes its developing charges, thereby accelerating its departure from the transition state.[86, 105]

Kinetic Mechanisms

Two conflicting opinions exist as to which step is rate-determining in protein phosphorylation—phosphoryl transfer or product release. These two different assessments are based on dissimilar interpretations of steady-state kinetic data. Roskowski and coworkers maintained that the phosphoryl transfer step was rapid and that ADP release was the rate determining step. They based these interpretations on the fact that various Mg^{2+} concentrations affected both k_{cat} and nucleotide binding.[126] In particular, they noted that k_{cat} increases when the binding affinity for ADP is reduced, implying that ADP release is slow. Other researchers, however, have deduced that phosphoryl transfer is slow since k_{cat} values are quite different depending on whether good and poor substrates are used.[80] In recent years, pre-steady-state kinetic techniques and viscosometric kinetic methods have provided more information on the kinetic mechanism.

Using viscosometric methods, viscosogens, such as glycerol or sucrose, were added to the reaction.[144, 145] For unimolecular kinetic steps, the kinetic parameters are not sensitive to solvent viscosity.[80] In contrast, the kinetic parameters of bimolecular steps are highly dependent on solvent viscosity. In phosphorylations catalyzed by protein kinases, the phosphoryl transfer step is unimolecular, while ADP release is a bimolecular event.[144, 146, 147] If a significant viscosity effect on k_{cat} is identified during phosphorylation, it implies that the

product release step is rate determining, and vice versa. For cAPK, a considerable viscosity effect was observed when Kemptide was used, indicating that product release (especially ADP release) is the rate-limiting step.[144] The use of PhK provided similar results.[81] However, for most other kinases, including Cdk2, p38, and Csk, analysis of their relative k_{cat} values versus their relative viscosities (η^{rel}) revealed that phosphoryl transfer and product release are both partially rate-limiting steps.[144] It should also be noted that for ERK2, the rate constant of phosphorylation was only one quarter of the rate constant associated with the ADP release step.[148]

Pre-steady-state kinetic experiments using rapid quench flow techniques permitted direct measurement of the rate of phosphoryl transfer.[149] Specifically, the rate of incorporation of ^{32}P into peptide substrates was measured. A rapid rise in phosphopeptide concentration at the beginning of the reaction, which is known as the "burst phase," was observed for cAPK.[149] The rate constant of the burst phase was measured at 250 s^{-1}, implying that phosphoryl transfer was not the rate-determining step.[128] However, no burst phase was observed in an experiment involving the cyclin-dependent kinase-activating kinase (CaK1p), indicating that the phosphoryl transfer step is slow.[128]

Neither viscosity effects nor pre-steady-state kinetics can provide direct and reliable measurements of the release rates of products from kinases. In order to better understand the product release process, another technique called catalytic trapping was developed.[150] This technique was adapted from rapid quench flow techniques, in which cAPK was preequilibrated with ADP or phosphopeptide and then rapidly mixed with ATP and a substrate peptide.[140, 144] If the release rate of a product was observed to be slow, the burst phase would

exhibit a delay. Conversely, if the release rate was fast, there would be no effect on the burst phase.[150] The results for cAPK showed that the ADP dissociation constant (23 s^{-1}) was similar in value to k_{cat} (20 s^{-1}), thereby confirming that the release of ADP from cAPK was the rate-determining step at levels of Mg^{2+} (10 mM free Mg^{2+}) when both sites were mostly occupied.[151]

Therefore, based on known viscosity effects spanning a considerable range of different kinases, as well as pre-steady-state kinetic experiments, the roles of both phosphoryl transfer and ADP release vary significantly according to the specific protein kinase under scrutiny.

1.3. Conclusion

Pin1, a phosphorylation dependent PPIase, has been found to be essential for regulating the cell cycle. A large number of mitosis-specific phosphoproteins involved in cell cycle have been confirmed as substrates of Pin1. Besides, Overexpression of Pin1 was observed in most cancers, making it a potential cancer target. The functions of Pin1 in the regulation of cell cycle, cell signaling transduction, gene expression and neeron function are all thought to occur via prolyl isomerization at specific pSer/pThr-Pro motifs in its substrates.

The requirement of the phosphorylation on Ser/Thr-Pro moiety in the substrates of Pin1 makes the upstream kinase(s) of Pin1 very important. Study of the interactions between Pin1, its upstream kinase(s) and its substrates will help us better understand the underlying mechanism for the regulation of cell cycle by Pin1.

Chapter 2. Scaled up Synthese of the Fmoc-Ser-cis-Pro-OH and Fmoc-Ser-trans-Pro-OH isosteres

2.1 Design of Ser-Pro isosteres

One of the objectives of this study was to demonstrate the differences in the phosphorylation of Ser-*cis*-Pro and Ser-*trans*-Pro isomers. Two possible conformers of the Ser-Pro amide bonds in the Cdc25c's peptide analogs for Cdc2 were used as substrates. Therefore, a pair of alkene amide bond isosteres were designed as conformationally locked substrate analogs of the Ser-Pro amide bonds (Figure 2.1). With respect to steric effects, an alkene bond can be an effective amide bond surrogate since they share a similar geometrical disposition of their substituents.[152-154] Moreover, olefinic groups have been successfully employed in a number of different peptides as trans conformational isosteres of an amide bond.[152-160] Although the isomerization of the cis β, γ-unsaturated carbonyl system to a more stable conjugated α, β-unsaturated system might limit the application of the cis alkene amide bond surrogate, several examples of these important isosteres have been reported in the literature.[158, 161-164]

In our group, alkene amide bond isosteres have been successfully incorporated as ground state analogue inhibitors for Pin1.[165] The peptidomimetic containing the Ser-*cis*-Pro alkene isostere inhibits Pin1 23-fold better than the peptidomimetic containing the Ser-*trans*-Pro alkene isostere.[165] The Ser-*cis*-Pro alkene isostere was successfully synthesized in our group by Scott A. Hart,[161-164] while an efficient route for synthesizing the Ser-*trans*-Pro alkene isostere was developed by Xiaodong Wang in our group.[164]

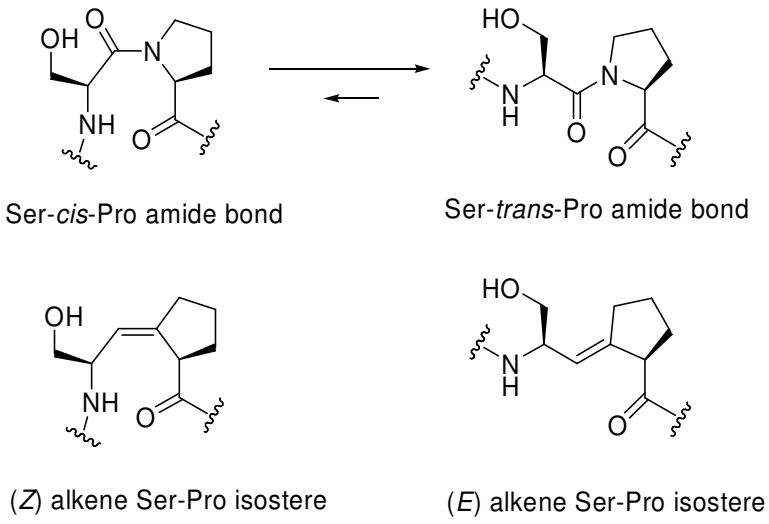

Figure 2.1 Design of Ser-*cis*-Pro and Ser-*trans*-Pro isosteres

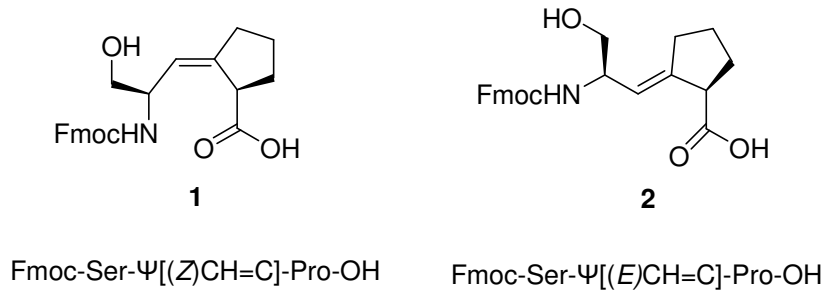

Figure 2.2 Fmoc protected (*Z*) and (*E*) alkene Ser-Pro isotere synthetic targets

The target molecules for synthesis were the Fmoc (fluorenylmethoxycarbonyl) protected (*E*)- and (*Z*)-alkenes shown in Figure 2.2, so that they could be used in solid-phase peptide synthesis. The key step for construction of the exocyclic (*Z*)-alkene bond in the Ser-*cis*-Pro isostere is via a [2, 3]-sigmatropic Still-Wittig rearrangement. The exocyclic (*E*)-alkene bond can be efficiently incorporated into the Ser-*trans*-Pro isostere via a [3, 3]-sigmatropic Ireland-Claisen rearrangement. One of the chiral centers of both mimics comes from *N*-Boc-*O*-benzyl-L-serine, which was used as the starting material for the synthesis of both alkene Ser-Pro mimics. The chiral center in the 5-membered ring of both

mimics was introduced during the two rearrangement reactions (Figures 2.2). The scaled-up syntheses of these two alkene isosteres are described below.

2.2 Scale-up Synthesis of Fmoc-Ser-Ψ[(E)CH=C]-Pro-OH

The synthesis of Fmoc-Ser-Ψ[(*E*)CH=C]-Pro-OH, **2**, utilized an Ireland-Claisen rearrangement as the key step. Typically, a γ, δ-unsaturated carboxylic acid is formed through the [3, 3]-sigmatropic Ireland-Claisen rearrangement by treating an allylic ester with a strong base. One unique feature of the Ireland-Claisen rearrangement is that an (*E*)-alkene product is always favored, regardless of the stereochemistry of its precursor. The 6-membered ring transition state of the Ireland-Claisen rearrangement for the synthesis of an (*E*)-alkene Ser-Pro isostere is shown in Scheme 2.1. Although the TMS enolate may assume either the (*Z*) or (*E*) configuration, the configuration of allylic carbon always assumes the (*R*) configuration because the bulky group CH(NHBoc)(CH_2OBn) of the precursor is preferred to be at the equatorial position in the stable 6-membered ring transition state.

In order to synthesize the allylic alcohol precursor with the *R* configuration at the allylic carbon via the Ireland-Claisen rearrangement, the Luche reduction was used to stereoselectively reduce the ketone intermediate through chelation of the carbonyl oxygen and the carbamate oxygen with a cerium ion (Ce^{3+}). Although the chelation of the carbonyl oxygen and the benzyl ether oxygen with cerium ion is also possible, the chelation of the carbonyl oxygen and the carbamate oxygen with cerium ion is preferred because the carbamate oxygen is more basic than the benzyl ether oxygen. According to this chelation model (Scheme 2.2), the formation of the alcohol product with the *R* configuration at the allylic carbon is favored. The corresponding transition state is shown in Scheme 2.2.

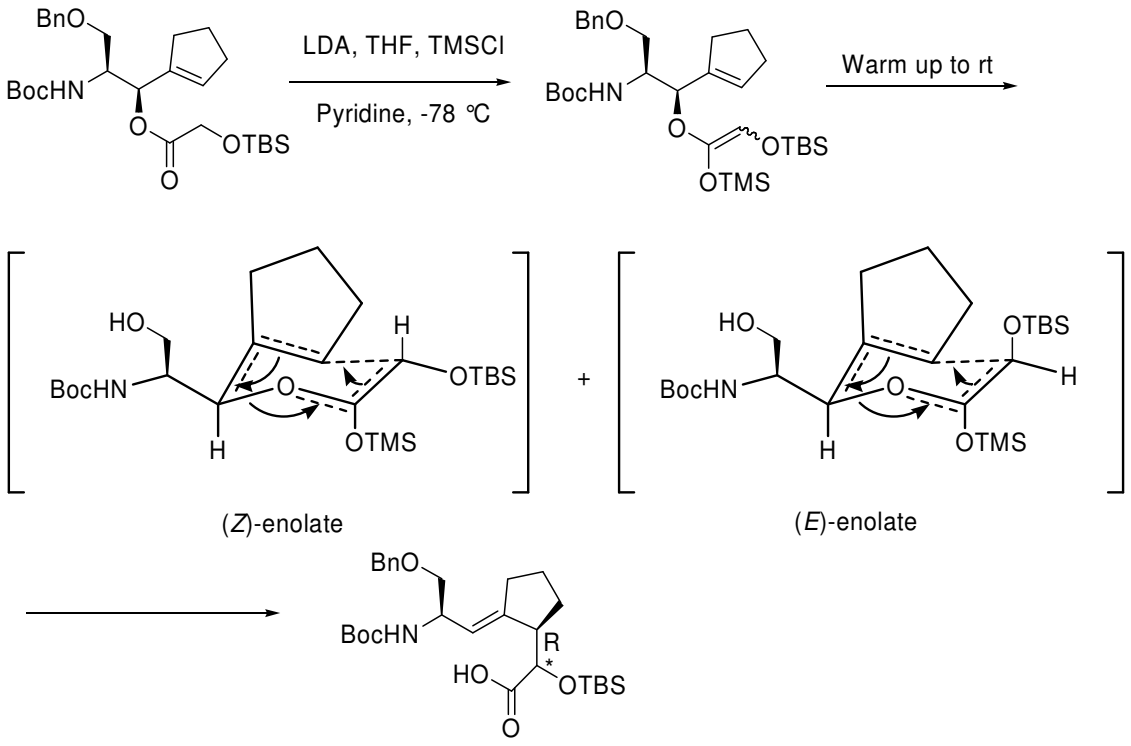

Scheme 2.1 Transition states of the Ireland-Claisen rearrangement

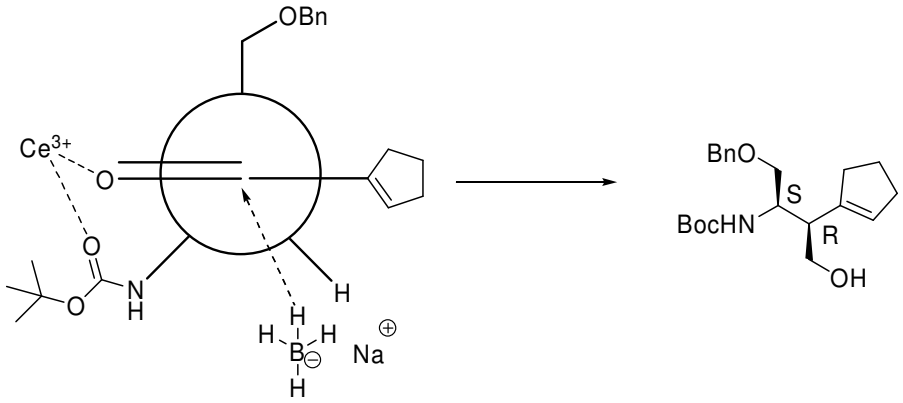

Scheme 2.2 Chelation controlled Luche reduction

N-Boc-*O*-benzyl-L-Serine was used as the starting material for the synthesis of Fmoc-Ser-Ψ[(*E*)CH=C]-Pro-OH, **2** (Scheme 2.3). The first step involved coupling with *N, O*-dimethyl hydroxylamine hydrochloride using DCC (1,3-dicyclohexylcarbodiimide) and HOBt (1-hydroxybenzotriazole) to afford Weinreb amide **3** in 97 % yield. Most of the DCU

(*N,N*-dicyclohexyl urea) was removed through filtration and flash chromatography, with the remainder removed via precipitation in cold dichloromethane. For the condensation of Weinreb amide **3** with cyclopentenyl lithium, 0.98 equivalent of *i*-PrMgCl was used to deprotonate the carbamate NH of **3** first, followed by treatment with 1.5 equivalents of cyclopentenyl lithium, freshly prepared from cyclopentenyl iodide, to afford the *α, β*-unsaturated ketone **4** in 70% yield. It should be noted that, without the use of *i*-PrMgCl, at least 3 equivalents of cyclopentenyl lithium would be required for a comparable yield in this condensation step. The 5-membered ring lithium-chelated tetrahedral intermediate for this reaction is shown in Scheme 2.4. It is this stable tetrahedral intermediate that makes the reaction stop at the ketone stage.[166] Upon hydrolysis during the aqueous acid work-up, the chelated intermediate was converted to ketone **4**.

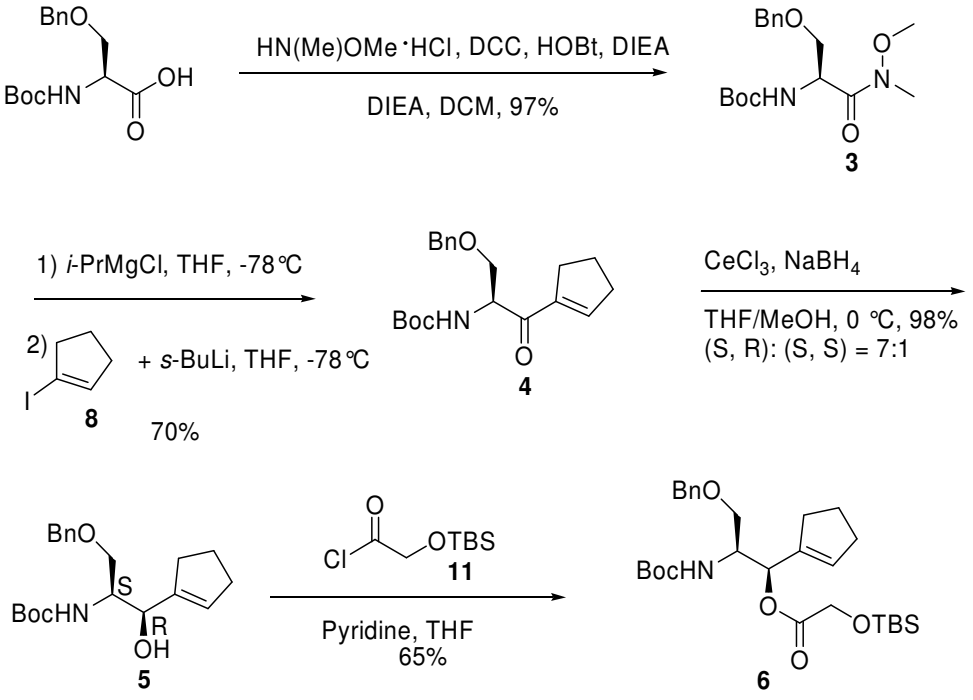

Scheme 2.3 Synthesis of allylic ester precursor for Ireland-Claisen Rearrangement

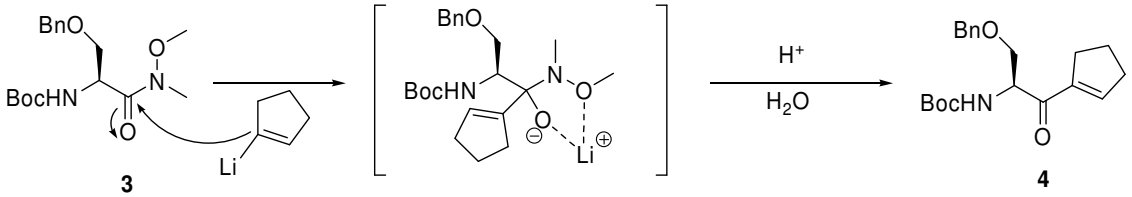

Scheme 2.4 Lithium chelated tetrahedral intermediate for the synthesis of **4**

The scale up for the condensation step turned out to be quite difficult. In fact, with respect to the 10-gram scale up, repeated attempts generated a mere 30% yield, which was much lower than the 70% yield obtained at the ≤ 5-gram scale. It was hypothesized that the low yield resulted from poor heat transfer in the larger scale. Therefore, a 5-gram scale was routinely used for this reaction.

The reagent cyclopentenyl iodide **8** was prepared by the method developed by Barton et al.[167] Cyclopentanone was used as the starting material, and the overall yield for the two step reaction was commonly 50% (Scheme 2.5).

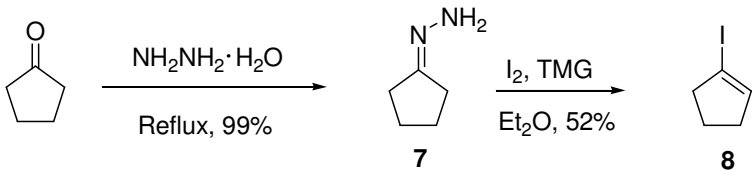

Scheme 2.5 Synthesis of reagent cyclopentenyl iodide **8**

A 7:1 mixture of (*S, S*) and (*S, R*) diastereomers was obtained via a typical Luche reduction of ketone **4** in fairly good yields (98%). The minor diastereomer (*S, S*) **5** was removed by either precipitation or flash chromatography. Since the stereochemistry of (*S, R*)-**5** had been previously determined via the Mosher method by Xiaodong Wang in our group,[164] the co-injection of the standard and the major diastereomer of **5** on HPLC verified the

stereochemistry.

The reagent *tert*-butyldimethylsilyloxyacetyl chloride **11**, was prepared according to standard procedures.[168] The commercially available reagent butyl glycolate was used as the starting material, and the overall yield for the first two steps was routinely around 70%. Vacuum distillation was used for the purification of **9**. The preparation of **11** was accomplished by reacting the product with a large excess of oxalyl chloride under reflux. Benzene was used in this step to remove the trace water from **10** by forming an azeotropic mixture with water. The *tert*-butyldimethylsilyloxyacetyl chloride **11** obtained was used directly, with isolation, in the esterification reaction (Scheme 2.6).

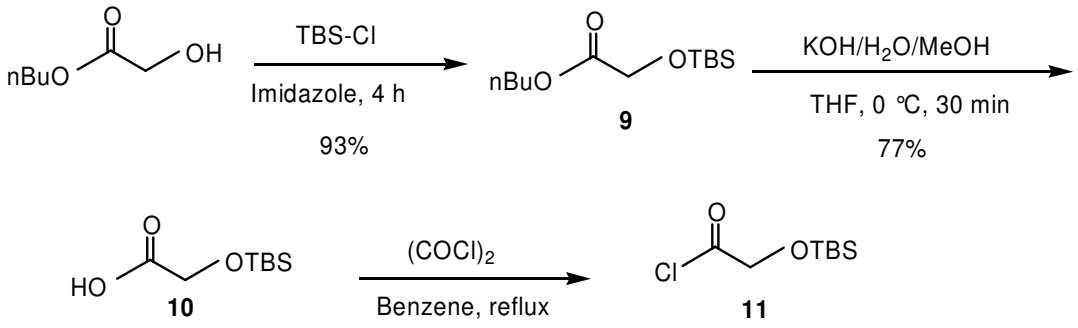

Scheme 2.6 Synthesis of reagent *tert*-butyldimethylsilyloxyacetyl chloride **11**

The yield for the esterification reaction of **5** was commonly around 65%. The quality of pyridine affects the reaction yields. Therefore, fresh distilled pyridine was routinely used in this reaction.

The Ireland-Claisen rearrangement from the ester precursor **6** to the acid intermediate **12** is the key step for the synthesis of Fmoc-Ser-Ψ[(*E*)CH=C]-Pro-OH, **2** (Scheme 2.7). Allylic ester precursor **6** was treated with LDA and TMSCl activated by pyridine to form the enolate at -82 °C, followed by a slow warm up to room temperature, and then stirring for 90

minutes to afford the unstable acid intermediate **12** which decomposes on silica-gel. The stable acid **13** was obtained by removing the TBS protecting group using TBAF in 52% overall yield for the two steps.

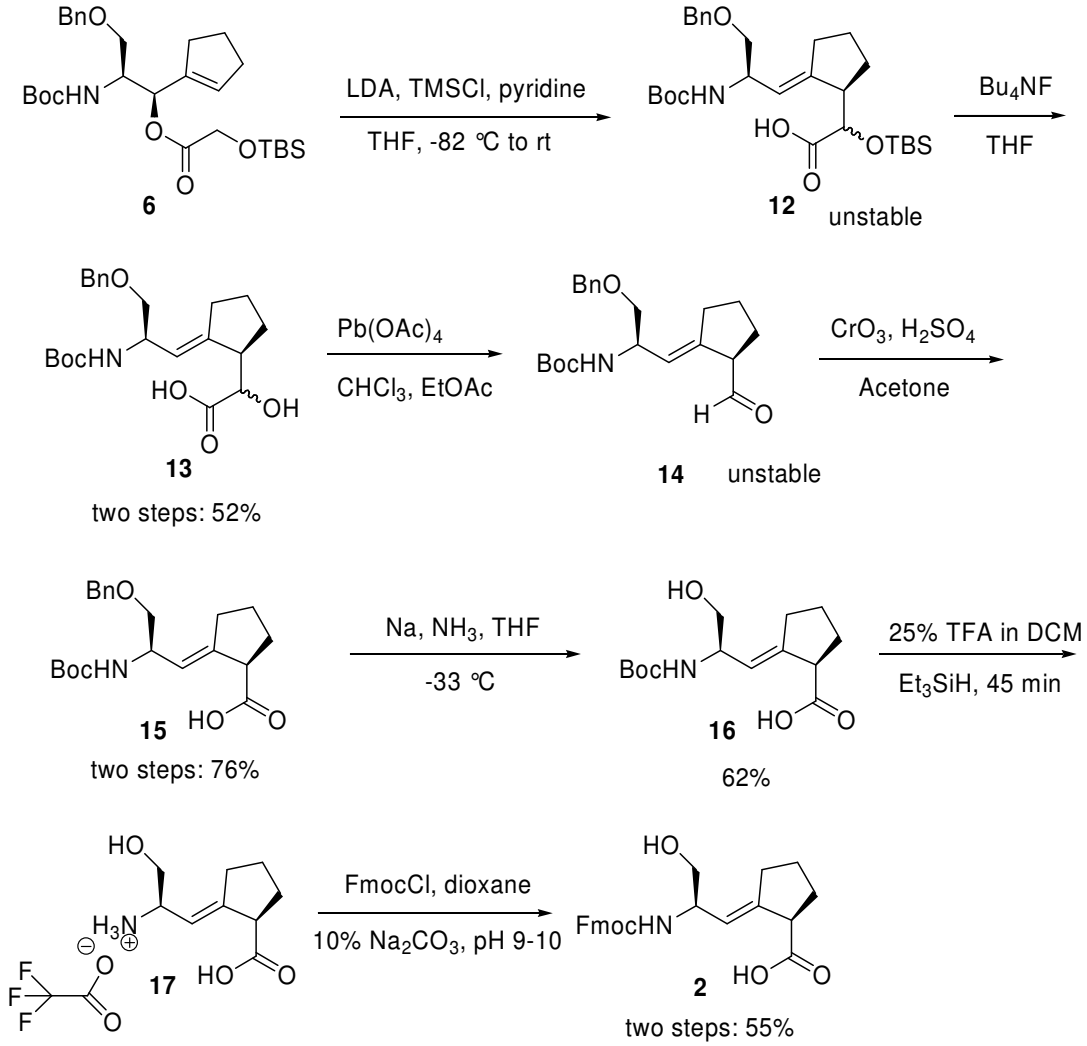

Scheme 2.7 Synthesis of Fmoc-Ser-Ψ[(*E*)CH=C]-Pro-OH **2**

Several factors have a huge effect on the success and yield for the Ireland-Claisen rearrangement. For example, very small amounts of solvent residues (e.g., ethyl acetate or water) in the ester precursor **6** may totally quench the reaction. In addition, since pyridine activated TMSCl was necessary for the success of this reaction, the quality of both the

TMSCl and the pyridine was very important. Acid **12** is unstable on silica gel, so flash chromatography purification was not performed. However, the α-hydroxyl acid **13** is normally stable on silica gel, so a mixture of diastereomers was obtained. Without separating out the major diatereomer, the mixture was degraded by one carbon and oxidized to β,γ-unsaturated aldehyde **14** by lead (IV) tetraacetate, followed by Jones oxidation to afford Boc-Ser(OBn)-Ψ[(*E*)CH=C]-Pro-OH **15** in an overall 76% yield for the two steps. The aldehyde **14** was found to be very unstable on silica gel or in basic aqueous work-up, so no purification was performed at this step. In basic condition, more stable α,β-unsaturated aldehyde is preferably formed through the isomerization of **14**. Thus, the freshly prepared **14** was used immediately in the Jones oxidation reaction. The isomerization of the β,γ-unsaturated aldehyde **14** to the more stable α,β-unsaturated aldehyde was attributed to the instability of aldehyde **14**. Because the Jones oxidation of aldehyde **14** to acid **15** is generally quite rapid, the precipitation of green Cr^{3+}signals the completion of this reaction. The (*E*)-alkene stereochemistry of **15** was verified by NOE experiment.[164] A Birch reduction to remove benzyl groups from **15** by sodium/liquid ammonia afforded the Boc-Ser-Ψ[(*E*)CH=C]-Pro-OH **16** in 62% yield without affecting the exocyclic alkene bond. Two factors are also important for this reaction. First, a large excess of sodium should be added to maintain the deep blue reaction solution. Second, during work-up the aqueous solution should initially be concentrated by rotary evaporation to remove most of the dissolved ammonia prior to acidification using 1N HCl. Boc protected acid **16** was converted to Fmoc-Ser-Ψ[(*E*)CH=C]-Pro-OH **2** via a two-step reaction with an overall yield of 55%. The reactivity of the unprotected side chain hydroxyl group and the free carboxylic acid

group of **16** was thought to be one reason for the low yield of the reaction. 450 mg of compound **2** was synthesized from this scale-up synthesis.

2.3 Scaled-up Synthesis of Fmoc-Ser-Ψ[(Z)CH=C]-Pro-OH

The synthesis of Fmoc-Ser-Ψ[(*Z*)CH=C]-Pro-OH **1** utilized a [2, 3]-sigmatropic Still-Wittig rearrangement as the key step. In the Still-Wittig rearrangement, a homoallylic alcohol product is formed by treating an allyl ether precursor with n-BuLi at low temperature. Since the reaction rate is dependent on the energy gap between the HOMO (anion) and the LUMO (allyl)—the less stable the carbanion, the quicker the rearrangement. An extremely unstable carbanion is generally formed in the Still-Wittig rearrangement as a result of the tin-lithium exchange. The two possible six-electron/five-membered cyclic transition states are shown in Scheme 2.8.

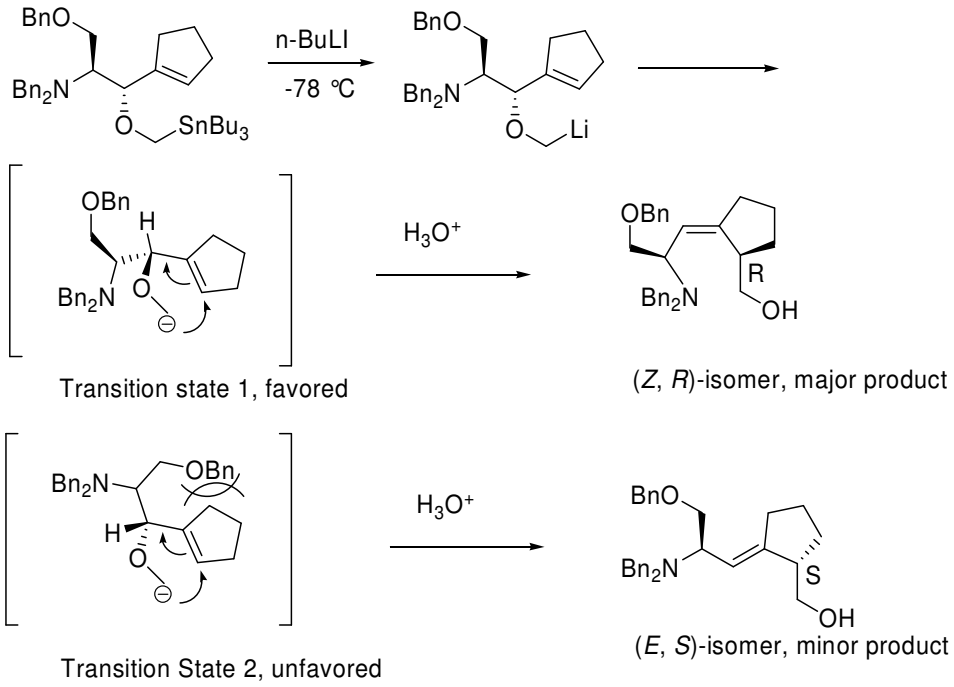

Scheme 2.8 Two possible transition states and the products for the Still-Wittig rearrangement

In transition state 1, β-face attack between the carbanion and allyl carbon constructs

the *Z*-exocyclic alkene bond and the second chiral center in the ring as R-configuration, while in transition state 2, α-face attack gave the (*E, S*)-isomer. The transition state 1 leading to the (*Z, R*)-alkene isomer was expected to be favored over transition state 2 leading to (*E, S*)-alkene isomer as a result of unfavorable steric interactions (Scheme 2.8). Computational studies by Scott Hart in our group[163] revealed that the counterion chelation in the Wittig rearrangement was crucial for the selectivities for (*Z*)- and (*E*)-alkene products. Specifically, with THF as the reaction solvent, in the resulting transition state, one THF molecule chelates with the Li^+ ion, and the Li^+ ion also chelates with the ether oxygen adjacent to the reacting carbanion and the amine, thus forming a five-membered chelated ring.[163] Ab Initio calculation indicated that the transition state leading to (*Z*)-alkene product was more stable by 0.6 kcal/mol than the transition state leading to (*E*)-alkene isomer in the presence of THF.[163] The calculation results were consistent with the predominantly production of (*Z*)-alkene as the major product with THF as the solvent. However, the ratio of these two isomer products varies as a function of the reaction temperature, the amount and concentration of the base, and the scale of the rearrangement reaction. This differs from the Ireland-Claisen rearrangement in which an (*E*) alkene isomer is isolated exclusively. As seen in Figure 2.6, the attacking by methylene anion from the bottom of the cyclopentyl ring transfers the chirality of allylic alcohol to the ring in a stereoselective manner. In order to construct the allylic chiral center with the *R* configuration, the allylic ether precursor should bear the *S* configuration because of chirality transfer associated with the Still-Wittig rearrangement.

In order to synthesize the required allylic ether precursor with the *S* configuration at the allylic carbon, $LiAlH_4$ was used for the stereoselective reduction of the ketone

intermediate. The Felkin-Ahn transition state for this reduction is illustrated in Scheme 2.9. Besides, the chelation of the carbonyl oxygen and benzyl ether oxygen and the lithium ion (Li^+) also gives the (S,S)-alcohol. This is why the single diastereomer (*S*, *S*)-alcohol was the only product achieved from this reduction.

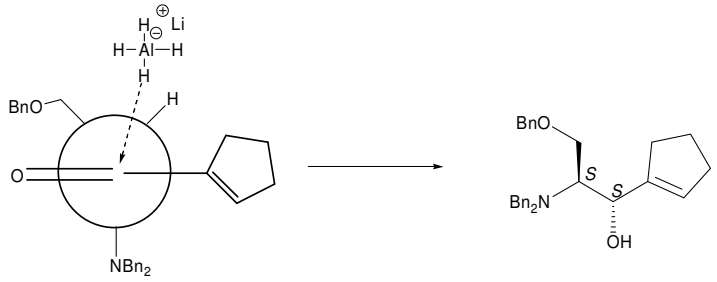

Scheme 2.9 Felkin-Ahn transition state for the reduction with $LiAlH_4$

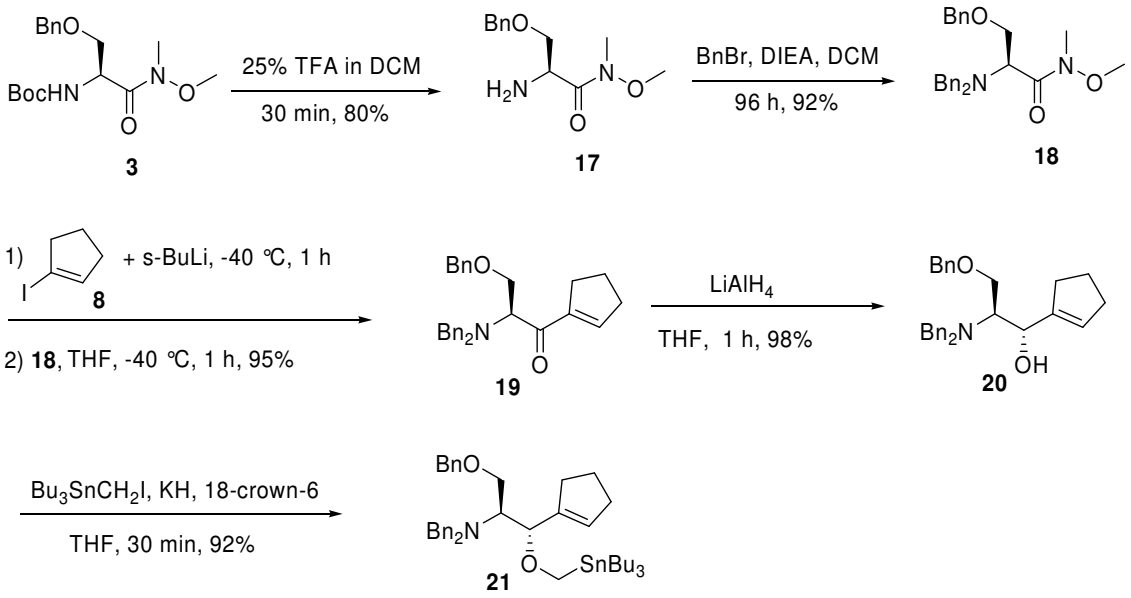

Scheme 2.10 Synthesis of the allylic ether precursor **21**

N-Boc-*O*-benzyl-L-serine was used as the starting material for the synthesis of Fmoc-Ser-Ψ[(*Z*)CH=C]-Pro-OH **1**. The first two steps switched the protecting group from Boc to dibenzyl for the amine. This was done because of the poor stereoselectivity for the Boc-protected material in the subsequent reduction and Still-Wittig rearrangement (Scheme

2.10). For the large scale reaction, the protection of the free amine by benzyl bromide was very slow; 4 days were required for the completion of the reaction on the 10-gram scale.

The condensation between the Weinreb amide **18** and the cyclopentenyl lithium, which was generated *in situ*, went smoothly and afforded a high yield (95%) of the *α,β*-unsaturated ketone **19**. Compared to the condensation reaction for the synthesis of the Fmoc-Ser-Ψ[(*E*)CH=C]-Pro-OH **2**, this reaction was much more easily controlled because of the lack of any free carbamate hydrogen in **18**. The *i*-PrMgCl reagent was not needed in this case. Moreover, this reaction was run in a -40 °C cold bath, and it was completed in just 90 min. The relatively high yield (> 95%) for this reaction can be guaranteed through the use of only 1 to 1.5 equivalents of cyclopentenyl iodide, which was much less than required for the synthesis of **4**. Additionally, the high yields for this condensation reaction were consistent—even when conducted on a 10-gram scale. Initially, an excess of $LiAlH_4$ (10 equivalents) was used for the stereoselective reduction of ketone **19**. Only a single diastereomer (*S, S*)-**20** was obtained from this reduction. Because of work-up difficulties, the amount of $LiAlH_4$ utilized in the reduction was reduced to two equivalents without losing stereoselectivity. The allylic ether precursor for the Still-Wittig rearrangement required iodomethyltributyl tin reagent **23** (Scheme 2.11).

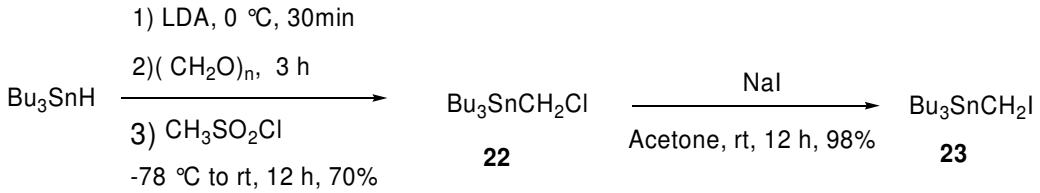

Scheme 2.11 Synthesis of iodomethyltributyltin reagent **23**

The iodomethyltributyl tin reagent **23** was prepared according to Steiz et al.[169] Specifically, tributylstannane was used as the starting material, reacted first with LDA

(lithium diisopropylamide), followed by reaction with paraformaldehyde to afford the tributylstannylmethoxide intermediate (Scheme 2.11). Without any purification, methanesulfonyl chloride was added at -78 °C to the solution of the tributylstannylmethoxide intermediate to afford the chloromethyltributyltin reagent **22** in a 70% yield for the large scale reaction.

The halogen exchange reaction of **22** with sodium iodide afforded the iodomethyltributyltin reagent **23** in 98% yield. The purification of chloromethyltributyltin and iodomethyltributyltin was easily accomplished by rapid filtration through a small amount of silica gel, followed by vacuum distillation. Since the polarities of chloromethyltributyltin and iodomethyltributyltin are very low, pure hexane can elute them from the column relatively quickly. Chloromethyltributyltin was distilled out in vacuum as a colorless liquid, bp 108-112 °C at 0.5 torr. Since iodomethyltributyltin has a higher boiling point than chloromethyltributyltin, bp 100-110 °C at 0.01 torr, greater vacuum was required for the distillation of the iodomethyltributyltin reagent **23**. Under a vacuum of 0.1 torr, the crude product had to be heated to ~150 °C to distill the iodomethyltributyltin, which also likely caused the product to burn. Rapid filtration through a short silica gel column was utilized for the purification of the iodomethyltributyltin reagent **23**.

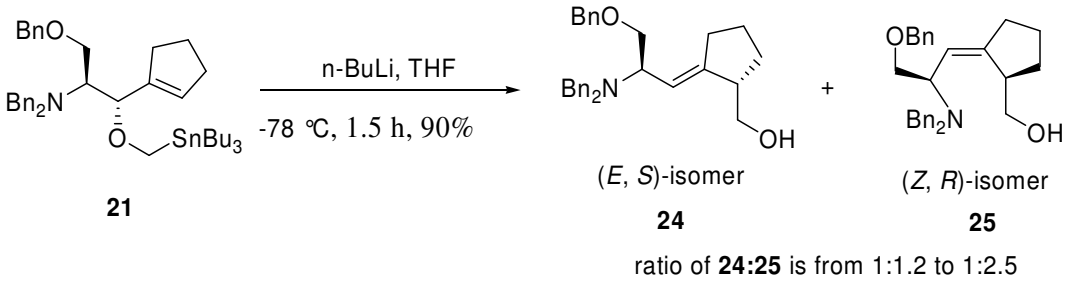

Scheme 2.12 Still-Wittig rearrangement

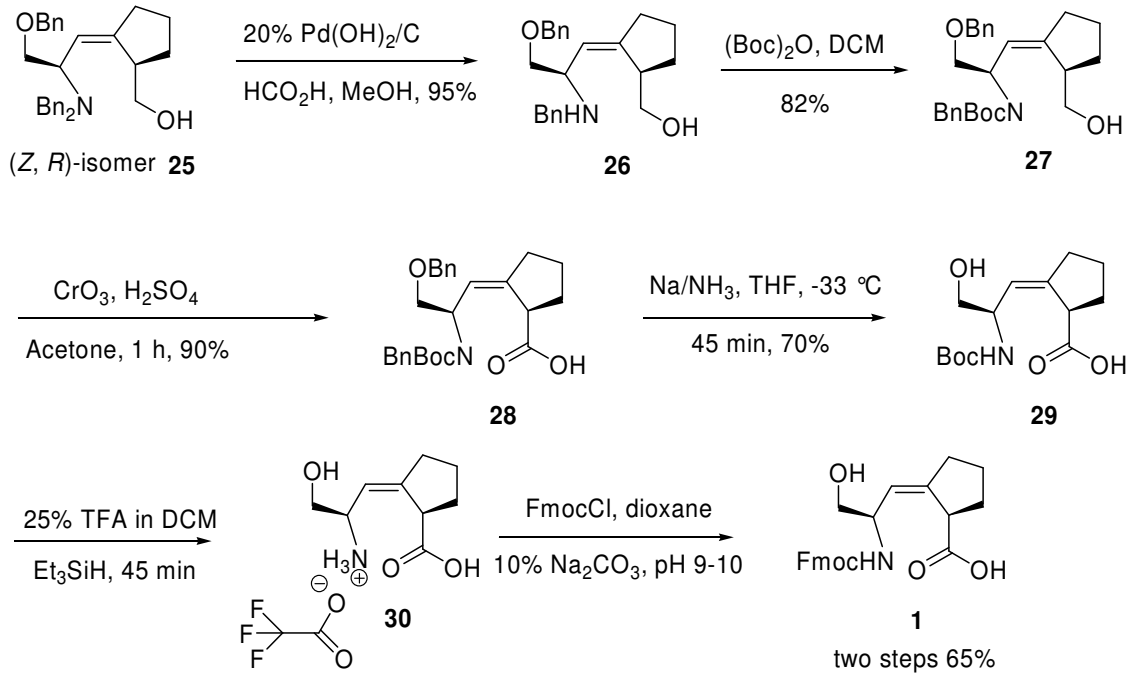

Scheme 2.13 Synthesis of Fmoc-Ser-Ψ[(*Z*)CH=C]-Pro-OH **1**

The Still-Wittig rearrangement of stannane **21** was identified as the key step in the synthesis of Fmoc-Ser-Ψ[(Z)CH=C]-Pro-OH isostere **1**. Unlike results obtained from the Ireland-Claisen rearrangement, the Still-Wittig rearrangement produced two diastereomers: 1) the desired product (*Z, R*)-alkene **25**, and 2) (*E, S*)-alkene product **24** (Scheme 2.12). The ratio of these two diastereomers (i.e., **24**:**25**) ranged from 1:1.2 to 1:2.5, which was highly dependent on reaction conditions such as temperature, concentration of the base, and size of scale-up. The two diastereomers were separated by flash chromatography, and their *E/Z* stereochemistry was determined by 1D-NOE NMR spectroscopy.[163] The yield for the Still-Wittig rearrangement was relatively high (> 90%), even for the large scale reaction.

With (*Z, R*)-alkene **25** in hand, the monodebenzylation of **25** was accomplished via catalytic transfer hydrogenation with formic acid on Pearlman's catalyst without affecting

either the benzyl ether or the exocyclic alkene bond (Scheme 2.13). For this reaction, keeping the reaction time short was essential for avoiding the formation of side product which results from the debenzylation on the oxygen. Generally, the reaction was completed in 10-30 min depending on the scale. The next step involved the reprotection of **26** by $(Boc)_2O$ to afford compound **27**. The rationale for keeping the second benzyl protection on the amine is associated with the failure of the Jones oxidation with only Boc-protected amine.[163] The Jones oxidation of the doubly protected Boc-benzyl-amine **27** produced acid **28** in 90% yield. An excess of Jones reagent (about two equivalents) was required to minimize the formation of any ketone side products (where carbonyl group is in the 5-membered ring, and the carbonyl group conjugates with the exocyclic alkene bond), which probably resulted from allylic oxidation and C-C bond cleavage. The Birch reduction was then used to remove the benzyl protecting groups on both the amine and the hydroxyl to yield Boc-Ψ[(*Z*)CH=C]Pro-OH **29** in 70% yield. Presumably, benzyl ether deprotection occurs somewhat more rapidly than benzyl amine deprotection. Similar to the synthesis of **16**, a large excess of sodium (~20 equivalents) was required to minimize the cyclization of the side chain oxyanion onto the Boc carbonyl to produce a cyclic carbonate. Fmoc-Ψ[(*Z*)CH=C]Pro-OH **1** was obtained by the protecting group switch from Boc to Fmoc in two steps with 65% total yield. The low yield was attributed to the presence of an unprotected side chain hydroxyl group and the carboxylic acid group. 520 mg of compound **1** was synthesized from this scale-up synthesis.

2.4 Conclusions

Two conformationally locked Ser-Pro amide bond isosteres,

Fmoc-Ψ[(*Z*)CH=C]Pro-OH **1** and Fmoc-Ψ[(*E*)CH=C]Pro-OH **2**, were designed and stereoselectively synthesized with high yields. Fmoc-Ψ[(*Z*)CH=C]Pro-OH **1** was synthesized in 12 steps with an overall yield of 15% from *N*-Boc-*O*-benzyl-L-serine on a large scale. The key step for the synthesis of **1** was the [2, 3]-sigmatropic Still-Wittig rearrangement. Fmoc-Ψ[(*E*)CH=C]Pro-OH **2**, was synthesized in 11 steps with an overall yield of 6% from *N*-Boc-*O*-benzyl-L-Serine on a large scale. The key step for the synthesis of **2** was the [3, 3]-sigmatropic Ireland-Claisen rearrangement.

Experimental

General. Unless otherwise indicated, all reactions were carried out under N_2 in flame-dried glassware. THF was distilled from sodium-benzophenone. CH_2Cl_2 was distilled from CaH_2. $(COCl)_2$ was distilled before each use. Brine, $NaHCO_3$ and NH_4Cl refer to saturated aqueous solutions, unless otherwise noted. Flash chromatography was performed on 230-400 mesh, ASTM, EM Science silica gel with reagent grade solvents. NMR spectra were obtained at ambient temperature in $CDCl_3$ unless otherwise noted. Proton (500 MHz) and carbon-13 (125 MHz) NMR spectra were measured on a JEOL, and proton (400 MHz) NMR spectra were measured on a Varian NMR spectrometer. ^{1}H NMR spectra are reported as chemical shift (multiplicity, coupling constant in Hz, number of protons). Compounds **1-29** have been reported previously, thus only ^{1}H-NMR data are given for the characterization.

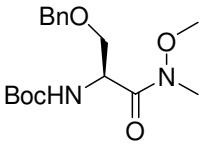

Boc-Ser(OBn) Weinreb amide, 3. *N*-Boc-Ser(OBn)-OH (8.85 g, 30.0

mmol), diisopropyl ethylamine (15.5 g, 120 mmol), and *N,O*-dimethylhydroxylamine hydrochloride (5.85 g, 60.0 mmol) were dissolved in 1:1 CH_2Cl_2/DMF (300 mL). The reaction was then cooled to 0 °C in an ice-water bath for 10 min. DCC (7.43 g, 36.0 mmol), HOBt (5.51 g, 26.0 mmol) and DMAP (290 mg, 2.40 mmol) were added to the flask, and the reaction was stirred at room temperature for 22 h. The reaction was filtered to remove DCU and the filtrate was concentrated. Ethyl acetate (400 mL) was added to the resulting slurry and the organic layer was washed with NH_4Cl (3 × 100 mL), $NaHCO_3$ (3 × 100 mL) and brine (100 mL). The organic layer was dried with anhydrous Na_2SO_4 and then concentrated. The remaining DCU was precipitated with a small amount of cold CH_2Cl_2 and filtered to afford 9.82 g (97%) of **3** as a colorless oil. ^{1}H NMR ($CDCl_3$): δ 7.30-7.25 (m, 5H), 5.42 (d, *J* = 8.7, 1H), 4.85 (Brs, 1H), 4.54 (d, *J* = 13, 1H), 4.47 (d, *J* = 13, 1H), 3.70 (s, 3H), 3.67 (m, 2H), 3.20 (s, 3H), 1.43 (s, 9H).

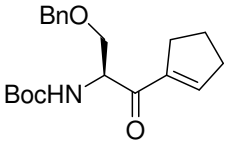

***α, β*-Unsaturated ketone, 4**. 1-Iodocyclopentenyl iodide **8** (4.12 g, 21.2 mmol) was dissolved in THF (50 mL), cooled to –78 °C, and s-BuLi (1.4 M in cyclohexane, 30 mL, 42 mmol) was added slowly to the cold solution. The reaction was stirred at -78 °C for 1 h. At the same time, a solution of Boc-Ser(OBn) Weinreb amide **3** (4.00 g, 11.8 mmol) in 40 mL THF was cooled to –78 °C for 10 min, *i*-PrMgCl (2 M in THF, 11.2 mmol, 5.6 mL) was added slowly and the reaction was stirred at –78 °C for 1 h. Then the cyclopentenyl lithium generated *in situ* was added to the reaction mixture of the Weinreb amide **3** and *i*-PrMgCl dropwise via cannula. The resulting mixture was stirred at –78 °C for 3 h. The

reaction was quenched with 20 mL NH_4Cl, diluted with 200 mL EtOAc, and washed with NH_4Cl (2 × 50 mL), $NaHCO_3$ (50 mL), brine (50 mL), dried over $MgSO_4$ and concentrated. Chromatography on silica with 5% EtOAc in hexanes afforded 3.4 g of ketone **4** (65%) as a pale yellow oil. ^{1}H NMR($CDCl_3$): δ 7.25-7.23 (m, 5H), 6.78 (m, 1H), 5.56 (d, *J* = 7.5, 1H), 5.00 (m, 1H), 4.51 (d, *J* = 10.5, 1H), 4.43 (d, *J* = 10.5, 1H), 3.70 (d, *J* = 2.5, 2H), 2.53 (m, 1H), 2.52 (m, 3H), 2.04-1.89 (m, 2H), 1.43 (s, 9H).

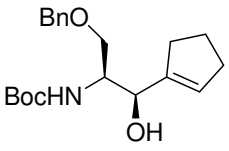

Allylic alcohol, 5. Ketone **4** (4.85 g, 11.2 mmol) was dissolved in 2.5:1 THF:MeOH (125 mL) and cooled to 0 °C. $CeCl_3$•$7H_2O$ (4.99 g, 13.4 mmol) was added, followed by $NaBH_4$ (0.84 g, 22 mmol). The reaction was stirred for 2 h at 0 °C, then quenched with NH_4Cl (500 mL), diluted with 200 mL EtOAc, washed with NH_4Cl (3 × 50 mL) and brine (100 mL), dried on Na_2SO_4, and concentrated to give 3.7 g (97%) alcohol **4** as a pale yellow solid which represents a 7:1 mixture of diastereomers. The major diastereomer was isolated from the mixture by recrystallization using EtOAc:*n*-hexanes system (1:9). ^{1}H NMR ($CDCl_3$): δ 7.29-7.25 (m, 5H), 5.65 (m, 1H), 5.34 (d, *J* = 9, 1H), 4.52 (d, *J* = 15, 1H), 4.43 (d, *J* = 15, 1H), 4.32 (brs, 1H), 3.83 (brs, 1H), 3.71 (dd, 1H), 3.68-3.69 (dd, 1H), 3.17 (d, *J* = 8.5, 1H), 2.29-2.26 (m, 4H), 1.88-.86 (m, 2H), 1.43 (s, 9H).

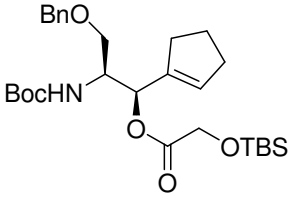

Allylic ester precursor, 6. Allylic alcohol **5** (1.20 g, 3.36 mmol) was

dissolved in 4 mL THF. Pyridine (1.02 g, 13.0 mmol) was then added and the reaction was cooled to 0 °C for 10 min. A solution of *tert*-butyldimethylsilyloxyacetyl chloride **11** (1.02 g, 4.42 mmol) in 4 mL THF was added dropwise at 0 °C and the resulting mixture was stirred for 16 h at rt, then diluted with 20 mL Et_2O, washed sequentially with 0.5 N HCl (2 × 10 mL), $NaHCO_3$ (10 mL), brine (10 mL), dried on Na_2SO_4, and concentrated. The product was purified by flash chromatography with 5% EtOAc in hexanes and 1.12 g (65%) of the allylic ester precursor **6** was obtained as yellow oil. ^{1}H NMR ($CDCl_3$): δ 7.29-7.25 (m, 5H), 5.67 (s, 1H), 5.58-5.57 (d, *J* = 8, 1H), 4.83 (d, *J* = 9.5, 1H), 4.49 (d, *J* = 11.5, 1H), 4.43 (d, *J* = 11.5, 1H), 4.19 (s, 2H), 4.05 (m, 1H), 3.53 (m, 1H), 3.48 (m, 1H), 2.41 (m, 1H), 2.27-2.26 (m, 3H), 1.82 (m, 2H), 1.40 (s, 9H), 0.90 (s, 9H), 0.07 (s, 6H).

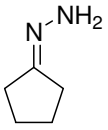

Hydrazone, 7. Cyclopentanone (44 mL, 0.50 mol) and hydrazine monohydrate (73 mL, 1.5 mol) were mixed at room temperature and refluxed for 3 h. The reaction was poured into 300 mL H_2O, extracted with CH_2Cl_2 (3 × 150 mL), washed with brine (200 mL), dried on Na_2SO_4 and concentrated to afford 47.71 g (97%) of **11** as colorless liquid. ^{1}H NMR ($CDCl_3$): δ 4.82 (s, 2H), 2.35-2.30 (m, 2H), 2.16-2.20 (m, 2H), 1.90-1.65 (m, 2H).

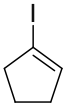

1-Iodocyclopentene, 8. I_2 (97.5 g, 384 mmol) was dissolved in Et_2O (600 mL), then a solution of tetramethylguanidine (265 mL, 2.09 mol) in Et_2O (400 mL) was added to the I_2 solution slowly at 0 °C. The reaction was stirred for 2.5 h. A solution of cyclopentanone

hydrazone **7** (17.3 g, 174 mmol) in Et_2O (200 mL) was added into the reaction solution dropwise at 0 °C and stirred for 16 h at rt, then heated at reflux for 2 h. The reaction was cooled to rt and filtered to remove the solid and concentrated. The solution was reheated at 80-90 °C for 3 h, cooled to rt, diluted with Et_2O (400 mL), washed sequentially with 2N HCl (3 × 150 mL, Warning! exothermic, add slowly!), $Na_2S_2O_3$ (3 × 100 mL), $NaHCO_3$ (2 × 100 mL), brine (100 mL), dried on $MgSO_4$, and then concentrated to give 22 g (65.4%) of **8** as a pale yellow liquid, which was stored under Argon at -20 °C. ^{1}H NMR ($CDCl_3$): δ 6.08-5.09 (m, 1H), 2.59 (m, 2H), 2.30 (m, 2H), 1.92 (m, 2H).

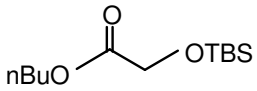

***n*-Butyl-*O*-TBS glycolate, 9**. *n*-butyl glycolate (20 g, 150 mmol) and imidazole (22 g, 330 mmol) were combined and cooled to 0 °C, then *tert*-butyldimethylsilyl chloride (24.9 g, 165 mmol) was added to the mixture. After stirring at rt for 16 h, pure *n*-butyl-*O*-TBS glycolate 33 g (95%) was obtained by vacuum distillation as a colorless oil. ^{1}H NMR ($CDCl_3$): δ 4.22 (s, 2H), 4.17 (t, 2H), 1.63 (m, 2H), 1.38 (m, 2H), 0.9 (s, 9H), 0.91 (m, 3H), 0.09 (s, 6H).

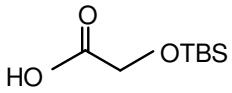

***tert*-Butyldimethylsilyloxyacetic acid, 10**. *n*-Butyl-*O*-TBS glycolate **9** (21.0 g, 85.4 mmol) was dissolved in 50 mL THF, cooled to about –5 °C in a salt/ice bath. A solution of KOH (4.78 g, 85.4 mmol) in MeOH (10 mL) and H_2O (19 mL) was added slowly, and the reaction was stirred for 1 h at 0 °C, diluted with H_2O (300 mL), and extracted with ether (200 mL). At 0 °C, the aqueous layer was acidified by 2N HCl to pH 3.5. The aqueous

layer was extracted twice with ether (200 mL), and the ether layer was washed with H_2O (200 mL) and brine (200 mL), dried over Na_2SO_4, and concentrated to yield 12 g (76.9%) of *tert*-butyldimethylsilyloxyacetic acid **10** as a colorless liquid, which was solid when stored at low temperature. ^{1}H NMR ($CDCl_3$): δ 4.4 (s, 2H), 0.92 (s, 9H), 0.14 (s, 6H).

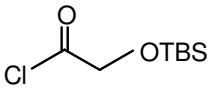

***tert*-Butyldimethylsilyloxyacetyl chloride, 11**. *tert*-Butyldimethylsilyloxyacetyl acid **10** (0.860 g, 4.32 mmol) was dissolved in benzene (15 mL), after which 5 mL of a benzene/water azotropic mixture was removed by distillation. Oxalyl chloride (1.10 g, 8.64 mmol) was added dropwise to the reaction, and the mixture was stirred at rt for 45 min, and then heated to reflux for another 45 min. Excess oxalyl chloride and benzene was removed by distillation. Without purification, the crude product was used immediately in the next esterification step. ^{1}H NMR ($CDCl_3$,): δ 4.5(s, 2H), 0.97 (s, 9H), 0.20 (s, 6H).

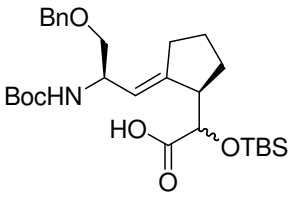

α-*O*-TBS acid, 12. To a solution of diisopropylamine (0.67 mL, 4.8 mmol) in 8 mL THF was added *n*-butyl lithium (2.5 M in hexanes, 1.75 mL, 4.37 mmol) at 0ºC. The mixture was stirred for 15 min to generate LDA. A mixture of chlorotrimethyl silane (1.45 mL, 11.4 mmol) and pyridine (1.00 mL, 12.4 mmol) in 3 mL THF was added dropwise to the LDA solution at –100ºC. After 5 min, a solution of allylic ester **6** (0.50 g, 0.95 mmol) in 3.5 mL THF was added dropwise and the reaction was stirred at –100ºC for 25 min, then warmed slowly (over 1.5 h) to room temperature, and stirred at room temperature for another

1.5 h. The reaction was quenched with 1N HCl (15 mL), and the aqueous layer was extracted with Et_2O (2 × 30 mL). The organic layers were combined, dried on $MgSO_4$, and concentrated to give the crude α-*O*-TBS acid **12**. Without further purification, **12** was used immediately in the next step.

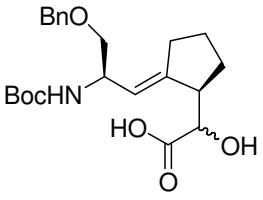

α-Hydroxy acid, 13. Tetra-*n*-butylammonium fluoride (1 M, 2 mL, 2 mmol) in THF was added to a solution of α-*O*-TBS acid **12** (0.95 mmol) in 2 mL THF at 0ºC. The reaction mixture was stirred at 0 ºC for 5 min, warmed to rt, and stirred for 1 h. The reaction was quenched with 0.5 N HCl (10 mL), extracted with EtOAc (100 mL), dried over $MgSO_4$ and concentrated. Purification by flash chromatograghy with 50% EtOAc in hexanes on silica yielded 393 mg of α-hydroxyl acid **13** as a colorless foam in an overall yield of 52% for the two steps. ^{1}H NMR (DMSO-d_6): 7.36-7.24 (m, 5H), 6.84 (d, J = 7.4, 1H), 5.27 (d, J = 7.7, 1H), 4.51-4.42 (m, 2H), 3.84 (d, J = 5.9, 1H), 3.40-3.32 (m, 2H), 3.30-3.25 (m, 1H), 2.70-2.61 (m, 1H), 2.41-2.37 (m, 1H), 2.25-2.10 (m, 1H), 1.74-1.67 (m, 2H), 1.55-1.42 (m, 2H), 1.37 (s, 9H).

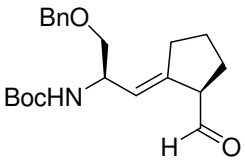

Aldehyde, 14. Lead tetraacetate (120 mg, 0.270 mmol) in $CHCl_3$ (0.7 mL) was added dropwise to a solution of α-hydroxyl acid **13** (100 mg, 0.242 mmol) in EtOAc (4 mL) at 0 °C. The reaction was stirred for 10 min at 0 °C, then quenched with ethylene glycol (0.5 mL), diluted with EtOAc (9 mL), washed with water (4 ×1.5 mL), brine (2 mL),

dried over Na_2SO_4 and concentrated to afford 91 mg of aldehyde **14** as a pale yellow oil (100% crude yield). ^{1}H NMR ($CDCl_3$) δ 9.38 (d, *J* = 2.8, 1H), 7.36-7.27 (m, 5H), 5.39 (dd, *J* = 2.2, 8.6, 1H), 4.95 (d, *J* = 7.1, 1H), 4.55 (d, *J* = 12.2, 1H), 4.47 (d, *J* = 12.2, 1H), 4.41 (brs, 1H), 3.50 (dd, *J* = 4.3, 9.3, 1H), 3.43 (dd, *J* = 5.0, 9.4, 1H), 3.25 (m, 1H), 2.55 (m, 1H), 2.24 (m, 1H), 1.99 (m, 1H), 1.86 (m, 1H), 1.72 (m, 2H), 1.43 (s, 9H).

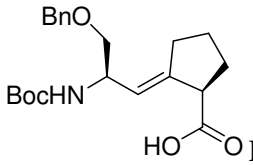

Boc-Ser(OBn)-Ψ[(*E*)CH=C]-Pro-OH, 15. The aldehyde **14** (91 mg) was dissolved in acetone (7 mL) and cooled to 0 °C. Jones reagent (2.7 M H_2SO_4, 2.7 M CrO_3, 0.20 mL, 0.48 mmol) was added dropwise to the solution. The reaction was stirred at 0 °C for 0.5 h, quenched with isopropyl alcohol (0.6 mL) and stirred for another 10 min. The green precipitate was removed by filtrationand the solvent was evaporated. The residue was extracted with EtOAc (3 ×10 mL), washed with water (1 × 2 mL) and brine (1 × 3 mL), dried over Na_2SO_4, and concentrated. Chromatography on silica with 30% EtOAc in hexane afforded 70 mg of Boc-Ser(OBn)-Ψ[(*E*)CH=C]-Pro-OH **15** as a colorless oil in 76% yield. ^{1}H NMR ($CDCl_3$) δ 7.30 (m, 5H), 5.55 (d, *J* = 6.7, 1H), 4.93 (brs, 1H), 4.53 (d, *J* = 12.1, 1H), 4.51 (d, *J* = 12.1, 1H), 4.39 (brs, 1H), 3.47 (dd, *J* = 3.5, 9.2, 1H), 3.41 (dd, *J* = 5.3, 9.6, 1H), 3.36 (t, *J* = 7.0, 1H), 2.54 (m, 1H), 2.29 (m, 1H), 2.04-1.84 (m, 3H), 1.66 (m, 1H), 1.43 (s, 9H).

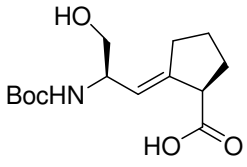

Boc-Ser-Ψ[(*E*)CH=C]-Pro-OH, 16. NH_3 (35 mL) was transferred from a gas cyclinder to the reaction round bottom flask at –40 °C cold bath and allowed to warm to reflux at –33 °C. Na (495 mg, 21.0 mmol) was added until a deep blue solution was sustained. Boc-Ser(OBn)-Ψ[(*E*)CH=C]-Pro-OH **15** (575 mg, 1.50 mmol) in THF (13 mL) was added directly to the Na/NH_3 solution via syringe. After stirring for 30 min at reflux, the reaction was quenched with NH_4Cl (20 mL) and then allowed to warm to rt. The reaction was concentrated to evaporate most of the NH_3 and more NH_4Cl (40 mL) was added. The mixture was extracted with $CHCl_3$ (5 × 30 mL). The aqueous layer was acidified with 1 N HCl and extracted with $CHCl_3$ (6 × 50 mL). The $CHCl_3$ layers were combined, washed with brine (1 × 30 mL), dried over $MgSO_4$ and concentrated to give 280 mg of Boc-Ser-Ψ[(*E*)CH=C]-Pro-OH **16** as a yellow oil in 65% yield. ^{1}H NMR (DMSO-d_6) δ 6.66 (d, J = 7.4*, 1H*), 5.31 (dd, J = 2.1*,* 8.7*, 1H*), 4.61 (brs, 1H), 4.06 (s, 1H), 3.27(dd, J = 7.1, 10.8, 1H), 3.20 (dd, J = 5.7, 10.5, 1H), 3.16 (m,1H), 2.39 (m, 1H), 2.22 (m, 1H), 1.80 (m, 3H), 1.52 (m, 1H),1.36 (s, 9H).

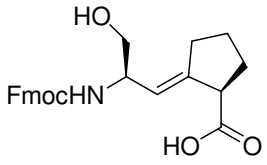

Fmoc-Ser-Ψ[(*E*)CH=C]-Pro-OH, 2. To solution of TFA (0.450 mL, 5.85 mmol) in CH_2Cl_2 (1.35 mL) was added Boc-Ser-Ψ[(*E*)CH=C]-Pro-OH **16** (133 mg, 0.450 mmol). Triethyl silane ($HSiEt_3$, 0.20 mL, 1.1 mmol) was added to the reaction and stirred at rt for 45 min. Most of the TFA was removed by rotary evaporation, and CH_2Cl_2 (10

× 10 mL) was evaporated to remove the remainder of the TFA in the residue. The residue was subjected to high vacuum until a constant weight was obtained. Without further purification, the crude amine-TFA salt was dissolved in $NaHCO_3$ aqueous solution (1.7 mL) and cooled to 0 °C. FmocCl (123 mg, 0.475 mmol) in dioxane (1.7 mL) was added slowly. The reaction was stirred at 0 °C for 2 h. Water (3 mL) was added and the aqueous layer was extracted with $CHCl_3$ (3 × 2 mL). The aqueous solution was acidified with 2N HCl to pH 3, and extracted with $CHCl_3$ (6 × 10 mL). The organic layers were combined, dried over $MgSO_4$ and concentrated. Chromatography on silica with gradient elution from 2% MeOH in $CHCl_3$ to 20% MeOH in $CHCl_3$ afforded 50 mg (45%) of Fmoc-Ser-Ψ [(*E*)CH=C]-Pro-OH **2** as a white solid. ^{1}H NMR (DMSO-d_6) δ 12.3 (brs, 1H), 7.90-7.30 (m, 9H), 5.35 (d, 1H), 4.30-4.10 (m, 4H), 3.50-3.10 (m, 4H), 2.36-2.23 (m, 2H), 1.78-1.77 (m, 4H).

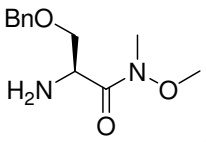

H-Ser(OBn)-N(Me)OMe, 17. *N*-Boc-Ser(OBn)-N(Me)OMe **3** (24.1 g, 71.2 mmol) was dissolved in CH_2Cl_2 (400 mL). TFA (125 mL) was added and the solution was stirred at rt for 30 min. The TFA and CH_2Cl_2 were removed by rotary evaporation, and $NaHCO_3$ was added to the residue until gas evolution ceased. The aqueous mixture was extracted with CH_2Cl_2 (8 × 300 mL), dried over $MgSO_4$, and concentrated. Chromatography on silica with 50% EtOAc in petroleum ether to remove impurities, followed by product elution with 10% MeOH in EtOAc, gave 13.1 g (80%) of the amine **17** as a clear oil. ^{1}H NMR δ 7.40-7.20 (m, 5H), 4.57 (d, J = 12.1, 1H), 4.52 (d, J = 12.1, 1H), 4.06 (m, 1H), 3.67 (s, 3H), 3.66-3.45 (m, 2H), 3.20 (s, 3H), 1.88 (br s, 2H).

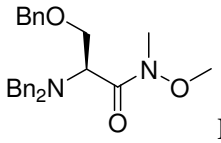

Bn-Ser(Bn)2-N(Me)OMe, 18. The amine **17** (13.0 g, 58.0 mmol) was dissolved in CH_2Cl_2 (50 mL), and benzyl bromide (24.8 g, 145 mmol) and DIEA (37.4 g, 290 mmol) were added. After stirring at rt for 96 h, the reaction was diluted with EtOAc (600 mL). The organic layer was washed with NH_4Cl (4 × 200 mL) and brine (200 mL), dried on $MgSO_4$, and concentrated. Chromatography on silica with 10% EtOAc in hexanes to remove benzyl bromide and then 50% EtOAc in hexane to elute the product gave 21.4 g (92%) of **18** as a clear oil. ^{1}H NMR δ 7.40-7.17 (m, 15H), 4.56 (d, J = 11.9, 1H), 4.48 (d, J = 11.9, 1H), 4.13 (m, 1H), 3.98-3.84 (m, 4H), 3.76 (d, J = 14.1, 2H), 3.28 (br s, 3H), 3.20 (br s, 3H).

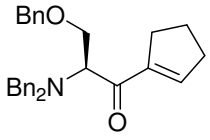

Ketone, 19. Cyclopentenyl lithium was generated by adding fresh *s*-BuLi (1.3 M in cyclohexane, 50 mL, 65 mmol) to a solution of freshly prepared cyclopentenyl iodide **8** (10.0 g, 51.5 mmol) in THF (100 mL) at –40 °C. The solution was stirred at –40 °C for 70 min. At the same time, in another reaction flask Weinreb amide **18** (7.40 g, 17.7 mmol) in THF (30 mL) was cooled to –40 °C and added slowly via cannula to the solution of cyclopentenyl lithium. The reaction mixture was stirred at –40 °C for 1 h, then quenched with NH_4Cl (20 mL), diluted with EtOAc (600 mL), washed with NH_4Cl (3 × 100 mL) and brine (100 mL), dried over Na_2SO_4, and concentrated. Chromatography on silica with 5% EtOAc in hexanes gave 7.1 g (95%) of the ketone **19** as a pale yellow oil. ^{1}H NMR($CDCl_3$) δ 7.39-7.20 (m, 15H), 6.11 (m, 1H), 4.55 (d, J = 12.3, 1H), 4.48 (d, J = 12.3, 1H), 4.24 (app t, J = 6.6, 1H), 3.90 (d, J = 6.6, 2H), 3.79 (d, J = 13.6, 2H), 3.71 (d, J = 14.1, 2H), 2.59-2.39 (m, 4H), 1.98-1.84 (m, 2H).

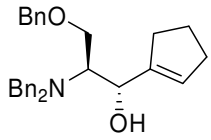

(*S, S*)-Alcohol, 20. Ketone **19** (6.80 g, 16.0 mmol) was dissolved in THF (250 mL), and $LiAlH_4$ (6.00 g, 160 mmol) was added in one portion. After stirring at rt for 1 h, the reaction was quenched with MeOH (50 mL) and NH_4Cl (50 mL). The reaction mixture was diluted with EtOAc (500 mL), and washed with NH_4Cl (150 mL), and 1 M sodium potassium tartrate (2 × 150 mL). The aqueous layers were back-extracted with CH_2Cl_2 (3 × 200 mL). The combined organic layers were dried over $MgSO_4$ and concentrated to yield 6.68 g (98%) of alcohol **20** as a colorless oil. ^{1}H NMR δ 7.49-7.24 (m, 15H), 5.65 (m, 1H), 4.62 (d, J = 11.9, 1H), 4.53 (d, J = 11.9, 1H), 4.48 (s, 1H), 4.26 (d, J = 10.1, 1H), 4.02 (d, J = 13.2, 2H), 3.80-3.70 (m, 3H), 3.58 (dd, J = 3.1, 10.6, 1H), 3.07 (m, 1H), 2.43-2.17 (m, 3H), 2.00-1.75 (m, 3H).

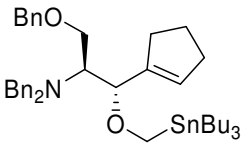

Stannane, 21. To a solution of alcohol **20** (2.20 g, 5.15 mmol) in THF (40 mL) were added 18-crown-6 (4.09 g, 15.5 mmol) in THF (10 mL), KH (1.03 g, 7.73 mmol, 35% suspension in mineral oil) in THF (10 mL), and freshly distilled Bu_3SnCH_2I (3.33 g, 7.73 mmol) in THF (10 mL). The resulting solution was stirred for 30 min at rt. The reaction was then quenched with MeOH, diluted with EtOAc (400 mL), washed with NH_4Cl (2 × 100 mL) and brine (100 mL), dried over $MgSO_4$, and concentrated. Purification by chromatography on silica with 3% EtOAc in hexanes gave 3.51 g (92%) of stannane **21** as a colorless oil. ^{1}H NMR ($CDCl_3$) δ 7.40- 7.26 (m, 15H), 5.60 (br s, 1H), 4.45 (d, J = 12.0, 1H), 4.37 (d, J = 12.0, 1H), 4.05 (d, J = 7.8, 1H), 3.99 (d, J = 13.7, 2H), 3.83 (d, J = 13.7, 2H),

3.74 (dm, J = 9.9, 1H), 3.60 (dd, J = 9.6, 5.7, 1H), 3.53 (dd, J = 9.6, 4.6, 1H), 3.41 (d, J = 9.6, 1H), 2.99 (m, 1H), 2.40-2.28 (m, 2H), 1.99 (br s, 2H), 1.82 (m, 2H), 1.54 (m, 6H), 1.33 (m, 6H), 0.91 (m, 15H).

Bu_3SnCH_2Cl **Chloromethyltributyltin, 22**. To a flame-dried flask with a septum-capped neck under dry N_2 was added dry THF (100 mL) and diisopropylamine (7.80 mL, 55.0 mmol). The reaction mixture was cooled to 0 °C for 10 min, and a solution of *n*-butyllithium in hexanes (1.44 M, 34.7 mL, 50.0 mmol) was added dropwise while stirring. After stirring at 0 °C for 15 min, tributylstannane (13.0 mL, 50.0 mmol) was added dropwise. The resulting light green solution was stirred at 0 °C for an additional 30 min, and paraformaldehyde (1.55 g, 50.0 mmol) was added. The reaction mixture was cooled to –78 °C and methanesulfonyl chloride (5.0 mL, 65 mmol) was added dropwise. The resulting reaction mixture was warmed to rt and stirred for 12 h, after which it was diluted with water (250 mL). The aqueous layer was extracted with hexane (3 × 100 mL), dried with Na_2SO_4, and concentrated by rotary evaporation. The crude product was quickly filtered through a small amount of silica (20.0 g) and eluted with hexanes. Further purification by vacuum distillation at 0.5 Torr yielded 13.0 g (70%) of chloromethyltributyltin **22** as a colorless liquid.

Bu_3SnCH_2I **Iodomethyltributyltin, 23**. A mixture of chloromethyltributyltin **22** (10.3 g, 30.0 mmol), sodium iodide (9.10 g, 61.0 mmol), and acetone (175 mL) was stirred at rt for 12 h. The reaction mixture was concentrated by rotary evaporation and diluted with water (250 mL). The mixture was extracted with CH_2Cl_2 (100 mL), dried with Na_2SO_4, and concentrated. The crude product was quickly filtered through a small amount of silica gel (20 g) eluting

with hexane to give 11.8 g (98%) of iodomethyltributyltin **23** as a colorless liquid. ^{1}H NMR ($CDCl_3$) δ 1.90 (s, 2H), 1.50 (m, 6H), 1.30 (m, 6H), 0.98 (m, 6H), 0.90 (m, 9H).

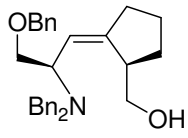

(*Z*)-Alkene, 25. Stannane **21** (9.60 g, 13.1 mmol) was dissolved in THF (150 mL) and cooled to –78 °C. *n*-BuLi (2.5 M in hexanes, 15 mL, 39 mmol) was cooled to –78 °C, and added slowly via cannula to the solution of stannane **21**. The resulting mixture was stirred at –78 °C for 1.5 h. The reaction was warmed to rt, quenched with MeOH (10 mL) and NH_4Cl (50 mL), and concentrated by rotary evaporation. The residue was diluted with EtOAc (700 mL), washed with NH_4Cl (2 × 150 mL) and brine (150 mL), dried on Na_2SO_4, and concentrated. Chromatography on silica with 15% EtOAc in hexanes yielded 3.0 g of (*Z*)-alkene **25** (53%) and 1.57 g of (*E*)-alkene **24** (28%) as clear oils. (*Z*)-alkene **25**: ^{1}H NMR ($CDCl_3$) δ 7.38-7.26 (m, 15H), 5.55 (br d, J = 8.7, 1H), 4.57 (d, J = 12.2, 1H), 4.53 (d, J = 12.2, 1H), 4.12 (brs, 1H), 3.89 (d, J = 13.3, 2H), 3.79 (m, 1H), 3.67 (m, 4H), 3.33 (m, 1H), 3.27 (m, 1H), 2.53 (m, 1H), 2.31-2.18 (m, 2H), 1.71- 1.47 (m, 4H); (*E*)- alkene **24**: ^{1}H NMR ($CDCl_3$) δ 7.38-7.27 (m, 15H), 5.43 (d, J = 9.4, 1H), 4.51 (d, J = 12.1, 1H), 4.47 (d, J = 12.1, 1H), 3.84 (d, J =13.9, 2H), 3.73 (m, 1H), 3.64-3.47 (m, 6H), 2.65 (m, 1H), 2.05 (m, 2H), 1.85 (m, 1H), 1.69 (m, 1H), 1.56 (m, 2H).

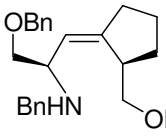

***N,O*-Dibenzyl alcohol, 26**. (*Z*)-Alkene **25** (1.44 g, 3.26 mmol) and 20% $Pd(OH)_2$/C (150 mg) were blanketed with N_2, after which MeOH (100 mL) was added,

followed by 96% HCOOH (20 mL). After stirring for about 30 min, the reaction solution was filtered immediately through Celite, concentrated and neutralized with solid $NaHCO_3$ until gas evolution ceased, extracted with CH_2Cl_2 (5 × 100 mL), dried over Na_2SO_4, and concentrated to give 1.1 g (95%) of the monobenzylamine **26**. Without further purification, *N,O*-dibenzyl alcohol **26** was used immediately in the next reaction: ^{1}H NMR ($CDCl_3$) δ 7.36-7.30 (m, 10H), 5.50 (d, J = 8.3, 1H), 4.56 (d, J = 1.6, 2H), 3.72 (d, J = 11.2, 1H), 3.66-3.60 (m, 3H), 3.55-3.50 (m, 1H), 3.48-3.45 (dd, J = 4.3, 10.8, 1H), 3.41-3.37 (m, 1H), 2.83 (m, 1H), 2.37-2.22 (m, 2H), 1.89-1.85 (m, 1H), 1.64 (m, 1H), 1.54-1.38 (m, 2H).

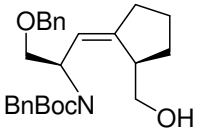

Boc-benzylamine, 27. The monobenzylamine **26** (1.10 g, 3.12 mmol) was dissolved in CH_2Cl_2 (60 mL), di-*tert*-butyl dicarbonate (1.70 g, 7.79 mmol) was added, and the resulting solution was stirred at rt for 17 h. The reaction mixture was concentrated by rotary evaporation. Purification by chromatography on silica with 20% EtOAc in hexanes gave 1.30 g (82%) of the Boc-benzylamine **27** as a pale yellow oil. ^{1}H NMR ($CDCl_3$) δ 7.36-7.16 (m, 10H), 5.36 (d, J = 8.9, 1H), 5.18 (brs, 1H), 4.47-4.37 (m, 4H), 3.48-3.46 (m, 5H), 2.87 (brs, 1H), 2.20 (m, 2H), 1.75 (m, 1H), 1.65 (m, 2H), 1.54 (m, 1H), 1.34 (brs, 9H).

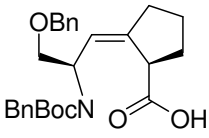

Boc-benzylamino Acid, 28. Alcohol **27** (2.20 g, 4.90 mmol) was dissolved in acetone (220 mL) and cooled to 0 °C. Jones reagent (2.7 M H_2SO_4, 2.7 M CrO_3; 4.50 mL, 12.0 mmol) was added, and the resulting solution was stirred at 0 °C for 40 min. The reaction

was quenched with *i*-PrOH (50 mL) and stirred for 5 min at rt. The reaction mixture was diluted with water (400 mL), extracted with CH_2Cl_2 (10 × 50 mL), dried over $MgSO_4$, and concentrated. Chromatography on silica with 20% EtOAc in hexanes gave 2.10 g (90%) of **28** as a pale yellow oil. ^{1}H NMR ($CDCl_3$) δ 7.34-7.16 (m, 10H), 5.53 (d, J = 9.2, 1H), 4.92 (br s, 1H), 4.47-4.27 (m, 4H), 3.69-3.24 (m, 3H), 2.46 (m, 1H), 2.28 (m, 1H), 2.11 (m, 1H), 1.89 (m, 2H), 1.62 (m, 1H), 1.38 (br s, 9H).

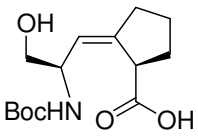

Boc-Ser-Ψ[(*Z*)CH=C]-Pro-OH, 29. NH_3 (40 mL) was transferred into 10 mL of THF at –78 °C and allowed to warm to reflux at –33 °C. Na (0.50 g, 22 mmol) was added until a deep blue solution was sustained. A solution of Boc-benzylamino acid **28** (0.50 g, 1.1 mmol) in THF (2 mL) was added to the Na/NH_3 solution slowly via cannula over a 5 min period. After stirring for 45 min at –33 °C, the reaction was quenched with NH_4Cl (5 mL) and allowed to warm to rt. The reaction mixture was concentrated by rotary evaporation to remove most of the NH_3. The residue (10 mL) was diluted with NH_4Cl (20 mL), acidified with 1 N HCl to pH 7, and the aqueous layer was extracted with $CHCl_3$ (10 × 50 mL). The organic layers were combined, dried on $MgSO_4$, and concentrated to gave 200 mg (70%) of Boc-Ser-Ψ[(*Z*)CH=C]-Pro-OH **29** as a pale yellow oil. ^{1}H NMR (DMSO-*d*6) δ 6.48 (d, J = 6.2, 1H), 5.20 (d, J = 8.4, 1H), 4.08 (m, 1H), 3.36 (m, 1H), 3.28 (dd, J = 5.7, 10.6, 1H), 3.13 (dd, J = 6.6, 10.6, 1H), 2.20 (m, 2H), 1.81 (m, 2H), 1.67 (m, 1H), 1.47 (m, 1H), 1.31 (s, 9H).

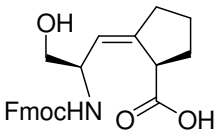

Fmoc-Ser-Ψ[(*Z*)CH=C]-Pro-OH, 1. Boc-Ser-Ψ[(*Z*)CH=C]-Pro-OH **29** (150 mg, 0.520 mmol) was dissolved in TFA (5 mL) and CH_2Cl_2 (15 mL) at 0 °C. The reaction mixture was stirred for 45 min at rt, then most of the TFA was evaporated by rotary evaporation. The remaining TFA in the residue was removed by evaporation of CH_2Cl_2 (10 × 10 mL). The trace TFA in the residue was further removed under high vacuum until a constant weight was obtained. Without further purification, the crude product was dissolved in a mixture of 10% Na_2CO_3 (3.0 mL) and $NaHCO_3$ (3 mL), then cooled to 0 °C for 10 min. A solution of FmocCl (148 mg, 0.580 mmol) in dioxane (6.0 mL) was added slowly, and the resulting solution was stirred at 0 °C overnight. The reaction mixture was diluted with H_2O (20 mL) and the aqueous layer was extracted with ether (2 × 20 mL). The aqueous layer was acidified with 1 N HCl to pH 1-2, and extracted with $CHCl_3$ (10 × 50 mL). The organic layers were combined, dried over $MgSO_4$ and concentrated to afford 126 mg (65%) of Fmoc-Ser-Ψ[(*Z*)CH=C]-Pro-OH **1** as a colorless foam. ^{1}H NMR (DMSO-*d6*) δ 12.1 (br s, 1H), 7.87 (d, *J* = 7.6, 2H), 7.71 (d, *J* = 7.6, 2H), 7.40 (app t, *J* = 7.4, 2H), 7.32 (app t, *J* = 7.4, 2H), 7.12 (d, *J* = 7.6, 1H), 5.31 (d, *J* = 9.2, 1H), 4.65 (br s, 1H), 4.24-4.17 (m, 4H), 3.44 (m, 1H), 3.38 (dd, *J* = 10.6, 5.4, 1H), 3.24 (m, 1H), 2.31 (m, 1H), 2.22 (m, 1H), 1.88 (m, 2H), 1.74 (m, 1H), 1.53 (m,1H).

Chapter 3. Synthesis of a Phosphorylated Prodrug for the Inhibition of Pin1

3.1. Prodrug Strategies for Phosphorylated Compounds

3.1.1. Prodrugs of Phosphates, Phosphonates and Phosphinates

Enzymatic phosphorylation of biologically active molecules is a major regulatory event during signal transduction and the cell cycle of a living system. Therefore, while many cellular drug targets display high-affinity interactions toward phosphorylated molecules, they are not able to bind their nonphosphorylated counterparts.[78, 95, 170] As a result, many phosphorous-containing molecules are viable drug candidates. However, one common problem for phosphorylated compounds as effective inhibitors or drugs is that they are generally not effective in penetrating cell membranes because of the negative charge on the phosphate group.[171] One general strategy for circumventing this problem involves masking the phosphate in a form that neutralizes this negative charge, thereby enhancing its cell permeability.[171-173] Upon cell entry, the mask can then be removed enzymatically and the inhibitors converted to their biologically active forms.[173]

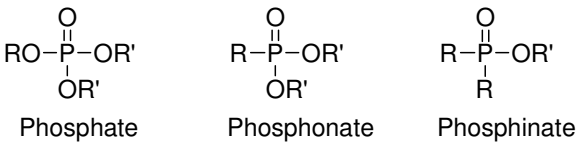

Figure 3.1. Structures of phosphate, phosphonate and phosphinate drugs

(Where R represents an alkyl or aryl group, and R' represents either a hydrogen atom or an anionic charge)

The general structures of phosphate, phosphonate and phosphinate drugs are shown in

Figure 3.1. There are several drug-delivery related problems that currently impede the use of these phosphorus-containing drugs. First, at nearly all physiological pH values, these drugs impart an ionic charge (mono- or di-), which makes them very polar.[173] Therefore, it is very difficult for these highly ionized species to undergo passive diffusion through cell membranes.[173] Second, the high polarity of these drugs leads to a lower volume of distribution and can hinder efficient renal clearance.[173] In addition, phosphatases present in the body can cleave the phosphate group from the phosphate drugs, especially those attached to a primary alcohol.[174, 175] Enzymatic dephosphorylation of phosphate drugs decreases the duration of their time of action.[174, 175]

Because of these shortcomings, chemically derivatizing the ionic phosphate, phosphonate, and phosphinate groups has been widely used to neutralize their anionic charges.[173, 174] The most commonly used derivatization technique for these phosphorus-coupled oxygens is the neutral esters.[173, 174] These derivatives are called "prodrugs" if the parent drugs can be released via enzymatic breakdown of the ester linkages of the phosphorous-coupled oxygens in the body.[173, 174] The advantage of using neutralized prodrugs is that the polarity of the drugs is decreased by increasing their lipophilicity.[173, 176, 177] With decreased polarity, some cells and tissues that formerly were not available to the non-modified parent drugs could then be accessed by these prodrugs.[173, 177] Thus, increasing the membrane permeability of phosphate, phosphonate and phosphinate drugs could improve their oral, brain, tumor and cellular delivery capabilities (especially to cells infected by viruses).[173, 174, 178-182] Another advantage of the neutralized drugs is especially important. Specifically, some serum phosphatases may nonspecifically cleave the phosphate groups

from the drugs, thereby causing them to fail in action.[173] By neutralizing the phosphate groups, these prodrugs would be stable towards nonspecific phosphatases as well.[173]

Choosing suitable bioreversible protecting groups for phosphate, phosphonate and phosphinate drugs is a major challenge. Several important issues should be considered in identify a proper prodrug system for these prodrugs. First, these prodrugs should display adequate chemical stability in plasma and the variable pH environments in the body.[173, 183] Second, these prodrugs should display adequate stability toward luminal contents as well as toward enzymes found in brush border membranes.[173, 177, 184] Final, these prodrugs should be able to be enzymatically converted into their parent drugs once they permeate the targeted cell membrane, thereby trapping them inside the targeted cells (Figure 3.2).[173, 177, 182, 183]

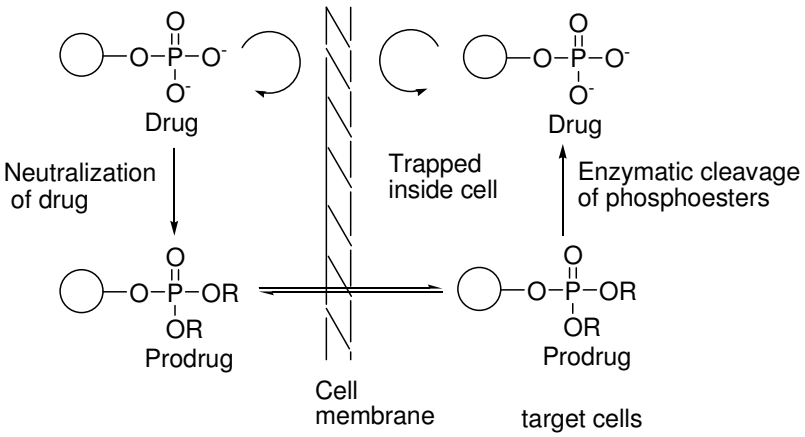

Figure 3.2. Permeation of prodrugs and their trapping inside target cells[173]

Bioreversible prodrugs of phosphate, phosphonate and phosphinate drugs have been designed by various strategies, which include SATE (*S*-acetylthioethanol),[185-187] BisPOM (bis-pivaloyoxymethyl),[188, 189] DET (dithiodiethanol)[185-187]. The design and properties of these strategies will be described in detail in the following.

3.1.2. Simple and Substituted Alkyl and Aryl Ester

Purine and pyrimidine nucleoside analogues have been found to be useful in the treatment of viral diseases.[190] AZT (3'-azido-2', 3'-dideoxythymidine), for example, has shown promise in inhibiting the AIDS virus.[187, 190-195] In order to enhance their bioavailability, some mono-5'-alkyl phosphate ester and di-5'-alkyl phosphate ester prodrugs (Figure 3.3 and Figure 3.4) have been evaluated.[196-198] Studies showed that the mono-alkyl or aryl esters of phosphate analogues failed to act as efficient prodrugs for the delivery of nucleoside-phosphate analogs.[199, 200] Specifically, limited passive diffusion through cell membranes was caused by a mono-ionic charge.[200]

As depicted in Figure 3.3, a series of alkyl prodrugs of hydrogen-phosphonate analogues of AZT were evaluated *in vitro*.[199] It was demonstrated that the short chain alkyl esters were more efficient than the longer chain alkyl ester prodrugs.[201] Moreover, the short chain alkyl ester prodrugs were found to be 5-10 times more potent than the parent phosphonate.[201]

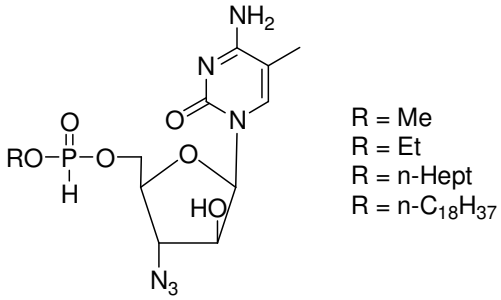

Figure 3.3. Alkyl prodrugs of AZT H-phosphonate analogue[199]

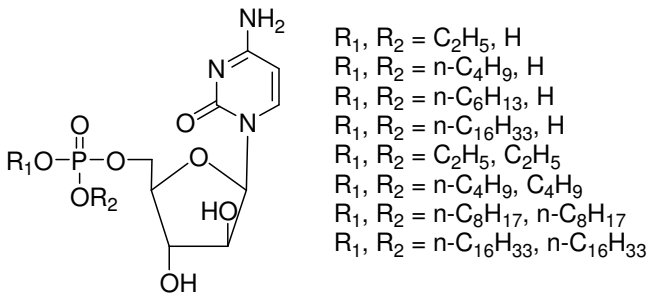

Figure 3.4. Alkyl ester prodrugs of araCMP[202]

In order to reduce polarity, dialkyl ester prodrugs were also studied (Figure 3.4).[196, 203] An inverse structure-activity relationship with respect to alkyl chain length was observed for diester prodrugs containing araCMP.[173, 196, 197] However, the highly stable alkyl esters resulted in little or no conversion to the active 5'-phosphate.[204] The short chain diesters, which are chemically and enzymatically stable, were predominantly detected unchanged in the serum.[204] As alkyl chain size increased, the diester prodrugs tended to break down into mono-phosphate esters more efficiently.[205] However, the mono-phosphate intermediates that accumulated in the serum failed to convert into the parent phosphate araCMP.[205]

Some simple aryl and substituted aryl phosphate ester prodrugs were also investigated for their ability to produce more chemically and enzymatically labile prodrugs. The most promising aryl phosphate ester prodrug appears to be the phenyl prodrug.[173]

Some halo alkyl ester prodrugs have been synthesized and their bioavailabilities have been evaluated (Figure 3.5).[206-208] The chemical lability of these prodrugs was shown to be as follows: trichloroalkyl > dichloroalkyl > monochloroalkyl. However, the observed activity was reported in this order: trichloroalkyl > monochloroalkyl > dichloroalkyl.[206-208]

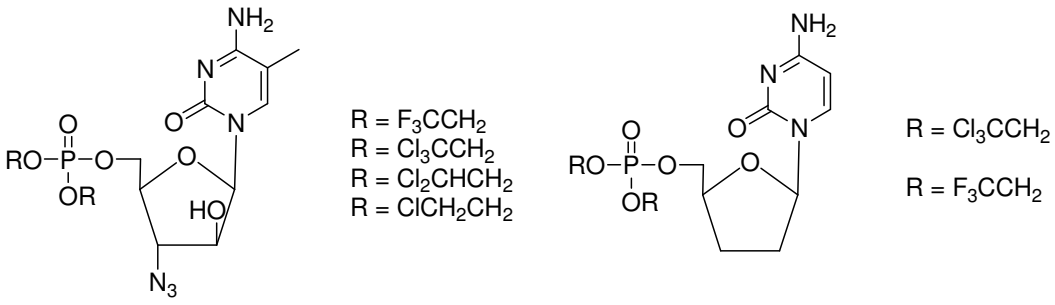

Figure 3.5. Haloalkyl diester prodrugs of an AZT analogue and a ddCD analogue[209]

These results imply that the presence of better leaving groups does not always result in more efficient conversion from a dialkyl ester prodrug to a monoalkyl ester intermediate and the parent phosphate. Thus, chemical lability is not the only factor for generating efficient prodrugs.

3.1.3. Acyloxyalkyl Phosphate Ester

The incorporation of acyloxyalkyl phosphate esters into prodrugs is another strategy that has been widely used.[173-175, 179, 188, 189, 210-212] These types of prodrugs can be used as neutral lipophilic prodrugs, which are able to permeate cell membranes by passive diffusion.[179, 198, 211, 212] They also can be easily removed by esterases to convert into their parent ionic phosphate compounds inside the cells (Scheme 3.1).[179, 198, 211, 212] The general mechanisms for the degradation of acyloxyalkyl phosphate ester prodrugs is the following: 1) The acyl group is cleaved by esterase to yield a hydroxymethyl analogue; 2) The hydroxymethyl analogue was then quickly decomposed to formaldehyde and the monoester prodrug; 3) The second acyl group can be cleaved by the same mechanism as in 1) and 2); alternatively, it can be cleaved by a different enzyme, a phosphodiesterase, in one step.[174, 213]

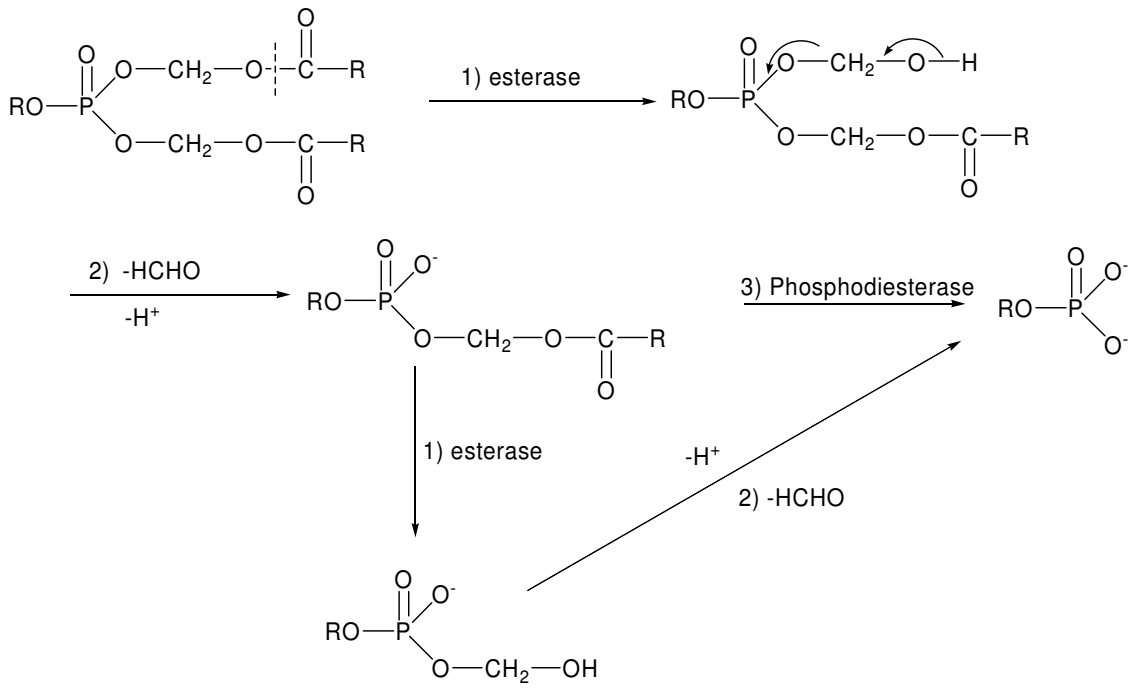

Scheme 3.1. Degradation of acyloxyalkyl prodrug by esterases[174, 213]

PMEA (9-(2-phosphonomethoxyethyl)adenine) is a potent and selective inhibitor of human immunodeficiency virus replication *in vitro*.[178, 205, 214] Its bis(pivaloyloxymethyl) prodrugs displayed substantially increased antiviral activity compared to PMEA (Figure 3.6).[178, 214, 215] In addition, a bis(pivaloyloxymethyl) prodrug of 2', 3'-dideoxyuridine-5'-monophosphate (ddUMP) also afforded much higher antiviral protection than its parent ionic phosphate counterpart, PMEA, *in vitro*.[211] Acyloxyalkyl ester prodrugs of PMEA also showed dramatically increased oral bioavailability.[214] Among them, the bis(pivaloyloxymethyl) prodrug achieved an oral bioavailability of 30%, and has been selected as a potential oral prodrug for further *in vivo* animal studies.[214] The hydrolysis of different acyloxyalkyl ester prodrugs was observed to be retarded by an increase in steric hindrance.[214] The hydrolysis rate for these prodrugs was observed as follows: acetyloxy > isobutyloxy > pivaloyloxy. However, the hydrolysis of the second acyloxymethyl was much

slower than the first promoiety.[173] This result was attributed to the poor binding of the esterase to the ionic mono-acyloxymethyl ester intermediate. One possible solution for this problem is the introduction of a spacer group, which can distance the acyl group from the mono-anionic phosphate intermediate. A series of mono- and bis(4-acyloxybenzyl) ester prodrugs of AZT analogues were synthesized and their hydrolysis rates were evaluated *in vitro*.[195, 216, 217] In the presence of porcine liver carboxyesterase, it was observed the mono- and bis(4-acyloxybenzyl) phosphate esters decomposed readily into the 5'-monophosphate AZT.[173]

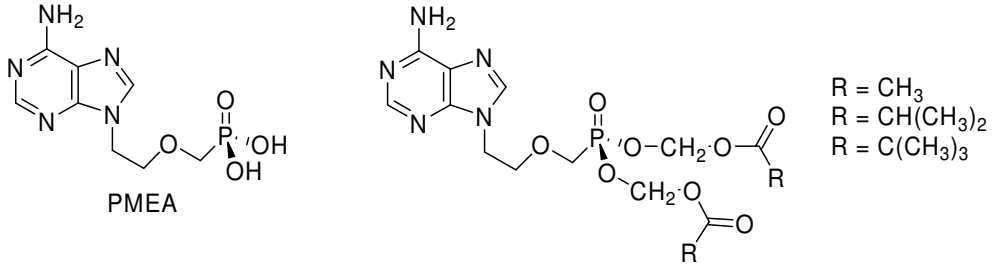

Figure 3.6. Various acyloxyalkyl ester prodrugs of PMEA[216]

3.1.4. Phospholipid Prodrugs

The general structure of a phospholipid prodrug is shown in Figure 3.7. The efficiency of phospholipid prodrugs in penetrating cell membranes is inversely related to the length of their acyl chain *in vitro*.[218-220]

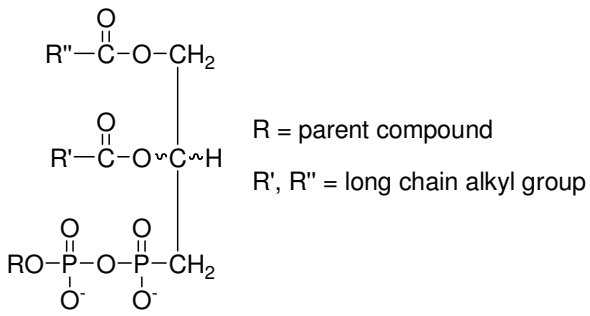

Figure 3.7. General structure of phospholipid prodrugs

3.1.5. SATE and DTE Prodrug Strategy

SATE (*S*-acetylthioethanol) and DTE (dithiodiethanol) are two bioreversible protecting groups widely utilized for prodrugs of nucleoside monophosphates.[187, 221] This strategy has been used for the compounds AZTMP (AZT-5'-monophosphate), PMEA and ddUMP (2',3'-dideoxyuridine 5'-monophosphate).[185-187, 222] SATE and DTE ester prodrugs readily decompose to unstable 2-thioethyl intermediates once they are inside cells by the activation of carboxyesterase or reductase. The unstable 2-thioethyl intermediate quickly breaks down to release episulfide, and the second promoiety is cleaved by the same mechanism (Scheme 3.2).[185, 186, 222]

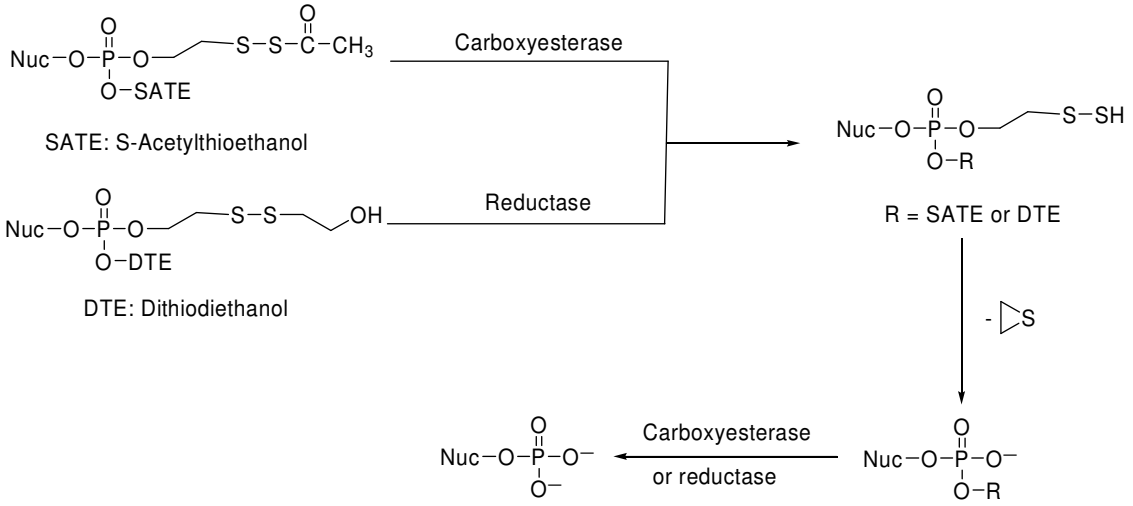

Scheme 3.2. Degradation mechanism of SATE or DTE prodrugs of nucleoside monophosphate[185, 186, 222]

3.1.6. Cyclic Prodrugs

One simple strategy to decrease the polarity of an ionic phosphate is to cyclize the phosphate. Along these lines, a cyclic trimethylene phosphate prodrug was studied by Winkler et al.[223] It was found that just one oxidation step was required for ring opening and

acrolein elimination follows. Therefore, a 4-pivaloyloxy group was introduced into the ring, which was transformed to a hydroxyl group in the presence of carboxylate esterase.[180] The model reaction in mouse plasma showed that such a prodrug could be quantitatively hydrolyzed to its parent phosphate. This strategy has been used for making prodrugs of fdUMP (5-fluoro-2'-deoxyuridylic acid monophosphate).[223]

3.1.7. Carbohydrate Prodrugs

Several selected carbohydrate phosphate prodrugs for AZTMP have been designed and evaluated.[224, 225] The glucose 6-phosphate diester was the most useful prodrug in the series (Figure 3.8).[224, 225]

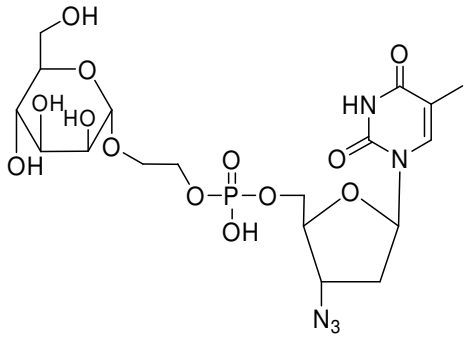

Figure 3.8 A mannopyranoside prodrug of AZTMP[224]

3.1.8. Miscellaneous prodrug strategies

Phosphoramidate prodrug strategy was also reported in literature.[226] These prodrugs are designed to undergo intracellular activation to generate an unstable phosphoramidate anion intermediate, followed by spontaneous cyclization.[226] Water acts as a nucleophile to attack the phosphorus, which leads to P-N bond cleavage and a nucleoside monophosphate.[226]

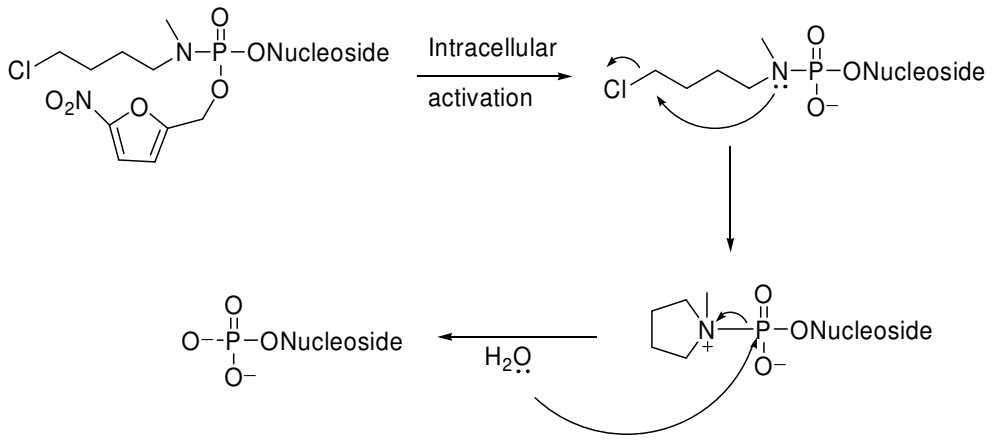

Scheme 3.3. Degradation of phosphoramidate prodrug[226]

3.2. Bis-pivaloyloxymethyl (POM) prodrugs

The acyloxyalkyl pivaloyloxymethyl (POM) was first introduced by Godtfkedsen to improve the absorption of ampicillin and α-methyldopa in the gastrointestinal tract.[188, 189] In early studies, the POM group was observed to be the best among many acyloxyalkyl groups which were designed to be hydrolyzed *in vivo*. Since this moiety was incorporated into a prodrug of nucleoside monophosphate by Farquhar in 1983,[227] the bisPOM ester prodrugs have been well characterized. As a result, they have been successfully used to achieve cellular delivery of ddUMP,[211] PMEA and the analogues of PMEA,[173, 197, 198, 201, 203] 2'-deoxy-5-fluorouridine 5'-monophosphate,[179] AZT,[207, 208] mannose-1-phosphate,[213] and N_3UMP (2'-azido-2'-deoxyuridine 5'-mono-phosphate).[228] These nucleoside monophosphate prodrugs were found to efficiently convert back to their parent compounds without any toxic by-products.

These bis(POM) derivatives are generally quite stable in buffer and plasma, and they are readily transformed to free phosphate derivatives inside various cell types.[229] After

entering cells by passive diffusion, one of the POM groups is cleaved by nonspecific carboxylate esterases to generate the hydroxymethyl analogue.[174, 213] This intermediate is inherently chemically labile, and it spontaneously dissociates to yield the monoPOM phosphodiester with elimination of one molecule of formaldehyde.[174, 213] The parent dianionic phosphate drugs are released by repeating the sequence with the second pivaloyloxymethyl group.[174, 213] Alternatively, the direct conversion of the monoPOM phosphoester into the parent drugs occurs as a result of interacting with the phosphodiesterases.[174, 213] This type of degradation path, which is illustrated in Scheme 3.1, has been verified by enzymatic testing.[174, 206, 212, 230] Figure 3.9 shows the bisPOM prodrug of tryptamine-phosphopantetheine, which is an inhibitor of CoA (cozenzyemA).[230, 231] Enzymatic and cellular study of this prodrug proved its degradation route inside the cells.[230] It also showed higher cellular activity compared to tryptamine-phosphopantetheine.[230]

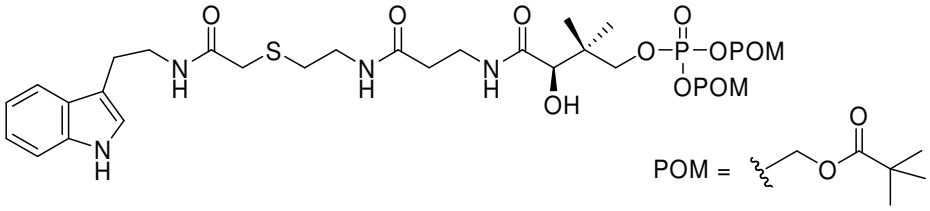

Figure 3.9 BisPOM prodrug of Tryptamine-phosphopantetheine[230]

The bisPOM prodrug strategy has been found to be very useful in improving the oral bioavailability of nucleotide drugs.[204] For example, the bisPOM ester of PMEA displayed an oral bioavailability of 30%, which was about 15-fold higher than the bioavailability (2%) observed for PMEA.[204] Moreover, BisPOM N_3UMP proved to be a stronger inhibitor of ribonucleotide reductase in permeabilized CHO cells with an IC_{50} of 3.0 μM, while its

dianionic parent drug 5'-monophosphate N_3UMP inhibited CHO cell growth with an IC_{50} value of up to 100 μM.[210, 211] The application of the bisPOM prodrug strategy for both antiviral and anticancer drugs has shown promise.[230-232] Based on the successful applications described above, it was decided to pursue a prodrug approach for the inhibition of Pin1 using the POM moiety in this study.

3.3. Strategies for the Synthesis of bisPOM Prodrugs

There are four common methods for introducing bisPOM onto the hydroxyl group of these drugs or inhibitors. The first strategy involves the initial phosphorylation of the hydroxyl compound, followed by the introduction of the bisPOM group by alkylation of the phosphate group (Scheme 3.4). The most efficient method for the phosphorylation of hydroxyl compounds (especially for oligodeoxynucleotide derivatives) is through the use of phosphoramidite intermediates.[233] Phosphites are sensitive compounds. Their high reactivity is due to the lone pair of electrons on the trivalent phosphorous atom.[233] The P(III) atoms in phosphites react with nucleophiles, after the nucleophilic substitution they are oxidized to P(V) atoms by oxidizing reagents.[233] This relatively straightforward sequence explains why P(III) chemistry using phosphoramidite intermediates to prepare phosphate derivatives of oligodeoxynucleotide is so popular and efficient.

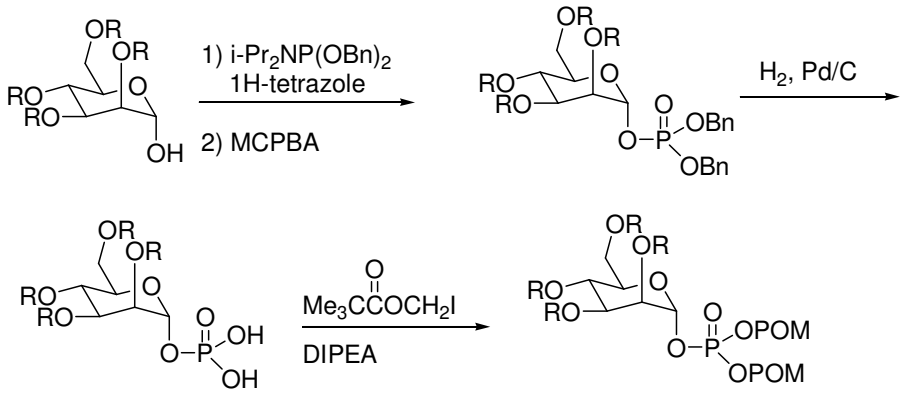

Scheme 3.4 Phosphoramidite method for the synthesis of bisPOM prodrugs[213]

One example of this phosphoramidite strategy is illustrated in Scheme 3.4.[213] The first step involves the reaction between the free hydroxyl group and dibenzyl di-isopropylphosphoramidite using 1H-tetrazole.[187, 213, 228, 234] Phospho triesters were obtained after *in situ* oxidation by MCPBA (meta-chloroperbenzoic acid) or t-BuOOH (*tert*-butyl hydroperoxide).[187, 213, 228, 234] The benzyl protecting groups were then removed by hydrogenation on Pd/C to afford the free phosphate.[187, 213, 228, 234] The resulting phosphates were converted into their POM esters by direct alkylation with bromomethylpivaloate in the presence of DIPEA (*N*-ethyl-di-isopropylamine).[187, 213, 228, 234] This four- to five-step procedure typically results in yields of less than 10%, which is not acceptable for drugs synthesized by such a lengthy synthetic route.

The second strategy for introducing bisPOM onto the hydroxyl group of a drug utilizes P(V) chemistry to accomplish the initial phosphorylation of the hydroxyl compounds, followed by direct esterification using chloromethyl pivaloate or iodomethyl pivaloate (Scheme 3.5.)[235] In the first step, free hydroxyl compounds were treated with two equivalents of phosphorous oxychloride in trimethyl phosphate at low temperature. Importantly, it is the

subsequent direct esterification of the phosphate salts formed with chloromethyl pivalate in Et_3N that facilitates the synthesis of the bisPOM prodrug. This method, however, also produces unacceptably low yield levels.[235]

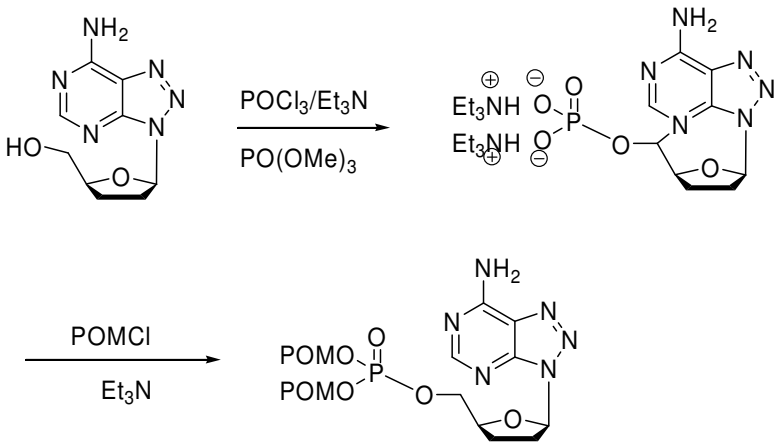

Scheme 3.5 The second method for the synthesis of a bisPOM prodrug[235]

The poor yields from the direct alkylation of phosphate compounds, described in the above two methods, limit their widespread application for preparing bisPOM prodrugs containing nucleotides. As a result, several modifications have been made to improve yields of these important bisPOM prodrugs.[210, 211] For example, it was reported by Cho[234] that both 5'-monophosphates of uridine and pyrimidine were alkylated efficiently via their corresponding stannyl intermediates with simple alkyl bromides in the presence of tetraalkylammonium bromide.[234] The yields resulting from the *O*-alkylation of dialkylphosphates were greater than 75%.[210, 211] The required tributylstannyl phosphate intermediate was prepared by simply mixing N_3dUMP (free acid) with Bu_3SnOMe in methanol at room temperature.[234] A solution of a tributylstannyl phosphate intermediate in CH_3CN was treated with iodomethyl pivalate in the presence of Bu_4NBr, which resulted in

the quantitative conversion of N_3dUMP to its bisPOM prodrug (Scheme 3.6)**.** [234]

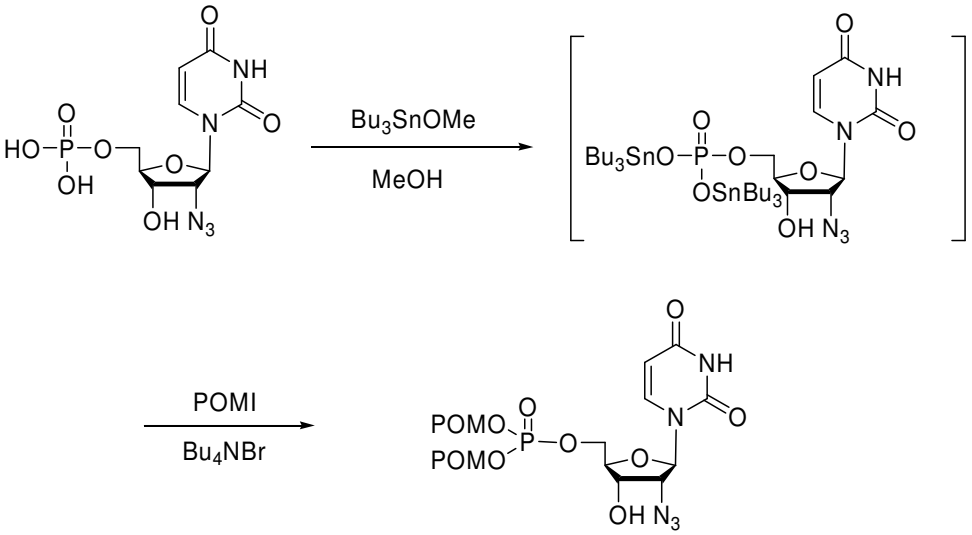

Scheme 3.6 Preparation of bisPOM ester of N_3dUMP via its stannyl intermediate[234]

The third method for introducing bisPOM onto the hydroxyl group of drugs or inhibitors utilizes the direct condensation of a hydroxyl compound with bisPOM-phosphate in the presence of a Mitsunobu reagent (Scheme 3.8).[179, 204] The synthesis of reagents used in this method: silver bisPOM phosphate and bisPOM phosphoric acid was shown in Scheme 3.7. However, the yield for this reaction is quite low, even for unhindered primary alcohols.[179, 231] One example of this method is illustrated in Scheme 3.7.[179]

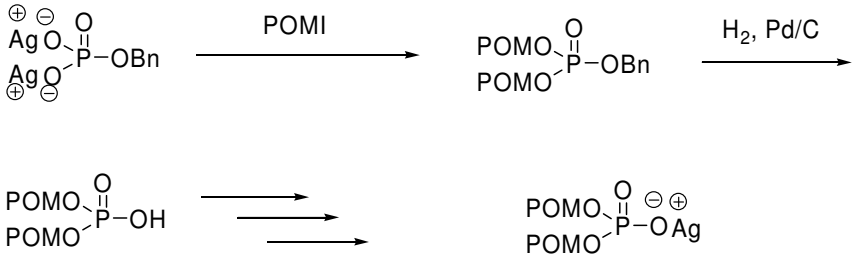

Scheme 3.7 The synthesis of silver bisPOM phosphate and bisPOM phosphoric acid[179]

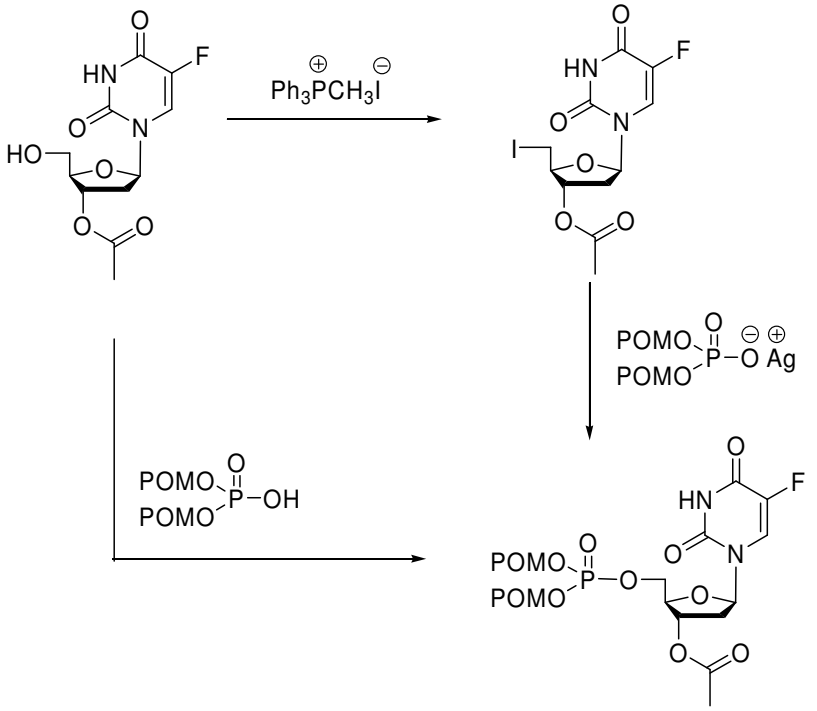

Scheme 3.8 The direct phosphorylation of the hydroxyl compound with bisPOM phosphate diester or bisPOM phosphoric acid[179]

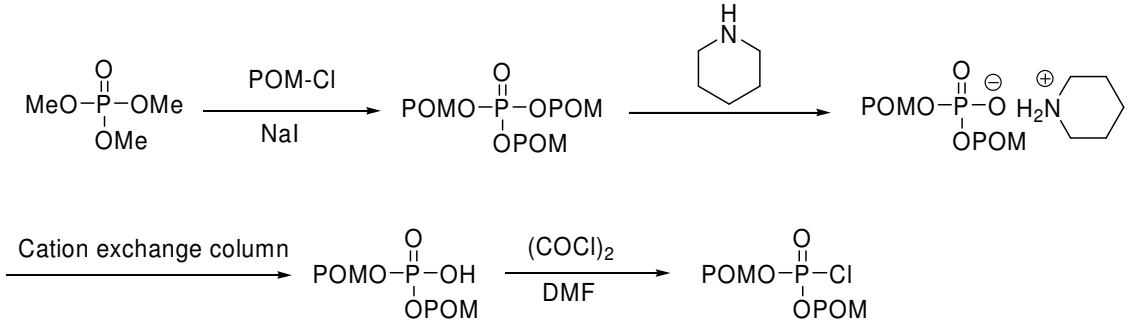

Scheme 3.9 Synthesis of bisPOM phosphoryl chloride[232]

The fourth method for preparing bisPOM prodrugs involves the direct phosphorylation of the hydroxyl compound using bisPOM-phosphoryl chloride (Scheme 3.9 and 3.10). Relatively high yields were achieved by this method for the synthesis of bisPOM-phosphoAZT and bisPOM-mannose-1-phosphate.[232] This method is particularly

useful since only one step is involved for the phosphorylation of the hydroxyl drug or inhibitor.

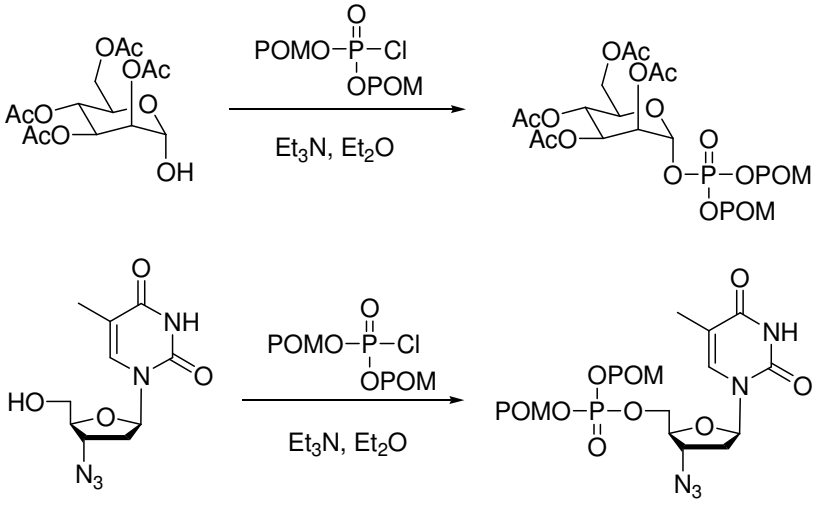

Scheme 3.10 Synthesis of bisPOM prodrug using bisPOM phosphoryl chloride[232]

3.4. Design of Phosphorylated Substrate-Analogue Inhibitors of Pin1

Cis-trans isomerization of proline-containing peptides has been implicated in a number of biologically important processes.[236] PPIase (Peptidyl-prolyl isomerase) enzymes catalyze the cis-trans isomerization of Xaa-Pro amide bonds in proteins.[236, 237] Pin1, a sub-type of PPIases,[37-39] is different from the other two PPIase families, the CyPs (cyclophilins) and the FKBPs (FK506 binding proteins).[236, 237] The CyPs and FKBPs are primarily of interest because they bind the immunosuppressant drugs, cyclosporin and FK506, respectively.[25] Pin1 isomerizes the prolyl residues preceded by phosphorylated Ser or Thr with selectivities up to 1300-fold greater (k_{cat}/K_m) over the nonphosphorylated peptides.[37, 39] Neither cyclophilins nor FKBPs effectively isomerize peptides with phosphorylated Xaa-Pro moieties.[37, 40]

Pin1 has been found to regulate mitosis through a simple conformational change.[39] Specifically, it is responsible for the cis-trans isomerization of phospho-Ser/Thr-Pro amide

bonds in a variety of key cell cycle regulatory phosphoproteins, including the Cdc25 phosphatase, the p53 oncogene, and the c-Myc oncogene.[39, 40, 58] Moreover, Pin1 is essential for regulation of mitosis from G2 to M stage.[40] Cells depleted of Pin1 are characterized by premature entry into mitosis, followed by mitotic arrest, nuclear fragmentation, and apoptosis. However, an overexpression of Pin1 inhibits the G2-to-M transition.[38, 40, 58, 238] Therefore, Pin1 acts as a negative regulator for mitotic activity in G2, preventing lethal premature entry into mitosis. Because Pin1 is present in higher concentrations during mitosis, it can be targeted primarily in the continuously dividing cancer cells.[68] In addition, Pin1 was found to be overexpressed in a large number of cancer cell types.[68] Therefore, Pin1 plays a vital role in the cell cycle, which makes it an ideal target for inhibition, both for discovery of anti-cancer drugs and for understanding the mechanisms of mitosis.

Alkenes as amide isosteres have been shown to be effective inhibitors of PPIases.[162, 165, 239] Alkenes as cis- and trans- amide isosteres have been designed and proven to be effective Pin1 inhibitors.[165] Previous studies in our group have shown that Pin1 binds the substrate analogue containing the cis-amide alkene isostere more tightly than the substrate analogue containing the trans-amide alkene isostere.[165] Specifically, two pentapeptide ground state analogue inhibitors **31**, **32** containing pSer-Ψ[(*Z*)CH=C]-Pro and pSer-Ψ[(*E*)CH=C]-Pro were synthesized and tested in both a protease-coupled PPIase assay and an A2780 ovarian cancer cell antiproliferative assay (Figure 3.10).[165] The Pin1 inhibition and antiproliferative activity data of compounds **31** and **32** revealed that the inhibitor of Pin1 containing the cis alkene isostere (IC_{50} = 1.3 μM against Pin1 and IC_{50} = 8.3 μM against A2780) was much more potent than the inhibitor containing the trans alkene isostere (IC_{50} = 28 μM against Pin1

and IC_{50} = 140 μM against A2780). Furthermore, X-ray structures of **31** and **32** bound in the catalytic site of Pin1 complement these inhibition results (X. J. Wang, Y. Zhang, J. P. Noel, F. A. Etzkoen, unpublished data). Based on our previous studies, only the cis alkene isostere pSer-Ψ[(*Z*)CH=C]-Pro was incorporated into the ground state analogue inhibitors of Pin1, **33** and **34** (Figure 3.11).

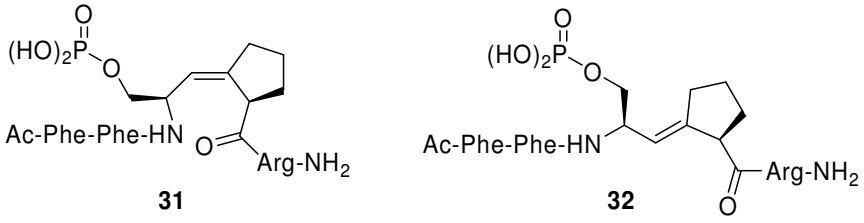

Figure 3.10 Two pentapeptide analogues inhibitors of Pin1 containing cis- and trans-amide alkene isosteres[165]

These X-ray structures of compounds **31** and **32** also show that the core pSer-Pro-Arg motif of both inhibitors was bound to the same catalytic site of Pin1. Interestingly, the two Phe residues at the N-termini of both inhibitors were disordered in the X-ray structures except for the carbonyl group (X. J. Wang, Y. Zhang, J. P. Noel, F. A. Etzkoen, unpublished data). Based on this observation, it was hypothesized that the core pSer-Ψ[(*Z*)CH=C]-Pro moiety would be sufficient for Pin1 enzymatic inhibition.

In order to develop a collection of more potent inhibitors of Pin1, different components flanking the pSer-Ψ[(*Z*)CH=C]-Pro core can be incorporated to obtain a small library. The docking of a series of inhibitors with various components flanking pSer-Ψ[(*Z*)CH=C]-Pro core into the catalytic site of Pin1 was studied in our group (Boobalan Pachaiyaooan, Felicia Etzkorn, unpublished data). The results of the computational study

demonstrated that compound **33** could be an efficient inhibitor of Pin1. In an effort to explore the methods to synthesize such a small library and to develop possible strategies to improve their inhibition against Pin1 and cancer cells, one ground state analogue inhibitor of Pin1, **33**, was designed as the basic target molecule. Due to the selectivity of Pin1 for the aromatic groups at both *N*- and *C*-termini,[39, 240, 241] Fmoc was designed for the *N*-terminus and tryptamine was designed for the C-terminus. Because of the negative charge of the phosphate group in inhibitors **31**-**33**, it is difficult for them to penetrate hydrophobic cell membranes. This, we believe, is the reason for the difference between the inhibition activity of Pin1 and the antiproliferative activity data of inhibitors **31**-**32**.[165] Therefore, a prodrug strategy was adopted to obtain more potent inhibitors. Based on the literature described above, the bisPOM prodrug strategy has proven to be particularly useful, since bisPOM derivatives are generally quite stable in buffer and plasma. More importantly, they are readily transformed to their free phosphate derivatives once they arrive inside the cells.[230, 232] Based on this information, a bisPOM-protected, ground-state-analogue inhibitor, **34**, was designed (Figure 3.11). By comparing the Pin1 inhibition activity and the A2780 cancer cell antiproliferative activities of these two inhibitors, we set out to learn whether the bisPOM prodrug strategy would be suitable here, which would provide an effective way to obtain more potent inhibitors of Pin1.

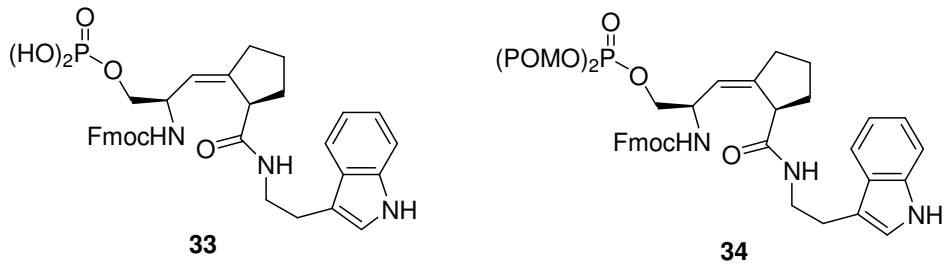

33 **34**

Figure 3.11 Designed phosphorylated Pin1 inhibitors without (**33**) and with (**34**) bis-POM prodrug masking group

Here we describe the synthesis of two Pin1 inhibitors containing pSer-Ψ[(*Z*)CH=C]-Pro isostere, **33** and **34**.. Their inhibition against Pin1 and antiproliferative activity towards human ovarian cancer cells *in vitro* are also reported. These inhibitors provide evidence to establish Pin1 as an anticancer drug target.

3.5. Synthesis of Fmoc BisPOM-pSer-Ψ[(Z)CH=C]-Pro-(2)-N-(3)-ethylaminoindole 34

Commonly, four general methods for the introduction of bisPOM onto free hydroxyl compounds have been described in section 3.3. The first two approaches involve 4-5 steps, beginning with hydroxyl compounds as the starting materials for synthesizing bisPOM protected phosphates. However, the overall yield from either of these approaches is routinely quite low (< 10%). Therefore, the third and fourth approaches were used in this study, since there is only one step required for the hydroxyl compounds. Because of the higher reactivity of bisPOM phosphoryl chloride compared to bisPOM phosphate, as well as the higher reported yields, the bisPOM phosphoryl chloride strategy was first explored to synthesize **34**.

BisPOM phosphate, **37**, was synthesized according to an established method (Scheme 3.11).[232] Commercially available trimethyl phosphate was used as the starting material.

Transesterification between an excess of chloromethyl pivalate and trimethyl phosphate was accomplished using NaI as the co-reagent in anhydrous acetonitrile under reflux.[242] Although it is very common for carboxylic esters, few examples for the transesterification of phosphorous esters have been reported in literature. The reaction on a large scale was quite slow and required one to two days to complete. It was also extremely sensitive to small amounts of water in the solvent, which may have resulted in poor yields. To improve the yield for the large scale reaction, anhydrous acetonitrile was used. The resulting trisPOM phosphate ester **35** was then partially hydrolyzed by treatment with piperidine, followed by cation exchange resin treatment to obtain the bisPOM phosphate **37**. It has been reported that secondary or tertiary amines can be used as dealkylating reagents for the selective hydrolysis of the tetraPOM ester of bisphosphonate.[243, 244] By optimizing reaction conditions and duration, it is even possible for piperidine to stop the hydrolysis quite selectively at the trisubstituted state for the bisphosphonate as the piperidinium salt in high yields.[243] The mechanism for this reaction can be understood if one considers the trisPOM phosphate ester as an *N*-alkylating reagent. In other words, the partially hydrolyzed product, bisPOM phosphate ester anion, forms an ionic bond with the trialkylammonium cation from the piperidine, which is insoluble in the reaction solvent and precipitates. Thus, no further hydrolysis of the bisPOM phosphate ester occurs.[243] The ammonium salt **36** formed can be easily converted to its acid form, bisPOM phosphoric acid, using a cation exchange resin. Because of their weak UV absorbance, PMA (Phosphomolybdic acid) was used for TLC (the thin-layer chromatography) studies of these intermediates. The synthesis of bisPOM phosphoric acid is outline in Scheme 3.11. Since it is very difficult to remove the piperidine

from the crude **36** completely, the yield for the reaction from **35** to **36** was always > 100%. For this reason, the percent yield was calculated for the two steps from **35** to **37**.

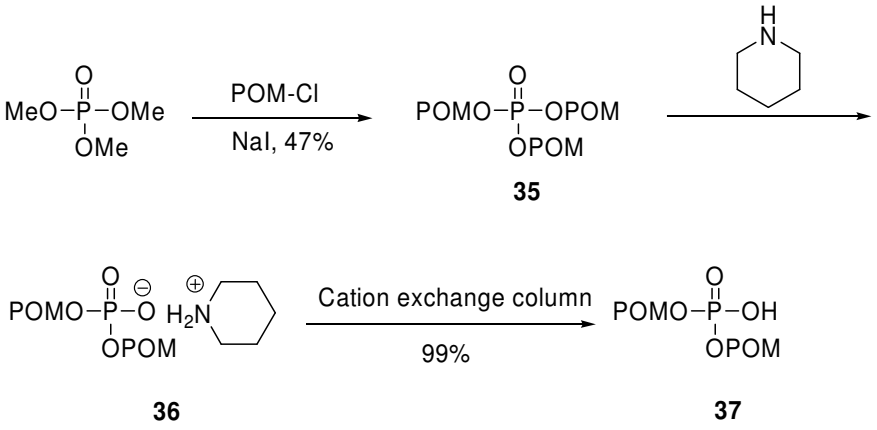

Scheme 3.11 Synthesis of bisPOM phosphate

Initially, bisPOM phosphoryl chloride **38** was prepared according to standard procedures.[232] However, we were unable to obtain the desired product during the phosphorylation step. To determine why, ^{31}P NMR was used to monitor the formation of the

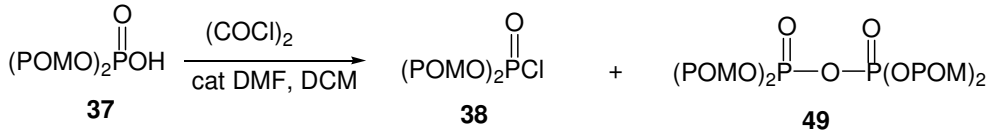

Scheme 3.12 Synthesis of bisPOM phosphoryl chloride **38**

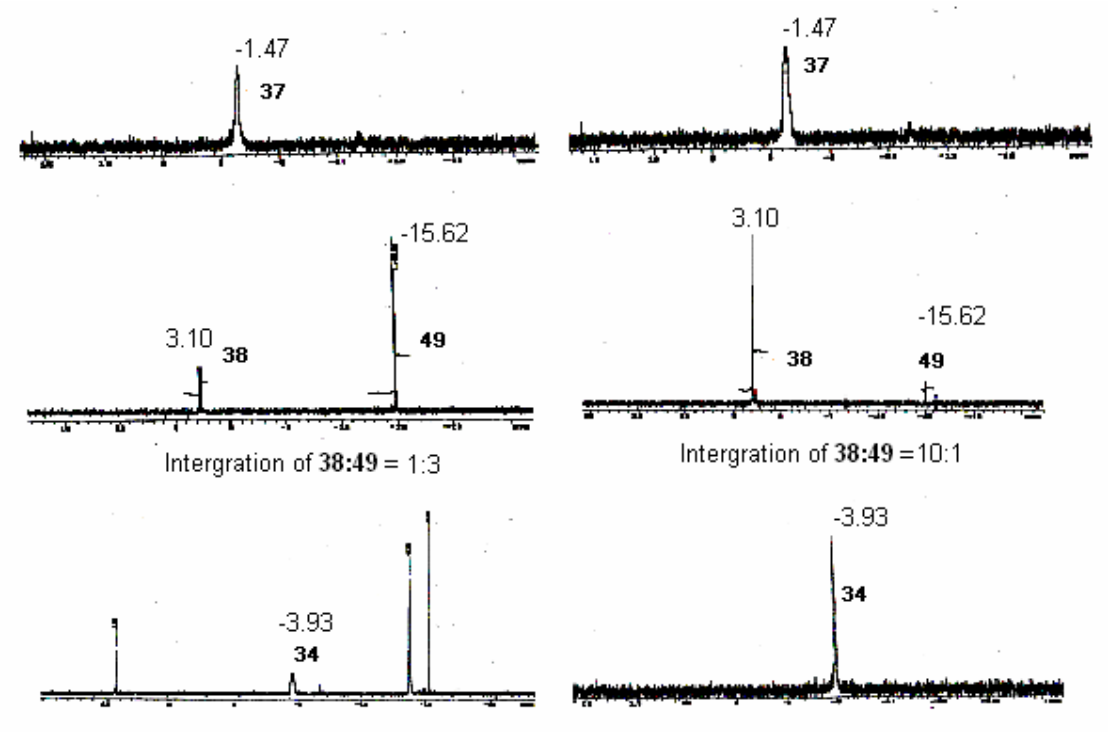

Figure 3.12. ^{31}P-NMR study of the phosphorylation step. **a**: $(COCl)_2$ was added to **37**, followed by DMF; **b**: **37** was added very slowly to the mixture of $(COCl)_2$ and DMF. **37**: bisPOM phosphate; **38**: BisPOM phosphoryl chloride; **49**: $(POM)_4$pyrophosphate; **34**: Fmoc-Ser(PO(OPOM)$_2$)-Ψ[(*Z*)CH=C]-Pro-(2)-*N*-(3)-ethylaminoindole.

bisPOM phosphoryl chloride **38** and the desired product **34** (Figure 3.11 and 3.12). In so doing we determined that the addition order of reagents was critical for the successful formation of the bisPOM phosphoryl chloride **38** (Figure 3.12). Specifically, if oxalyl chloride was added to the solution of bisPOM phosphoric acid **37**, the ^{31}P-NMR results showed that the formation of chloro bisPOM phosphate was not favored. Instead, pyrophosphate **49** was formed predominantly, which is not active towards phosphorylation of the intermediate **39**. The ratio of bisPOM phosphoryl chloride **38** to pyrophosphate **49** was 1:3. Therefore, the ^{31}P-NMR spectra results were quite complicated for the phosphorylation

step. The peak for the desired product (-3.80 ppm) was very minor compared with the other peaks. Instead, If the solution of bisPOM phosphoric acid **37** was added very slowly into the solution of oxalyl chloride in CH_2Cl_2 at 0 °C, the bisPOM phosphoryl chloride **38** was formed predominantly. In fact, only a small amount of the pyrophosphate product formed using this addition order, with the resulting ratio of bisPOM phosphoryl chloride **38** to pyrophosphate **49** at 10:1.[245] The bisPOM phosphoryl chloride was used immediately in the subsequent phosphorylation step because it was typically very unstable in storage.

Retrosynthetic analysis of the bisPOM-protected, phosphorylated compound, **34**, revealed that the key intermediate for the synthesis was the unphosphorylated intermediate **39** (Figure 3.13). Two synthetic routes based on differing protection strategies have been proposed for the synthesis of this key intermediate. Since the Fmoc protected Ser-Ψ[(*Z*)CH=C]-Pro-OH, **1**, isostere was readily available, it was used as the starting material. In the alternate proposed synthetic route, the bisPOM protecting group was introduced first, followed by a coupling reaction with tryptamine. The bisPOM would serve as the protecting group in the coupling reaction. By this method, the two steps of protection/deprotection during the reaction would be eliminated.

Because of the high reactivity of the hydroxyl group in Fmoc protected Ser-Ψ[(Z)CH=C]-Pro-OH isosteres, it is common to temporarily protect it during the reaction. However, there are examples in the literature that coupling reactions can proceed smoothly without any protecting group for the side chain hydroxyl groups of compounds containing a Ser, Thr or Tyr moiety.[246, 247] In order to eliminate the two protection and deprotection steps, a direct coupling between **1** and tryptamine was attempted. A model reaction using

Fmoc-Ser-OH as the starting material and EDC/HOAt as the coupling reagent was successful with high yield of product (Scheme 3.13).

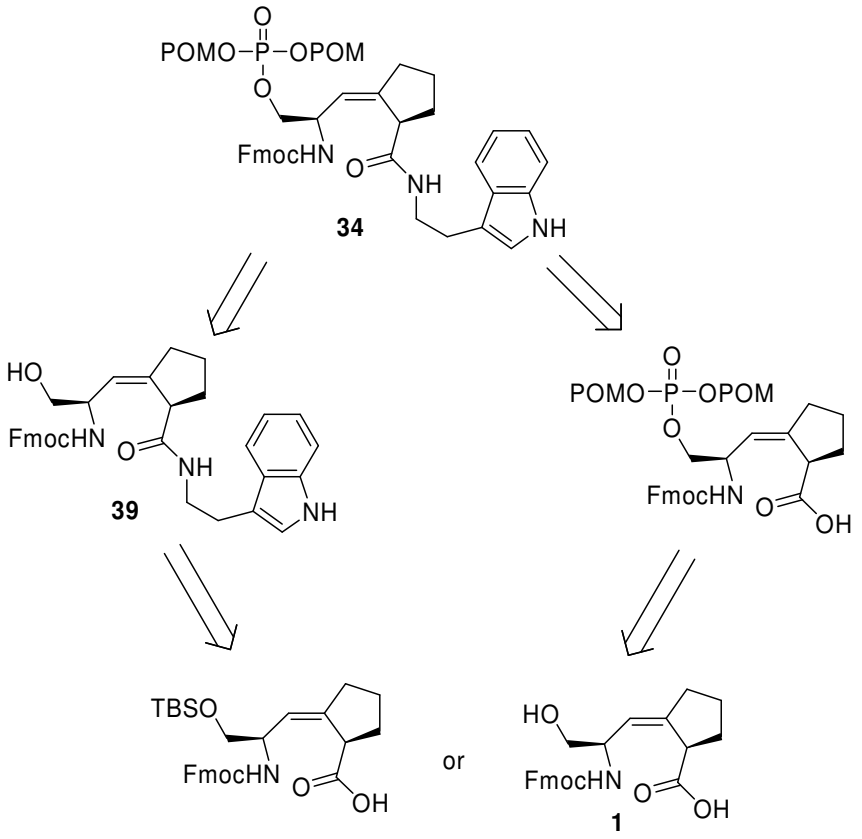

Figure 3.13 Retrosynthetic analysis of compound **34**

First, DIEA was used for this coupling reaction, which resulted in a very poor yield (ca. 30%). This was attributed to the possible formation of an 8-membered ring lactone from the trans esterification of the two Fmoc-Ser-OH molecules under basic conditions. Then, the coupling reaction without DIEA was tried, and a good yield (> 90%) was obtained with DMF as the solvent. DCM could not be used as the reaction solvent due to the low solubility of tryptamine in DCM. Based on these experiments, it was concluded that DIEA was not necessary for this coupling reaction, since tryptamine could act as the base.

The coupling reaction between Fmoc-SerΨ[(*Z*)CH=C]-Pro-OH, **1**, and tryptamine,

however, did not give amide **39** as the major product (Scheme 3.14). Instead, the 7-membered ring lactone **41** was produced in 55% yield. The formation of this lactone by-product was due to the internal esterification with tryptamine as the base. Clearly, such a low yield was unacceptable as the first step of the entire synthetic route.

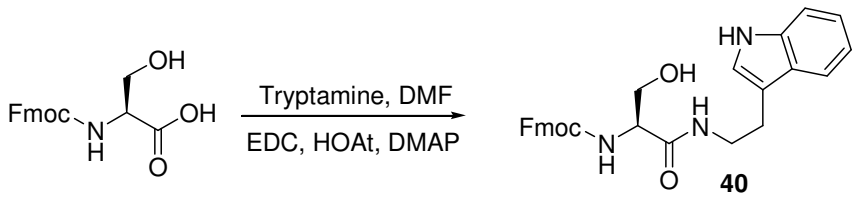

Scheme 3.13 Model reaction for the coupling with tryptamine

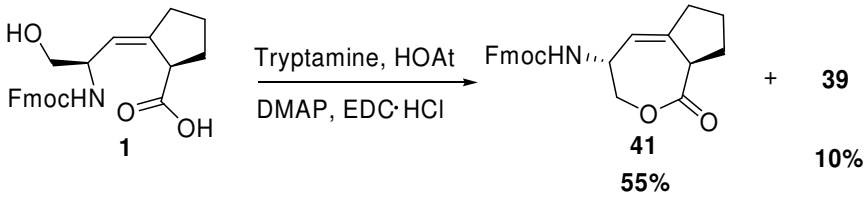

Scheme 3.14 Formation of 7-member ring lactone **41**

Different coupling reagents (e.g., HOAt and HATU, DCC, HOBt and HBTU) and a weaker base (2, 4, 6-collidine) were attempted in order to improve the yield of **39**. Despite various combinations, lactone **41** was still the major product with a yield exceeding 50%. From these results, we realized that the free hydroxyl group and the (*Z*)-alkene indeed affect the coupling reaction between **1** and tryptamine, thereby necessitating the use of a temporary protecting group. The synthesis of Fmoc-Ser(OTBS)Ψ[(*Z*)CH=C]-Pro-OH **42** was then attempted by reacting it with TBSCl (Scheme 3.15). With imidazole as the base in the reaction, we determined that the 7-membered ring lactone **41** was still the major product, with the yield < 25% for the desired product, **42**, which was also unacceptable.

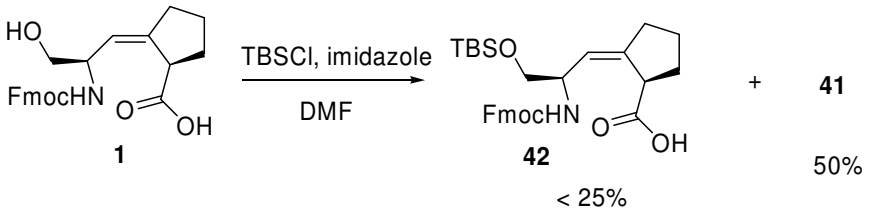

Scheme 3.15 Synthesis of Fmoc-Ser(TBS)Ψ[(*Z*)CH=C]-Pro-OH **42**

In order to synthesize **34**, we explored the possibility of introducing the bisPOM masking group first. A model reaction was run to test whether the phosphorylation would work without the use of a protecting group for the carboxylic group of **1**. Without any protecting group, the reaction between Fmoc-Ser-OH and acetic chloride led to the complex reaction (Scheme 3.16).

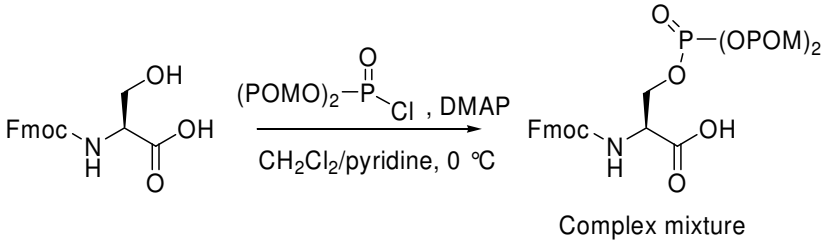

Scheme 3.16 Synthesis of Fmoc-Ser(bisPOM)-OH without protecting group

The second model reaction using TBS as the temporary protecting group in a "one pot" reaction was attempted (Scheme 3.17). In this procedure, Fmoc-Ser-OH was treated first with one equivalent of TBSCl and NMM (*N*-methyl morpholine), which selectively blocked the carboxyl group and left the side-chain hydroxyl group free. A mixture of Fmoc-Ser(bisPOM)-OH **43** and Fmoc-Ser(TBS)-OH **44** was obtained in 30% yields for each. To avoid the formation of Fmoc-Ser(TBS)-OH, the more labile temporary protecting group TMS was used, and the desired product **43** was synthesized successfully in 72% yield.

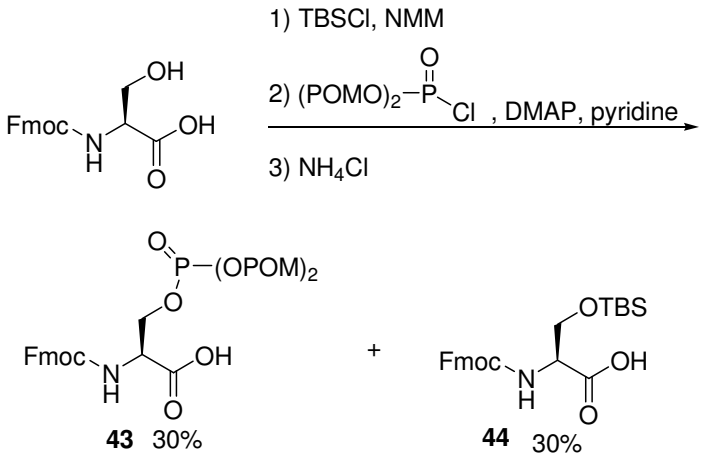

Scheme 3.17 Synthesis of Fmoc-Ser(bisPOM)-OH **43** with TBS as temporary protecting group

BisPOM phosphoryl chloride **38** was freshly prepared by a modification of the reported procedures.[232, 245] One equivalent of TMSCl was used to temporarily protect the carboxyl group of **1**, followed by the esterification of the hydroxyl group and bisPOM phosphoryl chloride **38** (Scheme 3.18). This reaction also produced the 7-membered ring lactone **41** as the major product.

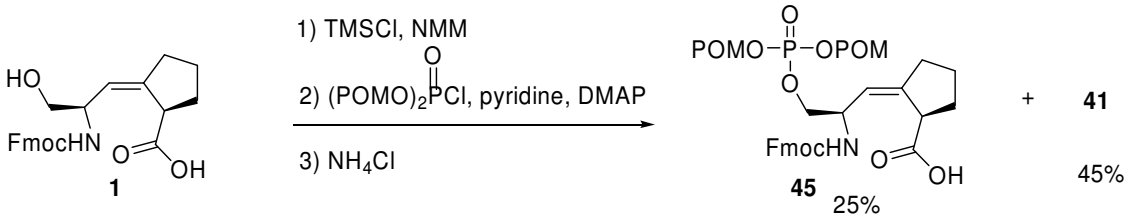

Scheme 3.18 Synthesis of Fmoc-Ser(bisPOM)Ψ[(*Z*)CH=C]-Pro-OH **45**

In summary, treating Fmoc-Ser(OH)Ψ[(*Z*)CH=C]-Pro-OH **1** with any base, including DIEA, collidine, imidazole, NMM or pyridine, resulted in the formation of the 7-membered ring lactone **41** as the major product.

In order to recover the Fmoc-Ser(OH)Ψ[(*Z*)CH=C]-Pro-OH **1** from the lactone **41**, the latter was hydrolyzed using 10% K_2CO_3 in a mixture of dioxane and H_2O (1:1) (Scheme 3.19). Analysis of the reaction mixture using LC-MS/MS showed that most of the lactone remained, while only 10% of the Fmoc-Ser(OH)Ψ[(*Z*)CH=C]-Pro-OH **1** was formed. Stronger hydrolytic conditions were not attempted since the Fmoc protecting group would be cleaved. These results imply that the reaction was reversible, and formation of the ring-opening product, Fmoc-SerΨ[(*Z*)CH=C]-Pro-OH, **1**, was not favored.

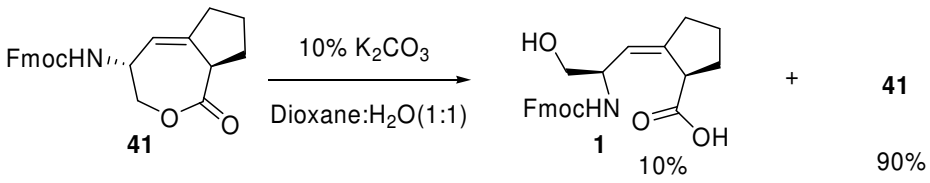

Scheme 3.19 Hydrolysis of lactone **41**

In order to circumvent the formation of the lactone during the synthesis of the bisPOM prodrug **34**, a different starting material, Boc-Ser(OH)-Ψ[(*Z*)CH=C]-Pro-OH **29**, was used. Protection of the side chain hydroxyl group with TBSCl was tried first (Scheme 3.20). Interestingly, no lactone byproduct formed during the reaction. Instead, the desired product Boc-Ser(TBS)-Ψ[(*Z*)CH=C]-Pro-OH **46** was obtained in 70% yield.

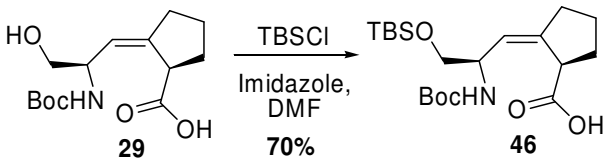

Scheme 3.20 Synthesis of Boc-Ser(TBS)-Ψ[(*Z*)CH=C]-Pro-OH **46**

Given the successful synthesis of **46**, an alternative synthetic route was designed for the bisPOM prodrug **34**, which is outlined in Schemes 3.20 and Scheme 3.21.

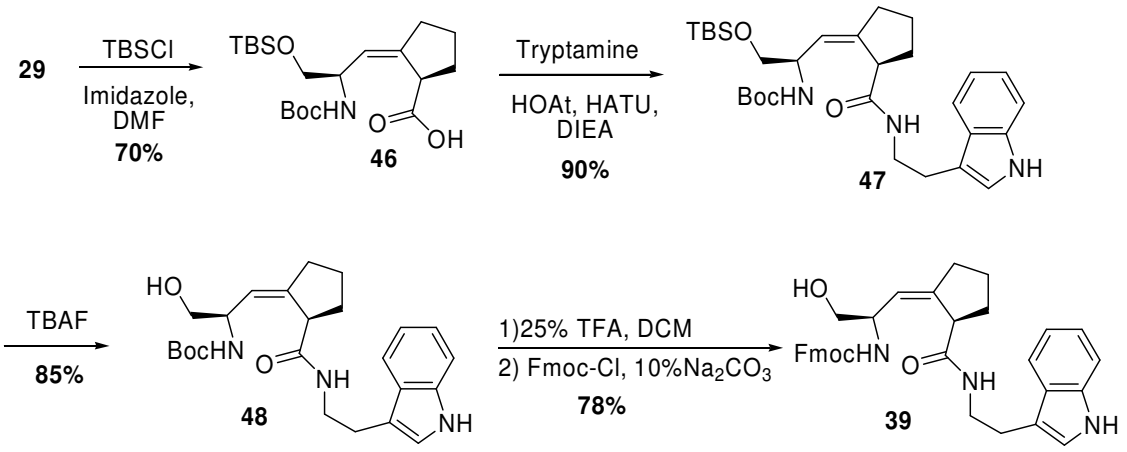

Scheme 3.21 Synthesis of the key intermediate **39**

The coupling reaction between **46** and tryptamine using HOAt and HATU as the coupling reagents in a solution reaction yielded **47** in 90% yield (Scheme 3.21). The TBS protecting group was cleaved using TBAF to afford **48** in an 85% yield. The Boc protecting group was then switched to Fmoc for the *N*-terminus of the mimic via a two-step reaction. Compared to the yield (only 52%) for Boc to Fmoc switch for Boc-Ser(OH)-Ψ[(*Z*)CH=C]-Pro-OH **29**, the yield was improved to 78% for Boc to Fmoc switch for compound **48** with tryptamine attached to the carboxyl group. The total yield for the conversion from **29** to **39** was 42%, which was much higher than the yield for the original synthetic route from **1** to **39** (10%).

The introduction of a bisPOM masking group to the hydroxyl group of **39** was first attempted using bisPOM phosphate **37** with DIC (diisopropylcarbodiimide) and HOAt as the coupling reagents (Scheme 3.22).[179, 227] ^{31}P-NMR was used to monitor the reaction progress. Even after two days, there was no phosphorus peak for the desired product (-3.8 to -4.0 ppm predicted from the calculation by ACD/XNMR predictor™, experimental value -3.93 ppm).

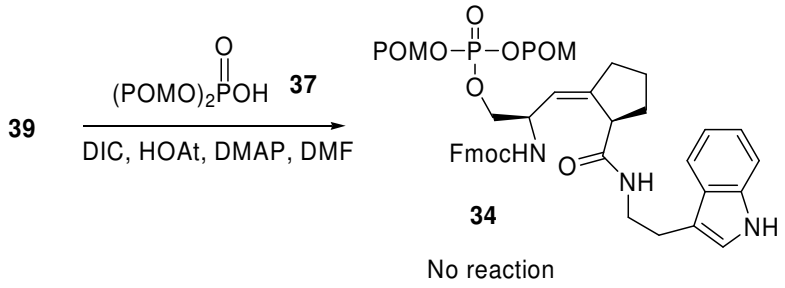

Scheme 3.22 Phosphorylation using bisPOM phosphate **37**

We then used the bisPOM phosphoryl chloride method to synthesize the bisPOM prodrug **34** since only one step was necessary to synthesize the required bisPOM phosphate. Moreover, reported yields have generally been higher using this method than the other two previously described. The phosphorylation of the model compound Fmoc-Ser-tryptamine, **40**, using a large excess of pyridine and bisPOM phosphoryl chloride, afforded Fmoc-bisPOM-Ser-tryptamine, **52,** as the major product in a 52% yield. The structure of **52** was shown in Scheme 3.25. ^{31}P-NMR was used in the phosphorylation step to monitor the formation of **34**.

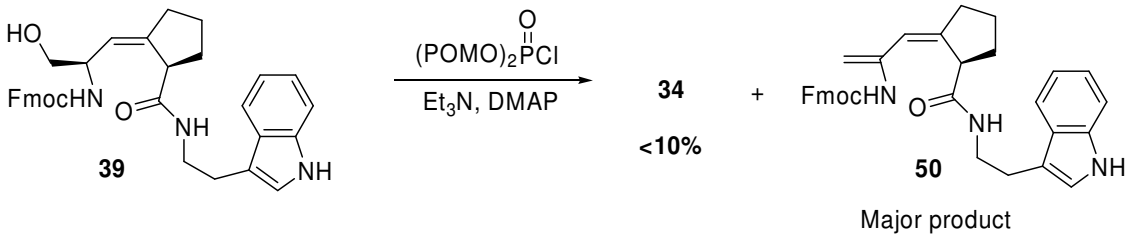

Scheme 3.23 Synthesis of **34** using Et_3N

The synthesis of **34** via reaction of **39** with bisPOM phosphoryl chloride using triethylamine was problematic, affording only a 10-20% yield of **34** under optimized

conditions (Scheme 3.23). Instead, the β elimination product was obtained as the major product from this reaction. Therefore, different weaker bases were tried in the phosphorylation step, and the results are shown in Table 3.1.

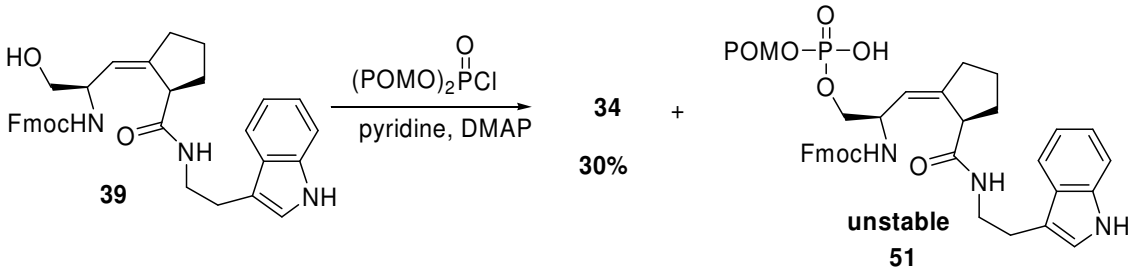

Scheme 3.24 Synthesis of bisPOM prodrug **34** using a large excess of pyridine

Base	Temperature	Yield
Et_3N	-40 °C	< 20%
Et_3N	rt	< 10%
DIEA	rt	< 20%
collidine	rt	< 20%
NMM	rt	< 20%
Pyridine (8 equivalents)	-40 °C	20%
Pyridine (8 equivalents)	rt	25%
Pyridine (large excess)	-40 °C	22%
Pyridine (large excess)	rt	30%

Table 3.1. Yields for the phosphorylation step of **39** using different bases.

These results indicated that a large excess of pyridine was the best choice for the phosphorylation step (Scheme 3.24). Moreover, an addition of a second batch of freshly

prepared bisPOM phosphoryl chloride slightly improved the yield; even so, the yield for the desired product **34** was still only 30%. LC-MS analysis of the crude product from the reaction showed that the mono-POM phosphate, **51,** was also formed, with most of the starting material recovered. No elimination product was observed with pyridine as the base. However, relatively high yield (52%) was achieved for model reaction of Fmoc-Ser-tryptamine, **40**, with bisPOM phosphoryl chloride. These results imply that a steric effect, which prevented the bulky bisPOM phosphate reagent **38** from approaching the hindered hydroxyl group of **39,** might have led to the poor yield we observed. It should also be noted that during the purification step using semi-prep HPLC, the mono POM phosphate product decomposed on the column. An intramolucular nucleophilic reaction was thought to be the reason for the unstability of mono POM phosphate product.

The bisPOM prodrug **34** was purified by reverse phase HPLC as a white solid.

3.6. Synthesis of Fmoc-pSer-Ψ[(Z)CH=C]-Pro-(2)-N-(3)-ethylaminoindole 33

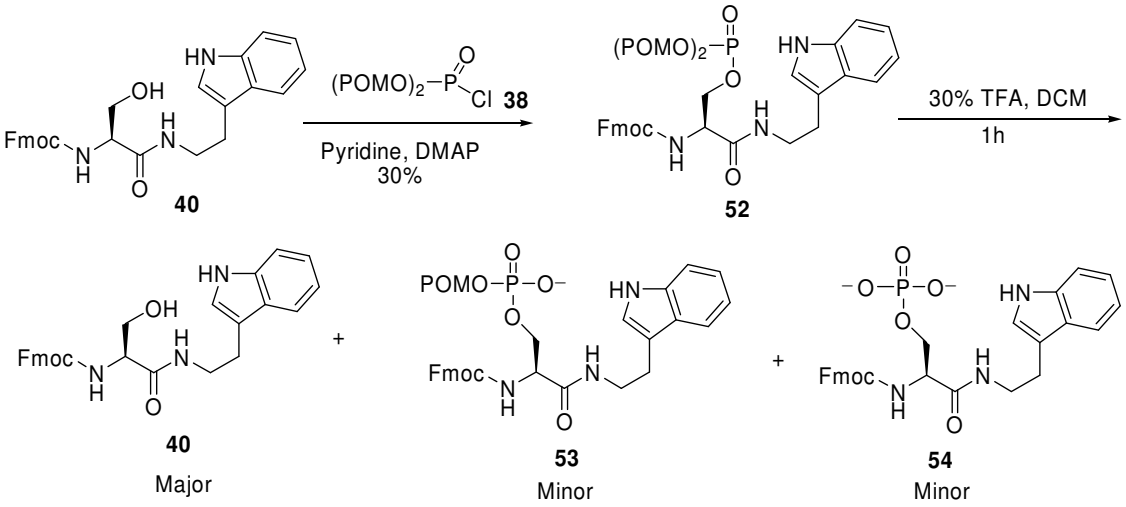

Scheme 3.25 Synthesis of bisPOM protected Fmoc-Ser-tryptamine **52** and hydrolysis of bisPOM Fmoc-Ser-tryptamine **52**

Three approaches were attempted for the synthesis of the unprotected phosphodipeptide isostere **33**. Since the bisPOM protected dipeptide isostere **34** was already available, we thought that it might work to deprotect the POM groups from the prodrug **34** to afford the unprotected phosphate **33**. To test this possibility, one model reaction was run using Fmoc-Ser(OH)-tryptamine **40** as the starting material. The phosphorylation of Fmoc-Ser(OH)-Tryptamine **40** was accomplished using bisPOM phosphoryl chloride **38**. The yield for the reaction was 30% (Scheme 3.25). Subsequently, 30% TFA in CH_2Cl_2 was used to deprotect the POM groups from **52**. LC-MS was used to monitor the reaction progress, which showed that after one hour at room temperature, three products were generated. The major product was the Fmoc-Ser(OH)-tryptamine **40**; the monoPOM protected product was the second most abundant, and only a very small amount of unprotected product was observed. Thus, the formation of the desired unprotected product was not favored under the reaction conditions. Surprisingly, no β elimination product was observed.

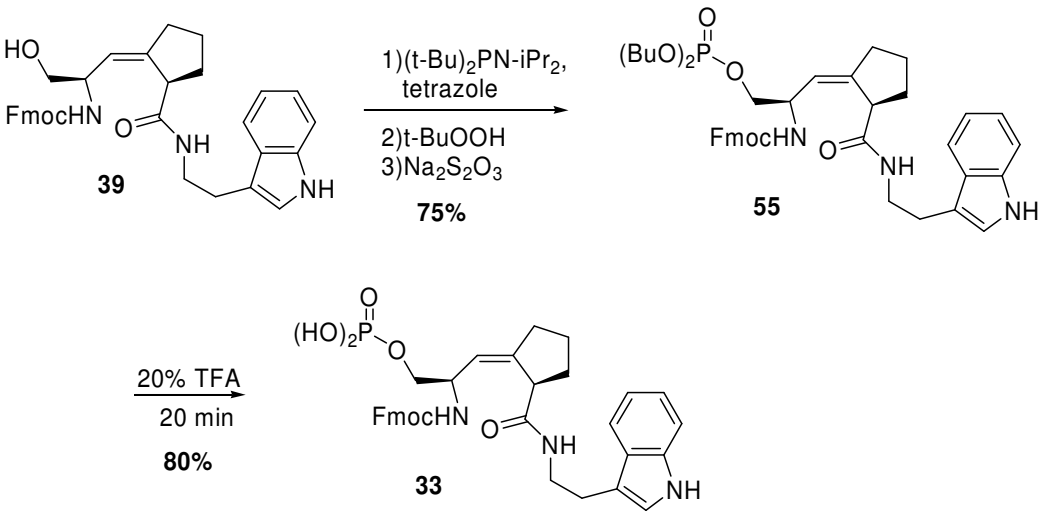

Scheme 3.26 Synthesis of **33**

The synthesis of **33** was accomplished using Boc-Ser-Ψ[(*Z*)CH=C]-Pro-tryptamine **39** as the starting material (Scheme 3.26). Phosphorylation of **39** was accomplished in a "one pot" reaction. Phosphitylation of **39** by *tert*-butyl diisopropylphosphoramidite and 5-ethylthio-1H-tetrazole, followed by oxidation with *tert*-butyl hydroperoxide afforded the *tert*-butyl protected phosphodipeptide isostere **55**. An excess of *tert*-butyl hydroperoxide was removed by washing with aqueous $Na_2S_2O_3$. We attempted to purify the crude product prior to the deprotection step, however it was unstable and decomposed on a silica gel column. Therefore, no purification was carried out before the final deprotection step. In the final step, 20% TFA in CH_2Cl_2 was used to remove the tert-butyl protecting group to afford the unprotected phosphodipeptide isostere **33**. The crude product was purified by reverse phase HPLC on a C18 semi-prep column to afford **33** as a white solid in 60% yield for the two step phosphorylation reaction.

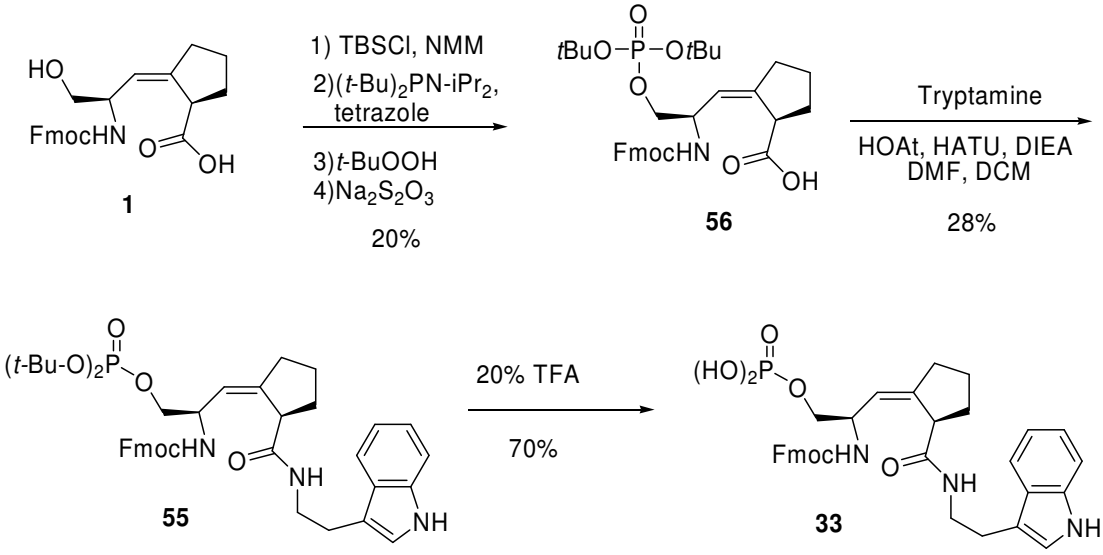

Scheme 3.27 Alternative route for the synthesis of **33**

We also synthesized the unprotected dipeptide isostere **33** using a different synthetic

route, prior to successfully establishing the efficient synthetic route for intermediate **39** (Scheme 3.27). Because the phosphorylation reaction would be run after synthesizing **39**, we thought that it might work if phosphorylation was accomplished first prior to the coupling step with tryptamine. This would place the protecting group on the hydroxyl group of the Ser and eliminate one deprotection step. Therefore, *tert*-butyl diisopropylphosphoramidite was used to phosphorylate Fmoc-SerΨ[(*Z*)CH=C]-Pro-OH, compound **1** in a "one pot" reaction (Scheme 3.27). One equivalent of TBSCl and NMM was used to selectively block the carboxyl group and leave the side chain hydroxyl group free. Phosphitylation by *tert*-butyl diisopropylphosphoramidite and 5-ethylthio-1H-tetrazole followed by oxidation with *tert*-butyl hydroperoxide and an aqueous acid work-up, thereby affording the *tert*-butyl protected phosphodipeptide isostere **56** in a 20% yield. The formation of 7-membered ring lactone, **41** was also observed as in the phosphorylation of Scheme 3.26. The formation of the 7-membered ring lactone, **41** was partly responsible for the low yield. The subsequent coupling reaction between **56** and tryptamine with EDC and HOAt gave the phosphodipeptide isostere **55** in a 28% yield. Steric effect may explain the low yield for the coupling reaction. Cleavage of **55** with 20% TFA gave the desired product **33** in 2.2% overall yield starting from **1**.

In summary, the efficient synthesis of compound **33** was achieved using intermediate **39** as the starting material. Phosphorylation followed by deprotection, which afforded the desired product **33** in an overall yield of 60%.

3.7. Pin1 Inhibition Studies of Inhibitor 33

Several PPIase inhibition studies have been reported.[20, 248, 249] For example, Rich et al. developed a protease-coupled assay for CyP and FKBP,[249] which we later modified to be used for Pin1[165] (Scheme 3.28). As shown in this scheme, the proteases, trypsin and chymotrypsin selectively cleave the amide bond between the P2' and P3' positions of Xaa-*trans*-Pro-containing peptides.[250] For this reason, the amide bonds between the P2' and P3' positions with a cis conformation have to isomerize to their trans conformation before they can be cleaved. Such conformational specificity was manipulated to measure the activity of PPIases.[249]

In our study, commercially available Suc-Ala-Glu-Pro-Phe-pNA was used as the substrate of Pin1.[165] The p-nitroanilide group was cleaved from the Suc-Ala-Glu-*cis*-Pro-Phe-pNA by α-chymotrypsin and its release was monitored by UV-VIS spectrometry at four different wavelengths (390 nm, 395 nm, 400 nm, 410 nm).[165] A large excess of α-chymotrypsin (60 mg/ml) was used in the assay to ensure that the cleavage step proceeded rapidly. Therefore, the rate limiting step in this assay was the isomerization step of Suc-Ala-Glu-*cis*-Pro-Phe-pNA to Suc-Ala-Glu-*trans*-Pro-Phe-pNA, and the rate for the isomerization was equal to the rate of the release of pNA.[165] In order to minimize the background thermal isomerization rate, the assay was run at 4 °C. The thermal isomerization rate was measured under the same conditions as in the assay, except that no Pin1 was added.

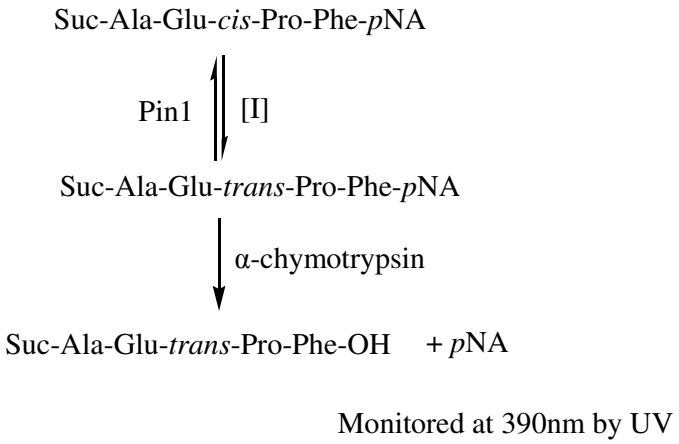

Scheme 3.28 Pin1 PPIase inhibition assay[165]

Although a peptide containing a pSer/pThr-Pro motif, such as AcFFpSPR-pNA, is generally a better substrate for Pin1 and has a higher k_{cat}/K_m value, the peptide we used in our assay, Suc-AEPF-pNA, was a satisfactory Pin1 substrate (k_{cat}/K_m = 3,410 mM^{-1}). Because glutamic acid contains a negative charge on the side chain, it mimics the phospho-serine. One advantage of this substrate is that the *C*-terminal phenylalanine makes it a specific substrate for α-chymotrypsin instead of trypsin, which can degrade Pin1.[20]

The Glu-Pro amide bond in the substrate exists 90% as the trans form in aqueous solution. Therefore, only 10% of the substrate concentration can be used, which results in a poor S/N ratio. Rich et al. improved this process by increasing the concentration of the cis Glu-Pro isomer on the peptide substrate up to 70% using TFE containing 0.47 M LiCl as the substrate solvent.[251] The Pin1 assay was conducted at a pH of 7.8 to ensure that the inhibitor existed in its diionized phosphate form, which is the actual physiological pH. Generally, a typical cis-trans isomerization of the substrate is complete in 90 seconds. In order to obtain the IC_{50} values of the inhibitor, the concentrations of Pin1 and the substrate were kept constant. Varying concentrations of inhibitor were pre-incubated with Pin1 in the

buffer for 2 min at 4 °C,[165] after which the percent inhibition was calculated using the following equation:

$$\% \text{ inhibition} = 100 \times (1 - (k_{obs,I} - k_{thermal})/(k_{obs,Pin1} - k_{thermal}))$$

Where $k_{obs,\ I}$ is the first-order rate constant in the presence of both Pin1 and the inhibitor, $k_{obs,Pin1}$ is the first-order rate constant in the presence of Pin1 without the inhibitor, and $k_{thermal}$ refers to the rate constant without both Pin1 and the inhibitor.

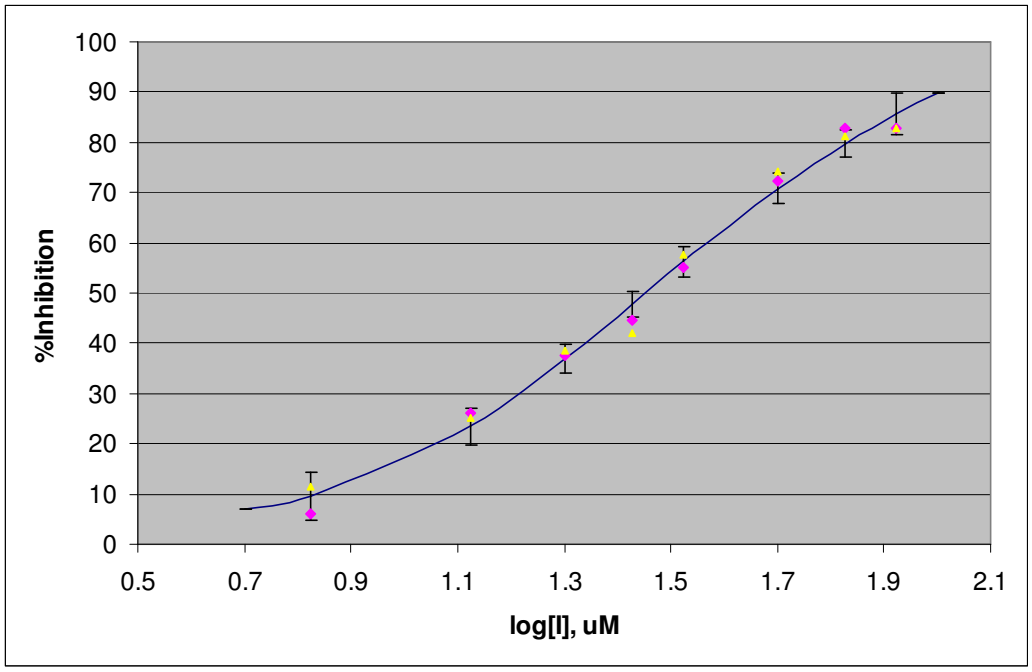

Figure 3.14 Dose response curve. Blue: inhibition against Pin1 by unprotected inhibitor **33**(IC_{50} = 24.8 ± 2.0 μM, ♦ and ▲).

The inhibition of compound **33** against Pin1 was measured in this Pin1 PPIase coupled assay *in vitro* (Figure 3.14). A plot of the percent % inhibition vs ln[I] produces a sigmoid curve, which was fit to a dose response curve. The IC_{50} value was calculated by plotting all of the data (percent inhibition of the Pin1 activity at different concentrations of inhibitor **33** in

the assay) in TableCurve^{TM} (Figure 3.14). The IC_{50} of inhibitor **33** against Pin1 was calculated to be 24.8 ± 2.0 μM.

3.8. Antiproliferative Activity of A2780 Studies of 33 and 34

In order to test if the bisPOM strategy would improve the cell permeability of inhibitor **33** through its hydrophobic cell membrane, compound **33** and compound **34** were tested for their antiproliferative activities towards A2780 ovarian cancer cells, as previously reported.[252, 253] IC_{50} values of **33** and **34** were obtained by plotting their percent inhibitions at different final concentrations in Tablecurve (Figure 3.15). IC_{50} values of **33** and **34** against A2780 were calculated to be 46.2 ± 3.0 μM and 26.9 ± 1.5 μM, respectively (Table 3.2).

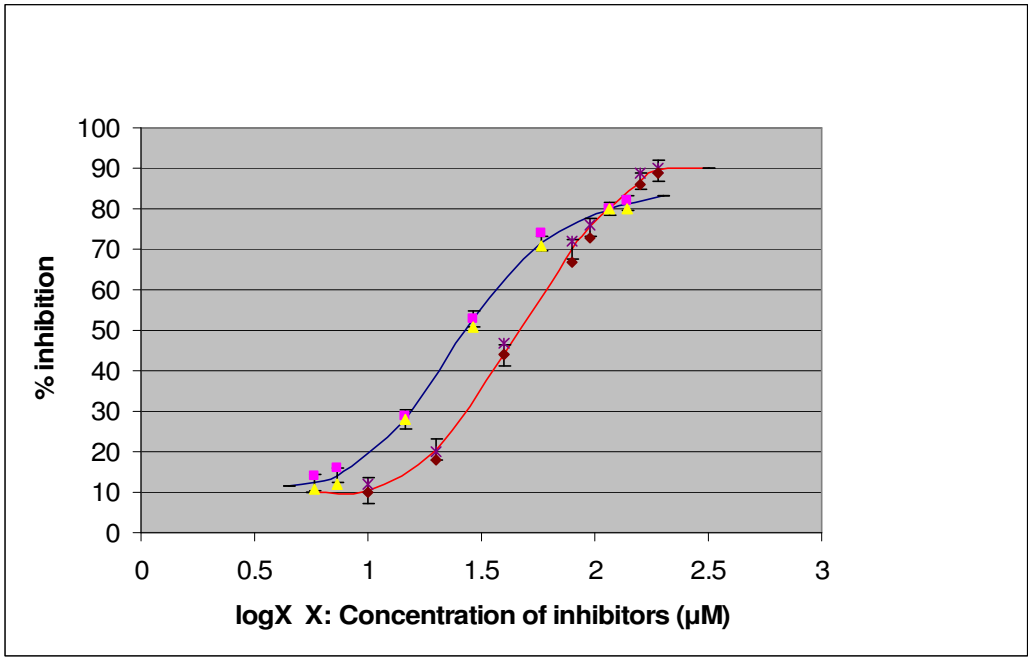

Figure 3.15. Dose Response curve. Blue: inhibition of antiproliferative activity against A2780 ovarian cancer cells by unprotected compound **33** (IC_{50} = 46.2 ± 3.0 μM, ■ and ▲). Red: inhibition of antiproliferative activity against A2780 ovarian cancer cells by bisPOM protected compound **34** (IC_{50} = 26.9 ± 1.5 μM, ♦ and *).

Table 3.2 Inhibition of Pin1 PPIase enzymatic activity and antiproliferative activity towards A2780 ovarian cancer cells for compounds **33** and **34**

Compound	Inhibition of Pin1 PPIase activity IC_{50} (μM)	Inhibition of A2780 proliferative activity IC_{50} (μM)
33	28.3 ± 2.1	46.2 ± 3.0
34	Not measured	26.9 ± 1.5

From the IC_{50} values of compound **33** and compound **34** towards A2780 ovarian cancer cells, an activity decrease of about twofold was observed for unmasked phosphate inhibitor **33** (46.2 ± 3.0 μM in cell based assay) compared to its IC_{50} value (28.3 ± 2.1 μM) in our Pin1 protease-coupled PPIase assay. The IC_{50} value of the bisPOM prodrug **34** was 26.9 ± 1.5 μM in the cell based assay, is the same as the IC_{50} value for the unprotected phosphate inhibitor **33** in the Pin1 protease-coupled PPIase assay. This result suggests that the introduction of a bis(POM) protection group on the phosphate of compound **34** helps entry into the cell by neutralizing the negative charge on the phosphate. However, only 1.7 fold difference in their IC_{50} values in the cell based assay also implies that the cell permeability of the free phosphate inhibitors of Pin1 is not a major issue that affects their potentency.

In addition, the IC_{50} value of compound **34** in our cell-based assay was comparable to the IC_{50} value of compound **33** in the Pin1 *in vitro* inhibition assay. This implies that the inhibition of Pin1 cause the inhibition of the proliferative activity towards A2780 ovarian cancer cells. The bis(POM) protection group helps the inhibitor penetrate the hydrophobic cell membrane very effectively, thereby verifying the role of Pin1 as a potential anticancer drug target.

3.9. Conclusions

We designed one ground state analogue inhibitor of Pin1, Fmoc-Ser($PO(OH)_2$)-Ψ[(*Z*)CH=C]-Pro-(2)-*N*-(3)-ethylaminoindole **33**, and its bisPOM prodrug Fmoc-Ser($PO(OPOM)_2$)-Ψ[(*Z*)CH=C]-Pro-(2)-*N*-(3)-ethylaminoindole **34**. The key intermediate, **39**, was synthesized efficiently using Boc-SerΨ[(*Z*)CH=C]-Pro-OH **29** as the starting material. Target compounds **33** and **34** were synthesized in yields of 24% and 12%, respectively from **29**.

We demonstrated that **33** showed a moderate inhibition towards PPIase Pin1 (IC_{50} = 28.3 ± 2.1 μM) by protease-coupled assay in vitro. **33** also inhibited A2780 ovarian cancer cell growth in vitro (IC_{50} = 46.2 ± 3.0 μM). The antiproliferative activity towards A2780 ovarian cancer cells of charged **33** was improved in **34** (IC_{50} = 26.9 ± 1.5 μM) by masking the charged phosphate with bisPOM protection group. This suggests that the bisPOM strategy is very efficient for improving the cell permeability of inhibitors of Pin1. These two inhibitors also provide additional evidence for establishing Pin1 as a potential anticancer drug target.

Experimental

General

Unless otherwise indicated, all reactions were carried out under N_2 in flame-dried glassware. THF and CH_2Cl_2 were dried by passage through alumina. Anhydrous (99.8%) DMF was available commercially and used directly from SureSeal™ bottles. Dimethyl sulfoxide (DMSO) was anhydrous and dried with 4 Å molecular sieves. Triethylamine (TEA) was distilled from CaH_2, and oxalyl chloride $(COCl)_2$ was distilled before each use.

Diisopropylethylamine (DIEA) was distilled from CaH_2 under a N_2 atmosphere. Brine, $NaHCO_3$, and NH_4Cl refer to saturated aqueous solutions unless otherwise noted. Flash chromatography was performed on 32-63 μm or 230-400 mesh, ASTM silica gel with reagent grade solvents. NMR spectra were obtained at room temperature in $CDCl_3$ unless otherwise noted. Proton (400 MHz) NMR spectra, carbon-13 (75 MHz) NMR spectra and phosphorus-31 (75 MHz) NMR spectra were measured on a Varian NMR spectrometer. Proton (500 MHz) NMR spectra, and carbon-13 (125 MHz) NMR spectra were measured on a JEOL NMR spectrometer. ^{1}H NMR spectra are reported as a chemical shift (multiplicity, coupling constant in Hz, number of proton). Rotamer peaks are indicated by listing ^{1}H chemical shifts separately; for ^{13}C the minor rotamer peak is listed in parentheses. Coupling constant *J* values are given in Hz. Electrospray ionization (ESI-MS) was carried out on a triple quadrupole ThermoFinnigan TSQ MS. Human Pin1 recombinant protein was prepared as described.[165] Analytical reverse phase liquid chromatography (RP-HPLC) was performed on a RP C18, 100 × 4.6 mm, 5 μm column (Varian Solaris). Preparative HPLC was performed using on a RP C18, 250 × 21.4 mm, 5 μm (Varian Solaris). HPLC solvents were A: water, B: CH_3CN. UV detection was performed at 220 nm unless otherwise noted.

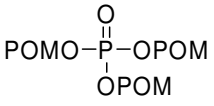

Tris(POM) phosphate, 35. Trimethyl phosphate (3.00 g, 21.4 mmol) was dissolved in anhydrous acetonitrile (18 mL), followed by adding chloromethyl pivalate (12.6 g, 83.4 mmol) and NaI (9.6 g, 64 mmol) sequentially. The reaction mixture was refluxed for 2 days. The cooled reaction mixture was diluted with Et_2O (200 mL), and the organic layer was washed with water (3 × 50 mL), brine (50 mL), dried over anhydrous Na_2SO_4 and

concentrated to afford a 10.1 g crude product. The crude product was purified by silica gel column chromatography (Hexanes:Ethyl acetate = 85:15) to afford 4.4 g of tris(POM) phosphate **35** as viscous oil (47% yield). ^{1}H NMR ($CDCl_3$) δ 5.66 (d, *J* = 13.7, 6H), 1.23 (s, 27H). ^{31}P NMR ($CDCl_3$) δ –4.12 (s).

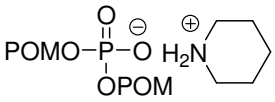

Complex of bisPOM phosphate and piperidine, 36. Tris(POM) phosphate **35** (0.50 g, 1.4 mmol) was dissolved in piperidine (3.50 mL) and the reaction mixture was stirred at rt for 24 h. The piperidine was removed by rotary evaporation and further evaporated at high vacuum until constant weight was obtained. (0.730 g, 157.0% yield). ^{1}H NMR ($CDCl_3$) δ 5.52 (d, *J* = 12.1, 4H), 2.98 (m, 6H), 2.50 (m, 2H), 1.73 (m, 6H), 1.56 (m, 6H), 1.17 (s, 18H). ^{31}P NMR ($CDCl_3$) δ –3.28 (s).

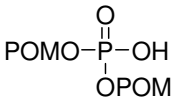

BisPOM phosphate, 37. A cation exchange column was prepared by swirling 45 mL of Dowex 50 × 8-400 ion exchange resin with distilled water (100 mL). The resin was rinsed using distilled water until the eluted solution became clear. The complex of BisPOM phosphate and piperidine **36** (0.45 g, 1.1 mmol) containing 30% piperidine was dissolved in distilled H_2O, after which it was loaded onto the cation exchange column. Distilled water was used to elute the bisPOM phosphoric acid from the column. The eluent was collected until its pH reached 7.0. The elutions were combined, frozen, and lyophilized to afford bisPOM phosphate **37** as a white solid (0.26 g, 99% yield). ^{1}H NMR ($CDCl_3$) δ 8.62 (br s, 1H), 5.60 (d, *J* = 14.2, 4H), 1.20 (s, 18H). ^{13}C NMR ($CDCl_3$) δ 176.9, 82.91, 82.85, 38.92, 26.95 ppm. ^{31}P NMR ($CDCl_3$) δ –1.47 (s).

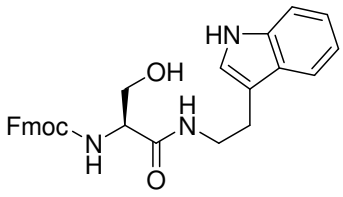

Fmoc-Ser(OH)-tryptamine, 40. Fmoc-Ser-OH (327 mg, 1.00 mmol) was dissolved in DMF (25 mL) and cooled to 0 °C for 5minutes. HOAt (135 mg, 1.00 mmol) and EDC • HCl (210 mg, 1.10 mmol) were added to the solution sequentially. Finally, tryptamine (176 mg, 1.10 mmol) was slowly added into the solution followed by the addition of DMAP (134 mg, 0.100 mmol). The reaction was then stirred at rt for 3 h. The reaction was diluted with 250 mL of ethyl acetate. The organic layer was washed with water (2 × 50 mL) and brine (50 mL) and concentrated by rotary evaporation. The product was purified by flash chromatography (DCM:MeOH = 96:4) to afford Fmoc-Ser(OH)-tryptamine **40** as a pale yellow solid (440 mg, 95%). ^{1}H-NMR ($CDCl_3$), δ 7.53 (d, *J* = 8.1, 2H), 7.39 (app t, *J* = 5.6, 2H), 7.16 (m, 4H), 7.06 (m, 2H), 6.93 (app t, *J* = 7.5, 1H), 6.84 (m, 2H), 6.52 (d, *J* = 7.7, 1H), 6.17 (br s, 1H), 4.43 (br s, 1H), 4.12 (m, 3H), 3.96 (m, 1H), 3.80 (m, 1H), 3.65 (m, 1H), 3.39 (d, *J* = 7.1, 2H), 2.77 (t, *J* = 7.1, 2H). ^{13}C NMR ($CDCl_3$) δ 171.0, 162.8, 143.9, 141.2, 136.7, 128.9, 127.8, 127.4, 127.2, 125.3, 122.8, 121.5, 121.1, 119.9, 119.0, 118.5, 112.1, 111.6, 67.1, 63.0, 47.2, 40.1, 36.4, 31.4 ppm.

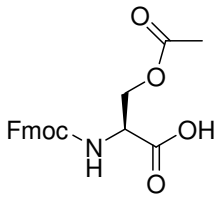

Fmoc-Ser(OAc)-OH: To a solution of Fmoc-Ser(OH)-OH (200 mg, 0.611 mmol) in 4 mL THF, *N*-methylmorpholine (67 μL, 0.61 mmol) was added followed by TBSCl (92 mg, 0.61 mmol) at 0 °C. The reaction became cloudy, after which it was stirred at 0 °C for 10 min, and another 30 min at rt. The reaction was cooled to –40 °C and pyridine

(0.5 mL) was added in one portion followed by adding acetyl chloride (65 μL, 0.92 mmol) dropwise. The reaction was stirred at –40 °C for 3 h. NH_4Cl (1 mL) was added to quench the reaction. The reaction was diluted with chloroform (20 mL). The organic layer was washed with 5% citric acid (2 × 10 mL), 5% $NaHCO_3$ (10 mL), H_2O (10 mL) and brine (10 mL), and dried over Na_2SO_4. The organic solvent was evaporated by rotary evaporation and the residue was purified via silica gel flash chromatography ($CHCl_3$:MeOH = 10:1) to afford 67 mg of Fmoc-Ser(Ac)-OH (30%) as a pale yellow oil. ^{1}H-NMR ($CDCl_3$), δ 7.87 (d, *J* = 7.5, 2H), 7.71 (d, *J* = 7.4, 2H), 7.40 (t, *J* = 7.5, 2H), 7.32 (t, *J* = 7.4, 2H), 7.14 (d, *J* = 6.1, 2H), 4.42 (d, *J* = 8.0, 1H), 4.32 (m, 1H), 4.23 (app t, J = 6.7, 2H), 4.14 (m, 2H), 1.95 (s, 2H).

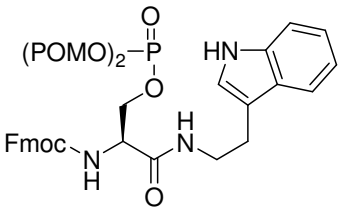

Fmoc-Ser(bisPOM)-tryptamine, 52. Fmoc-Ser(OH)-tryptamine **40** (7.0 mg, 0.016 mmol) and DMAP (1.0 mg) was dissolved in 1 mL of THF : pyridine (1:1), and cooled to –40 °C for 10 min. A solution of freshly prepared bisPOM phosphoryl chloride **38** (0.08 mmol) in THF (0.5 mL) was added to the reaction mixture dropwise via syringe over 15 min. The reaction mixture was stirred at –40 °C for 3 h. A second batch of bisPOM phosphoryl chloride **38** (0.08 mmol) in DCM (0.4 mL) was added dropwise to the reaction mixture and the reaction was stirred at –40 °C for another 3 h. The reaction was warmed to rt over 2 h and water (1.0 mL) was added to quench the reaction. The organic solvent was removed by rotary evaporation. Chloroform (20 mL) was added to the residue and washed with 5% citric acid (1 mL), 5% $NaHCO_3$ (1 mL), H_2O (1 mL), brine (1 mL), and dried over anhydrous $MgSO_4$. The solvent was evaporated and the residue was

purified by flash silica gel chromatography to afford Fmoc-Ser(bisPOM)-tryptamine **52** (1.0 mg, 12% yield). ^{1}H-NMR ($CDCl_3$), δ 7.74 (app t, *J* = 7.0, 2H), 7.54 (app t, *J* = 7.4, 2H), 7.38 (app t, *J* = 6.0, 2H), 7.28 (app t, *J* = 6.2, 4H), 7.15 (t, *J* = 7.1, 1H), 7.07 (t, *J* = 7.5, 1H), 6.93 (m, 1H), 5.52 (d, *J* = 13.4, 4H), 4.38 (m, 4H), 4.22 (m, 1H), 4.15 (m, 1H), 3.57 (t, *J* = 6.2, 2H), 2.94 (m, 2H). ^{31}P NMR ($CDCl_3$) δ –3.30 (s).

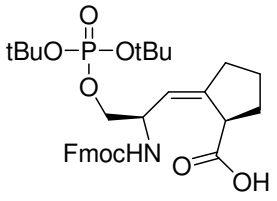

Fmoc-Ser(PO(*t*Bu)$_2$)-Ψ[(*Z*)CH=C]-Pro-OH, 56.

Fmoc-Ser-Ψ[(*Z*)CH=C]-Pro-OH, **1** (33 mg, 0.081 mmol) was dissolved in THF (3 mL). *N*-methylmorpholine (8 mg, 0.08 mmol) was added to the reaction solution, followed by TBSCl (12 mg, 0.081 mmol). The reaction was stirred at rt for 30 min. (tBuO)$_2$P(N-iPr)$_2$ (50 μL, 0.16 mmol) in THF (2 mL) was added to the reaction solution dropwise followed by tetrazole (42 mg, 0.32 mmol). The mixture was stirred at rt overnight, then cooled to – 40 °C for 10 min. *tert*-Butyl hydroperoxide (5 M in decane, 32 μL, 0.16 mmol) was added to the reaction solution dropwise. The mixture was stirred at –40 °C for an additional 40 min. The cold bath was removed and the reaction was stirred at rt for another 30 min. The mixture was cooled to 0 °C and 10% aq. $Na_2S_2O_3$ (3 mL) was added. After stirring for 10 min, the mixture was transferred to a separatory funnel using Et_2O (3 × 30 mL). The combined organic layers were washed with 10% aq. $Na_2S_2O_3$ (2 × 20 mL) and brine (20 mL), dried over Na_2SO_4, and concentrated to afford 160 mg of the crude product **56**, as a pale yellow oil. The crude product was purified by semipreparative C_{18} HPLC at 15 mL/min, 10% to 90% B for 20 min.

Purified Fmoc-Ser(PO(tBu)$_2$)-Ψ[(Z)CH=C]-Pro-OH **56** (20 mg, 42%) was obtained as a white solid. ^{1}H-NMR ($CDCl_3$), δ 7.73 (d, J = 7.5, 2H), 7.58 (d, J = 6.1, 2H), 7.36 (t, J = 7.3, 2H), 7.27 (t, J = 7.4, 2H), 5.88 (brs, 1H), 5.42 (d, J = 7.5, 1H), 4.48 (br s, 1H), 4.35 (m, 2H), 4.17 (m, 1H), 3.94 (m, 2H), 3.61 (m, 1H), 3.50 (m, 1H), 2.43 (m, 1H), 2.27 (m, 1H), 2.15 (m, 1H), 1.59 (m, 2H), 1.44 (s, 18H). ^{31}P-NMR ($CDCl_3$) δ –8.49 (s). ESI-MS gave the molecular ion $[M+H]^+$ m/z = 600.34, $[M+Na]^+$ m/z = 622.29, $[M- 2tBu + 2H]^+$ m/z = 488.

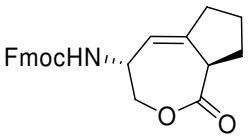

Lactone, 41. Fmoc-Ser-Ψ[(Z)CH=C]-Pro-OH, **1** (40.0 mg, 0.096 mmol) and imidazole (33 mg, 0.48 mmol) were dissolved in DMF (2.0 mL), and TBSCl (29 mg, 0.19 mmol) was added. The mixture was stirred for 16 h, and NH_4Cl (2 mL) was added. The mixture was stirred for an additional 50 min, and diluted with EtOAc (20 mL), washed with NH_4Cl (2 × 10 mL), dried over Na_2SO_4, and concentrated. Chromatography on silica gel with 2% MeOH in $CHCl_3$ afforded **41** (28 mg, 55%) as a white powder. ^{1}H NMR ($CDCl_3$) δ 7.77 (d, J = 8.0, 2H), 7.57 (d, J = 8.0, 2H), 7.40 (app. t, J = 7.5, 2H), 7.32 (app. t, J = 6.5, 2H), 5.50 (br s, 1H), 4.73 (d, J = 8.5, 1H), 4.52? (br s, 1H), 4.46 (d, J =6.0, 2H), 4.39 (t, J = 12, 1H) 4.22 (m, 2H), 3.92 (m, 1H), 2.37 (br s, 2H), 2.27 (two d, J = 7.1, 7.7, 1H), 1.97 (two d, J = 6.0, 7.1, 1H), 1.73 (two d, J = 6.0, 6.1, 1H), 1.60 (two d, J = 5.9, 7.8, 1H). ^{13}C-NMR ($CDCl_3$) δ 173.2, 155.3, 143.6, 142.4, 141.3, 127.8, 127.0, 124.9, 120.0, 66.7, 66.3, 49.0, 47.1, 43.9, 35.1, 29.3, 24.4 ppm. HRMS calculated for $C_{24}H_{23}NO_4$ (MH^+) m/z = 390.1705, found m/z = 390.1715.

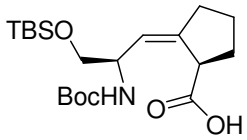

Boc-Ser(TBS)-Ψ[(*Z*)CH=C]-Pro-OH, 46. Boc-Ser-Ψ[(*Z*)CH=C]-Pro-OH **29** (synthesized by the published method)[164] (111 mg, 0.388 mmol) and imidazole (136 mg, 2.00 mmol) were dissolved in DMF (2.0 mL), and TBSCl (151 mg, 1.00 mmol) was added with stirring. The reaction was stirred for 18 h at rt, then NH_4Cl (5 mL) was added. The mixture was stirred for an additional 60 min, and then diluted with EtOAc (20 mL), washed with NH_4Cl (2 × 10 mL), and brine (10 mL). The organic layer was dried over $MgSO_4$, and concentrated by rotary evaporation. Chromatography on silica gel with 30% EtOAc in hexane afforded 150 mg (70%) of **46** as a pale yellowish oil. ^{1}H-NMR ($CDCl_3$) δ 11.10 (br s, 1H), 5.96 and 4.91 (br s, 1 H), 5.42 (d, *J* = 5.8, 1H), 4.23 (br s, 1H), 3.61 and 3.59 (d, *J* = 4.4, 1H), 3.55 and 3.48 (br s, 2H), 2.41 (m, 1H), 2.23 (m, 1H), 2.04 (br s, 1H), 1.90 (m, 1H), 1.80 (br s, 1H), 1.55 (m, 1H), 1.37 (s, 9H), 0.83 (s, 9H), - 0.01 (s, 6H). ^{13}C-NMR ($CDCl_3$) δ 178.5, 155.4 (157.0), 144.1 (145.4), 122.2, 79.1 (79.9), 65.3, 51.8 (52.7), 45.8, 33.6, 31.1, 28.2, 25.7, 24.0, 18.2, –5.5 ppm. HRMS calculated for $C_{20}H_{38}NO_5Si$ (MH^+) *m/z* = 400.2519, found *m/z* = 400.2485.

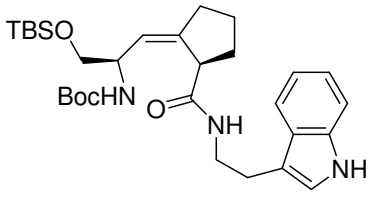

Boc-Ser(TBS)-Ψ[(*Z*)CH=C]-Pro-(2)-*N*-(3)-ethylaminoindole, 47. Boc-Ser(TBS)-Ψ[(*Z*)CH=C]-Pro-OH, **46** (150 mg, 0.376 mmol) was dissolved in DMF (20 mL), and cooled to 0 °C for 10 min. HOAt (101 mg, 0.751 mmol), HATU (287 mg, 0.751 mmol) and DMAP (10 mg, 0.075 mmol) were added. DIEA (260 μL, 1.50 mmol) was then added to the stirred solution dropwise. Tryptamine (120 mg, 0.751 mmol) was added slowly.

The mixture was stirred for 6 h, diluted with EtOAc (200 mL), washed with water (2 × 50 mL) and brine (20 mL). The aqueous layer was back-extracted with CH_2Cl_2 (2 × 75 mL). The organic layers were combined, dried with Na_2SO_4 and concentrated. Chromatography on silica gel with 2% MeOH in $CHCl_3$ afforded 184 mg (90%) of **47** as a colorless oil. ^{1}H-NMR ($CDCl_3$), δ 8.82 (br s, 1H), 7.71 (br s, 1H), 7.65 (d, *J* = 7.6, 1H), 7.33 (d, *J* = 8.1, 1H), 7.13 (app t, *J* = 7.6, 1H), 7.05 (app t, *J* = 7.5, 1H), 6.97 (s, 1H), 5.32 (d, *J* = 8.8, 1H), 5.05 (s, 1H), 4.08 (m, 1H), 3.64 (m, 1H), 3.55 (m, 1H), 3.50 (two d, *J* = 6.2, 6.3, 2H), 3.35 (d, *J* = 7.0, 1H), 3.00 (app t, *J* = 7.7, 2H), 2.31 (m, 2H), 2.15 (m, 1H), 1.79 (m, 1H), 1.54 (m, 2H), 1.44 (s, 9H), 0.88 (s, 9H), 0.04 (s, 6H). ^{13}C-NMR ($CDCl_3$) δ 171.9, 156.0, 144.3, 136.2, 127.5, 123.8, 121.9, 121.4, 118.7, 113.1, 111.1, 79.5, 64.9, 52.6, 47.5, 40.5, 38.5, 36.4, 32.8, 30.8, 28.3, 25.7, 25.0, 23.3, 18.2, –5.6. HRMS calculated for $C_{30}H_{48}N_3O_4$ (MH^+) *m/z* = 542.3414, found *m/z* = 542.3403.

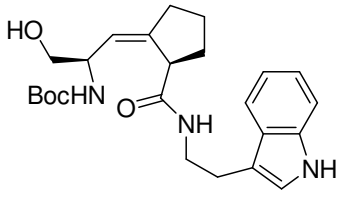

Boc-Ser-Ψ[(*Z*)CH=C]-Pro-(2)-*N*-(3)-ethylaminoindole, 48. Boc-Ser(TBS)-Ψ[(*Z*)CH=C]-Pro-(2)-*N*-(3)-ethylaminoindole, **47** (92 mg, 0.17 mmol) was dissolved in THF (2.5 mL), and cooled to 0 °C for 10 min. A solution of TBAF (117 mg, 0.342 mmol) in THF (2.5 mL) was added dropwise at 0 °C. The mixture was stirred at rt for 4 h. The reaction was quenched with NH_4Cl (25 mL), and extracted with EtOAc (2 × 80 mL). The organic layer was washed with brine (20 mL), dried with Na_2SO_4 and concentrated. Chromatography on silica gel with 2% MeOH in $CHCl_3$ afforded 85 mg (85%) of **48** as a colorless oil. ^{1}H-NMR ($CDCl_3$), δ 8.60 (br s, 1H), 7.73 (br s, 1H), 7.63 (d, *J* = 7.8, 1H), 7.33

(d, *J* = 8.1, 1H), 7.15 (app t, *J* = 7.5, 1H), 7.07 (app t, *J* = 7.4, 1H), 6.99 (s, 1H), 5.33 (s, 1H), 5.30 (d, *J* = 8.8, 1H), 4.04 (m, 1H), 3.87 (br s, 1H), 3.60 (m, 1H), 3.53 (m, 2H), 3.45 (m, 1H), 3.34 (d, *J* = 7.6, 1H), 3.01 (m, 2H), 2.29 (m, 1H), 2.17 (m, 2H), 1.80 (m, 1H), 1.52 (m, 2H), 1.41 (s, 9H). ^{13}C-NMR ($CDCl_3$) δ 173.5, 156.5, 144.4, 136.1, 127.5, 123.4, 122.1, 121.7, 119.1, 118.8, 113.1, 111.1, 79.7, 64.7, 53.4, 47.4, 40.5, 33.4, 31.6, 28.3, 24.7, 23.8. HRMS calculated for $C_{24}H_{34}N_3O_4$ (MH^+) *m/z* = 428.2549, found *m/z* = 428.2553.

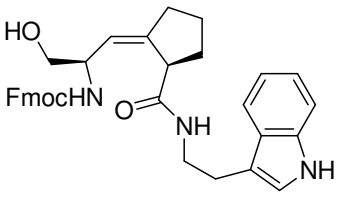

Fmoc-Ser-Ψ[(*Z*)CH=C]-Pro-(2)-*N*-(3)-ethylaminoindole, 39. Boc-Ser-Ψ[(*Z*)CH=C]-Pro-(2)-*N*-(3)-ethylaminoindole **48** (62 mg, 0.14 mmol) was dissolved in CH_2Cl_2 (3 mL), and cooled to 0 °C for 10 min. TFA (1 mL) was added dropwise. The mixture was stirred at 0 °C for 10 min after which the cold bath was removed. The mixture was stirred at rt for an additional 45 min and the solvent was evaporated. CH_2Cl_2 was added and evaporated (3 × 20 mL). The remaining TFA was removed under high vacuum overnight. Without further purification, the crude product was dissolved in a mixture of 10% aq. Na_2CO_3 and $NaHCO_3$ (3:1, 2 mL), then cooled to 0 °C for 10 min. A solution of Fmoc-Cl (43 mg, 0.17 mmol) in dioxane (2 mL) was added dropwise. After stirring at 0 °C for 20 h, the mixture was diluted with water (20 mL) and extracted with EtOAc (2 × 25 mL). The aqueous layer was acidified with 1M HCl to pH 3-4 and extracted with EtOAc (3 × 30 mL) and CH_2Cl_2 (3 × 30 mL). The organic layers were combined, washed with brine (20 mL), dried with Na_2SO_4, and concentrated. Chromatography on silica gel with 10% MeOH in $CHCl_3$ afforded 63 mg (78 %) of **39** as a colorless oil. ^{1}H-NMR ($CDCl_3$), δ 7.95 (br s, 1H), 7.77 (d, *J*

= 7.5, 2H), 7.57 (d, *J* = 7.8, 2H), 7.53 (d, *J* = 6.2, 2H), 7.41 (app t, *J* = 7.5, 2H), 7.32 (app t, *J* = 6.8, 2H), 7.24 (s, 1H), 7.10 (app t, *J* = 7.5, 1H), 6.97 (app t, *J* = 7.4, 1H), 6.83 (br s, 1H), 5.23 (m, 2H), 4.37 (dd, *J* = 6.9, 10.5, 1H), 4.26 (d, *J* = 7.0, 9.3, 1H), 4.15 (app t, *J* = 6.6, 1H), 3.83 (m, 1H), 3.5-3.37 (m, 4H), 3.23 (d, *J* = 6.8, 1H), 3.00 (m, 1H), 2.86 (m, 1H), 2.32 (m, 1H), 2.19 (m, 2H), 1.84 (m, 1H), 1.54 (m, 2H). ^{13}C-NMR ($CDCl_3$) δ 172.9, 156.7, 145.5, 143.9, 141.4, 136.2, 127.9, 127.3, 125.2, 125.1, 122.6, 122.2, 121.8, 120.2, 119.3, 118.9, 113.4, 111.2, 66.7, 64.6, 53.7, 47.9, 47.2, 40.7, 33.6, 31.7, 24.6, 24.0. HRMS calculated for $C_{34}H_{36}N_3O_4$ (MH^+) *m/z* = 550.2706, found *m/z* = 550.2711.

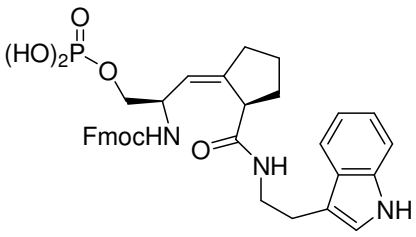

Fmoc-Ser(PO(OH)$_2$)-Ψ[(*Z*)CH=C]-Pro-(2)-*N*-(3)-ethyl-aminoindole, 33. Fmoc-Ser-Ψ[(*Z*)CH=C]-Pro-(2)-*N*-(3)-ethylaminoindole, **39** (31 mg, 0.056 mmol) was dissolved in THF (3 mL). Tetrazole (36 mg, 0.22 mmol) and (tBuO)$_2$P(N-iPr)$_2$ (40 μL, 0.11 mmol) were added. The mixture was stirred at rt for 20 h, then cooled to –40 °C for 10 min. *tert*-Butyl hydroperoxide (5 M in decane, 22 μL, 0.11 mmol) was added dropwise. The mixture was stirred at –40 °C for 40 min. The cold bath was removed and the reaction was stirred at rt for an additional 30 min. The mixture was cooled to 0 °C and 10% aq. $Na_2S_2O_3$ (3 mL) was added. After stirring for 10 min, the mixture was transferred to a separatory funnel using Et_2O (3 × 30 mL). The combined organic layers were washed with 10 % aq. $Na_2S_2O_3$ (2 × 20 mL) and brine (20 mL), dried with Na_2SO_4, and concentrated to afford 40 mg of the crude Fmoc-Ser(PO(O-tBu)$_2$)-Ψ[(*Z*)CH=C]-Pro-(2)-*N*-(3)-ethylaminoindole, **55**,

as a colorless oil. ^{1}H-NMR ($CDCl_3$), δ 8.30 (s, 1H), 7.70 (t, *J* = 10, 2H), 7.50-7.40 (m, 3H), 7.35 (m, 2H), 7.25 (m, 3H), 7.06 (app t, *J* = 7.5, 1H), 6.92 (m, 2H), 5.67 (m, 1H), 5.30 (m, 1H), 4.27 (d, *J* = 9.0, 1H), 4.10 (m, 2H), 3.90 (m, 2H), 3.50 (m, 3H), 3.35 (m, 1H), 2.95 (m, 2H), 2.22 (m, 3H), 1.90 (m, 1H), 1.45 (s, 9H). ^{31}P-NMR ($CDCl_3$) δ –9.65 (s). ESI-MS donated the molecular ion $[M+H]^+$ *m/z* = 742.3, $[M+Na]^+$ *m/z* = 764.3. Without further purification (decomposing on silica gel), Fmoc-Ser(PO(O*t*Bu)$_2$)-Ψ[(*Z*)CH=C]-Pro-(2)-*N*-(3)-ethylaminoindole **55** (40 mg, 0.054mmol) was dissolved in CH_2Cl_2 (4 mL), and cooled to 0 °C. TFA (1mL) was added to the reaction mixture slowly, followed by the addition of water (0.2 mL) as a scavenger. After stirring at 0 °C for 10 min, the cold bath was removed and the reaction mixture was stirred at rt for an additional 30 min, and the solvent was evaporated. CH_2Cl_2 was added and evaporated (5 × 20 mL). The remaining TFA was removed under high vacuum overnight until a constant weight was obtained. The crude product was purified by semipreparative C_{18} HPLC at 15 mL/min, 10 % to 90 % B over 20 min. Purified **33** (12 mg, 70% yield) eluted at 19.6 min as a white solid. Purity was 98.8 % by analytical C_{18} HPLC (2 mL/min, 10 % to 90 % B over 13 min, retention time 11.79 min). ^{1}H-NMR (CD_3OD), δ7.73 (app t, *J* = 6.3, 2H), 7.55 (app t, *J* = 7.9, 2H), 7.39 (d, *J* = 7.3, 1H), 7.32 (two d, *J* = 7.6, 8.1, 3H), 7.21 (m, 2H), 7.03 (app t, *J* = 7.3, 1H), 6.97 (s, 1H), 6.90 (app t, *J* = 7.5, 1H), 5.43 (d, *J* = 9.3, 1H), 4.40 (m, 1H), 4.24 (m, 2H), 4.08 (app t, *J* = 6.6, 1H), 3.91 (m, 1H), 3.86 (m, 1H), 3.47 (m, 1H), 3.41 (t, *J* = 1.5, 2H), 2.91 (m, 2H), 2.41 (m, 1H), 2.30 (m, 1H), 2.00 (m, 1H), 1.72 (m, 1H), 1.57 (m, 1H). ^{13}C-NMR (CD_3OD) δ 147.3, 145.4, 145.2, 142.5, 138.1, 128.8, 128.7, 128.1, 126.3, 126.2, 125.0, 123.4, 122.3, 120.8, 119.5, 119.4, 113.3, 112.2, 68.1, 67.9, 52.7, 41.7, 35.2, 35.1, 33.1, 30.8, 26.0, 25.5. ^{31}P- NMR (CD_3OD) δ –1.164 (s). ESI-MS gave

the molecular ion $[M+H]^+$ *m/z* = 630.33, $[M+Na]^+$ *m/z* = 652.24, $[M-H_3PO_4]^+$ *m/z* = 532.20. HRMS calculated for $C_{34}H_{37}N_3O_7P$ (MH^+) *m/z* = 630.2369, found *m/z* = 630.2340.

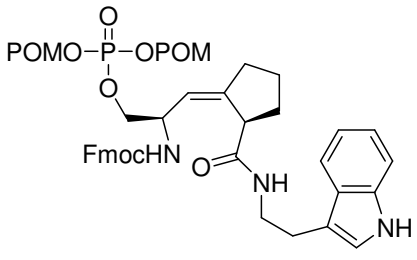

Fmoc-Ser(PO(OPOM)$_2$)-Ψ[(*Z*)CH=C]-Pro-(2)-*N*-(3)-ethylaminoindole, 34. BisPOM phosphate **37** was synthesized by a modification of the published procedure.[232] Oxalyl chloride (90 μL, 1.92 mmol) was added dropwise to CH_2Cl_2 (1.5 mL) at 0 °C. DMF (7 μL) was added in one portion. A solution of hydrogen bisPOM phosphate (62 mg, 0.192 mmol) in CH_2Cl_2 (1.5 mL) was added dropwise at 0 °C over 15 min. The reaction mixture was stirred at rt for 2 h. The solvent and $(COCl)_2$ were removed by rotary evaporation. The remaining oxalyl chloride was removed in vacuo until a constant weight was obtained. The product was obtained as a slightly yellowish oil (50 mg, 80%). Without further purification, the bisPOMphosphoryl chloride was used immediately in the next step. ^{1}H-NMR ($CDCl_3$), δ 5.71 (m, 4H), 1.23 (s, 18H). ^{13}C-NMR ($CDCl_3$) δ 83.52, 83.45, 31.0, 27.0 ppm. ^{31}P-NMR ($CDCl_3$), δ 3.80 (s). Fmoc-Ser-Ψ[(*Z*)CH=C]-Pro-(2)-*N*-(3)-ethyl-aminoindole, **39** (21 mg, 0.038 mmol) was dissolved in THF (1.5 mL), and cooled to –40 °C. Pyridine (0.75 mL) was added, and the mixture was stirred at –40 °C for 20 min. DMAP (2.5 mg) was added, then a solution of bisPOM phosphoryl chloride **38** (50 mg, 0.145 mmol) in THF (0.9 mL) was added to the reaction mixture dropwise via syringe at –40 °C. The mixture was stirred at –40 °C for 2 h. A second batch of bisPOM phosphoryl chloride solution, (20 mg, 0.058 mmol) in THF (0.5 mL) was added. The mixture was stirred for an additional 30

min. The cold bath was removed and the reaction mixture was stirred at rt for 6 h. Water (2 mL) was added to quench the reaction and the reaction mixture was diluted with EtOAc (40 mL). The organic layer was washed with water (2 × 20 mL). The aqueous layer was back-extracted with EtOAc (3 × 20 mL). The combined organic layers were washed with brine (20 mL), dried with Na_2SO_4, and concentrated. The crude product was purified using semipreparative C_{18} HPLC (15 mL/min, 60% B for 5 min, then 60% to 95% B over 20 min). Purified **34** (3 mg, 20%) eluted at 23.0 min as a white solid. Purity > 99% by analytical C_{18} HPLC (1.5 mL/min, 10% B for 5 min, then 10% to 90% B over 20 min, retention time 24.7 min). ^{1}H-NMR ($CDCl_3$), δ 8.04 (s, 1H), 7.76 (app t, *J* = 6.7, 2H), 7.57 (d, *J* = 8.4, 1H), 7.54 (app t, *J* = 4.0, 2H), 7.40 (m, 2H), 7.30 (m, 3H), 7.10 (app t, *J* = 8.1, 1H), 6.97 (app t, *J* = 7.4, 2H), 6.88 (s, 1H), 5.63 and 5.60 (m, 4H), 5.42(br s, 1H), 5.26 (d, *J* = 6.9, 1H), 4.42 (br s, 1H), 4.29 (d, *J* = 7.0, 1H), 4.16 (app t, *J* = 6.4, 1H), 4.11 (br s, 1H), 3.98 (m, 1H), 3.49 (m, 2H), 3.37 (br s, 1H), 3.27 (m, 1H), 2.93 (m, 2H), 2.35 (m, 1H), 2.21 (m, 2H), 2.03 (m, 1H), 1.83 (m, 1H), 1.62 (m, 1H), 1.25 and 1.23 (s, 18H). ^{13}C-NMR ($CDCl_3$) δ 177.2, 172.6, 156.1, 148.0, 144.0, 141.4, 136.3, 127.9, 127.3, 125.2, 122.2, 122.1, 120.3, 120.1, 119.4, 118.9, 113.4, 111.3, 83.0, 69.0, 67.0, 51.3, 48.0, 47.2, 40.4, 38.9, 33.6, 31.6, 27.0, 24.7, 23.9. ^{31}P-NMR ($CDCl_3$) δ –3.934 (s). ESI-MS donated the molecular ion $[M+H]^+$ *m/z* = 858.25; $[M+Na]^+$ *m/z* = 880.37. HRMS calculated for $C_{46}H_{57}N_3O_{11}P$ (MH^+) *m/z* = 858.3731, found *m/z* = 858.3805.

Pin1 Inhibition Assay

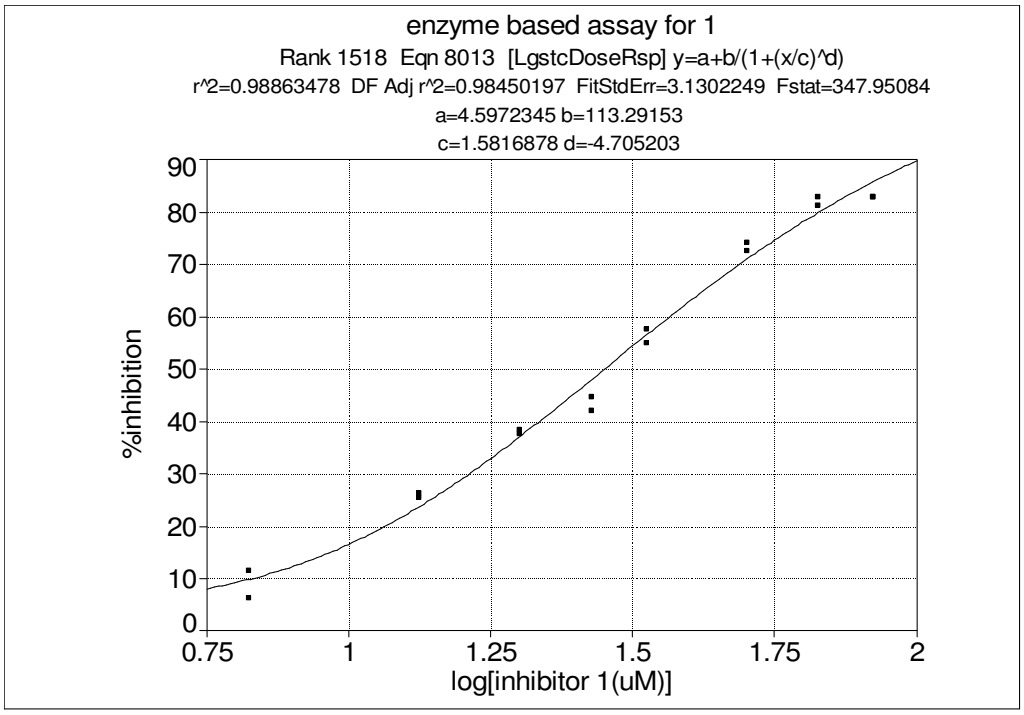

Figure 3.16. Dose response curve for inhibition of Pin1 by compound **33** (IC_{50} = 28.3 ± 2.1 μM).

The Pin1 inhibition assay involving compound **33** was performed as published.[165] The assay buffer (1.05 mL of 35.0 mM HEPES, pH 7.8; final concentration 31 mM HEPES), Pin1 (10 μL of 8.0 μM stock solution, concentration measured by Bradford assay, final concentration 67 nM) and inhibitors (10 μL of varying concentrations in 1: 2 DMSO: H_2O) were preequilibrated in the cuvette at 4 °C for 10 min. The thermal isomerization rate constant k_3 was determined in the absence of Pin1. Immediately before the assay was started, 120 μL of ice-cooled chymotrypsin solution (60 mg/mL in 0.001 M HCl; final concentration 6 mg/mL) was added. The peptide substrate, Suc-Ala-Glu-Pro-Phe-*p*NA (10 μL), dissolved in dry 0.47 M LiCl/TFE, was added to the cuvette via syringe, and the solution was mixed vigorously by inversion three times. The final volume in a semi-micro 1.0 cm path length polystyrene cell

was 1.2 mL. After a mixing delay of 6-8 s, the progress of the reaction was monitored at 4 °C by absorbance at 390 nM for 90 s. The inhibitor **33** (10 μL at concentrations of 800 μM, 1.6, 2.4, 3.2, 4.0, 6.0, 8.0, 10.0 mM in 1:2 DMSO: H_2O) was pre-equilibrated in the cuvette at 4 °C for 10 min. The assay was performed in duplicate, and all of the data were used for calculating the IC_{50}. The plot of % inhibition vs. log [I] (μM) produced a sigmoidal curve (Figure 3.16). The concentration of **33** for 50% inhibition of Pin1 activity (IC_{50}) was obtained by fitting all the experimental data to a dose response curve (95% confidence level) using equation (1) in TableCurve (version 3 for win32), where [I] is the inhibitor concentration (μM).

$$\%Inhibition = a + \frac{b}{\{1 + (\log[I]/c)^d\}} \qquad (1)$$

In the equation, a = 4.60, b = 113.29, c = 1.58, and d = 4.71 are the fitted constants; $r^2 = 0.989$. The calculated value of IC_{50} was 28.3 ± 2.1 μM.

A2780 Cell Based Assay

We are grateful to Margaret Brodic and Professor David G. I. Kingston for performing the A2780 assay. The antiproliferative activity towards a A2780 human ovarian cancer cell line was measured as published.[252, 253] The concentrations of **33** used were 190.8, 159.0, 95.4, 79.5, 39.7, 19.9, 9.9 μM (duplicates), and the concentrations of **34** were 140.0, 116.7, 58.3, 29.2, 14.6, 7.3, 5.8 μM (duplicates). The IC_{50} values were calculated by a curve-fitting program. The plot of % inhibition of proliferation activity against A2780 ovarian cancer cells vs. log [I] (μM) produced a sigmoidal curve for each inhibitor (Figures 3.17 and 3.18). The concentrations of **33** and **34** for 50% inhibition of Pin1 activity (IC_{50}) were obtained by fitting

all the experimental data to a dose response curve (95% confidence level) using equation (1) in TableCurve (Version 3 for win32)

.

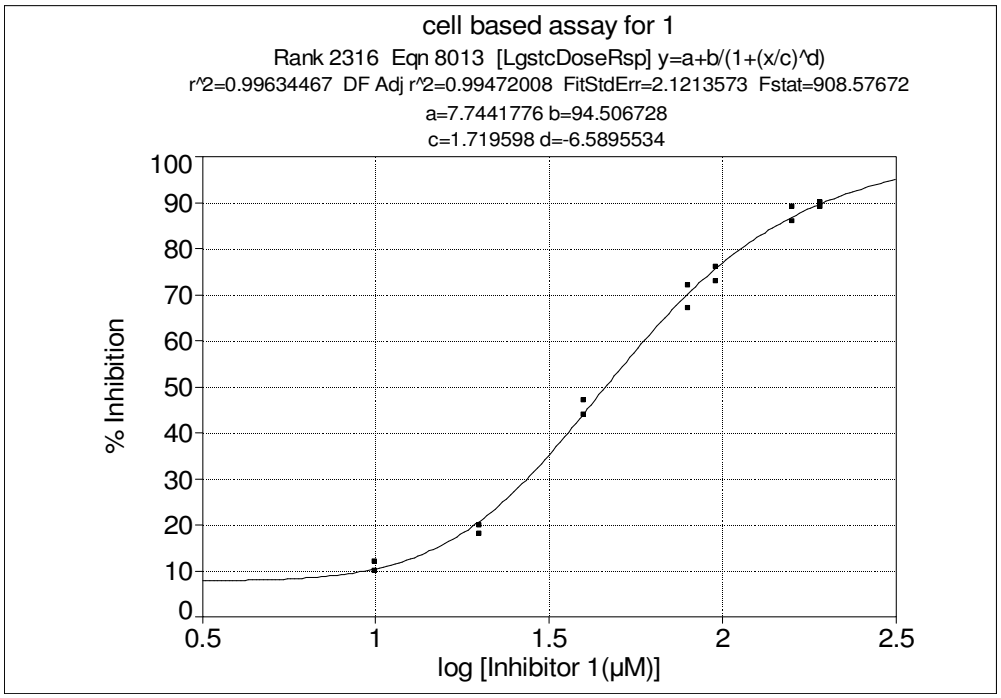

Figure 3.17 Dose response curve for the inhibition of A2780 ovarian cancer cells proliferation activity of **33** (IC_{50} = 46.2 ± 3.0 μM).

Where [I] is the inhibitor concentration (μM).

$$\%Inhibition = a + \frac{b}{\{1 + (\log[I]/c)^d\}} \qquad (1)$$

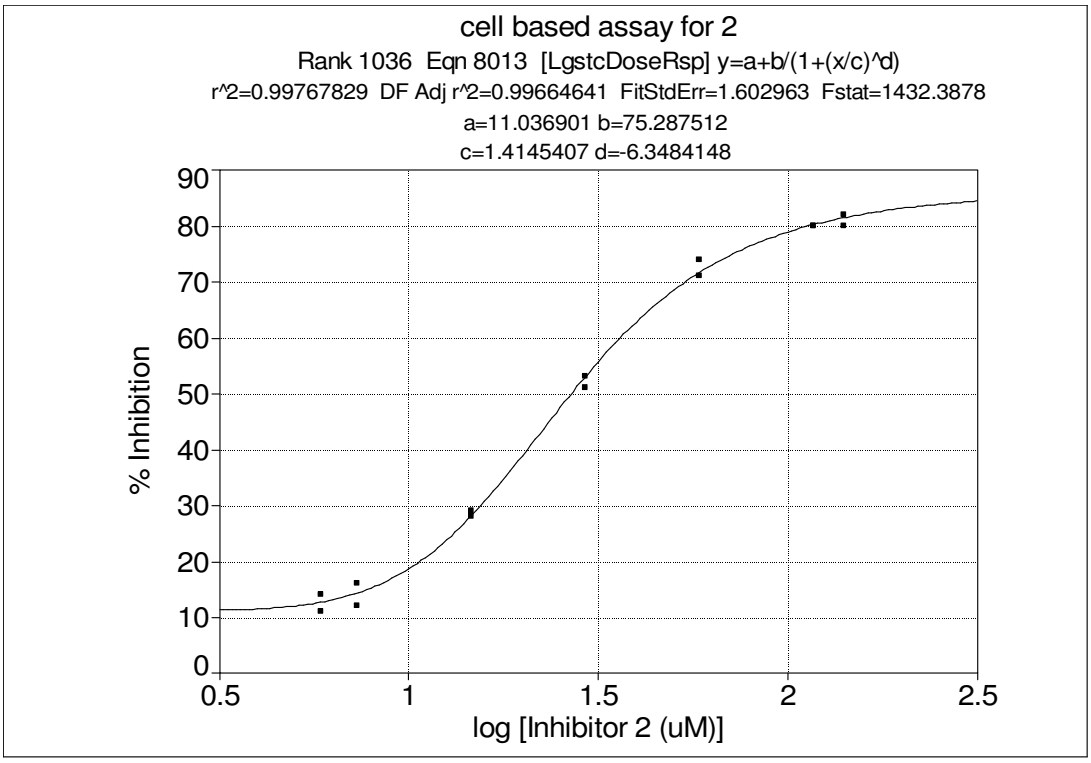

Figure 3.18 Dose response curve for the inhibition of A2780 ovarian cancer cells proliferation activity of **34** (IC_{50} = 26.9 ± 1.5 μM).

For **33**, from equation (1), a = 7.74, b = 94.51, c = 1.72, and d = 6.59 are the fitted constants; r^2 = 0.996. The IC_{50} value of 46.2 ± 3.0 μM was obtained from the equation.

For **34**, from the equation, a = 11.04, b = 75.29, c = 1.41, and d = 6.35 are the fitted constants; r^2 = 0.998. The IC_{50} value of 26.9 ± 1.5 μM was obtained as from the equation.

Chapter 4. Study of the Substrate Conformational Specificity of the Kinase Upstream of Pin1

4.1. Substrate Conformational Specificity of Proline-directed Kinases and Phosphatases

Since prolyl amide bonds in proteins exist in the discrete cis and trans conformations, these conformers of proline-containing proteins may be discriminated by enzymes according to their structural differences. It is also possible that only one conformer is required for the active biological form. For example, the protease α-chymotrypsin shows trans conformational specificity towards its substrates, even when the isomeric bond is remote from the scissile position.[254] In proline-directed Ser/Thr phosphorylation/dephosphorylation, the reaction center is the side chain hydroxyl group. It is also possible that proline-directed kinases or phosphatases may distinguish these two conformers, with only one conformer serving as the substrate. For example, in 2000, Fischer reported that the proline-directed p42 mitogen-activated protein kinase (ERK2) displayed conformational specificity for its substrate, with only trans conformers being recognized and phosphorylated by ERK2.[47] The initial rate of phosphorylation of the substrate peptide Pro-Arg-Ser-Pro-Phe-4-nitroanilide by ERK2 was observed to be dependent on the concentration of the trans proline conformer of the substrate through thermal cis/trans isomerization.[47]

The crystal structure of a complex consisting of a proline-directed kinase CDK2 and its peptide substrate HHASPRK in the presence of an inactive ATP analogue also showed the structure of the substrate arrangement in the active site of a proline-directed kinase. The trans conformation of the prolyl bond in the bound peptide substrate indicated that CDK2

specifically bound the trans conformation of the peptide substrate.[46] The major proline-directed phosphatase PP2A is also conformation specific, because it only effectively dephosphorylates the trans pSer/Thr-Pro isomer.[48] Importantly, Pin1 was found to catalyze prolyl isomerization of specific pSer/Thr-Pro motifs both in Cdc25C and tau protein to facilitate their dephosphorylation by PP2A.[48]

Given the fact that reversible mitotic protein phosphorylation on Ser/Thr-Pro-containing MPM-2 epitopes plays an essential role in regulating the timing of mitotic progression, the conformational specificities of these proline-directed kinases and phosphatases could add a level of complexity to the phosphorylation/dephosphorylation process, thus an additional level of regulation of the timed cell cycle events. Furthermore, these conformational specific kinases and phosphatases stress the important role of the phosphorylation dependent PPIase, Pin1, in the regulation of the cell cycle. Indeed, conformational changes induced by Pin1 may not only change the function of proteins, but could also provide additional mechanisms for cell signaling.

4.2. Interaction Between Pin1 and its Protein Substrate Cdc25 in Cell Cycle Regulation

4.2.1. Regulation of Cell Cycle by Cdc25 and Pin1

Cell cycle regulation involves the appropriately timed structural modification of proteins through the processes of phosphorylation, dephosphorylation, and ubiquitin-mediated protein degradation. The transition from G2 to mitosis is specifically governed by the abrupt activation of the Cdc2/cyclin B complex (Figure 4.1).

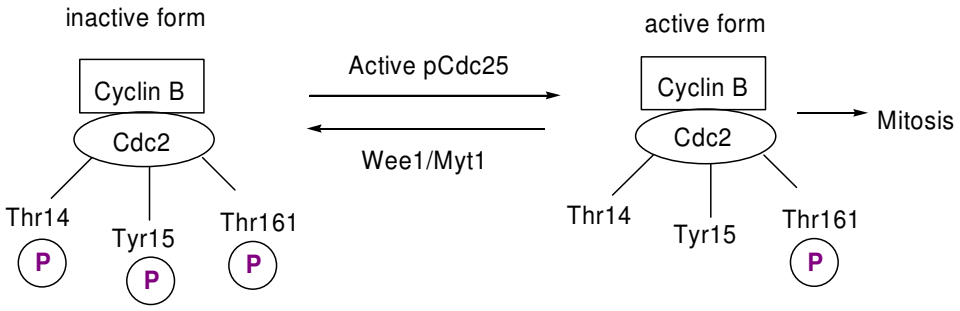

Figure 4.1. Regulation of the G2/M transition by activation of the Cdc2/Cyclin B complex[50]

The activity of the Cdc2/cyclin B complex is positively regulated by phosphorylation on Thr161, and negatively regulated by phosphorylation on its Thr14 and Tyr15 by Wee1 and Myt1 kinase.[50] A dual specific phosphatase Cdc25, which is another key cell cycle regulator, selectively dephosphorylates the pThr14 and pTyr15 of Cdc2 , activating the Cdc2/cyclin B complex, thereby initiating the process of mitosis.[50] The activity of the Cdc25 phosphatase is also governed by the phosphorylation of 12-20 different residues by at least three types of kinases (Cdc2, Plk and Jun/SAPK).[50, 98, 255-257] After the removal of the 14-3-3 protein and delocalization of Cdc25 from the cytoplasm to the nucleus, Cdc25 phosphatase assumes an active form and leads cell entry into mitosis by selectively dephosphorylating Cdc2 on Thr14 and Tyr15.[98, 257] One of the kinases that phosphorylates and activates Cdc25, at least *in vitro*, is the Cdc2/cyclin B complex, which is also a target of the Cdc25 phosphatase.[255] This suggests a positive feedback mechanism between Cdc2 and Cdc25, thereby explaining the autoamplification of mitosis-promoting factor (MPF) activity in oocytes injected with catalytic amounts of Cdc25.[256] This positive feedback loop also explains the abrupt activation of the Cdc2/cyclin B complex at the G2/M transition.

Significantly, the phosphorylated Cdc25 phosphatase is a known substrate of Pin1.[39] The interaction between Pin1 and the phosphorylated Cdc25 phosphatase, is cell cycle

regulated, and such interaction is significantly increased just before mitosis.[40, 257] This pre-mitosis interaction is believed to be an important event regarding the phosphatase activity of Cdc25c. Wild-type Pin1 inhibits both mitotic cell division in *Xenopus* embryos and entry into mitosis in *Xenopus* extracts.[38-40] Moreover, depletion of the Pin1 protein in Hela cells or Pin1/Ess1p in yeast, or inhibition of Pin1 expression by antisense RNA in Hela cells both result in mitotic arrest.[38, 40] In contrast, Pin1 overexpression, , induces G2 arrest through failure to activate the Cdc2 mitotic kinase.[38] An earlier study showed that the mitotically phosphorylated form of Cdc25 interacts with Pin1 *in vitro*.[40] Moreover, the interaction between Pin1 and Cdc25 significantly increases just prior to mitosis.[257]

Based on the above two observations, the fact that Pin1 has an inhibitory effect on the entry into mitosis could be at least partially explained by the inhibition of the mitotic activation of Cdc25 by Pin1. And the inhibition of the phosphatase activity of Cdc25c by Pin1 could also be a result of the interaction between Pin1 and the specific phosphorylated Ser/Thr-Pro motifs in Cdc25.[40] Determining the details of the interaction between Pin1 and the Cdc25 phosphatase will help us understand the specific signal transduction and regulatory events in the cell cycle from G2 to mitosis.

4.2.2. Regulation of the Phosphatase Activity of Cdc25c

Since the interaction between Pin1 and Cdc25c affects the phosphatase activity of Cdc25c, and such interaction depends on the phosphorylation of Cdc25c, it is important for us to understand how the phosphatase activity of Cdc25c is regulated prior to mitosis. In the transition from G2 to mitosis, the activity of Cdc25c increases 10-fold. That increase involves a series of events: 1) The *N*-terminal regulatory domain of Cdc25c is phosphorylated on

12-20 different positions by at least two kinases: Cdc2/cyclinB and polo-like kinase (Plk1);[255-259] 2) Cdc25c relocalizes from the cytoplasm to the nucleus;[98] 3) At some specific pSer/Thr-Pro sites of Cdc25c that are important for its activity, Pin1 interacts with phosphorylated Cdc25c to induce a conformational change, thereby altering the activity of Cdc25c.[98, 257]

It has been shown that the phosphorylation of Cdc25c by Cdc2/cyclinB and Plk1 kinases positively regulates the phosphatase activity of Cdc25c.[98, 257] Moreover, the phosphorylation of Ser216 on Cdc25c is accomplished by CHK1 kinase, which negatively regulates the phosphatase activity of Cdc25c following DNA damage.[257, 260] In addition, it was observed that the phosphatase activity of Cdc25c is negatively controlled by the SAPK/JNK kinase (stress-activated protein kinase) at the Ser^{168}-Pro position of Cdc25c.[261]

The interaction between Cdc25 phosphatase and Pin1 is mediated by the phosphorylation of Cdc25 phosphatase at specific positions.[40, 98] Specifically, if Cdc25 was phosphorylated by Cdc2 kinase in *Xenopus* extracts, the phosphatase activity of Cdc25 was inhibited 40% by substoichiometric Pin1 treatment. If Cdc25 was phosphorylated by Plk1 kinase alone, Pin1 had no effect on the phosphatase activity of Cdc25. If Cdc25 was phosphorylated by both Cdc2 and Plk1 kinase, Pin1 enhanced the activity of Cdc25 phosphatase by 1.8-fold. Therefore, depending on the phosphorylation state of Cdc25, Pin1 can either inhibit or enhance Cdc25 phosphatase activity.

In order to explain the apparent inconsistency between the fact that Pin1 inhibits entry into mitosis by inhibiting the activity of Cdc25c, and the fact that Pin1 either inhibits or activates the phosphatase activity of Cdc25c depending on its phosphorylation state, the

following model was suggested.[98] During the lag phase, Cdc2—rather than Plk1—is active, which then phosphorylates Cdc25. In this case, Pin1 inhibits the phosphatase activity of Cdc25.[98] If Pin1 is depleted, Cdc25c will not be properly inhibited, which results in the earlier activation of Cdc2 and thus premature entry into mitosis.[98] During the abrupt G2/M transition, both Plk1 and Cdc2 are activated. So at that point, Pin1 acts as a catalyst to promote conformational change that increases the activity of Cdc25c.[98]

4.2.3. Interaction Between Pin1 and Cdc25

In both HeLa cells and *Xenopus* extracts, the interaction between Pin1 and Cdc25c is highly regulated by the cell cycle, increasing significantly just prior to mitosis.[40, 257] Therefore, Pin1 interacts with specific phosphorylated Ser/Thr-Pro sites on Cdc25c that are essential for its mitotic activity. To examine whether Pin1 can regulate the activity of Cdc25c, Pin1 was incubated with mitotically phosphorylated Cdc25c.[40] It was found that Pin1 reduced Cdc25c activity to a level similar to that of Cdc25c incubated with interphase extracts, indicating that Pin1 indeed prevents the mitotic activation of Cdc25c.[40]

Pin1 promotes conformational changes in Cdc25c, which has been confirmed by three different assays: "changes in protease digestion patterns, changes in the ability of an antibody with overlapping specificity with the Pin1 recognition site to react with Cdc25, and changes in the enzymatic activity of Cdc25."[98]

With respect to the specific mechanisms for the interaction between Pin1 and Cdc25c, two models have been proposed: 1) Pin1 stoichiometrically binds Cdc25c in response to phosphorylation, or 2) Pin1 catalyzes cis/trans isomerization of the specific pSer/Thr-Pro motifs in Cdc25c.[98] In the first model, Pin1 binding might generate some local stress in the

molecule by rotating the peptide bonds or by some other local perturbations, and such constraints would prevent cis/trans isomerization.[98] In the second model, Pin1 could catalyze a lasting conformational change. These two models are discriminated by the fact that Pin1 modifies the conformation of Cdc25 at a stoichiometry of less than 0.0005.[98] So the first model can be ruled out.

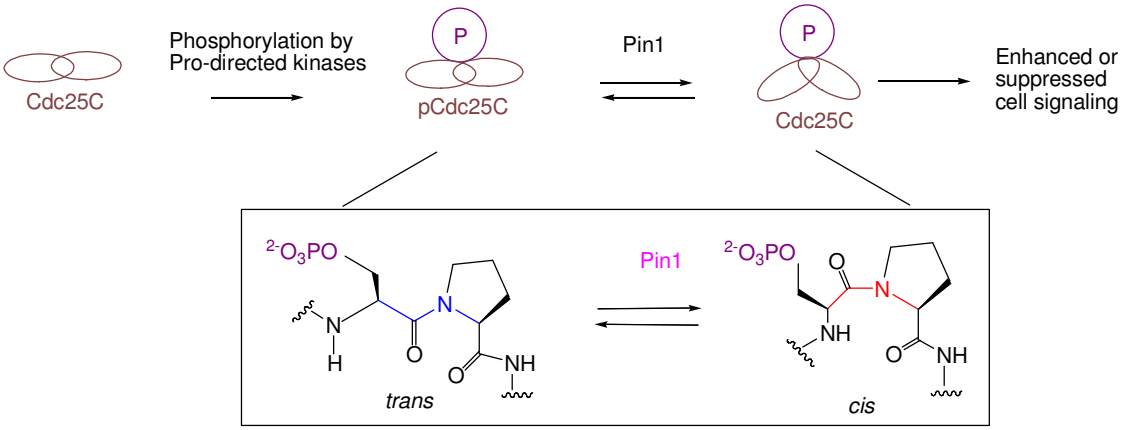

Figure 4.2. Interaction of Pin1 and Cdc25C phosphatase

Based on the fact that Pin1 is a phosphorylation dependent PPIase, a two-step mechanism for the interaction between Pin1 and Cdc25 has been suggested (Figure 4.2):[39, 40, 98] The first step involves the phosphorylation of the Cdc25 phosphatase at specific Ser-Pro or Thr-Pro sites by the mitosis-specific proline-directed kinases, thereby creating binding sites for Pin1.[98] In the second step, Pin1 binds the phosphorylated Ser/Thr-Pro motifs of the phosphorylated Cdc25 phosphatase and induces local conformational changes through prolyl isomerization.[39, 98] These local conformational changes alter the activity of the phosphoCdc25, thus leading to either enhanced or suppressed cell signaling. [39, 40, 98] This mechanism is shown in Figure 4.2. What remains unsolved in this mechanism is what the mitotically active conformation of Cdc25 is *in vivo*. Therefore, investigating how Cdc25 is activated during the

G2/M transition may answer some fundamental questions in cancer biology.

Pin1 only speeds the interconversion of the two conformers; it does not change the relative free energy between the starting material and the product and it does not shift the equilibrium between the two conformers. In order for Pin1 to be essential for mitosis, the equilibrium levels of cis and trans conformation of phosphoCdc25 must be changed from outside this cis-trans interconversion, either upstream or downstream of the Cdc25-Pin1 interaction. Specific phosphorylation, therefore, is one likely upstream event to shift the equilibrium. Thus, mitotic phosphorylation of Cdc25c has at least two consequences: 1) to generate a binding site for Pin1, and 2) to change the cis-trans equilibrium of two conformers around a proline residue. Although phosphorylation could lead to a shift of equilibrium, the new state would be reached much more slowly compared to other biological processes without Pin1 catalysis.

With the proposal of the above model, there is one unanswered questions that was investigated in this study: What is the initial state at the specific binding sites of Cdc25c for Pin1?

In order to answer this question, peptidomimetics containing (*Z*) or (*E*)-alkene isosteres as conformationally locked surrogates of *cis*- or *trans*-Ser-Pro motifs were designed and used as kinase substrates. Based on the observation that some Proline-directed kinases are conformationally specific toward their substrates, it was hypothesized that the upstream kinase, which phosphorylates specific Ser/Thr-Pro motifs in Cdc25c and creates binding sites for Pin1, would also be conformationally specific toward its substrates. This upstream kinase might discriminate between the two conformations of unphosphorylated Cdc25c at specific

Ser/Thr-Pro motifs, and only one conformation would be phosphorylated by this upstream kinase (Figure 4.3).[40, 48, 98, 257]

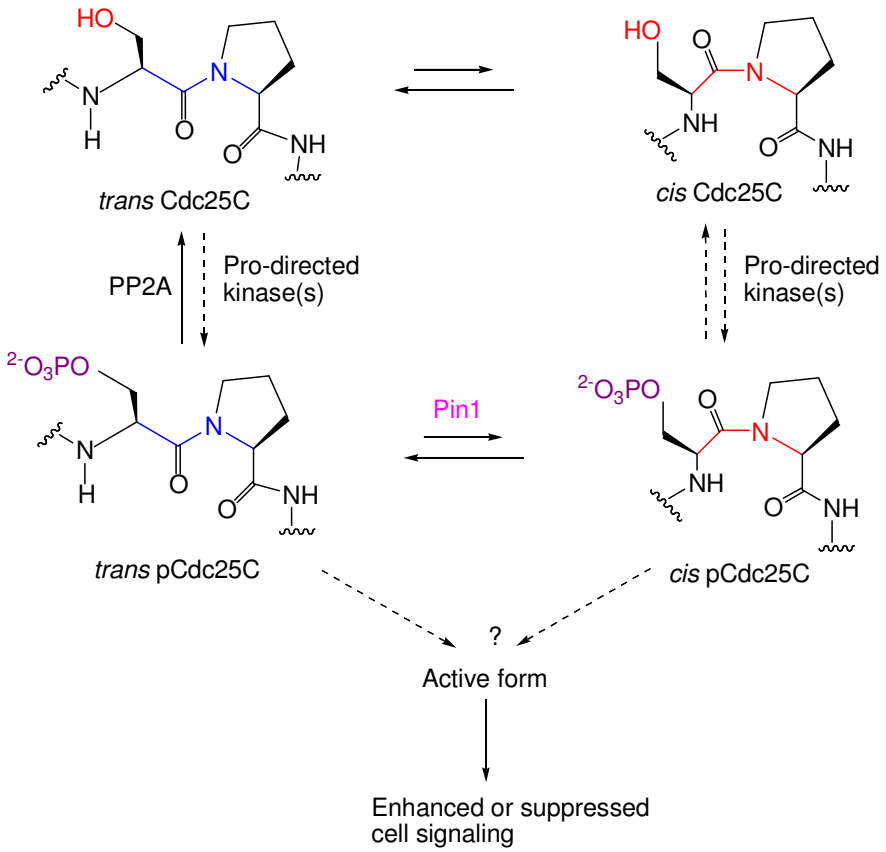

Figure 4.3. Two steps mechanism for the interaction between Pin1 and Cdc25 phosphatase[40, 48, 98, 257]

In the proposed mechanism shown in Figure 4.3, the dephosphorylation of phosphoCdc25c by PP2A phosphatase has been shown to be conformation specific, wherein only the trans conformer of phosphoCdc25c was dephosphorylated by PP2A.[47] In addition, Pin1 has been shown to facilitate the dephosphorylation of phosphoCdc25c by acting as a PPIase to speed up the conversion of the cis conformation of phosphoCdc25c to the trans conformer of phosphoCdc25c at specific pSer/pThr-Pro motifs in Cdc25c.[48] We are interested in the Pro-directed kinase that works in opposition to PP2A phosphatase on

Cdc25c.

4.2.4. Possible Positions of pCdc25c Phosphatase for the Interaction with Pin1 PPIase Domain

In order to understand the complex relationship between Pin1 and Cdc25c, we need to know the exact binding position of pCdc25c for the Pin1 PPIase domain. All pSer-Pro or pThr-Pro motifs in pCdc25c might be the interaction position(s) between Pin1 and Cdc25c. The screening of the sequence of human Cdc25c revealed several Ser/Thr-Pro motifs in Cdc25c, including Thr^{48}-Pro, Thr^{67}-Pro, Ser^{122}-Pro, Thr^{130}-Pro, Ser^{168}-Pro and Ser^{214}-Pro.[262] Among these, the WW domain of Pin1 was found to bind two conserved pThr-Pro sites in Cdc25c: $pThr^{48}$-Pro and $pThr^{67}$-Pro in Cdc25c by screening the synthetic short peptides.[49] The interaction between the WW domain of Pin1 and Cdc25c was also shown to be phosphorylation dependent, as confirmed by a peptide scan.[49] Furthermore, a synthetic phosphorylated peptide based on the sequence around the Thr^{48}-Pro motif in Cdc25c, EQPLpTPVTDL, was found to compete with Cdc25c in binding with the WW domain of Pin1, while the nonphosphorylated peptide showed no binding at all.[49]

The WW domain of Pin1 binds to $pThr^{48}$-Pro and $pThr^{67}$-Pro in Cdc25c by acting as a phospho-Ser/Thr-binding module and placing the phosphor-Ser/Thr-Pro specific isomerase domain (PPIase domain) close to its substrate.[49] Based on the amino acid preference values in each of the 6 positions surrounding the pSer/Thr-Pro motif in the substrates for the optimal binding with Pin1 PPIase domain, it was predicted that $pSer^{168}$-Pro in Cdc25c was the binding site for Pin1 PPIase domain by a weighted screening of the SWISS-PROT sequence database.[39] The binding between Pin1 and pCdc25c at $pSer^{168}$-Pro was also confirmed

experimentally using the synthetic phosphopeptide YLGS^{168}PITT based on the sequence of Ser^{168}-Pro of Cdc25c.[39] A molecular modeling study using Tripos Sybyl to compare the free energies of the docking complex between Pin1 active site and different Ser-Pro positions of Cdc25C was also carried out, and the modeling results confirm that the Ser^{168}-Pro of Cdc25c was the binding site for Pin1.[263]

In order to study the phosphorylation of Ser^{168}-Pro of Cdc25c by mitotic kinases, a series of peptides based on the sequence around the Ser^{168}-Pro motif of Cdc25c phosphatase with different *C*-terminal and *N*-terminal lengths were designed. These peptides were used in kinase reactions to screen for the optimal length for their phosphorylation at Ser residue by the upstream kinase of Pin1.

4.2.5. Possible Upstream Kinases of Pin1 for Interaction with Cdc25c

Cdc2/cyclinB and Plk1 kinases together can phosphorylate Thr^{48}-Pro, Thr^{67}-Pro, Thr^{122}-Pro, Thr^{13}0-Pro, Ser^{168}-Pro and Ser^{214}-Pro motifs in Cdc25 prior to entry into mitosis.[255, 256] The phosphorylation of Cdc25c by Cdc2/cyclinB and Plk1 kinases positively regulates the phosphatase activity of Cdc25c.[256-259] Because Cdc2 kinase is a Pro-directed kinase and a key regulator for the cell entry into mitosis, it was chosen as the upstream kinase for this project. The elucidation of the conformational specificity of the Cdc2 kinase toward its substrates will help us to better understand the regulation of the process of cell cycle.

4.3. The Conformational Specificity of Upstream Kinases for Interaction between Cdc25c and Pin1.

In order to elucidate the conformational specificity of Cdc2 kinase, (*Z*) and (*E*)-alkene

isosteres were designed as conformationally locked surrogates for the cis and trans Ser-Pro amide bonds in Cdc25c (Figure 4.4). These two alkene isosteres were then incorporated into the optimal peptide substrate for Cdc2 kinase to produce two peptidomimetics. These two peptidomimetics were separately incubated with pure Cdc2 kinase to identify which one is phosphorylated by Cdc2 kinase, and which one is not.

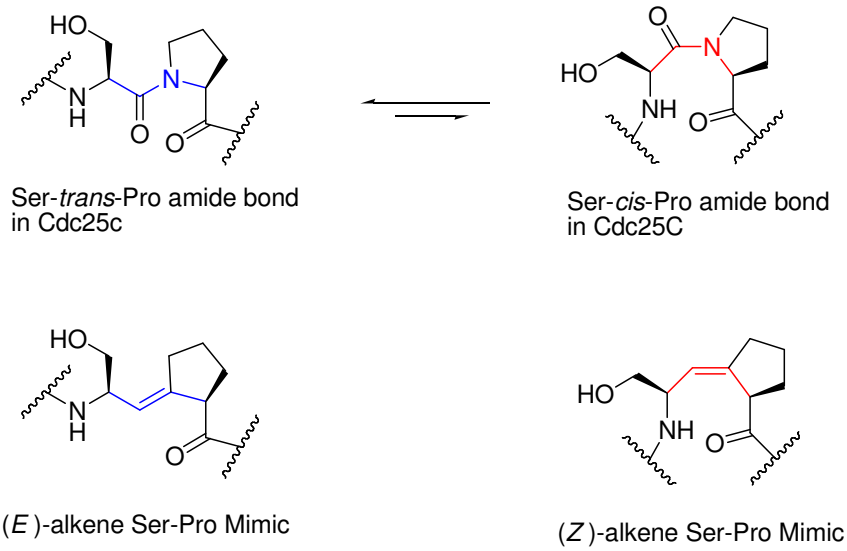

Figure 4.4. Alkene isosteres as the conformationally locked surrogates for *cis* and *trans* Ser-Pro amide bonds in Cdc25c

4.4. Techniques for Detecting Phosphopeptides and Phosphoproteins

Protein phosphorylation plays a central role in many cellular processes, including signal transduction, gene expression, the cell cycle, cytoskeletal regulation and apoptosis.[95, 170] Due to the central role of phosphorylation in the regulation of biological processes, significant effort has focused on developing techniques for analyzing protein phosphorylation.

In prokaryotic cells, phosphorylation mainly occurs at the histidine (His), glutamic acid

(Glu) and aspartic acid (Asp) sites.[264] In eukaryotic cells, phosphorylation is mainly at the serine (Ser), threonine (Thr) and tyrosine (Tyr) sites. Other phosphorylation sites include arginine (Arg), lysine (Lys), and cysteine (Cys).[264] Their structures are shown in Figure 4.5.

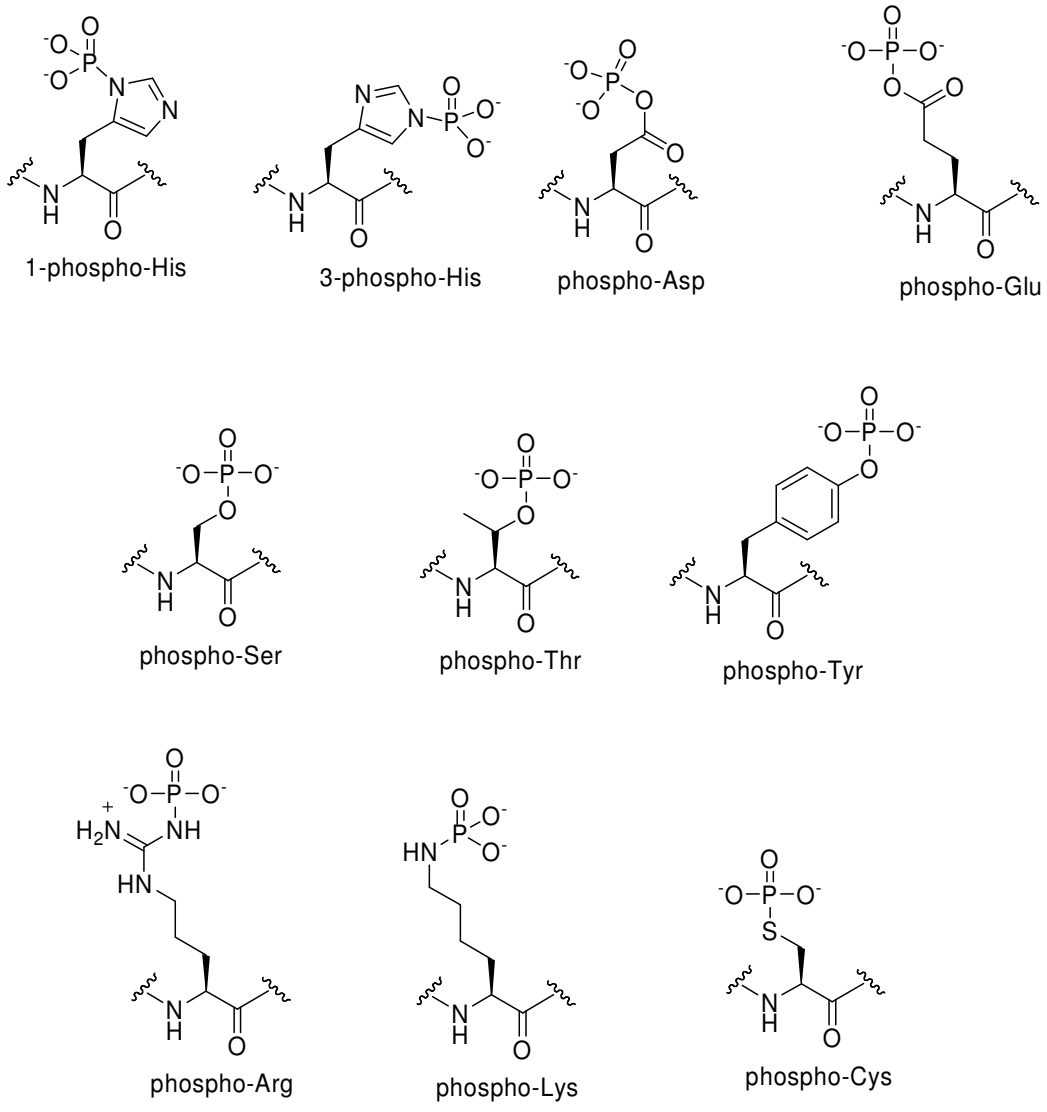

Figure 4.5. Chemical structures of phosphor-amino acid residues formed biologically

In characterizing protein or peptide phosphorylation, the following questions must be answered:

1) Has the the protein or peptide actually been phosphorylated?

2) What is the quantitative extent of phosphorylation?

3) Where are the phosphorylation sites in proteins or peptides?

In the following discussion, the techniques available for answering these important questions of the phosphorylation of peptides and proteins will be reviewed.

4.4.1 Enrichment of Phosphopeptides and Phosphoproteins

Phosphorylation of peptides is often sub-stoichiometric, such that phosphopeptides are always present in much lower concentrations compared to their unphosphorylated peptides. Also, the negatively charged modification (e.g., phosphorylation) can hinder proteolytic digestion by trypsin. Therefore, analyzing phosphoproteins or phosphopeptides is always a challenge. For example, when analyzing a phosphopeptide by mass spectrometry, its signal is always suppressed relative to its unphosphorylated counterpart.[265, 266] Therefore, enrichment of the phosphoprotein or phosphopeptide is necessary for its analysis. Several strategies have been developed to enrich the sample before the analysis.

The simplest method for enrichment is via fractionation by high performance liquid chromatography (HPLC). Fractions containing phosphopeptides can be monitored by mass spectrometry or by prior labeling with ^{32}P, followed by radioactivity detection. It is important to note that the addition of a phosphate group makes a peptide more hydrophilic, so care must be taken not to lose phosphopeptides during the fractionation process.[265, 267]

High affinity antibodies can be used to immunoprecipitate a specific protein from a complex mixture. However, a specific antibody is needed for each protein. Thus, a more

desirable alternative is an antibody that is able to immunoprecipitate any protein containing phosphorylated residues. Currently, non-sequence-specific antibodies directed against phosphoserine, phosphothreonine or phosphotyrosine have been developed. Unfortunately, only the anti-phosphotyrosine antibodies are able to display sufficiently tight binding to enable effective immunoprecipitation, so this method is presently confined to the analysis of peptides or proteins containing phosphotyrosine residues.[268]

Immobilized metal affinity chromatography (IMAC) is another valuable and widely used method for enrichment of phosphopeptides and proteins.[268] This method is based on the high affinity of negatively charged phosphate groups towards a metal-chelated stationary phase, especially Fe^{3+} and Ga^{3+} IMAC. IMAC enables phosphopeptides to be selectively bound to the column while other unphosphorylated proteins or peptides remain unbound and can be eluted first. The phosphopeptides can then be released using high pH or a phosphate buffer. The advantage of this method is that it can be used to enrich any phosphoprotein or peptide including phosphoserine, phosphothreonine and phosphotyrosine. The limitation of IMAC is that some unphosphorylated peptides, typically acidic groups (Asp, Glu) and electron donors (His) may display an affinity for immobilized metal ions.[268] However, esterification of any acidic residues prior to IMAC enrichment can be used to reduce such binding.[268] It should also be noted that some multiple phosphorylated peptides may be lost in the elution because of their high affinity towards the IMAC column.

Another widely used method for enriching phosphopeptides is via chemical modification. In this method, mixtures of peptides are exposed to high pH, whereby β elimination occurs only for the peptides containing pSer or pThr as a result of losing H_3PO_4

or PO_4^{3-} (Figure 4.6). A Michael addition then occurs between the resulting double bond and added ethanedithiol. A biotin tagging group can be attached to the thiol at acidic or neutral pH via biotinylation.[269] Biotinylated peptides can then be isolated from nonphosphorylated peptides via avidin affinity chromatography. This method, however, is not suitable for the enrichment of phosphoproteins or phosphopeptides that contain pTyr because phosphotyrosine is much more stable than phosphoserine or phosphothreonine in the alkaline state and does not undergo β elimination.[268, 269]

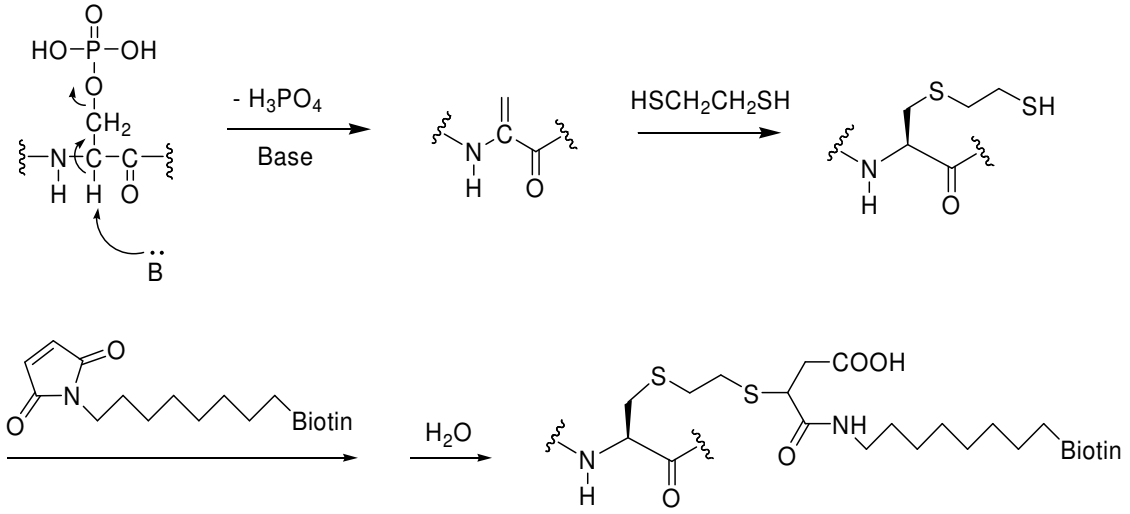

Figure 4.6. Chemical modification of phosphate group to enrich the phosphopeptide[269]

In this method, it is necessary to block the thiol group of the cysteines in the peptide because the biotin group can also be attached to the thiol via a sulfhydryl-reactive group. Generally, performic acid oxidation is preferred over alkylation since alkylated cysteine residues may undergo β elimination in a similar way to pSer or pThr.[269] The major disadvantage of the chemical modification method is it requires several steps. Thus, a large amount of sample is needed for the analysis.

4.4.2. Detection of Phosphopeptides and Phosphoproteins

Once the phosphopeptide has been enriched, phosphorylation can be detected. The traditional method is via radiolabelling of the phosphate group by ^{32}P.[268] Specifically, a radioactive phosphate is first incorporated into a protein or peptide by incubation of the peptide, Mg^{2+} and [γ-^{32}P]-ATP with a kinase *in vitro*.[268] The ^{32}P-labeled peptides and proteins can then be precipitated on filter paper, followed by thoroughly washing the filter paper to remove nonpeptide bound radioactivity.[268] After that, the filter paper is placed in a scintillation vial and counted to determine the presence and amount of phosphorylated peptides. Sodium dodecyl sulfate-polyacryamide gel electrophoresis (SDS-PAGE) is used to separate the proteins and the dried gel to X-ray film is exposed to locate the ^{32}P-labelled phosphoproteins by autoradiography.[268] Although this method is sensitive, it is tedious and the resulting radioactive waste must be discarded carefully.

Edman sequencing is another technique that can be used for detecting phosphopeptides and phosphoproteins.[268] However, with the improvement of mass spectrometry in recent years, this technique is used more frequently to determine the presence of phosphopeptide.[266, 270-275] Detection of peptide phosphorylation by mass spectrometry is based on a mass difference of 80 Da (HPO_3) (or multiples) between the phosphorylated and dephosphorylated forms.[268, 270] Resulting differences in the peptide map before and after treatment with phosphatase can further aid in the analysis. The standard procedure for the detection of phosphopeptides or phosphoproteins using MALDI-MS is as follows: 1) detect the molecular ion $[M+H]^+$; 2) treat with alkaline phosphatase, and 3) detect the $[M+H-HPO_3]^+$ ion, which is $[M+H]^+$ - 80. This method is suitable for phosphoSer,

phosphoThr and phosphoTyr residues.[264, 266, 268, 274] The comparison of three methods for detecting phosphopeptides and phosphoproteins is summarized in Table 4.1.

Table 4.1. Comparison of techniques for the detection of phosphopeptides and phosphoproteins

	^{32}P labeling	Edman sequencing	Mass spectrometry
Radioactivity	Large amounts needed	May be used	Not required
Sensitivity	Most sensitive	Less sensitive (pmol)	Highly sensitive (fmol)
Site determination	difficult	Possible (difficult for Tyr)	Precise site determination
Coverage	Full coverage difficult	Full coverage possible	Full coverage difficult
High-throughput	Not possible, labor intensive	Difficult	Possible for LC-MS/MS
Purified protein required	Yes	Yes	No

Neutral loss scanning is another useful technique in mass spectrometry.[264, 266, 268, 274] This method uses tandem MS, such as a triple quadrupole mass analyzer, to detect the neutral loss of the elements H_3PO_4 (98 Da) after collision induced dissociation (CID). Specifically, Q1 scans the entire mass range, Q2 is the collision cell, while Q3 scans the entire range with *m/z* difference of 98/n to look for phosphopeptide ions carrying a charge of +n. Only peptides ions losing H_3PO_4 in Q2 can pass through Q3. In the positive ion mode of MALDI-TOF, peptides containing pSer or pThr show a predominant neutral loss of 98 Da (β-elimination) and a loss of 80 Da (due to HPO_3). For peptides containing pTyr, which is resistant to β-elimination, only a loss of 80 Da is typically observed. Moreover, in the positive ion mode of ESI-MS/MS using neutral loss scan, a spacing of 69 Da (due to dehydroalanine) or 83 Da

(due to dehydroaminobutyric acid) is sometimes observed, which can indicate the exact location of pSer and pThr, respectively.[268] In the neutral loss scan mode, the value of the neutral loss is dependent on the charge states of the parent ions. For example, for a doubly charged peptide containing pSer, a neutral loss of 49 will be observed instead of 98 (Figure 4.7).

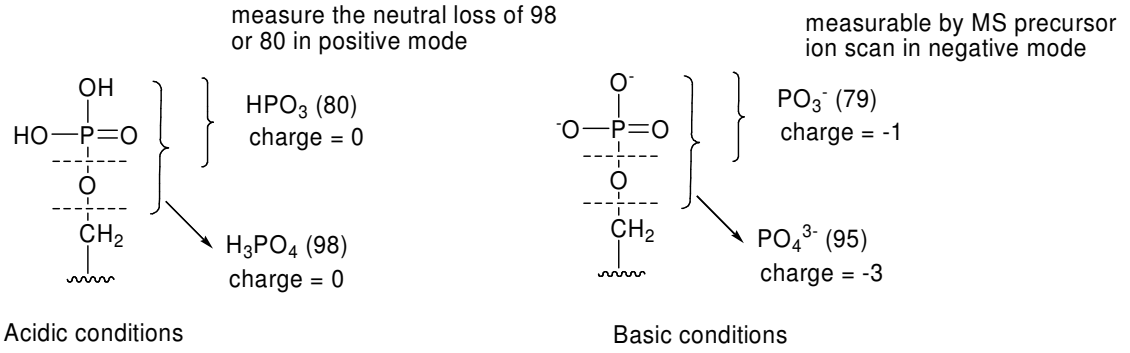

Figure 4.7. Cleavage of phosphate group in different scan modes of mass spectrometry

Precursor ion scanning, another commonly used method in ESI-MS/MS to detect phosphopeptides and phosphoproteins,[274] utilizes the detection of phosphate-specific fragments to signal the presence of a phosphorylated peptide. A triple quadrupole mass spectrometer operating in negative ion mode is generally used for this method. In the negative mode of ESI-MS/MS, the reporter ion for the phosphoSer, phosphThr and phosphoTyr residues is PO_3^- (79) (Figure 4.7). First, the proteolytic digest is desalted, making it basic under alkaline conditions, after which it is infused into the MS/MS system. Q1 scans the full ranges, then CID is induced in Q2, while Q3 is set to selectively pass only *m/z* 79 ions (due to PO_3^-). In this method, PO_3^- is the fragment-specific ion that serves as the characteristic reporter ion for the phosphorylated peptides. This method is very useful because the detection of the PO_3^- anion by mass spectrometry is very specific and sensitive

compared to a neutral loss scan. This method has enabled synthetic phosphorylated peptides to be characterized at concentrations as low as 10 fmol/μl. In addition, the fragment ion (PO_3^-) 79 is independent of the charge states of the parent ions, making it much more efficient for detecting all phosphopeptides in complex mixtures. This method is applicable for phosphoSer, phosphoThr, and phosphoTyr residues. Precursor ion scanning can also be performed in the positive mode using ESI-MS/MS instruments, which facilitates the precise detection of the immonium ion of phosphoTyr (216.043). This mode, however, is not applicable for phosphoSer and phosphoThr residues since they are labile under the same conditions. The different scan modes in tandem mass spectrometry are summarized below in Tables 4.2 and 4.3

Table 4.2. Scan modes for the detection of phosphopeptides in tandem MS

	Q1	Q2	Q3
Precursor ion scan	scanned	CID	fixed
Neutral loss scan	scanned	CID	scanned
Product ion scan	fixed	CID	scanned
Multiple reactions monitor	fixed	CID	fixed

Despite the efficiency of many of these techniques, the use of mass spectrometry to detect the presence of phosphopeptides and phosphoproteins is not without its problems. First, electrospray ionization (ESI) in most of the mass spectrometers is typically carried out in positive (+) mode, which is not efficient for detecting phosphopeptides containing negative charges on the phosphate group. Therefore, the signal intensities for phosphopeptides in mass

spectrometers are commonly quite low in negative mode. Second, the intensities of these phosphopeptides peaks are always suppressed by large amounts of non-phospho-counterparts. Third, phosphoserine and phosphotherine residues are labile, which can undergo β-elimination during the analysis process. Finally, because phosphopeptides are hydrophilic, they do not bind to the common preconcentrating material.

	Phosphatase treatment	CID neutral loss scan in + mode	CID precursor ion scan in - mode	CID precursor ion scan in + mode
MALDI-MS	$[M+H]^+$ - 80 (HPO_3) pSer, pThr, pTyr	$[M+H]^+$ - 98 (H_3PO_4) pSer, pThr $[M+H]^+$ - 80 (HPO_3) pTyr	n.a	n.a
ESI-MS/MS	n.a	$[M+H]^+$ - 98 (H_3PO_4) pSer, pThr	Detect PO_3^- (79) pSer, pThr, pTyr	Detect 216^+ pTyr

Table 4.3. Summary of the techniques used for the detection of phosphopeptides and phosphoproteins by mass spectrometry

4.4.3. Quantitative Analysis of Phosphopeptides and Phosphoproteins

After the presence of phosphorylated peptides has been confirmed, it is important to determine their stoichiometry—for example, the ratio of phosphorylated to unphosphorylated peptides. An easy way to do this involves the use of HPLC separation of the phosphopeptide from its unphosphorylated counterpart as identified by MS. We can then compare the integration of these two peaks.

Another classic technique is the radiolabelling method.[268] After the introduction of ^{32}P in a kinase reaction, the ^{32}P-labeled phosphopeptide can be located on TLC plates or 2D

SDS-PAGE by autoradiography, after which it can be quantitated by Cerenkov radioactivity counting.[268] Using the radiolabelling method, one can assess the relative spot intensities in order to quantify the relative amounts of phosphopeptides from different sources.

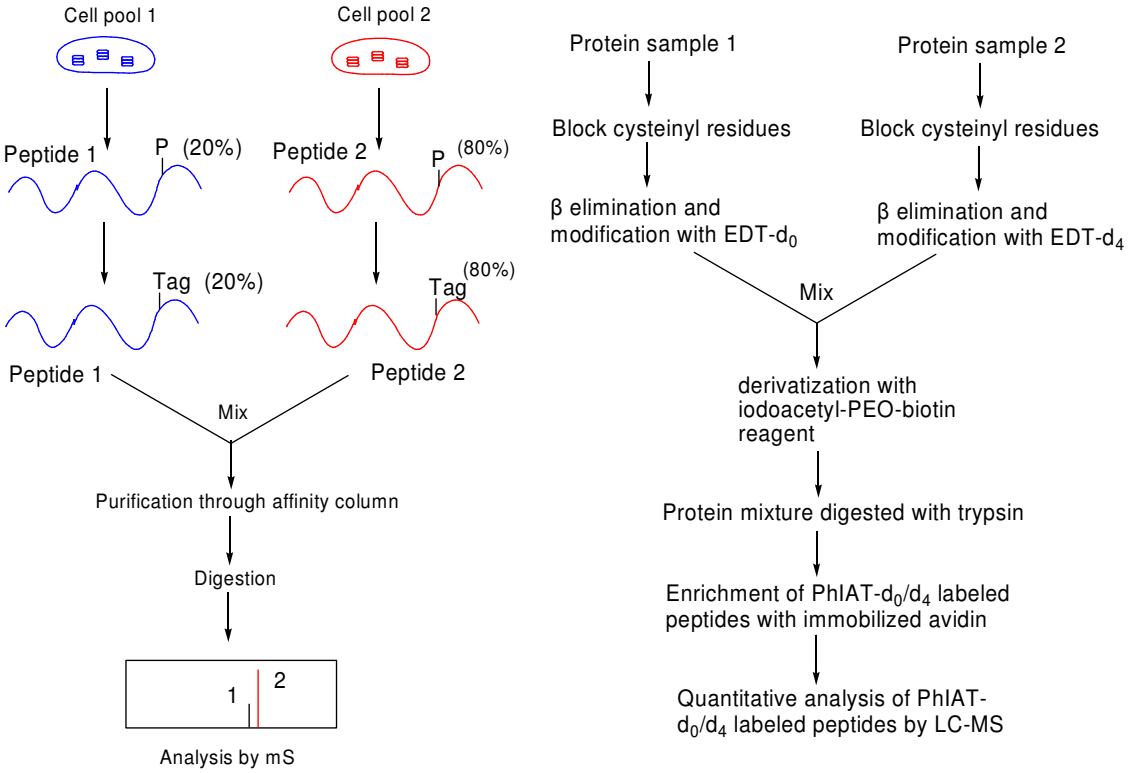

Figure 4.8. Quantitation of phosphorylation by ICAT coupled with MS[276]

Recently, ICAT (isotope-coded affinity tag) chemistry has been used to "tag" or affix a chemical marker to a peptide containing a specific type of amino acid (Figure 4.8).[276, 277] This process, when used with various mass spectrometry systems, has facilitated the quantitation of phosphorylation.[276, 277] Using this method, mass tags with different masses are introduced to the phosphorylation position via a β elimination reaction and a Michael addition of the nucleophile to the resulting carbon-carbon double bond.[276] In one sample, the nucleophile is unlabeled, while in the second sample, the nucleophile is deuterated. The two

samples are then mixed and injected into a mass spectrometer. The comparison of the peak intensities within each pair can identify the relative amounts of these two phosphopeptides which are derived from different sources.

4.4.4. Determination of the Phosphorylation Position in Phosphopeptides and Phosphoproteins

One of the important concerns with respect to phosphorylation is: Where are the phosphorylation sites in proteins or peptides? The classic approach for identifying a phosphorylation site is radiolabelling by ^{32}P, coupled with Edman sequencing analysis.[268] In this method, ^{32}P radioactivity is incorporated into a phosphopeptide using [γ-^{32}P] ATP. Phosphoproteins then can be degraded chemically or enzymatically into small peptides, and the small peptides can then be separated by 2D SDS-PAGE or a combination of electrophoresis/chromatographic analysis. Sequence analysis of each fragment can then be performed by gas phase or solid phase *N*-terminal Edman sequencing.[268] The detection of ^{32}P radioactivity is the only criterion for locating phosphorylated amino acids. The disadvantage of this method is that it is tedious and subject to error. Moreover, this method is not suitable for high throughput experiments.[268]

Mass spectrometry has become a very useful technique in the elucidation of phosphorylation sites in recent years.[269-271, 273, 275, 278] In the MS/MS mode using a triple quadrupole mass analyzer system, a collision-induced dissociation (CID) of samples produced by ESI occurs in Q2, followed by peptide mapping in Q3. Although the loss of phosphate as HPO_3 or H_3PO_4 is a favored fragmentation event (which can dominate backbone cleavage), phosphoamino acid sequences can still be assigned according to their

weaker backbone fragment ions. Some programs, such as PEPSEARCH and SEQUEST,[273] are able to identify peptide sequences and phosphorylation sites from uninterpreted MS/MS spectra. Since the phosphate group is labile in CID mode, modification of the phosphate group can be used. Most commonly, β elimination is used to convert pSer or pThr to *S*-ethylcysteine or *β*-methyl-*S*-ethylcysteine residues via the addition of a base and ethanethiol.[272] Since the labile phosphate group was removed, the modified peptides can fragment more evenly within the peptide backbone, affording more complete sequencing information.[272]

Electron transfer dissociation (ETD), combined with Fourier transform ion cyclotron resonance (FTICR-MS), is another useful technique for identifying phosphorylation sites.[275, 279] ETD induces more extensive fragmentation of the peptide backbone than CID.[275, 279-281] Moreover, the loss of phosphoric acid, phosphate, or water does not occur when using the ETD method, making it very useful for analyzing peptide sequences and phosphorylation sites.

Post-source decay is another peptide mapping technique in mass spectrometry. It is particularly useful in distinguishing the phosphorylated sites of peptides containing pSer/Thr-Pro moieties.[282] When the phosphorylation position is immediately to the amino-terminal side of a proline residue, cleavage of the intervening amide bond is highly preferred. This makes the identification of a phosphorylation site much easier.[271] The downside is that this technique requires the more expensive MALDI-TOF MS instrument.

4.4.5. Fragment Ions in Mass Spectrometry

Three types of fragment ions are commonly formed during CID or ETD in mass

spectrometry. The nomenclature for these fragment ions are shown in Figure 4.9. The b and y type ions are derived from the cleavage of the amide bond (C-N bond), while the c and z type ions are derived from the cleavage of the αC-N bond. In CID, b and y type ions are predominantly formed.[283] At relatively high collision energy, the formation of b type ions is preferred, while y type ions are preferred at relatively low collision energy. In ETD, c and z type ions are commonly dominant, which preserve post modification such as phosphorylation.[275, 279] Therefore, ETD is very useful for detecting the post modification of proteins and peptides.[275, 279]

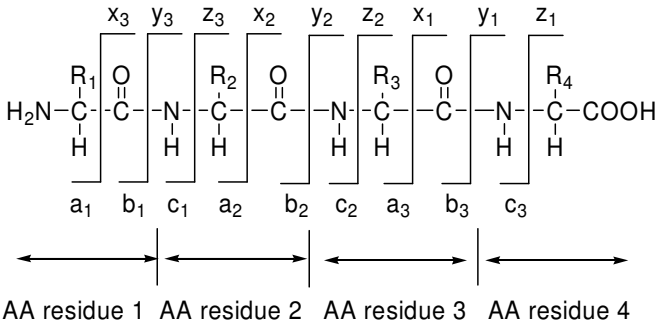

Figure 4.9. Nomenclature of fragment ions from mass spectrometry

With regard to the mechanism by which b and y type ions are formed during CID, it has been shown that this occurs through an oxazolone pathway or via direct cleavage of the amide bond. These mechanisms are depicted in Figure 4.10 and Figure 4.11, respectively.[283, 284]

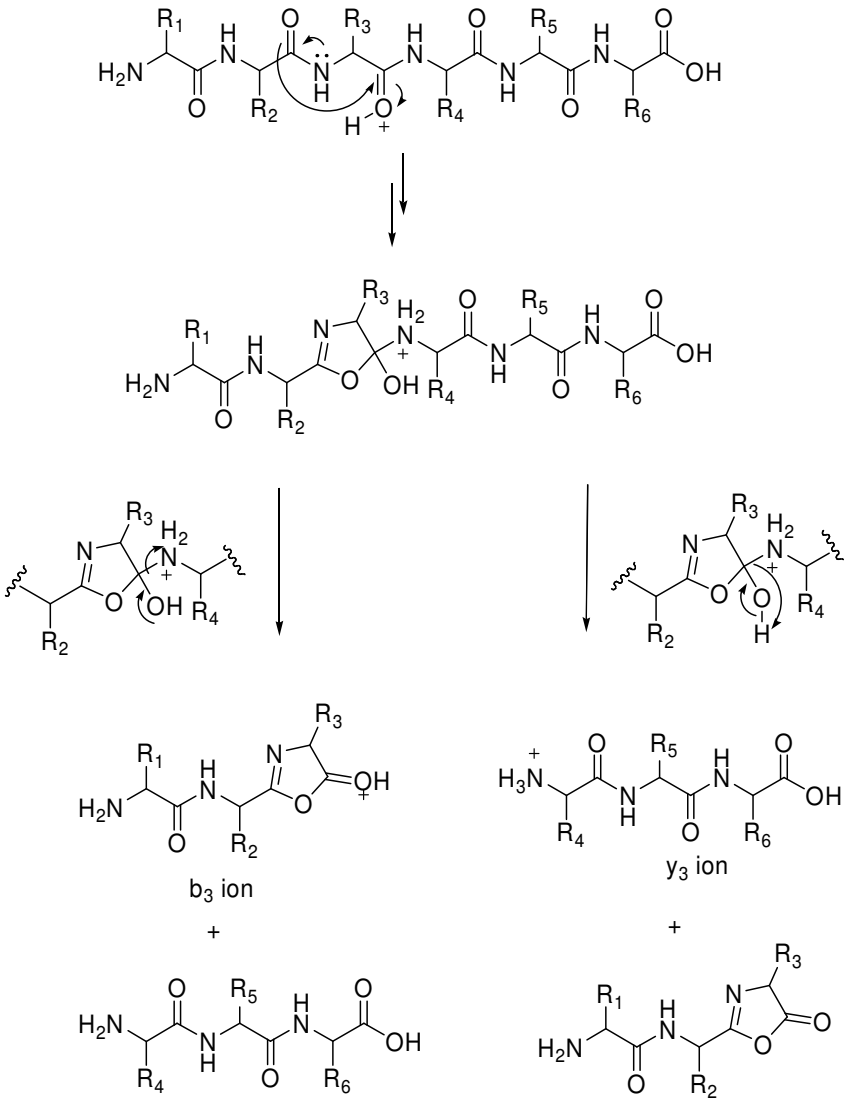

Figure 4.10 Formation of b and y type ions in CID through an oxazolone pathway[283, 284]

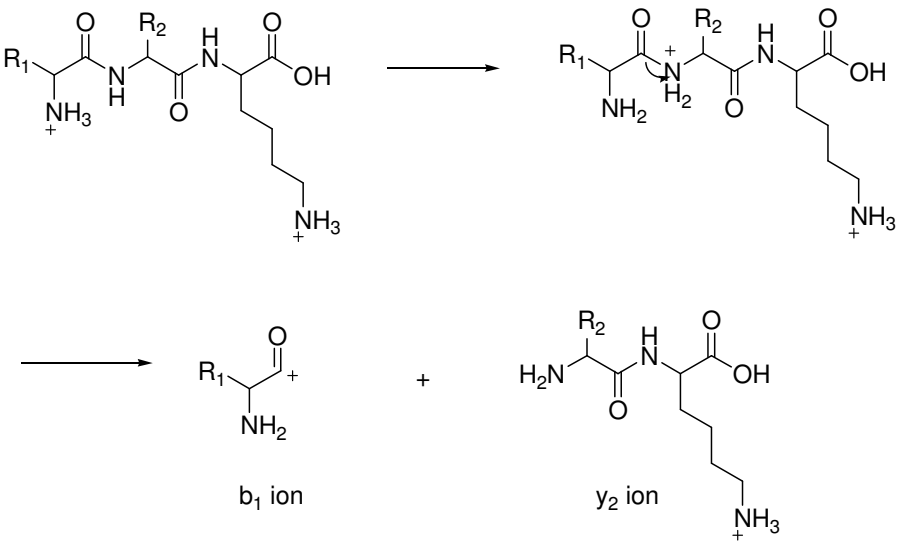

Figure 4.11. Formation of b and y type ions through the cleavage of amide bond from doubly charged parent ions[279, 283, 284]

4.5. Optimization of the Peptide Substrate Derived from the Sequence Around Ser168-Pro in Cdc25c for Cdc2 Kinase

4.5.1. Synthesis of Eight Peptides Containing Ser168-Pro Moiety of Cdc25c by Solid Phase Peptide Synthesis

In this study we investigated the conformational specificity of the Cdc25c substrate for Cdc2 kinase, as well as its relationship with Pin1. Before the (*Z*)- and (*E*)-alkene isosteres were incorporated into the appropriate peptide substrates, however, it was necessary to optimize the Cdc2 kinase reaction conditions. These include the lengths and concentrations of the peptide substrates, the concentrations of ATP and Mg^{2+}, temperature and time. Among these factors, the length of the peptide substrates was the most important factor. This is due to the fact that Cdc2 kinase will not recognize a peptide substrate if it is too short; conversely, it would be quite difficult to synthesize a long-chain peptide with incorporation of alkene isosteres. Therefore, the optimal length for the peptide substrates had to be determined first.

Once that information was ascertained, the model peptide substrate could be used as the control substrate to optimize the other conditions for Cdc2 kinase reaction.

In order to minimize the length of the peptide substrate of Cdc2 kinase, a series of peptides based on the sequence around Ser^{168}-Pro motif of human Cdc25c phosphatase with different *C*-terminal and *N*-terminal lengths were designed. These peptides were incubated with Cdc2 kinase in a suitable kinase buffer. An LC-MS/MS technique was used to determine whether these peptides could be efficiently phosphorylated at the Ser position by Cdc2 kinase *in vitro*.

Based on the sequence of Ser^{168}-Pro of human Cdc25c, the following eight peptides with varied *C*-terminal and *N*-terminal lengths were designed: AcMKYLG**SP**ITTVNH_2 (**57**), AcYLG**SP**ITTVNH_2 (**58**), AcKYLG**SP**ITTNH_2 (**59**), AcG**SP**ITTVNH_2 (**60**), AcLG**SP**ITTNH_2 (**61**), AcYLG**SP**ITNH_2 (**62**), AcG**SP**ITNH_2 (**63**), AcLG**SP**INH_2 (**64**). Acetyl groups and amide groups were used as protecting groups on the *N*-termini and *C*-termini of the peptides to neutralize their charges and improve the substrate binding to the kinase. Using these peptides, we tried to determine which terminus of the peptide around the Ser-Pro core was more important for the recognition by Cdc2 kinase, as well as the necessary minimum length of the peptide substrates.

Rink amide MBHA resin was used for the synthesis of the control peptides via the Fmoc solid phase peptide synthesis strategy. First, resin was swelled in CH_2Cl_2 and NMP for 20 min each. piperidine was used to remove the Fmoc group from the resin. The Kaiser test was used to determine the presence or absence of primary amino groups, wherein a dark blue resin indicated the presence of primary amino groups, while yellow indicated the absence of

primary amino groups. However, for some longer peptides containing more than 15 amino acids, the Kaiser test was neither reliable nor accurate. In the case of coupling with proline or removal of proline, the Chloranil test was used to check for presence of secondary amine group.

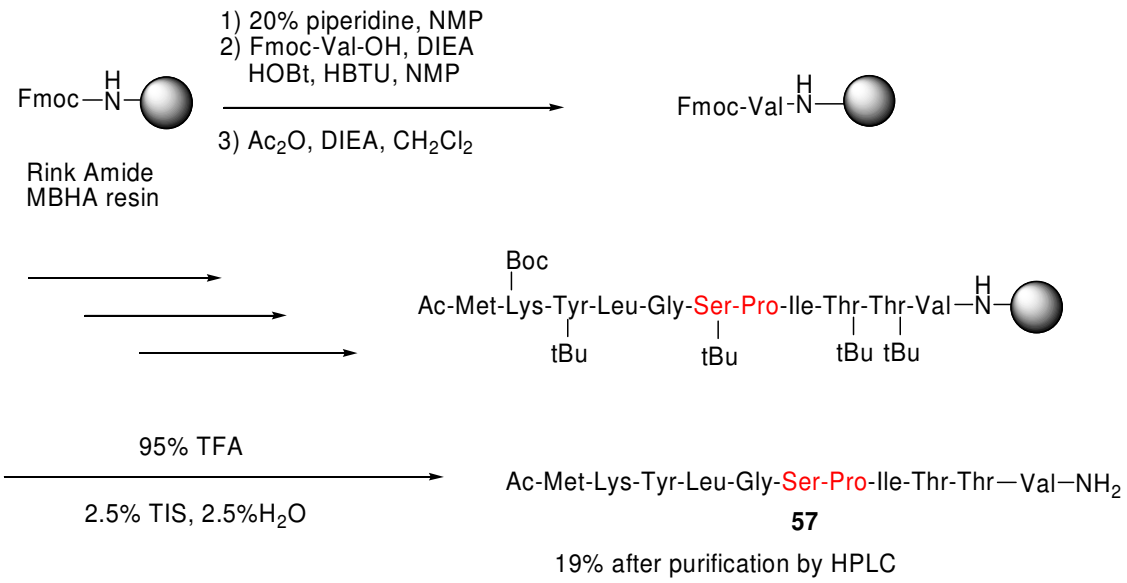

Scheme 4.1. Solid phase peptide synthesis of peptide AcMKYLGSPITTVNH$_2$

Fmoc protected amino acids were used in the coupling reaction with free primary amino groups on Rink amide resins. HBTU and HOBt were used as the coupling reagents and DIEA served as the base. For serine, threonine and tyrosine, which all have side chain hydroxyl groups, *tert*-butyl protected Fmoc amino acids were used in the coupling reaction. With the exception of the first amino acid, each coupling step generally took about 20 minutes to complete. If the Kaiser test gave a blue color after the first coupling, a second coupling was performed. If, however, the Kaiser test still gave a blue color after the second coupling, the resin was then capped with acetic anhydride and DIEA in dichloromethane for 30 minutes. TFA in CH_2Cl_2 was used to cleave the peptides from the resin. Triisopropylsilane

(TIS) and water were used as cation (t-Bu^+) scavengers. The crude peptides were precipitated in cold ether. The synthesis of 11-mer peptide $AcMKYLGSPITTVNH_2$ is described in Scheme 4.1.

4.5.2 Purification of the Crude Peptides by RP-HPLC and Characterization of these Peptides.

Analysis of the purity of these peptides was performed using a reverse phase analytical HPLC(Table 4.4). It should be noted that TFA was used as the ion-pairing agent to enhance interactions between the peptide and column packing. The crude peptides were purified via semi-preparative reverse HPLC

Table 4.4. Amounts, percent yields of eight peptides after purification by RP-HPLC

Peptide sequences	Mass (mg)	Percent yield (%)
$AcMKYLG\mathbf{SP}ITTVNH_2$	15	19
$AcYLG\mathbf{SP}ITTVNH_2$	8	13
$AcKYLG\mathbf{SP}ITTNH_2$	15	23
$AcG\mathbf{SP}ITTVNH_2$	26	57
$AcLG\mathbf{SP}ITTNH_2$	10	21
$AcYLG\mathbf{SP}ITNH_2$	30	60
$AcG\mathbf{SP}ITNH_2$	30	90
$AcLG\mathbf{SP}INH_2$	10	30

Table 4.5. Molecular weights and determined masses of eight peptides

Peptide sequences	Calculated $[M+H]^+$	Experimental $[M+H]^+$
AcMKYLG**SP**ITTVNH_2	1251.51	1251.5
AcYLG**SP**ITTVNH_2	992.14	992.3
AcKYLG**SP**ITTNH_2	1021.18	1021.3
AcG**SP**ITTVNH_2	715.81	715.4
AcLG**SP**ITTNH_2	729.83	730.0
AcYLG**SP**ITNH_2	792.32	792.1
AcG**SP**ITNH_2	515.57	515.6
AcLG**SP**INH_2	527.63	527.4

NMR spectra for these purified peptides were taken in DMSO-d_6. The experimental $[M+H]^+$ values of these purified peptides using FAB-MS in the positive ion mode matched the calculated $[M+H]^+$ values of these peptides very well, indicating the syntheses were successful (Table 4.5).

4.5.3. Synthesis and Purification of Four Phosphopeptide Standards

In order to increase the sensitivity for detecting phosphopeptides from the kinase reaction by mass spectrometry, standard phosphopeptides are commonly used to optimize the parameters of mass spectrometer. For this reason, four standard phosphopeptides were synthesized by Fmoc solid phase peptide synthesis strategy: AcMKYLGp**SP**ITTVNH_2 (**65**), AcYLGp**SP**ITTVNH_2 (**66**), AcKYLGp**SP**ITTNH_2 (**67**) and AcYLGp**SP**ITNH_2 (**68**). The procedure was similar to the synthesis of their unphosphorylated counterparts except for the

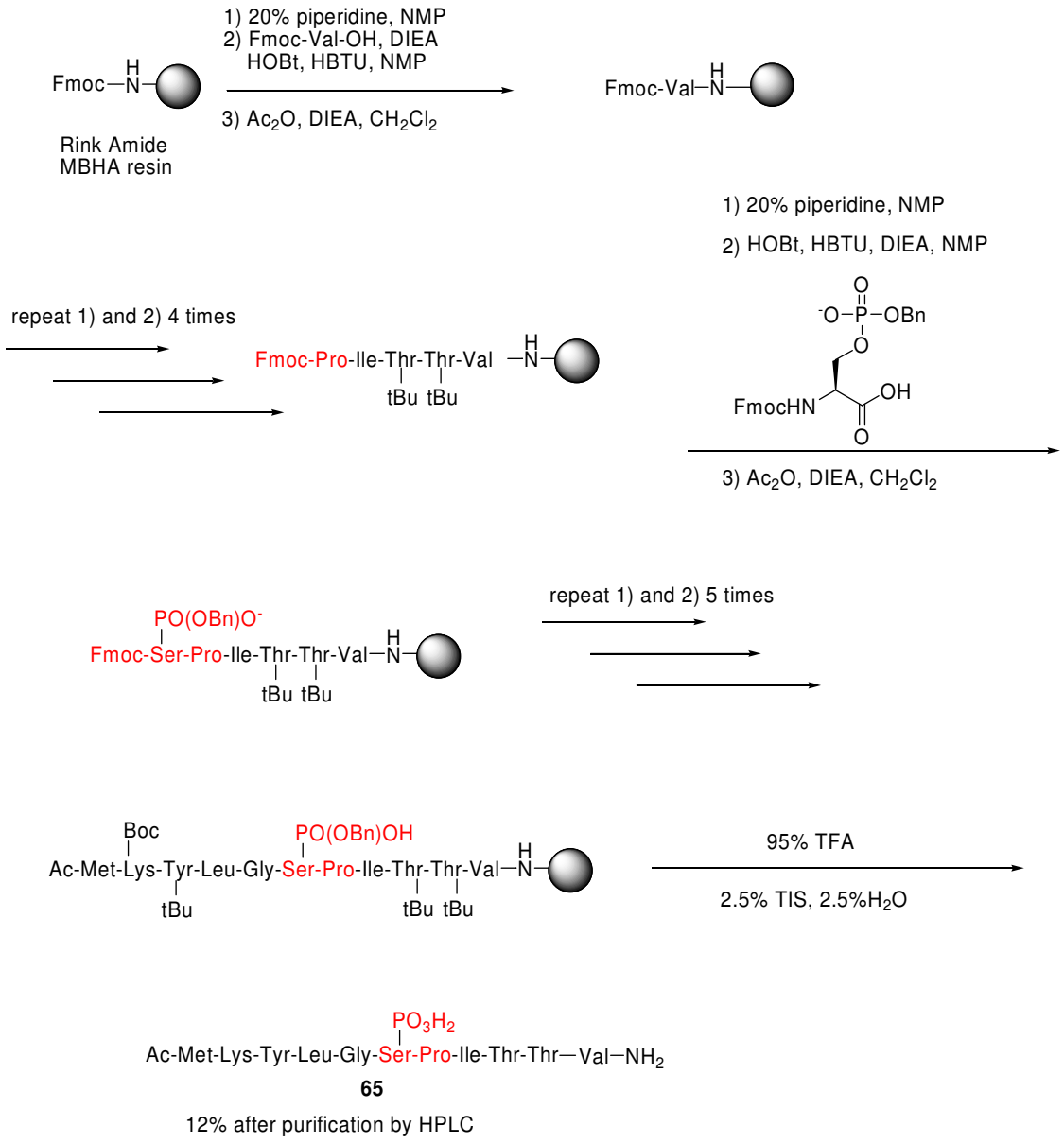

Scheme 4.2. Synthesis of AcMKYLGpSPITTVNH$_2$ **12**

coupling of the phosphoSer residue. Commercially available Mono-benzyl protected phosphoSer was used for the coupling step because it resists the β-elimination reaction during the solid phase synthesis process. The benzyl protecting group was removed simultaneously when the peptides were cleaved from the resins by 95% TFA. The synthesis of the resulting 11-mer phosphopeptide AcMKYLGp**SP**ITTVNH$_2$ is outlined in Scheme 4.2.

Purification of the phosphopeptides was performed on semi-prep reverse phase HPLC using 250 × 21.4 mm, 5 μm column (Varian Solaris). No TFA was added to the HPLC solvents to prevent the β-elimination reaction of the phosphopeptides.

Table 4.6. Amounts and percent yields for the synthesis of phosphopeptides

Phosphopeptides	Mass (mg)	Percent yield (%)
AcMKYLGp**SP**ITTVNH_2	2.2	9.7%
AcYLGp**SP**ITTVNH_2	1.7	11%
AcKYLGp**SP**ITTNH_2	3.5	15%
AcYLGp**SP**ITNH_2	1.5	5.6%

Table 4.7. Calculated and experimental $[M+H]^+$ values for phosphopeptide standards

Phosphopeptides	Calculated $[M+H]^+$	Determined $[M+H]^+$
AcMKYLGp**SP**ITTVNH_2	1330.5	1330.4
AcYLGp**SP**ITTVNH_2	1071.14	1071.3
AcKYLGp**SP**ITTNH_2	1100.18	1100.2
AcYLGp**SP**ITNH_2	871.32	893.2

4.5.4. Phosphorylation of the Eight Peptide Substrates Using Mitotic Extract

Since Cdc25c is phosphorylated at multiple Ser-Pro or Thr-Pro positions during the G2/M transition, mitotic extracts prepared just prior to the transition should be capable of phosphorylating Cdc25c *in vitro.* Thus, mitotic extracts from *Xenopus* embryos at the transition stage G2/M of cell cycle prepared by Aucland in Dr. Sible's lab (Department of

Biology, Virginia Tech) were used to determine if these peptide substrates were phosphorylated (Figure 4.12). Because 20 mM each of ATP and $MgCl_2$ had already been added to the mitotic extract during its preparation, no additional ATP or $MgCl_2$ were added to the kinase incubation mixture. $CaCl_2$ was added to trigger the extract entry into mitosis. After the peptide substrates were incubated with the mitotic extract at room temperature for 100 min, 50% acetic acid was used to quench the reaction. Sample preparation included filtration to remove the high MW proteins in the reaction mixture, as well as desalting with C18 analytical HPLC. The samples were analyzed by LC-MS/MS

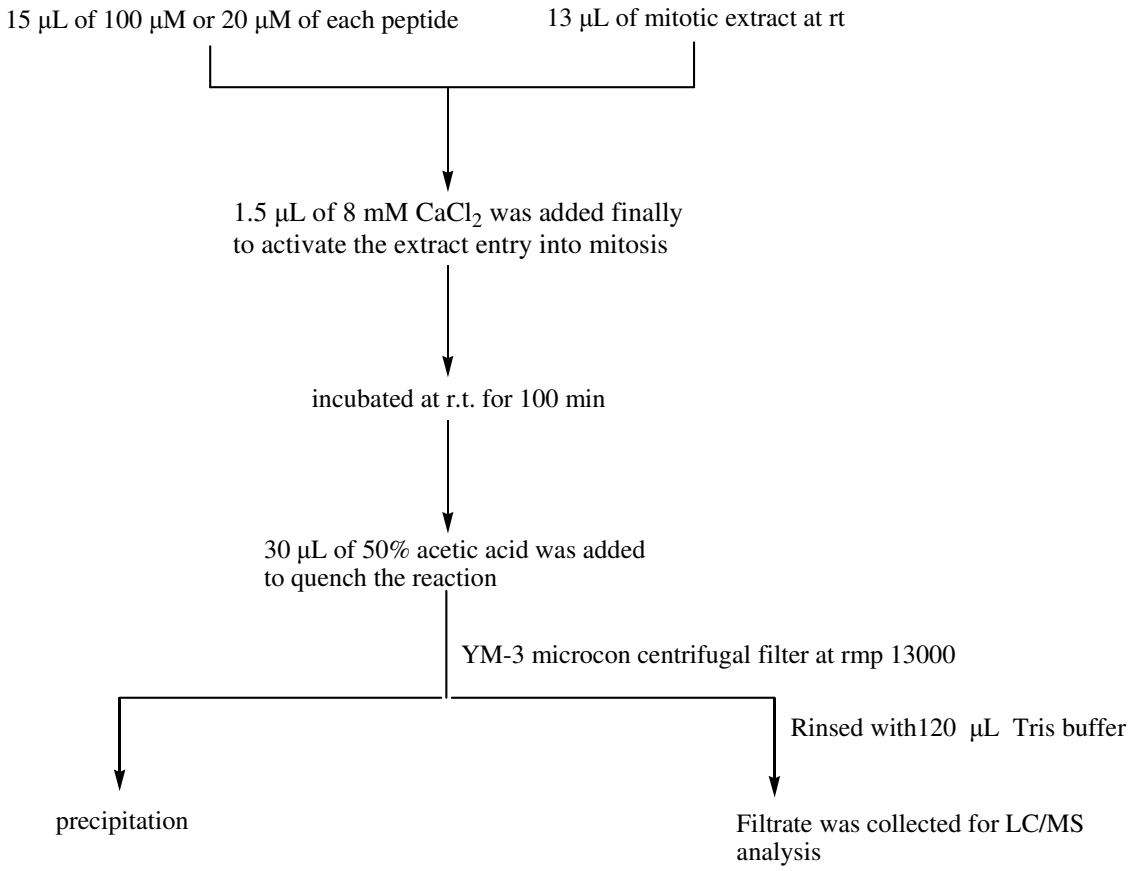

Figure 4.12. Phosphorylation of peptide substrates by mitotic extract

A Q1 full scan using LC-MS to screen the molecular weights of the phosphopeptides from the injected mixture proved to be unsuccessful. There was a large and broad junk peak (retention time was from 17.0 min to 23.0 min) in all of the injected samples. This large junk peak not only overlapped with the elution ranges for the peptide substrates and the phosphorylated peptide products in the chromatograms, but also suppressed the signals of the desired phosphopeptides. This peak was thought to come from the complex mitotic extract, which contained a variety of proteins, phosphoproteins and other biomolecules. Thus, the molecular ions of the phosphopeptides and their respective chromatographic peaks could not be obtained in the Q1 full scan experiment. Figure 4.13 illustrates the total ion chromatogram of the Q1 full scan LC-MS analysis of the incubation of AcMKYLGp**SP**ITTVNH_2 with mitotic extract.

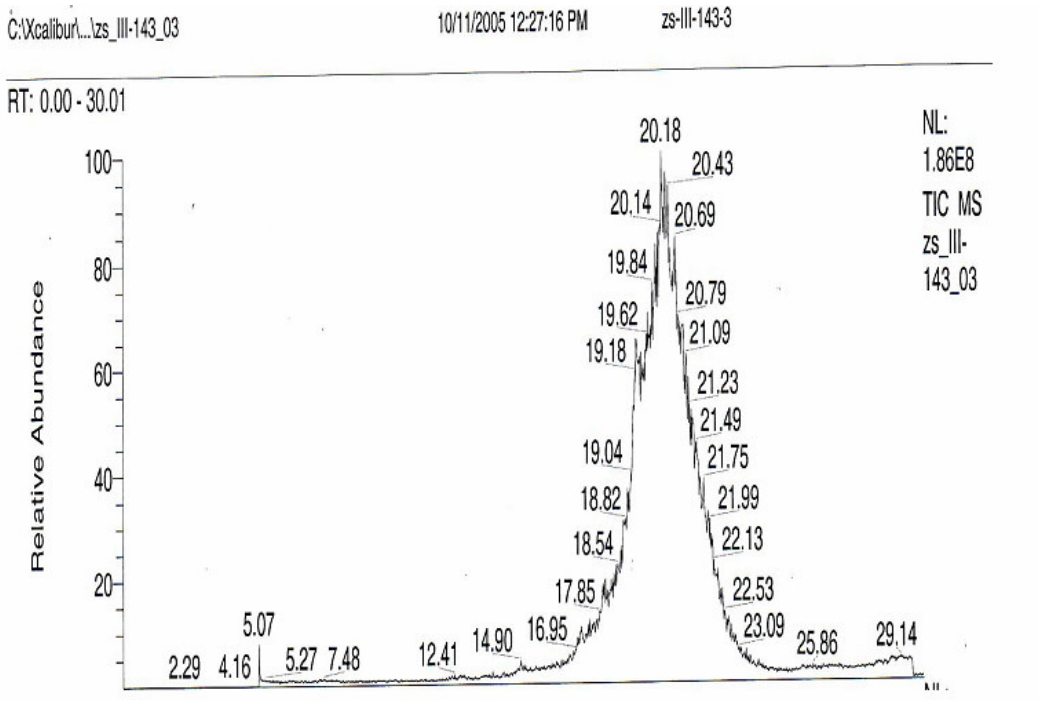

Figure 4.13. Q1 full scan LC-MS analysis of theproducts from incubation of AcMKYLG**SP**ITTVNH_2 with mitotic extracts

Single ion monitoring (SIM) in LC-MS was attempted to increase the detection sensitivity. In the SIM procedure, Q1 only scans a very narrow mass range around the desired MW of the phosphopeptide AcMKYLGp**SP**ITTVNH_2. However, as in the previous trial, a large junk peak remained in all the samples (Figure 4.14). No obvious peaks corresponding to the desired MWs of phosphopeptides were obtained.

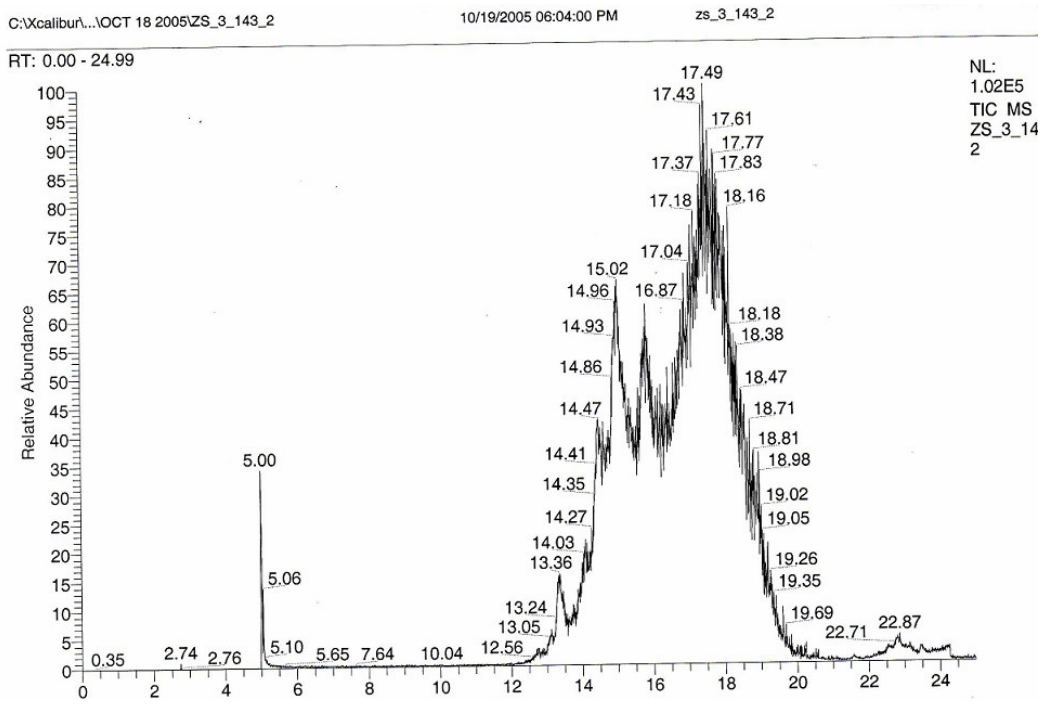

Figure 4.14. SIM scan LC-MS analysis of the incubation of AcMKYLG**SP**ITTVNH_2 with mitotic extracts

Neutral loss scan (H_3PO_4 98) in positive ion mode is the most commonly used method for detecting phosphopeptides and phosphoproteins by mass spectrometry.[268] This method was also used to detecte phosphopeptides resulting from the incubation with mitotic extract. However, no obvious peaks were observed for the desired MWs of the phosphopeptides (Figure 4.15). Moreover, the signal was very noisy (10^3 cps), indicating that only very small amounts of the desired phosphopeptides formed during the incubation with mitotic extracts.

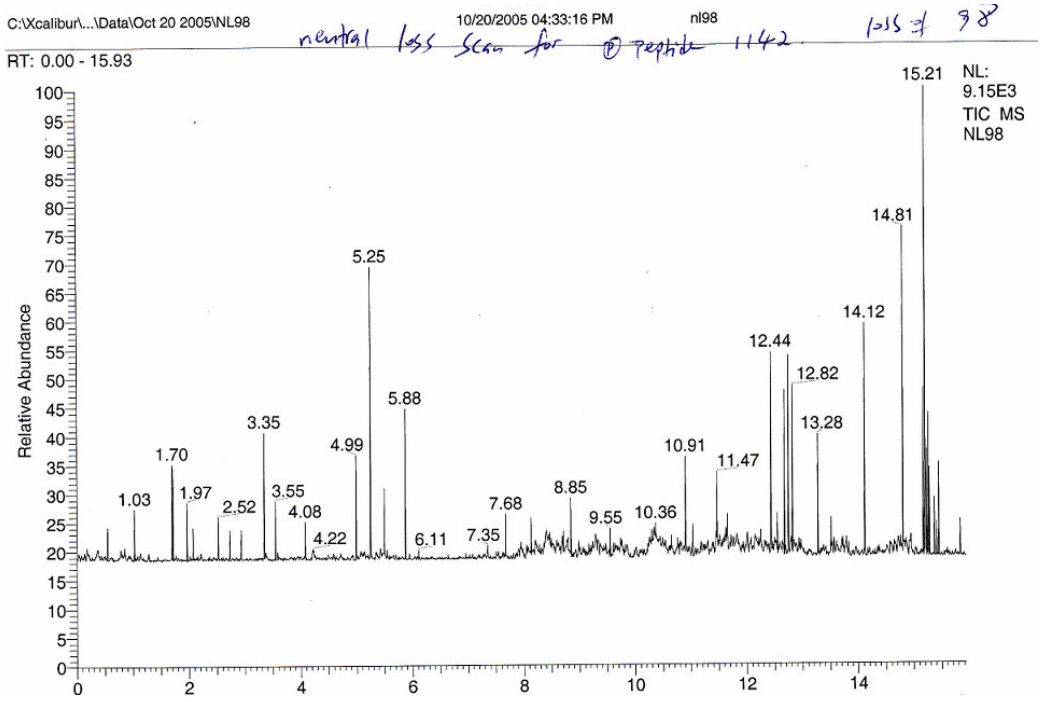

Figure 4.15. Neutral loss scan for the incubation of AcMKYLG**SP**ITTVNH_2 with mitotic extracts

In summary, the phosphorylation of peptide substrates with mitotic extract was not successful. We propose the following reasons for this result:

1) The activity of the mitotic extract may be poor. And it is difficult to measure the actual concentration of Cdc2 kinase in the mitotic extracts.

2) The complex mitotic extract made the analysis of the phosphopeptides by mass spectrometry very difficult. The large junk peak observed from the mitotic extracts had a huge suppression effect on the desired signals of the phosphopeptides.

3) The complex mitotic extract made the sample preparation difficult. The recovery of the phosphopeptides may not be efficient during the sample preparation involving multiple steps.

These disappointing results with the mitotic extract led us to use pure Cdc2

kinase/cyclin B complex to phosphorylate these peptide substrates.

4.5.5. Phosphorylation of Peptide Substrates Using Pure Cdc2/cyclin B

Recombinant human Cdc2/cyclin B complex was purchased from Sigma and New England Biolabs. Cdc2 kinase is composed of two subunits, a 34 kDa catalytic subunit (Cdc2) and a 55 kDa regulatory subunit (cyclin B).[53] Both subunits are essential for the activity of Cdc kinase during mitosis and meiosis in eukaryotes.[53]

4.5.5.1. Phosphorylation of Control Peptide Substrate in Cdc2 Kinase Reaction

In order to verify the activity of the purchased Cdc2/cyclin B complex and optimize conditions for subsequent kinase reactions, a known substrate for Cdc2 kinase was used. Histone H1 is the most commonly used Cdc2 kinase substrate that is commercially available.[285] In order to detect phosphorylation by mass spectrometry, small peptide substrates are necessary. Some well-known peptide substrates for Cdc2 kinase include Ac**SP**GRRRRKNH$_2$ and PK**TP**KKAKKL, which are derived from the p34^{Cdc2} *in vitro* phosphorylation sites of histone H1.[286-288] Because the peptide substrate AcSPGRRRRKNH$_2$ has the same protecting groups at the *C*-terminus and *N*-terminus, it was used as the control peptide in the positive control experiments.

A typical experimental procedure for Cdc2 kinase reaction is depicted in Figure 4.16. The Cdc2 kinase reaction conditions that needed to be optimized in this procedure include the following: concentration of peptide substrates, concentration of ATP, concentration of $MgCl_2$, amount of Cdc2 kinase, incubation temperature, incubation time, and quench conditions.

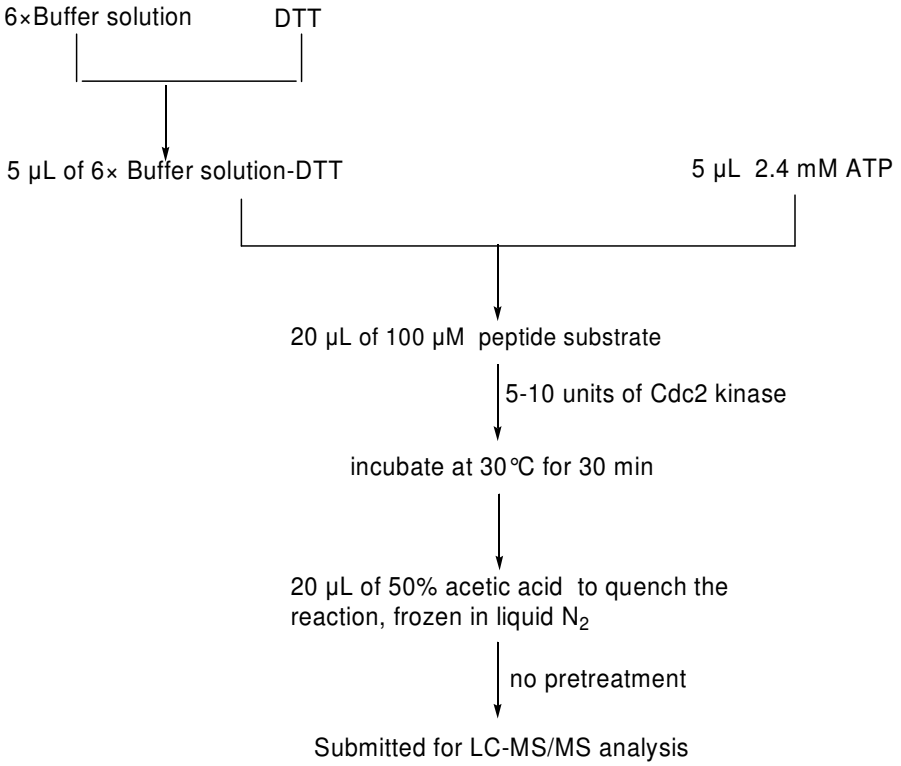

Figure 4.16. Procedure for the Cdc2 kinase reaction

In order to detect the phosphorylated peptide, AcpSPGRRRRKNH$_2$, in the positive control experiment, single ion monitoring (SIM) for 1135 ([MH]$^+$) or 568 ([MH$_2$]$^{2+}$) in positive ion mode, precursor ion scan for 79 (PO_3^-) in negative ion mode and neutral loss scan for 98 (H_3PO_4) in positive ion mode were tried.

The chromatogram for the SIM scan is shown in Figure 4.17. Two peaks (retention times = 2.89 min and 9.70 min) were obtained. The product ion scan for the first peak at 2.89 min gave fragments in which no [M + H – H_3PO_4]$^+$ or [M + H – HPO_3]$^+$ fragment ions were observed. This indicated that the first peak was not a phosphopeptide. The product ion scan for the second peak at 9.70 min gave the fragment ion with the loss of H_3PO_4. Therefore, the second peak represented the desired product Ac-pSPGRRRRK-NH$_2$. The occurrence of two peaks with a MW of 1135 Da was due to the low resolution of the mass spectrometry. A

neutral loss scan for 98 at positive mode confirmed the formation of Ac-pSPGRRRRK-NH_2 at 9.70 min. A precursor ion scan for 79 at negative mode failed to produce the signal for phosphopeptide, which we believe was due to the low sensitivity of mass spectrometry in negative ion mode than in positive ion mode. Without the standard Ac-pSPGRRRRK-NH_2, it was not possible to conduct quantitative analysis of the concentration of phosphorylated peptide, Ac-pSPGRRRRK-NH_2.

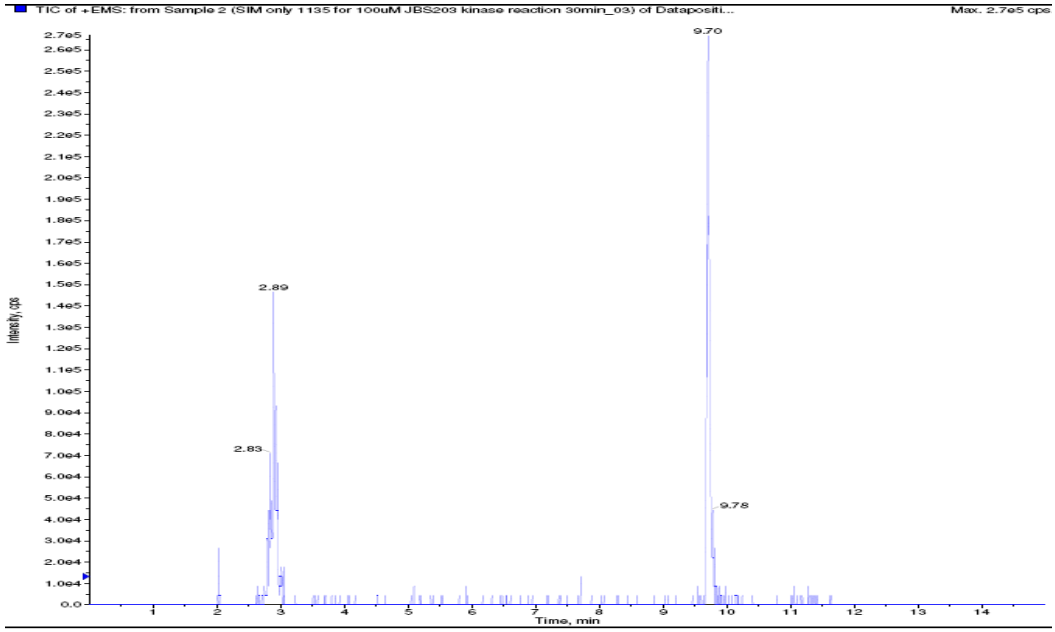

Figure 4.17 SIM scan for 1135 ($[MH]^+$) in control experiment with Ac-pSPGRRRRK-NH_2, a histone H1 peptide for Cdc2 kinase

4.5.5.2. Method Development for the Quantitative Analysis of Target Phosphorylated Peptide Substrates by LC-MS/MS

Due to the success of the positive control experiment using AcSPGRRRRKNH_2 peptide substrate, the eight synthetic peptide substrates derived from Cdc25c were then

incubated with the pure Cdc2 kinase under the same kinase conditions. The kinase reaction mixtures were then analyzed by LC-MS/MS. In order to determine the concentrations of phosphopeptides formed during the kinase reaction, standard synthetic phosphopeptides were used to develop a quantitative method for each peptide. A multiple reaction monitoring (MRM) scan was used for the quantitative analysis of these phosphopeptides. In a typical MRM scan, Q1 only allows the parent ions with specific *m/z* values to pass through, followed by the fragmentation of these specific parent ions in Q2 (collision cell). Subsequently, Q3 also only allows the fragment ions with specific *m/z* values to pass through.[273, 274, 278] MRM scan experiments, using triple quadrupole or triple quadrupole-ion trap instruments, are designed to detect the target molecules very specifically. Knowing the mass of the target compound, as well as its most abundant fragment ion, allowed us to design an MRM experiment to specifically detect the target molecule. In addition, MRM provides maximum detection sensitivity because Q1 and Q3 only scan very narrow mass ranges. The drawback of MRM is that standard target molecules are required to optimize the parameters for the mass spectrometer.[273, 274, 278]

First, MRM experiment was tried on triple quadrupole instrument for the standard peptide Ac-MKYLGp**SP**ITTVNH_2. However, the sensitivity was very low. In contrast, triple-quadrupole-ion trap instrument gave relatively high sensitivity. This agrees with that fact that ion trap instrument commonly gives the better sensitivity for the detection of phosphopeptides than regular triple quadrupole mass spectrometer. Therefore, triple quadrupole-ion trap mass spectrometer was used in the flowing experiments.

Different MRM experiments were developed for each synthetic standard

phosphopeptide. A 20 μM standard phosphopeptide solution in 1:1 mixture of water and methanol was injected at 10 μL/min directly into an ion trap mass spectrometer (Sciex Qtrap 3200) to tune the parameters (Table 4.8). The exact molecular ion of each phosphopeptide was found. For example, the $[MH]^+$ for AcMKYLGpSPITTVNH$_2$, **57**, was determined to be 1330.4 Da (Figure 4.18). A product ion scan experiment of the molecular ion was performed to find out the most abundant fragment ions at different collision energies. The three most abundant fragment ions were chosen for the MRM experiment. Finally, MRM experimentation, which enables one to detect the transitions from the molecular ion to its three most abundant fragment ions, was performed. To optimize the sensitivity for each transition, the various mass spectrometry parameters were modified, including ionization spray voltage (IS) , sheath gas pressure (GS1), auxillary gas pressure (GS2), temperature (TEM), collision energy (CE), collision cell entrance potential (CEP), collision cell exit potential (CXP), declustering potential (DP), and time per transition (Dwell time) (Table 4.8).

For quantitative analysis using MRM, a series of concentrations of each phosphopeptide were used: 50 μM, 40 μM, 30 μM, 20 μM, 15 μM, 10 μM, 5 μM, 3 μM, 2 μM, 1.5 μM, 1 μM, 0.5 μM, 0.2 μM and 0.1 μM. A standard curve was made for each phosphopeptide by plotting their peak heights at each concentration. Q1 and Q3 represent the *m/z* values of the parent ions and their corresponding fragment ions selected for the MRM transitions. Figure 4.18 depicts the chromatogram for the MRM experiment using standard phosphopeptide AcMKYLGpSPITTVNH$_2$ at different concentrations.

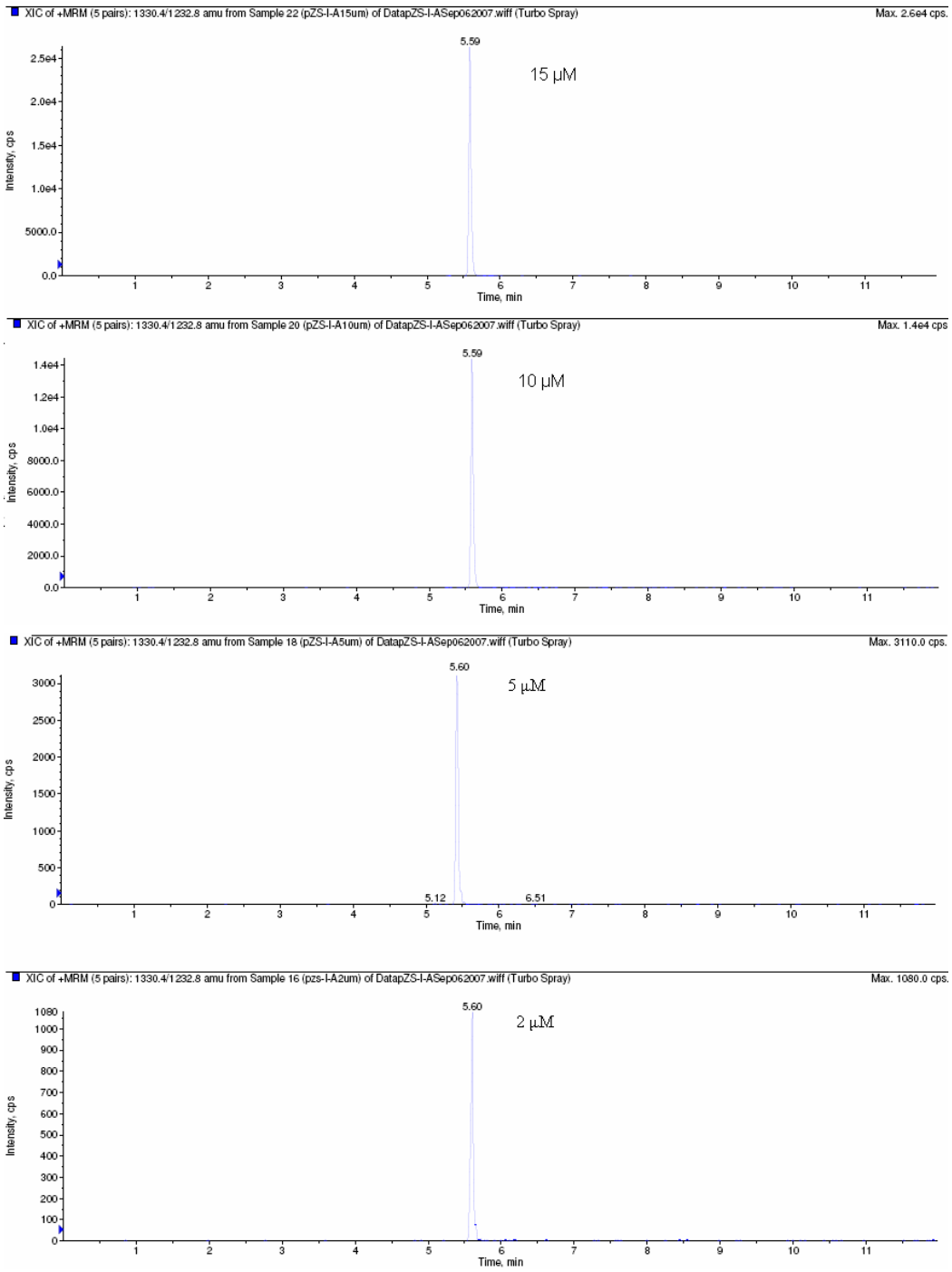

Figure 4.18. Chromatograms for the MRM experiment (1330.4 → 1232.8) for AcMKYLGpSPITTVNH$_2$ at concentrations: 15, 10, 5 and 2 µM

4.5.5.3. Optimization of the Length of Peptide Substrates Derived from Cdc25c at Ser^{168} in Cdc2 Kinase Reactions

Due to our success in detecting the phosphorylation of a control peptide substrate during the Cdc2 kinase reaction, synthetic peptide substrates with different lengths derived from Cdc2 at Ser^{168} were incubated with Cdc2 kinase and ATP using the same conditions as in the control experiments. The longest synthetic peptide substrate $AcMKYLGSPITTVNH_2$ (11-mer) was investigated first.

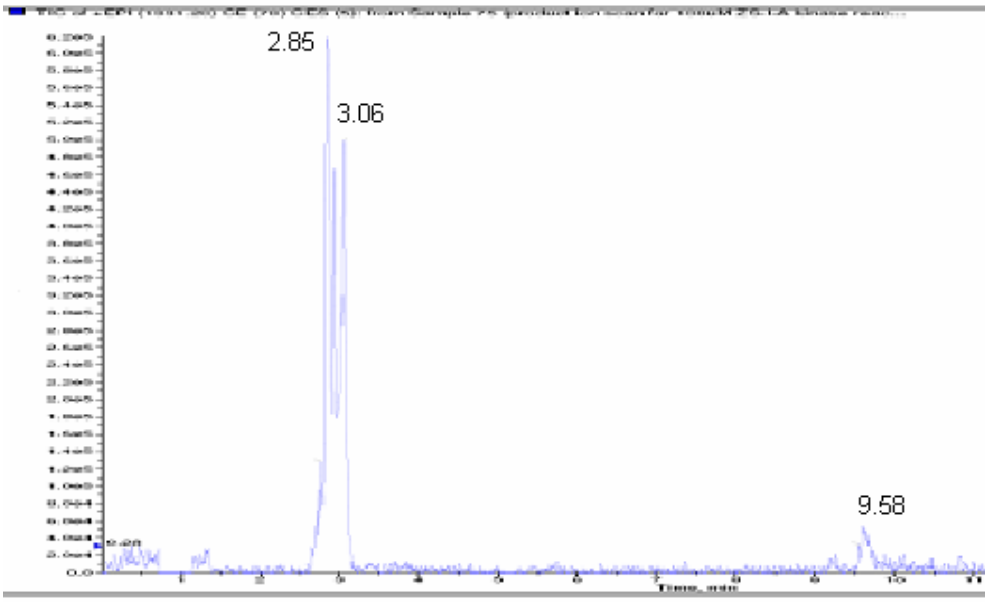

Figure 4.19. Chromatogram for SIM scan experiment for Cdc2 kinase reaction with synthetic $AcMKYLGSPITTVNH_2$ peptide substrate

A SIM scan experiment was attempted first in order to detect the phosphorylation of $AcMKYLGSPITTVNH_2$ in the Cdc2 kinase reaction. As shown in Figure 4.19, two peaks were observed at 3.10 min and 9.58 min. The product ion scan for the peak at 3.10 min showed that it was not a phosphorylated peptide, while the peak at 9.58 min was the desired

phosphorylated peptide AcMKYLGpSPITTVNH$_2$. However, the signal was too low and the noise was high. Product ion scan and neutral loss scan experiments also resulted in poor S/N. The phosphorylation of the peptide substrate AcMKYLGSPITTVNH$_2$ in Cdc2 kinase reaction was finally confirmed by the MRM transition (1330.4 → 1232.8) using ion trap mass spectrometer, which is shown in Figure 4.20.

Figure 4.20. Chromatogram for MRM experiment (1330.4 → 1232.8) for the incubation of AcMKYLGSPITTVNH$_2$ peptide substrate with ATP and Cdc2 kinase

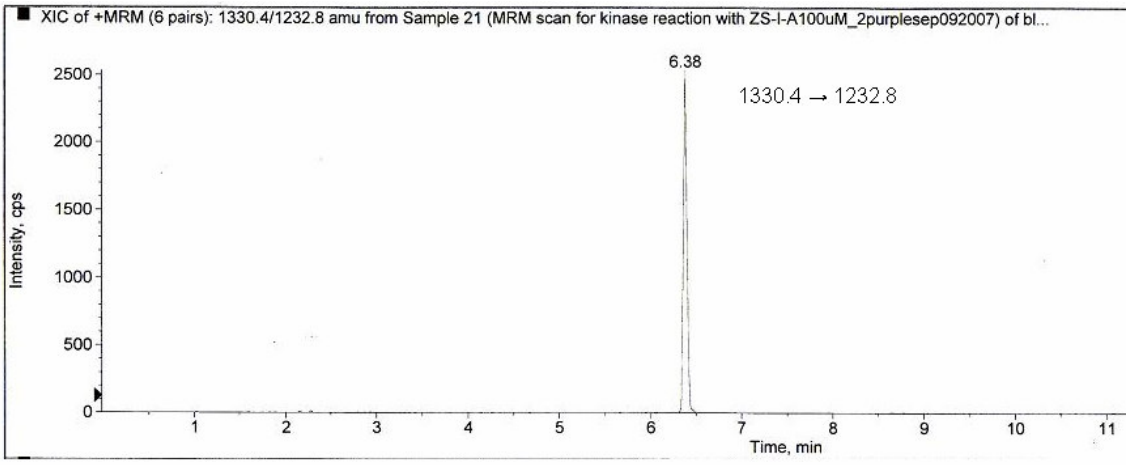

The MRM transition (1330.4 → 1232.8) confirmed the phosphorylation of the peptide substrate AcMKYLGSPITTVNH$_2$ in the Cdc2 kinase reaction. However, it did not indicate which position was phosphorylated in the peptide substrate since there were several possible positions (e.g., Tyr, Ser and Thr). In order to determine the phosphorylation position in the resulting phosphorylated peptide substrate derived from the kinase reaction, the following MRM transitions were chosen for monitoring:

1) 1330.2 ($[M + H]^+$) → 578.1 (b_4 ion, AcMKYL$^+$) indicated the phosphorylation was not on Tyr residue.

2) 1330.2 ($[M + H]^+$) → 801.0 (b_6 ion, $AcMKYLGpS^+$) indicated the phosphorylation was on Ser residue and not on either Thr residue.

3) 1330.2 ($[M + H]^+$) → 1015.0 (b_8 ion, $AcMKYLGpSPI^+$) indicated the phosphorylation was not on either Thr residue.

From the intensity (about 2500 cps(counts per second)) of the MRM transition (1330.4 → 1232.9), the concentration of the target phosphopeptide $AcMKYLGpSPITTVNH_2$ was estimated to be 4.0 μM, which represented a 6% yield for the phosphorylation. (Figure 4.21)

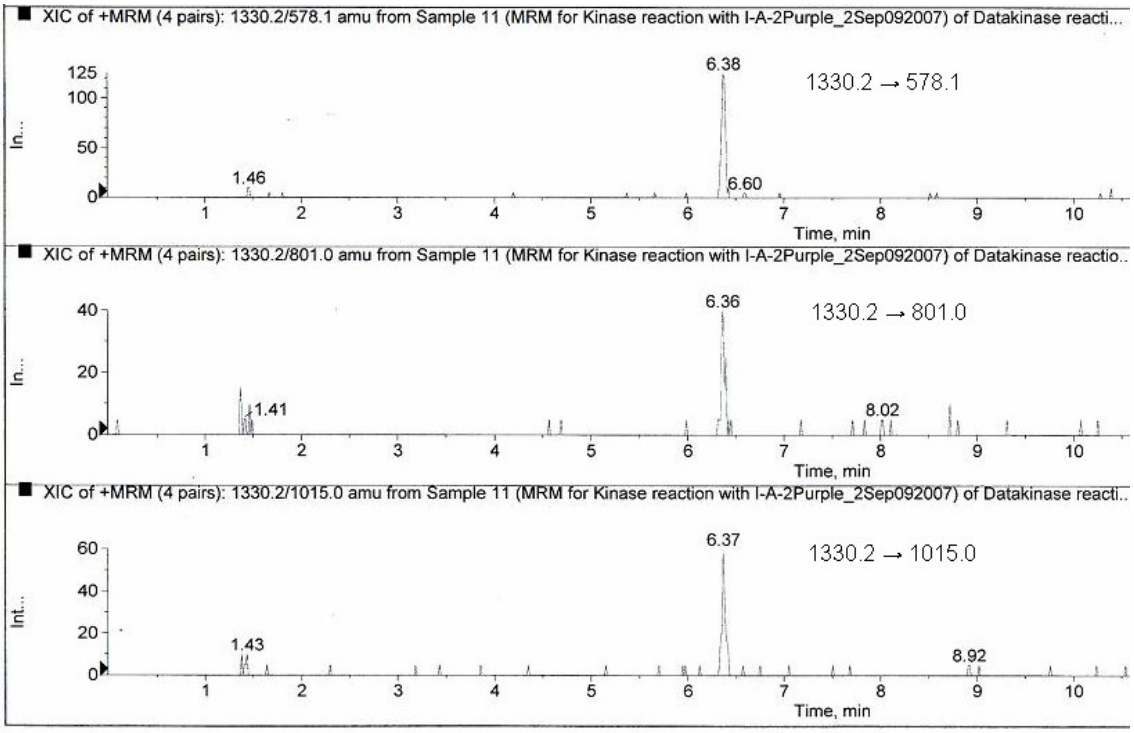

Figure 4.21. Chromatogram for the MRM experiment (1330.2 → 578.1, 1330.2 → 801.0, 1330.2 → 1015.0) for the incubation of the $AcMKYLGSPITTVNH_2$ peptide substrate with ATP and Cdc2 kinase

After the successful phosphorylation of the longest synthetic peptide substrate in the

Cdc2 kinase reaction, three shorter synthetic peptide substrates were investigated to determine the minimum peptide length for recognition by Cdc2 kinase. Since MRM transitions for the loss of phosphoric acid (H_3PO_4, 98) generally give the most sensitive detection in LC-MS/MS, the following MRM transitions were chosen for detecting the phosphorylation of these peptide substrates:

1) 1071.6 ([AcYLGp**SP**ITTVNH_2 + H]$^+$) → 973.8 ([AcYLGp**SP**ITTVNH_2 + H – H_3PO_4]$^+$)

2) 893.2 ([AcYLGp**SP**ITNH_2 + Na]$^+$) → 795.2 ([AcYLGp**SP**ITNH_2 + Na – H_3PO_4]$^+$)

3) 1100.2 ([AcKYLGp**SP**ITTNH_2 + H]$^+$) → 1002.5 ([AcKYLGp**SP**ITTNH_2 + H – H_3PO_4]$^+$)

However, none of these shorter peptide substrates were phosphorylated by Cdc2 kinase using the specific MRM transitions. This indicates that AcMKYLGSPITTVNH_2 was the minimum peptide length for recognition by Cdc2 kinase. The kinase reaction of 9-mer AcKYLG**SP**ITTNH_2 afforded a weak signal (95 cps) for the MRM transition 1100.2 → 1002.4 at 7.60 min (Figure 4.22). However, compared to the signal (2500 cps) of the MRM transition 1330.4 → 1232.8 for the longest peptide substrate AcMKYLGSPITTVNH_2, it is a much worse peptide substrate compared to the 11-mer for Cdc2 kinase.

In summary, the Ser^{168}-Pro position of Cdc25c was confirmed as one of the positions phosphorylated by Cdc2 kinase during the G2/M transition. Moreover, In order for the recognition of the synthetic peptide substrates by Cdc2 kinase, we determined that the 11-mer peptide AcMKYLGSPITTVNH_2 represents the minimum peptide length and it is a reasonable substrate for Cdc2 kinase.

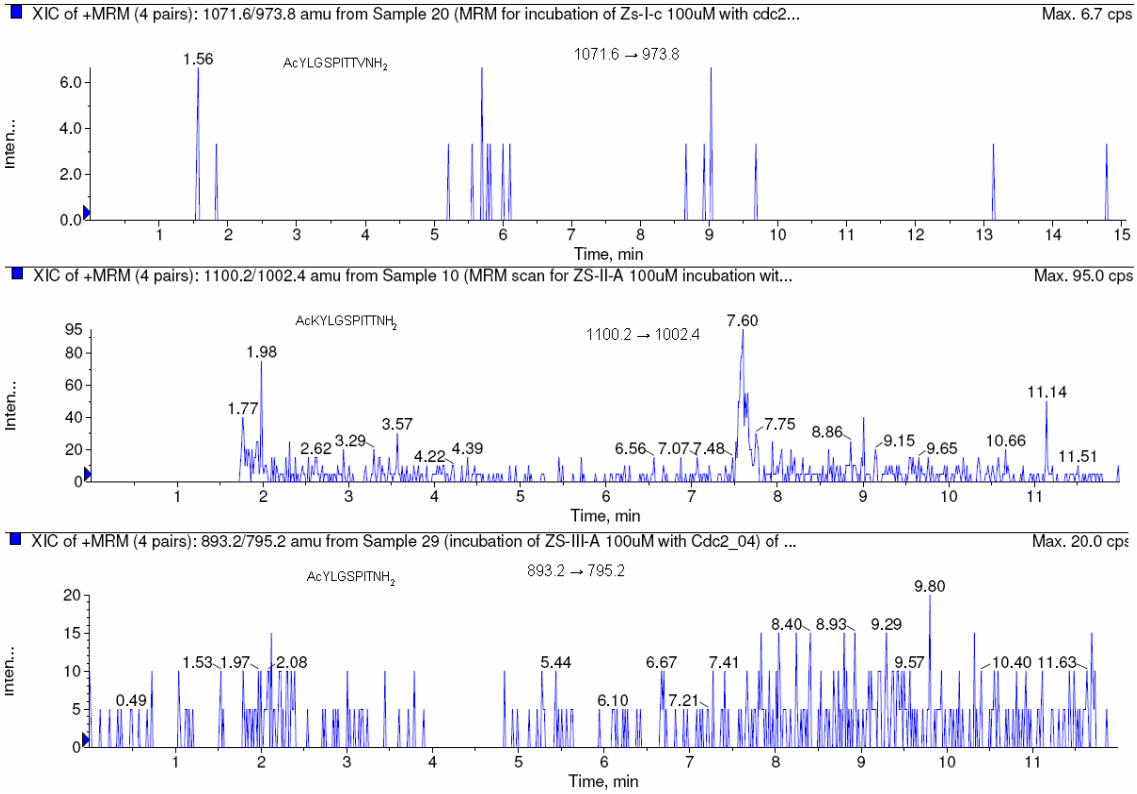

Figure 4.22. MRM experiments for the incubation of shorter peptide substrates with ATP and Cdc2 kinase

4.6. Synthesis of Peptidomimetics Containing the Alkene Ser-Pro Isosteres

In order to study the conformational specificity of Cdc25 substrate at Ser168-Pro for Cdc2 kinase, the (*Z*)-alkene and (*E*)-alkene Ser-Pro isosteres were designed as conformationally locked surrogates for the Ser-*cis*-Pro and Ser-*trans*-Pro amide bonds in synthetic peptide substrates. As noted above, since the 11-mer peptide is the minimum-length substrate, two target peptidomimetics Ac-MKYLGS-Ψ[(*Z*)C=CH]-PITTV-NH_2 and Ac-MKYLGS-Ψ[(*E*)C=CH]-PITTV-NH_2 were designed and synthesized by SPPS.

It has been reported that Fmoc-Ser(OH)-OH and Fmoc-Thr(OH)-OH can be used directly in Fmoc peptide synthesis strategy without any protection on the side chain hydroxyl

group.[289] To prove this, Fmoc-Ser(OH)-OH was also used in our model peptide synthesis (Scheme 4.5).

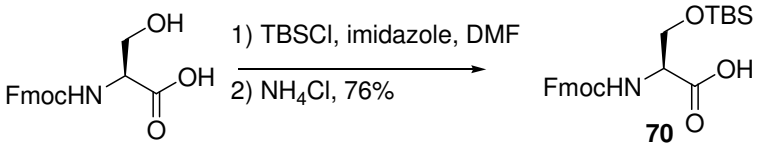

Scheme 4.3. Synthesis of Fmoc-Ser(TBS)-OH **70**

Given that the side chain free hydroxyl group of the alkene isosteres may affect peptide synthesis, we chose to protect the hydroxyl group on the side chain with *tert*-butyl dimethylsilyl, which is orthogonal to Fmoc. In order to confirm that the TBS protection strategy would be effective during peptide synthesis, Fmoc-Ser(TBS)-OH, **70**, was synthesized and used in a model peptide synthesis (Scheme 4.5). Side chain protection was particularly important for both the cis and trans alkene isosteres. This was due to the fact that the cis isostere is known to cyclize intramolecularly to form a 7-membered ring lactone (see Chapter 3) in the presence of free hydroxyl group, while the trans isostere is likely to quickly undergo an isomerization from β,γ- to α,β-unsaturated system during coupling with a side chain hydroxyl group. Thus, three equivalents of *tert*-butyl dimethylsilyl chloride (TBSCl) were used to silylate both the side chain hydroxyl group and the carboxylic acid functional group in both alkene isosteres.[165] The TBS ester of the carboxylic acid was formed temporarily in the reaction, and a mildly acidic aqueous workup deprotected only the TBS ester without affecting the TBS ether on the side chain hydroxyl group. (Scheme 4.4)

The yield for the synthesis of Fmoc-Ser(TBS)-Ψ[(*Z*)C=CH]-Pro-OH, **42**, was only 25% due to the formation of the 7-membered ring lactone.

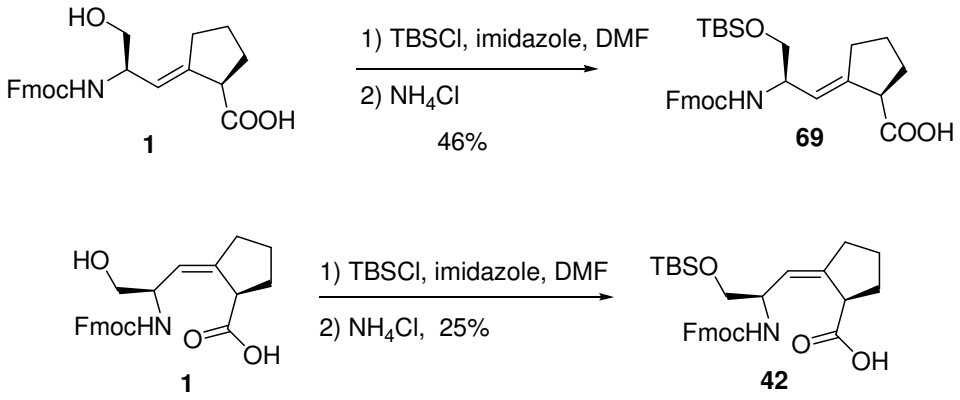

Scheme 4.4. Synthesis of the TBS protected trans (top) and cis (bottom) isostere

The TBS group was readily removed under the resin-cleavage conditions with TFA. After purification by semi-prep HPLC, an 11% yield was obtained using TBS protected build block **70**, which is comparable to the yield (12%) using Fmoc-Ser(tBu)-OH. However, only a 7% yield was obtained using the unprotected building block Fmoc-Ser(OH)-OH. An LC-MS/MS analysis of the crude peptide revealed that the reaction was more complex without any protecting group compared to using protected building blocks. Therefore, the TBS protected alkene isostere building blocks were used for the synthesis of the target peptidomimetics **71** and **72**.

Rink amide MBHA resin was used for the solid phase peptide synthesis of the two target peptidomimetics, AcMKYLGS-Ψ[(*Z*)C=CH]PITTVNH$_2$ (**71**) and AcMKYLGS-Ψ[(*E*)C=CH]PITTVNH$_2$ (**72**) (Scheme 4.6). For the coupling step with the (*Z*)-alkene building block **42,** standard coupling using HOBt/HBTU and DIEA as base in NMP was utilized. For the coupling step with the (*E*)-alkene building block **69**, the more efficient coupling reagent HOAt/HATU was used, and the much weaker base, collidine, was used to prevent the β,γ- to α,β-alkene isomerization of the (*E*)-alkene building block.

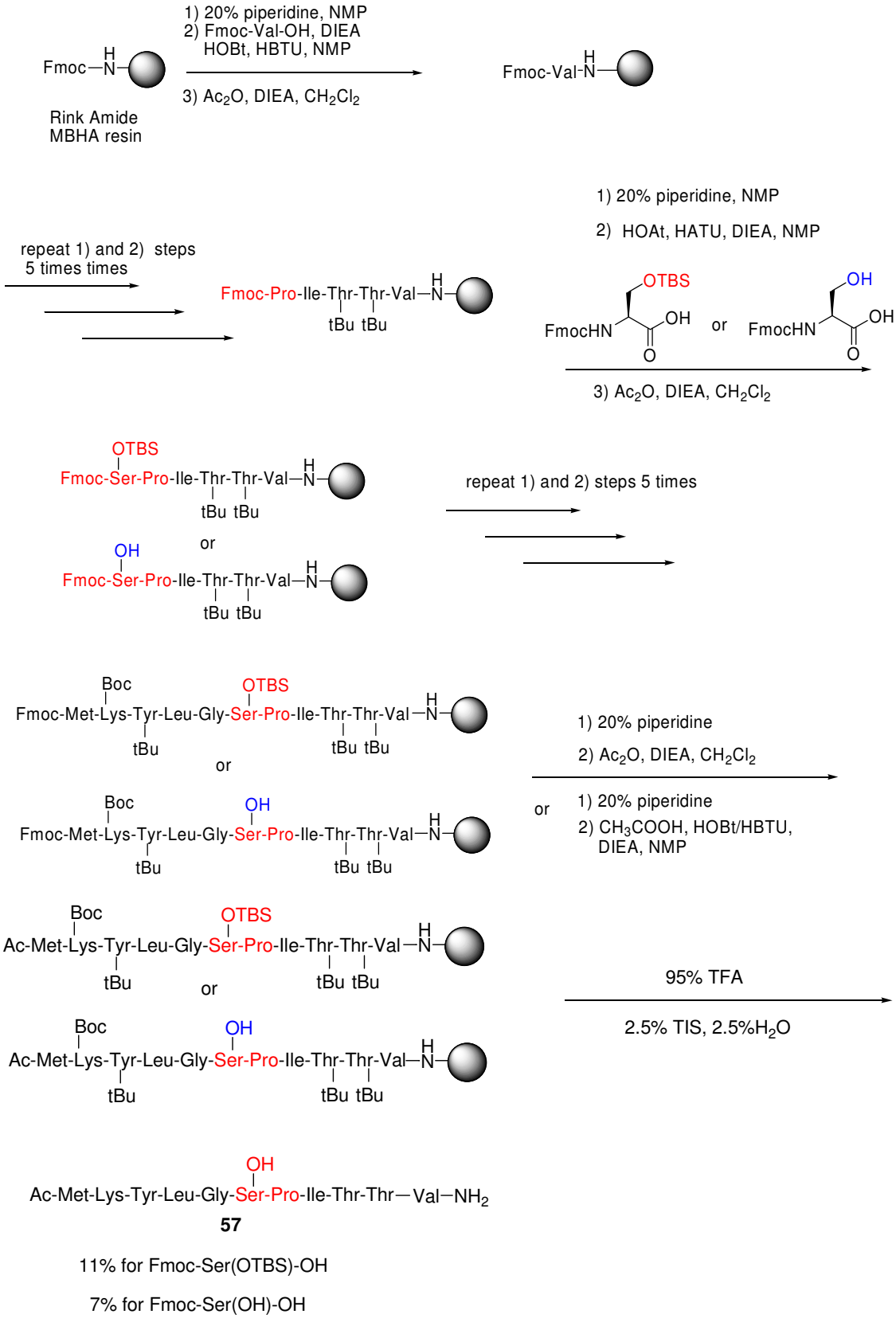

Scheme 4.5. Model peptide synthesis using Fmoc-Ser(OH)-OH and Fmoc-Ser(TBS)-OH **70**

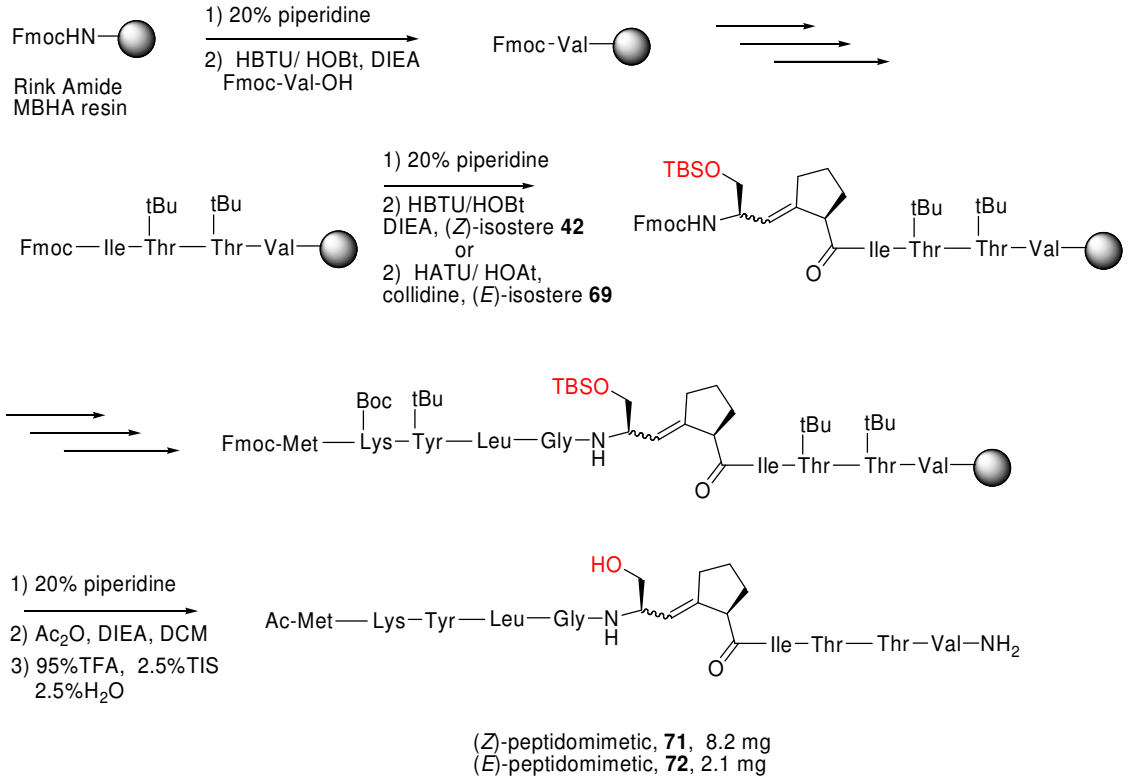

Scheme 4.6. Solid phase peptide synthesis of the two target peptidomimetics **71** and **72**

Only 0.9 equivalents of **42** or **69** were used in the coupling step to conserve the precious intermediates, and the completion of the coupling reactions was monitored by the disappearance of **42** or **69** by analytical reverse phase HPLC. The coupling time for the (*Z*)-alkene building block **42** was 3.5 h, and 3 h for the (*E*)-alkene building block **69**. The TBS protecting group was removed simultaneously when the peptide was cleaved from the resin by 95% TFA. After the purification of crude peptides by HPLC, 8.2 mg of AcMKYLGS-Ψ[(*Z*)C=CH]PITTVNH$_2$ (**71**) was obtained in 10.5% yield and 2.1 mg of AcMKYLGS-Ψ[(*E*)C=CH]PITTVNH$_2$ (**72**) was obtained in 5% yield (Scheme 4.6).

In order to obtain the highest detection sensitivity for the phosphorylation of peptidomimetics **71** and **72** in Cdc2 kinase reaction by LC-MS/MS, their phosphorylated

counterparts AcMKYLGS(PO_3H_2)-Ψ[(*Z*)C=CH]PITTVNH_2 (**73**) and AcMKYLGS(PO_3H_2)-Ψ[(*Z*)C=CH]PITTVNH_2 (**74**) were synthesized as standards in the MRM LC-MS/MS experiments. In principle, there are two strategies for synthesizing phosphopeptides: 1) the building block approach using protected phosphoamino acids, and 2) the global phosphorylation approach using post-synthetic phosphorylation of the unprotected hydroxyl groups. Due to the success of the building block approach in our lab (Scheme 4.9),[165] this method was chosen for the synthesis of phosphopeptidomimetics **73** and **74**.

The unsymmetrical phosphoramidite, *O*-benzyl-*O*-β-cyanoethyl-*N,N*-diisopropyl-phosphoramidite, **75**, was used successfully as the phosphorylation reagent in our group.[165] The β-cyanoethyl group can be removed by piperidine simultaneously with Fmoc deprotection to afford the phosphate monoanion, which is the most stable form of phosphoserine in Fmoc strategy solid phase peptide synthesis.[165, 290] The phosphorylation reagent **75** was synthesized in 95% yield from chloro-*O*-β-cyanoethyl-*N,N*-diisopropyl-phosphoamidite (Scheme 4.7).[165]

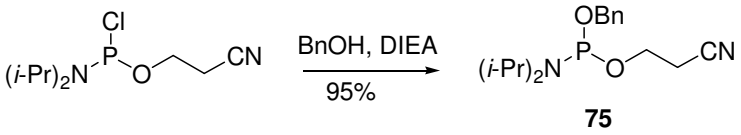

75

Scheme 4.7. Synthesis of phosphorylation reagent **75**

The synthesis of two phosphorylated alkene isostere building blocks Fmoc-Ser(PO(OBn)(OCH_2CH_2CN))-Ψ[(*Z*)C=CH]-Pro-OH **76** and Fmoc-Ser(PO(OBn)(OCH_2CH_2CN))-Ψ[(*E*)C=CH]-Pro-OH **77** was accomplished in a "one-pot" reaction (Scheme 4.8).[165] In this procedure, Fmoc-Ser-Ψ[(*Z*)C=CH]-Pro-OH **1** and

Fmoc-Ser-Ψ[(*Z*)C=CH]-Pro-OH **2** were first treated with one equivalent of TBSCl and *N*-methyl morpholine (NMM), which selectively protected the carboxyl group and left the side chain hydroxyl group free. Phosphitylation of the TBS ester intermediate was performed using the phosphorylation reagent **75** and 5-ethylthio-1H-tetrazole as the base. After oxidation with *tert*-butyl hydroperoxide and mild aqueous acid (NH_4Cl) work up, the protected phosphorylated alkene isostere building blocks **76** and **77** were produced in 65% and 79% yields, respectively.

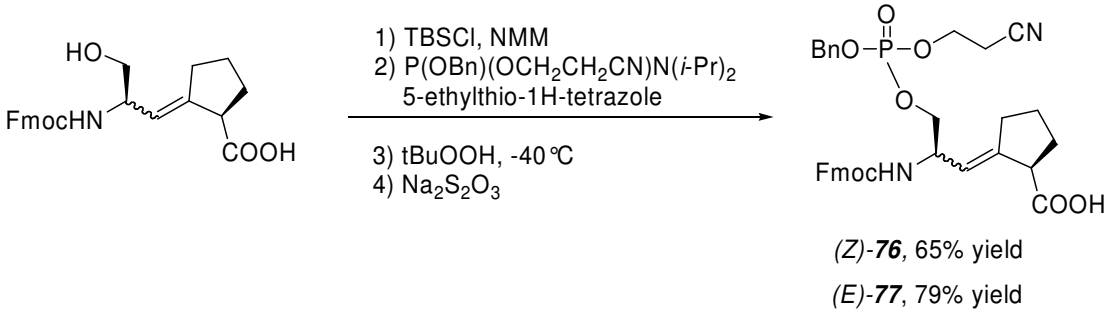

Scheme 4.8. Synthesis of phosphorylated building blocks **76** and **77**

Standard Fmoc solid phase peptide synthesis chemistry using Rink amide MBHA resin was utilized for the synthesis of the target phosphopeptidomimetics **73** and **74** (Scheme 4.9). Similar to the synthesis of the unphosphorylated peptidomimetics **71** and **72**, only 0.9 equivalents of the phosphorylated building blocks were utilized in the coupling step. Analytical HPLC was used to monitor the disappearance of **76** and **77**. The coupling of the cis isostere **76** utilized HOBt/HBTU and DIEA for 3 h at 30 °C, while the coupling of the trans isostere **77** utilized HOAt/HATU and collidine for 2.5 h at 30 °C. Immediately after coupling **76** and **77** onto the resin, 20% piperidine was used to remove the β-cyanoethyl group and deprotect the Fmoc simultaneously. The following coupling conditions were used

for all other amino acids: 1) 20 min coupling for each amino acid. Double coupling was performed if the Kaiser test indicated the first coupling was incomplete; 2) HOBt/HBTU was used as the coupling reagent and DIEA as the base. The benzyl protecting group was removed simultaneously when the peptide was cleaved from the resin by 95% TFA.

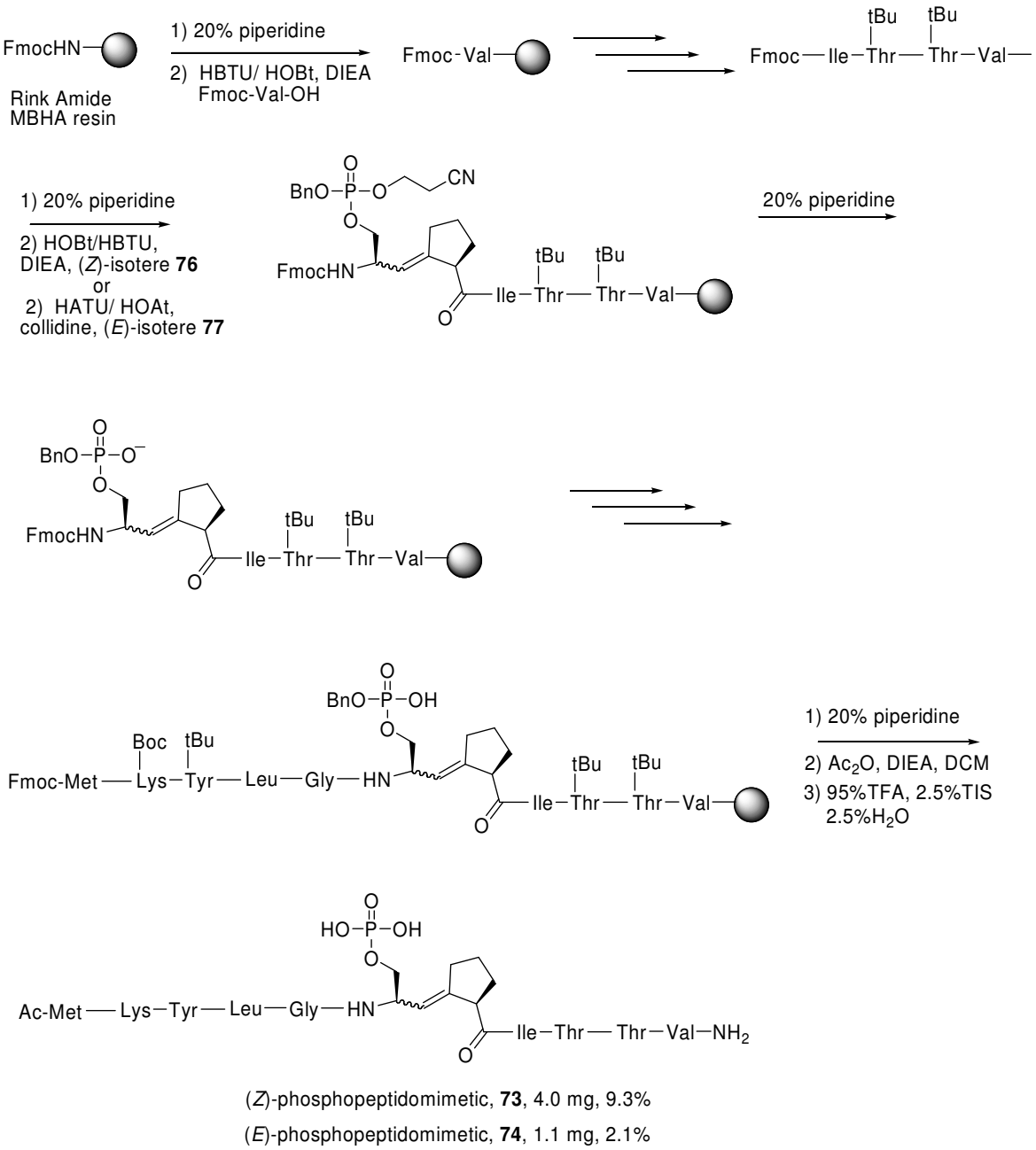

(*Z*)-phosphopeptidomimetic, **73**, 4.0 mg, 9.3%

(*E*)-phosphopeptidomimetic, **74**, 1.1 mg, 2.1%

Scheme 4.9. Solid phase peptide synthesis of two phosphopeptidomimetics **73** and **74**

To purify the crude phosphopeptidomimetics by semi-prep HPLC, no TFA was added to the mobile phase to prevent β-elimination of the phosphate group. After purification, 4.0 mg of AcMKYLGS(PO_3H_2)-Ψ[(*Z*)C=CH]PITTVNH_2 **73** was obtained in 9.3% yield and 1.1 mg of AcMKYLGS(PO_3H_2)-Ψ[(*E*)C=CH]PITTVNH_2 **74** was obtained in 2.1% yield.

In summary, peptidomimetics **71** and **72** containing (*Z*)- and (*E*)-alkene isosteres were synthesized efficiently using TBS protected alkene isostere building blocks **42** or **69** by Fmoc solid phase peptide synthesis. Their phosphorylated counterparts **73** and **74**, were synthesized efficiently using the synthetic phosphorylated alkene isostere building blocks **76** and **77** via the building block phosphorylation strategy.

4.7. The Conformational Specificity of Cdc2 kinase for Cdc25c at Ser^{168}-Pro

In order to detect the phosphorylation of peptidomimetic substrates **71** and **72** in the Cdc2 kinase reaction, phosphorylated peptidomimetics **73** and **74** were used as the standards for the MRM experiment in LC-MS/MS. Tables 4.9 show the MRM transitions and parameters using a Qtrap mass spectrometer for detecting the phosphorylation of the cis peptidomimetic substrate **71** and the trans peptidomimetic substrate **72**.

Since **73** and **74** are configurational isomers, the typical mass spectrometer cannot differentiate between them. Therefore, the MRM experiment for their detection turned out to be same. The transition 1313.2 → 1215.1 corresponds to the transition from $[M + H]^+$ to $[M + H - H_3PO_4]^+$, while the transition 1335.2 → 1237.3 corresponds to the transition from $[M + Na]^+$ to $[M + Na - H_3PO_4]^+$. These two MRM transitions were based on the neutral loss of one molecule of phosphoric acid from the molecular ion in the positive ion mode. Standard curves were made for **73** and **74** by plotting the intensities of these two MRM transitions at

different concentrations. The resulting standard curves were used to determine the formation and quantity of phosphopeptidomimetics in the Cdc2 kinase reaction.

The reaction conditions for the phosphorylation of cis and trans peptidomimetic substrates **71** and **72** using Cdc2 kinase were exactly same as the optimized conditions utilized for the phosphorylation of AcMKYLGSPITTVNH_2, **57**, which served as the control peptide (Figure 4.18). Desalting the sample was carried out by analytical HPLC using 95% water in acetronitrile for 2 min at the beginning of the LC-MS/MS analysis.

Figure 4.23 depicts the MRM chromatogram for the phosphorylation of the trans peptidomimetic **72** in Cdc2 kinase reaction. One significant peak at 6.50 min was observed for both MRM transitions (1313.2 → 1215.1) and (1335.2 → 1237.2).

Figure 4.24 illustrates the MRM chromatogram for the phosphorylation of the cis peptidomimetic **71** in Cdc2 kinase reaction. Two very weak peaks at 6.54 min and 6.66 min were observed for the MRM transition 1313.2 → 1215.1, while no signal was observed for the MRM transition 1335.2 → 1237.2.

The intensity (40 cps) of the two peaks (6.54 min and 6.66 min) for the MRM transition 1313.2 → 1215.1 involving the Cdc2 kinase reaction of the cis peptidomimetic **71** was much weaker compared to the intensity (265 cps) for the peak at 6.50 min for MRM transition 1313.2 → 1215.1 involving the Cdc2 kinase reaction of the trans peptidomimetic substrate **72.** This indicates that the trans peptidomimetic substrate **72** is a much better substrate for Cdc2 kinase than the cis peptidomimetic substrate **71**. In order to further explore the weak signals for the cis peptidomimetic substrate **71** (Figure 4.24), thermal phosphorylation of both peptidomimetic substrates by ATP was performed under the exact

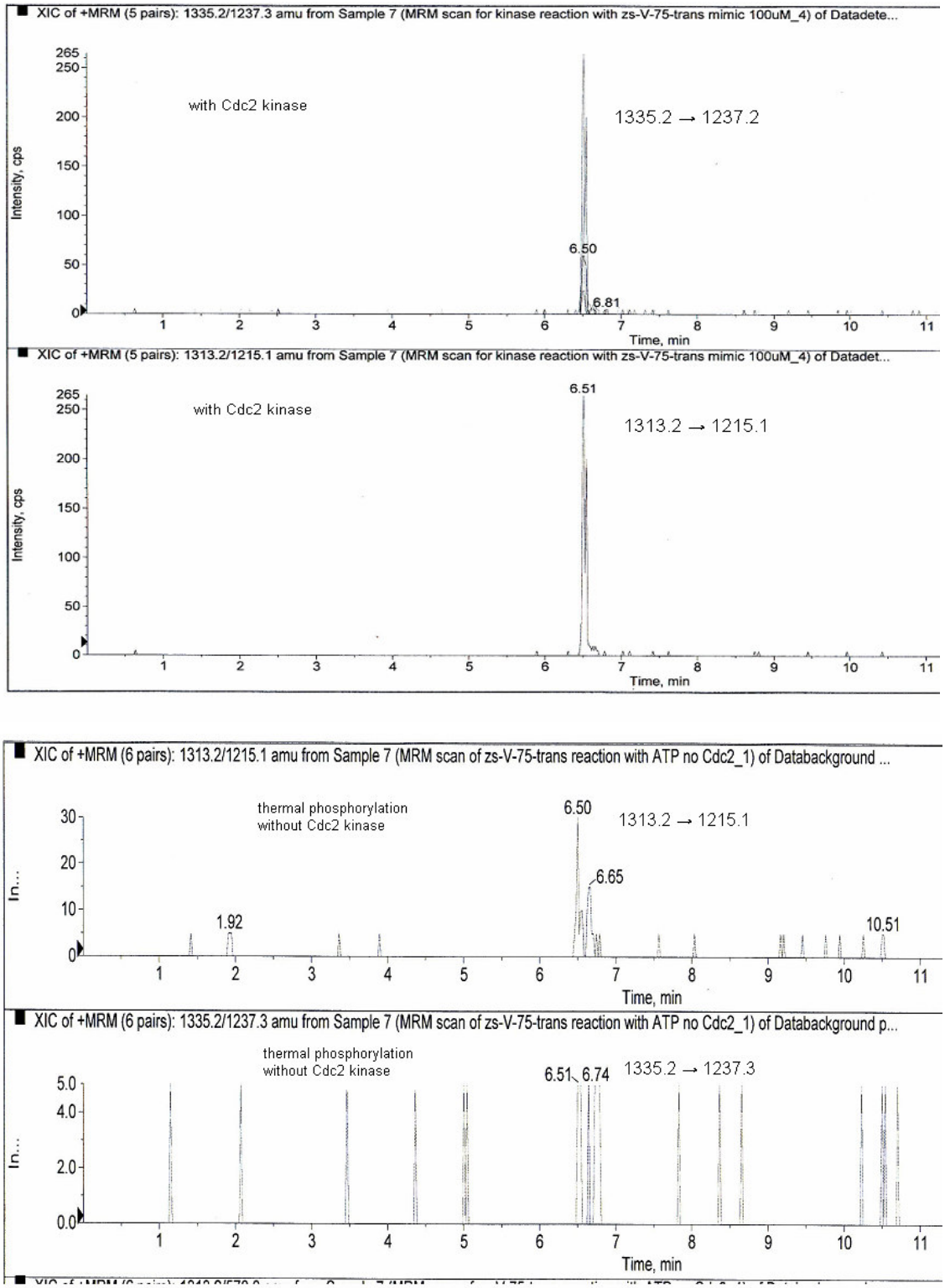

Figure 4. 23. Chromatogram obtained for MRM experiment to detect the phosphorylation of the trans peptidomimetic substrate **72** with Cdc2 kinase or without Cdc2 kinase.

same reaction conditions, except that no Cdc2 kinase was added. Figure 4.23 and Figure 4.24 also show the chromatograms obtained by MRM for the thermal phosphorylation reaction of the cis peptidomimetic substrate **71** and the trans peptidomimetic substrate **72,** respectively.

By comparing the signal for the MRM transition 1313.2 → 1215.1 in the Cdc2 catalyzed phosphorylation reaction, and the signal from the thermal phosphorylation reaction of the cis peptidomimetic substrate **71**, we determined that they had very similar intensities and the same retention times for the two weak signals. This indicated that the phosphorylation signal in the Cdc2 kinase reaction of **71** resulted from thermal phosphorylation by ATP. In other words, Cdc2 kinase did not recognize and catalyze the phosphorylation of the cis peptidomimetic **71**. In the absence of Cdc2, the thermal phosphorylation of **71** produced two phosphorylated products, which indicated that the thermal phosphorylation of **71** was not specific at the Ser^{168}-Pro position.

The phosphorylation signal associated with the thermal phosphorylation reaction of the trans peptidomimetic substrate **72** (30 cps) was comparable in intensity to the signal for the cis peptidomimetic substrate **71** (30 cps). However, it was much weaker compared to the Cdc2 catalyzed phosphorylation reaction of the trans peptidomimetic substrate **72** (265 cps). This result indicates that the Cdc2 kinase indeed only recognizes and phosphorylates the trans peptidomimetic substrate **72**. With the catalysis of Cdc2 kinase, only one phosphorylated product was formed, while two phosphorylated products were obtained for the thermal phosphorylation of **72** (Figure 4.23).

In summary, the experiments described above demonstrate the conformational specificity of Cdc2 kinase for Cdc25c substrate—specifically, that only the trans Cdc25c

substrate at the Ser[168]-Pro position can be recognized and phosphorylated by Cdc2 kinase.

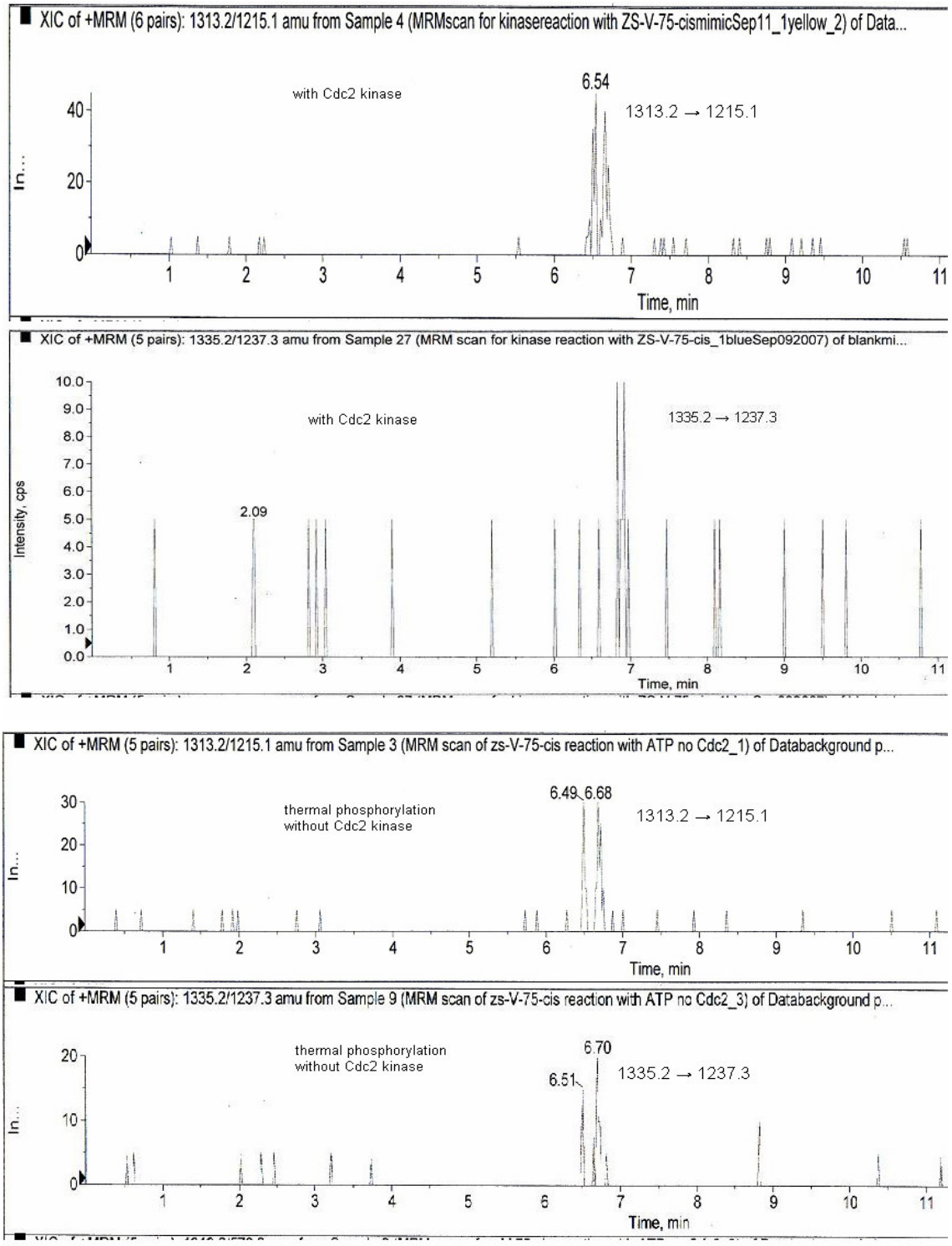

Figure 4.24. Chromatograms of the MRM experiment to detect the phosphorylation of the cis peptidomimetic substrate **71** with Cdc2 kinase and without Cdc2 kinase

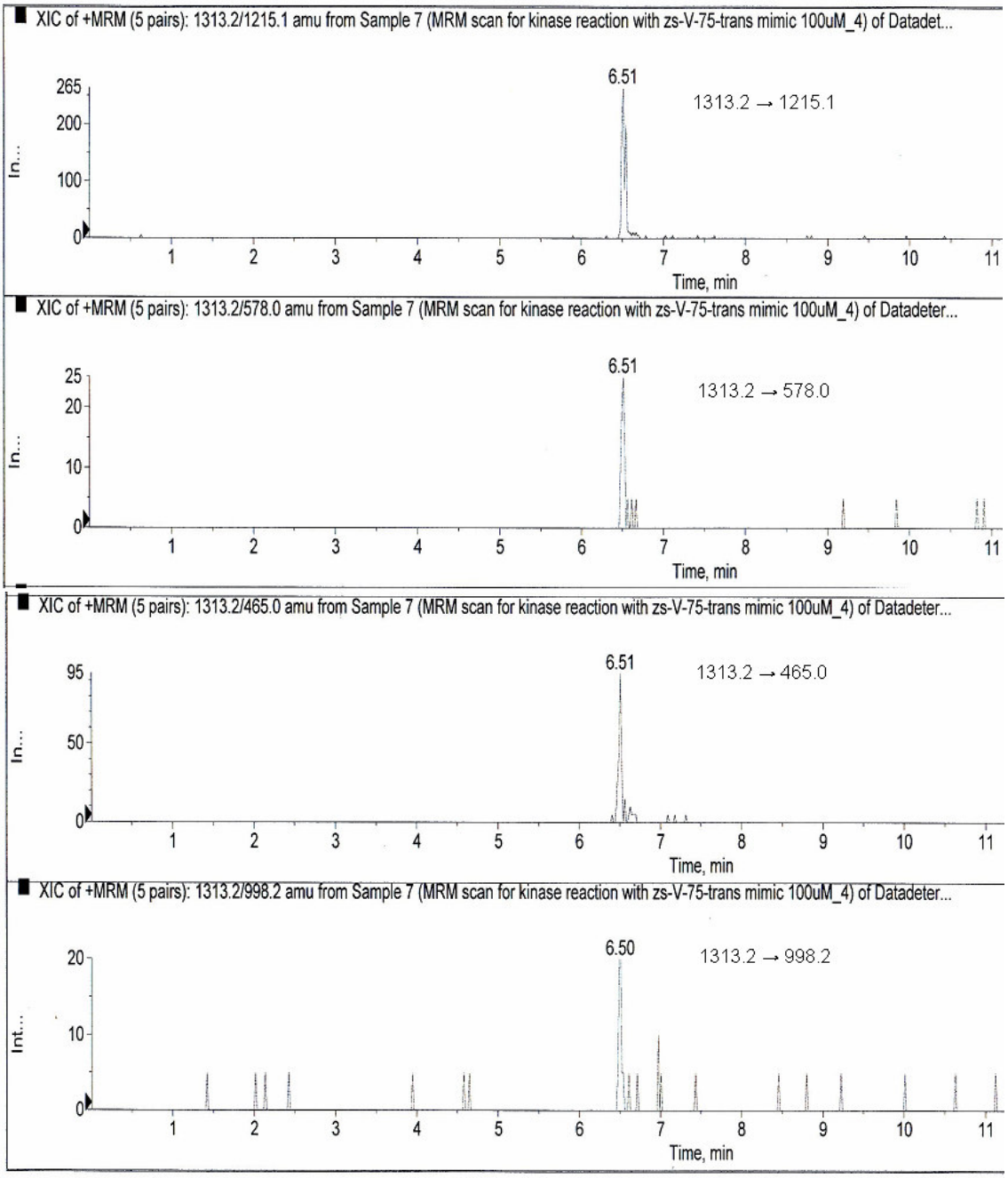

Figure 4.25. MRM experiments for determining the phosphorylation position of the trans peptidomimetic substrate **72** in the Cdc2 kinase reaction

To determine the exact phosphorylation position in the Cdc2 kinase reaction of the trans peptidomimetic substrate **72**, the following MRM experiments were designed. The

parameters of the Qtrap mass spectrometer used in the reaction were optimized using the standard phosphopeptidomimetic **74** (Tables 4.10).

The MRM transition 1313.2 → 578.0 corresponds to the transition from $[M + H]^+$ to $AcMKYL^+$ (b_4 ion), while the MRM transition 1313.2 → 465.0 corresponds to the transition from $[M + H]^+$ to $AcMKY^+$ (b_3 ion) (Figure 4.25). These two MRM transitions eliminate the possibility that phosphorylation occurred on the Tyr residue. The MRM transition 1313.2 → 998.2 corresponds to the transition from $[MH]^+$ to AcMKYLGpSΨ[(*E*)C=CH]P^+ (b_7 ion), indicating that phosphorylation did occur on the Ser residue of the peptidomimetic substrate **72**.

4.8. Discussion

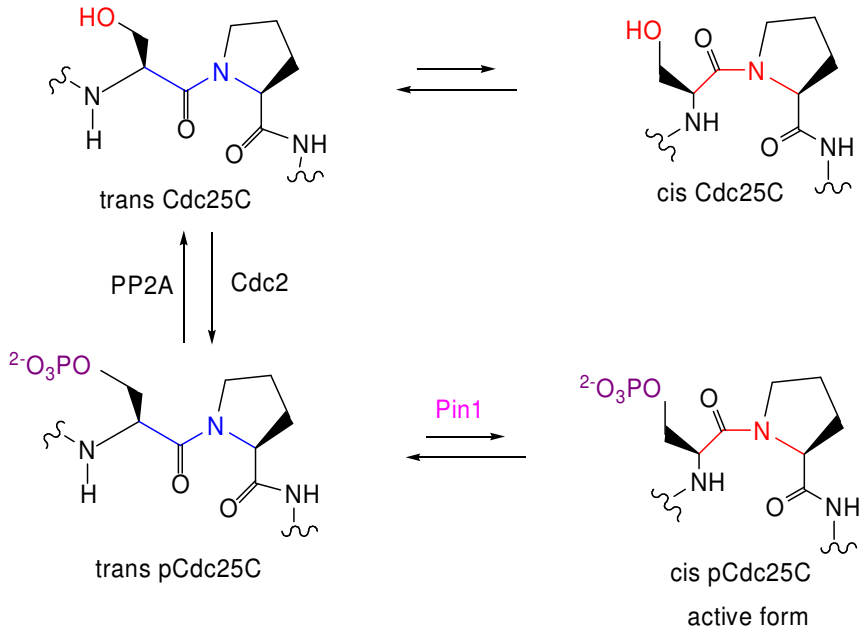

Figure 4.26. Mechanism for the interaction between Pin1 and Cdc25 phosphatase

From our experimental results, we conclude that Cdc2 kinase, which is the upstream kinase for the interaction between Pin1 and Cdc25 phosphatase, is conformational specific towards its substrates. Only the Ser-*trans*-Pro conformer can be recognized and

phosphorylated by Cdc2 kinase. Together with the observation that PP2A phosphatase is also conformational specific towards its substrates (which only pSer-*trans*-Pro conformer can be dephosphorylated), the mechanism for the interaction between Pin1 and Cdc25 phosphatase is outlined in Figure 4.26. The initial substrate for the interaction between Pin1 and Cdc25 phosphatase is the trans conformer of Cdc25 at its Ser^{168}-Pro position. From Figure 4.26, we can see that the phosphorylation or dephosphorylation of Cdc25 phosphatase by conformational specific kinase(s) and phosphatase(s) is the driving force for the cis-trans isomerization of Cdc25 phosphatase. In fact, it is the conformational specificities of the major kinases (such as Cdc2) and phosphatases (such as PP2A) that make Pin1 necessary for the cell cycle regulation. Without Pin1, the equilibrium can only be reached very slowly. However, under the help of Pin1, the equilibrium can be rebuilt at the time scale of cell cycle events.

Besides, the conformational change of Cdc25 phosphatase at Ser^{168}-Pro position catalyzed by Pin1 should induce the enhanced or suppressed cell signals. From the mitotic functions of Pin1 and Cdc25 phosphatase, it is further predicted that the cis conformation of phosphorylated Cdc25C phosphatase at Ser^{168}-Pro is the active form, which can dephosphorylate Cdc2 kinase at its pThr14 and pTyr15 positions and lead the cell entry into mitosis.

4.9. Conclusion

We designed, synthesized and purified eight peptide substrates for Cdc2 kinase based on the sequence of human Cdc25c around the Ser168-Pro motif. The optimal peptide substrate for the Cdc2 kinase was identified to be the 11-mer, Ac-MKYLG**SP**ITTV-NH_2, **57**.

Two peptidomimetic substrates containing (*E*)- and (*Z*)-alkene isosteres were designed, synthesized, purified, and used in Cdc2 kinase reaction. Using LC-MS/MS, we determined that Cdc2 kinase specifically recognizes and phosphorylates the trans peptidomimetic substrate **72** at the Ser^{168}-Pro position, while Cdc2 kinase is unable to catalyze the phosphorylation of the cis peptidomimetic substrate **71** at the Ser^{168}-Pro position. The conformational specificity of Cdc2 kinase for its substrates makes Pin1 necessary for the regulation of the cell cycle. After the phosphorylation of protein substrates by conformational specific kinases, such as Cdc2 kinas, ERK2 kinase, Pin1 helps rebuild the equilibrium between the phosphorylated proteins very quickly, therefore providing an additional regulation mechanism for the cell cycle.

Experimental

General. Peptide synthesis grade DMF, DIEA, and NMP were purchased. Brine, $NaHCO_3$, and NH_4Cl refer to saturated aqueous solutions unless otherwise noted. Flash column chromatography was performed using silica gel (230-400 mesh, ASTM, EM Science) with reagent grade solvents. ^{1}H-NMR spectra were obtained at 500 MHz or 400 MHz at ambient temperature in $CDCl_3$ unless otherwise noted. ^{13}C-NMR and ^{31}P-NMR spectra were obtained at 125 and 162 MHz respectively, unless otherwise noted. Coupling constants *J* are reported in Hz. Analytical HPLC was performed on a Beckman HPLC with a Polaris reverse phase C18 column (Varian), 10 μm, 100 × 4.6 mm; Xbridge reverse phase C18 column (Waters), 2.5 μm, 50 × 4.6 mm or Vydac reverse phase C4 column, 5.0 μm, 250 × 4.6 mm. Preparative HPLC was performed on a Varian HPLC with a Polaris reverse phase C18 column (Varian), 5 μm, 100 × 21.2 mm, or on a Vydac reverse phase C4 column, 10 μm, 250

× 22 mm. Unless otherwise noted, solvent A for HPLC was 0.1% TFA in H_2O, and solvent B was 0.1% TFA in CH_3CN. Unless otherwise noted, LC-MS/MS analysis was performed on an Agilent 1100 HPLC coupled to an Applied Biosystem (ABI) Qtrap 3200 mass spectrometer system. LC-MS/MS was performed on an Eclipse XDB reverse phase C18 column (Agilent), 5 μM, 150 × 4.6 mm. Solvent C for LC-MS/MS analysis was 0.1% formic acid in H_2O and solvent D was 0.1% formic acid in CH_3CN.

Ac-Met-Tyr-Leu-Gly-Ser-Pro-Ile-Thr-Thr-Val-NH_2, 57. Manual solid phase peptide synthesis of **57** was performed in 5 mL disposable polypropylene columns using standard Fmoc chemistry. Rink amide MBHA resin (100 mg, 0.064 mmol, 0.64 mmol/g) was swelled in CH_2Cl_2 (3 mL, 60 min) and NMP (3 mL, 10 min). For each amino acid coupling cycle, Fmoc group was removed in two steps with 20% piperidine in NMP (4 mL) for 5 min, then 15 min. After washing with NMP (3 × 3 mL), and CH_2Cl_2 (3 × 3 mL), a Kaiser test was performed using a small amount of damp resin. The resin was rinsed with NMP (3 × 3 mL), a solution of the first amino acid, Fmoc-Val-OH (65.0 mg, 0.192 mmol), HBTU (73.0 mg, 0.192 mmol), HOBt (26 mg, 0.192 mmol) and DIEA (55 μL, 0.384 mmol) in NMP (2 mL) were added to the resin and shaken for 30 min. The resin was washed with NMP (3 × 3 mL), CH_2Cl_2 (3 × 3 mL) and NMP (3 × 3 mL). A second coupling was performed if the Kaiser test indicated that the coupling reaction has not been completed. The resin was capped with 10% Ac_2O (30 μL, 0.315 mmol) and 10% DIEA (30 μL, 0.33 mmol) in CH_2Cl_2 (3 mL) for 30 min if the Kaiser test still indicated that the coupling was incomplete after the second coupling reaction. The deprotection step of Fmoc protecting group, the coupling step with Fmoc-protected amino acids, and the capping steps for Fmoc-Pro-OH, Fmoc-Ser(*t*Bu)-OH,

Fmoc-Gly-OH, Fmoc-Leu-OH, Fmoc-Met-OH were repeated until the whole sequence of **57** was introduced onto the resin. The resin was then treated with 20% piperidine in NMP (2 × 4 mL, 5 min, 15 min) to remove the Fmoc group on the *N*-terminus. Acetylation of the *N*-terminus was carried out with 10% Ac_2O (30 μL, 0.310 mmol) and 10% DIEA (30 μL, 0.330 mmol) in CH_2Cl_2 (3 mL) for 30 min. The resin was washed with NMP (5 × 3 mL), CH_2Cl_2 (5 × 3 mL), MeOH (5 × 3 mL), and ether (3 × 3 mL), then the resin was dried in a desiccator under vacuum overnight. The dried resin was then treated with a mixture of 95% TFA, 2.5% H_2O and 2.5% triisopropylsilane (TIS) (3 mL) for 3 h, filtered and rinsed with CH_2Cl_2 and MeOH. The combined solutions were concentrated to a small volume by rotary evaporation. The crude peptide was precipitated with cold ether (50 mL), collected by filtration and dried in vacuum to afford 39 mg (49%) of the crude peptide as a white solid. The crude peptide **57** was dissolved in a mixture of 2.2 mL of H_2O and 0.4 mL of CH_3CN, and purified by preparative HPLC using a Polaris C18 preparative column. The purified peptide **57** was eluted at 10.8 min as a white solid (15 mg, 18.8%) with a flow rate of 20 mL/min, 10% B for 2 min, 10% to 28% B over 10 min, 28% to 90% B over 3 min, 90% B for 4 min. The purity (> 99%) of purified peptide **57** was checked by analytical HPLC (2 mL/min, 10% B for 5 min, 10 to 90%B over 10 min, ret. time 10.9 min) on analytical Polaris C18 column. ^{1}H NMR (DMSO-*d6*) δ 9.13 (s, 1H), 8.04 (dd, *J* = 8.0, 4.0, 2H), 7.98 (brs, s, 2H), 7.87 (brs, s, 2H), 7.78 (d, *J* = 8.0, 1H), 7.60 (m, 4H), 7.30 (s, 1H), 7.07 (s, 1H), 6.98 (d, *J* = 8.0, 2H), 6.60 (d, J = 8.0, 2H), 4.97 (m, 3H), 4.60 (dd, *J* = 6.8, 8.0, 1H), 4.42 (m, 2H), 4.32-4.18 (m, 6H), 4.09 (dd, *J* = 6.4, 10.6, 1H), 4.0 (m, 2H), 3.71-3.48 (m, 5H), 2.87 (m, 2H), 2.70 (m, 3H), 2.40 (m, 2H), 2.0 (m, 5H), 1.82 (s, 6H), 1.74 (m, 2H), 1.56 (m, 2H), 1.44 (m,

6H), 1.22 (m, 2H), 1.01 (d, J = 6.4, 6H), 0.86-0.75 (m, 18H). ESI-MS (+), calculated for $C_{57}H_{95}N_{13}O_{16}S$ $[M + H]^+$) m/z = 1250.51, found m/z = 1250.40. The presence of b_3, b_4, b_6, b_8, b_9, b_{10} ions (m/z = 465.1, 578.3, 722.5, 932.6, 1033.6 and 1134.6) in a product ion scan experiment of $[M + H]^+$ (m/z = 1250.4) in LC-MS/MS confirmed the sequence of **57**.

Ac-Met-Tyr-Leu-Gly-Ser(PO_3H_2)-Pro-Ile-Thr-Thr-Val-NH_2, 65. The solid phase peptide synthesis of **65** was performed in a manner similar to that for **57** except that Fmoc-protected Ser(PO(OBn)OH)-OH (Novabiochem) was used in the coupling reaction on a smaller scale (50 mg of Rink amide MBHA resin, 0.032 mmol). The crude peptide was purified by preparative HPLC using a Polaris C18 preparative column. The purified peptide **65** was eluted at 9.7 min as a white solid (2.3 mg, 6.5%) with a flow rate of 20 mL/min, 10% B for 2 min, 10% to 28% B over 10 min, 28% to 90% B over 3 min, 90% B for 4 min. Analytical HPLC (2 mL/min, 10% B for 5 min, 10 to 90%B over 10 min, ret. time 9.7 min) on analytical Polaris C18 column showed > 95% purity.. ESI-MS (+), calculated for $C_{57}H_{96}N_{13}O_{19}PS$ $[M + H]^+$) m/z = 1330.50, found m/z = 1330.40. The presence of b_3, b_4, b_5, b_6, b_7, b_8, b_9 ions (m/z = 465.1, 578.3, 635.3, 802.4, 899.5, 1012.7 and 1113.8) in a product ion scan experiment of $[M + H]^+$ (m/z = 1330.40) in LC-MS/MS confirmed the sequence of **65**.

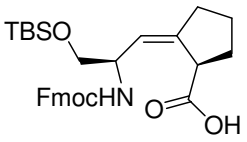

Fmoc-Ser(TBS)-Ψ[(*Z*)CH=C]-Pro-OH, 42. Fmoc–SerΨ[(*Z*)CH=C]–Pro–OH, **1** (43 mg, 0.11 mmol) was dissolved in DMF (0.8 mL). To the reaction solution at rt, imidazole (36 mg, 0.53 mmol) was added, followed by the slow addition of TBSCl (40 mg, 0.26 mmol). The mixture was stirred at rt for 16 h, and NH_4Cl (5

mL) was added. The mixture was stirred for an additional 50 min, diluted with EtOAc (60 mL), washed with NH_4Cl (2 × 10 mL), brine (10 mL), dried with $MgSO_4$, and concentrated. Chromatography on silica gel with 5% MeOH in $CHCl_3$ afforded 14 mg (25%) of **42** as a yellowish oil. ^{1}H NMR (CD_3OD) δ 7.74 (d, *J* = 7.6, 2H), 7.61 (d, *J* = 7.3, 2H), 7.34 (app. t, *J* = 7.5, 2H), 7.26 (app. t, *J* = 7.1, 2H), 5.38 (d, *J* = 8.5, 1H), 4.33-4.15 (m, 4H), 3.61 (m, 1H), 3.52 (m, 2H), 2.42 (m, 1H), 2.29 (m, 1H), 1.97 (dd, *J* = 7.0, 13.7, 2H), 1.82 (m, 1H), 1.58 (m, 1H), 0.85 (s, 9H), 0.02 (s, 6H). ^{13}C-NMR (CD_3OD) δ 177.2, 156.8, 145.1, 144.3, 141.4, 127.5, 126.9, 125.1, 121.6, 119.7, 66.7, 65.4, 52.6, 46.1, 33.8, 31.5, 29.5, 25.2, 24.8, 24.5, 17.9, -5.1, -6.4. ESI-MS(+) calculate for $C_{30}H_{39}NO_5Si$ $[M + H]^+$ = 522.7, found *m/z* = 522.3.

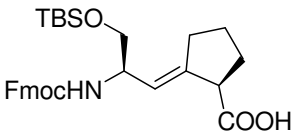

Fmoc-Ser(TBS)-Ψ[(*E*)CH=C]-Pro-OH, 69.

Fmoc–SerΨ[(*E*)CH=C]–Pro–OH, **2** (106 mg, 0.260 mmol) was dissolved in DMF (1.0 mL). Imidazole (89 mg, 1.3 mmol) was added to the reaction mixture at rt followed by the slow addition of TBSCl (98 mg, 0.65 mmol). The mixture was stirred at rt for 16 h, and NH_4Cl (20 mL) was added. The mixture was stirred for an additional 50 min, and then diluted with EtOAc (50 mL), washed with NH_4Cl (2 × 10 mL), brine (10 mL), dried with $MgSO_4$, and concentrated. Chromatography on silica gel with 5% MeOH in $CHCl_3$ afforded 60 mg (46%) of **69** as a clear oil. ^{1}H NMR (CD_3OD) δ 7.73 (d, *J* = 7.5, 2H), 7.57 (t, *J* = 7.4, 2H), 7.37 (t, *J* = 7.3, 2H), 7.28 (t, *J* = 7.4, 2H), 5.54 (d, *J* = 8.3, 1H), 4.37-4.32 (m, 2H), 4.20 (t, *J* = 7.0, 1H), 3.64-3.56 (m, 2H), 3.33 (m, 1H), 2.56 (m, 1H), 2.31 (m, 1H), 1.98-1.89 (m, 3H), 1.65 (m, 1H), 0.86 (s, 1H), 0.01 (s, 1H). ^{13}C NMR (CD_3OD) δ 179.8, 155.9, 143.8, 141.2, 129.8, 127.6, 127.0, 125.0, 121.8, 119.9, 66.7, 65.1, 52.4, 49.3, 47.2, 29.9, 29.4, 26.2, 25.8, 25.6, 25.0, 18.2,

-3.7, -5.5. ESI-MS(+) calculate for $C_{30}H_{39}NO_5Si$ $[M + H]^+$ = 522.7, found *m/z* = 522.2.

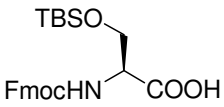

Fmoc-Ser(TBS)-OH, 70. Fmoc-serine (1.1 g, 3.2 mmol) and imidazole (1.10 g, 16.0 mmol) were dissolved in DMF (6.4 mL) at rt. TBSCl (1.2 g, 8.0 mmol) was added slowly and the reaction mixture was stirred for 16 h. NH_4Cl (40 mL) was added and the reaction mixture was stirred for another 50 min. The reaction mixture was diluted with 200 mL CH_2Cl_2, washed with NH_4Cl (2 × 40 mL), H_2O (40 mL), dried on Na_2SO_4 and concentrated. Chromatography on silica gel with 5% MeOH in $CHCl_3$ gave1.39 g (98%) of **70** as a colorless oil. ^{1}H NMR δ 11.5 (brs, 1H), 7.76 (d, *J* = 7.5, 2H), 7.63 (t, *J* = 8.4, 2H), 7.40 (t, *J* = 7.4, 2H), 7.32 (t, *J* = 7.2, 2H), 5.76 (d, *J* = 8.5, 1H), 4.53 (d, J = 8.2, 1H), 4.42 (t, J = 6.4, 2H), 4.26 (t, J = 7.3, 1H), 4.17 (dd, *J* = 2.6, 12.8, 1H), 3.94 (dd, *J* = 3.7, 7.1, 1H), 0.92 (s, 9H), 0.09 (d, *J* = 5.3, 6H). ESI-MS(+) calculated for $C_{24}H_{31}NO_5Si$ $[M + H]^+$ = 442.2, found *m/z* = 442.2.

Ac-Met-Lys-Tyr-Leu-Gly-Ser-Ψ[(*Z*)C=CH]-Pro-Ile-Thr-Thr-Val-NH$_2$, 71. The solid phase peptide synthesis of **71** was performed in a manner similar to that for **57** except that the reaction was conducted on a smaller scale (76 mg Rink amide MBHA resin, 0.05 mmol, 0.66 mmol/g). Fmoc-Ser(TBS)-Ψ[(*Z*)C=CH]-Pro-OH (0.040 mmol, 20 mg), **42**, was coupled with HOAt (0.080 mmol, 11 mg), HATU (0.080 mmol, 30 mg), and DIEA (0.15 mmol, 20 mg) for 3.5 h at 30 °C. The coupling reaction was monitored by analytical C18 HPLC (conditions as below) for the disappearance of **42**. The resin was capped with 10% Ac_2O and 10% DIEA in DCM (2.5 mL) for 30 min after the coupling reaction with **42.** The crude peptidomimetic was purified using a preparative reverse phase Vydac C4 column at 15 mL/min, 10% B to

40% B over 10 min, 40% B to 36% B over 6 min. 0.1%TFA was added to both A and B HPLC solvent for the purification of **71**. Purified **71** (8.2 mg, 10.5% yield) eluted at 14.60 min as a white solid. Analytical HPLC on an Xbridge C18 analytical column (1.0 mL/min, 10% B for 2min, 10% B to 90% B over 15 min, retention time 8.83 min) showed > 99% purity. ESI-MS (+), calculated for $C_{58}H_{96}N_{12}O_{15}S$ $[M + H]^+$) *m/z* = 1233.52, found *m/z* = 1233.2 and *m/z* = 1255.3 for $[M + Na]^+$. The presence of b_3, b_4, b_7, b_8, b_{10}, y_6, y_9, and $[y_{10} + Na]^+$ ions (*m/z* = 465.2, 578.4, 915.7, 1016.5, 1216.7, 652.8, 1056.6 and 1211.6) in a product ion scan experiment of $[M + H]^+$ (*m/z* = 1233.2) in LC-MS/MS confirmed the sequence of **71**.

Ac-Met-Lys-Tyr-Leu-Gly-Ser-Ψ[(*E*)C=CH]-Pro-Ile-Thr-Thr-Val-NH_2, 72. The solid phase peptide synthesis of **72** was performed in a manner similar to that for **57** except that the reaction was conducted on a smaller scale (76 mg Rink amide MBHA resin, 0.05 mmol, 0.66 mmol/g). Fmoc-Ser(TBS)-Ψ[(*E*)C=CH]-Pro-OH, **69**, (0.040 mmol, 20 mg), **69**, was coupled with HOAt (0.12 mmol, 16 mg), HATU (0.12 mmol, 44 mg), and 2, 4, 6-collidine (0.23 mmol, 32 μL) for 3 h at 30 ℃. The coupling reaction was monitored by analytical C18 HPLC (conditions as below) for the disappearance of **69**. The resin was capped with 10% Ac_2O and 10% DIEA in DCM (2.5 mL) for 30 min immediately after the coupling reaction with **69**. The crude peptidomimetic was purified using a preparative reverse phase Vydac C4 column at 15 mL/min, 10% B to 70% B over 13 min, 70% B to 80% B over 5 min and 80% B to 90% B over 1 min. 0.1%TFA was added to both A and B HPLC solvents for the purification of **72**. Purified **72** (2.1 mg, 5% yield) eluted at 12.10 min as a white solid. Analytical HPLC on an Xbridge C18 analytical column (1.0 mL/min, 10% B for 2min, 10% B to 90% B over 15 min, retention time 8.36 min) showed > 99% purity. ESI-MS (+),

calculated for $C_{58}H_{96}N_{12}O_{15}S$ $[M + H]^+$) *m/z* = 1233.52, found *m/z* = 1233.2 and *m/z* = 1255.1 for $[M + Na]^+$. The presence of b_3, b_4, b_7, b_8 and y_6 ions (*m/z* = 465.1, 578.0, 915.2, 1016.3 and 652.1) in a product ion scan experiment of $[M + H]^+$ (*m/z* = 1233.2) in LC-MS/MS confirmed the sequence of **72**.

Ac-Met-Lys-Tyr-Leu-Gly-Ser(PO_3H_2)-Ψ[(*Z*)C=CH]-Pro-Ile-Thr-Thr-Val-NH_2, 73.

The solid phase peptide synthesis of **73** was performed in a manner similar to that for **71** except that the reaction was conducted on a smaller scale (60 mg Rink amide MBHA resin, 0.04 mmol, 0.66 mmol/g). Fmoc-Ser(PO(OBn)OCH_2CH_2CN)-Ψ[(*Z*)C=CH]-Pro-OH (0.032 mmol, 20 mg), **76**, was coupled with HOAt (0.035 mmol, 8.0 mg), HATU (0.035 mmol, 15 mg), and DIEA (0.070 mmol, 15 μL) for 3.0 h at 30 °C. The coupling reaction was monitored by analytical C18 HPLC (conditions as below) for the disappearance of **76**. The resin was capped with 10% Ac_2O and 10% DIEA in CH_2Cl_2 (2.5 mL) for 30 min immediately after the coupling reaction of **76**. After the Kaiser test gave yellow color, 20% piperidine was used to remove the *β*-cyanoethyl group and deprotect the Fmoc simultaneously in 3.5 h. The crude phosphopeptidomimetic was purified using a preparative reverse phase Vydac C4 column at 15 mL/min, 10% B to 45% B over 9 min, 45% B to 42% B over 5 min and 42% B to 90% B over 1 min. No TFA was added to the HPLC mobile phases for the purification of **73.** Purified **73** (4.0 mg, 9.3% yield) eluted at 13.10 min as a white solid. Analytical HPLC on an Xbridge C18 analytical column (1.0 mL/min, 10% B for 2min, 10% B to 90% B over 15 min, retention time 8.48 min) showed> 99% purity. ESI-MS (+), calculated for $C_{58}H_{97}N_{12}O_{18}PS$ $[M + H]^+$) *m/z* = 1313.50, found *m/z* = 1313.2 and *m/z* = 1235.2 for $[M + Na]^+$. The presence of b_3, b_4, b_7 and b_8 ions (*m/z* = 465.0, 578.0, 998.2 and 1099.2) in a product ion scan

experiment of $[M + H]^+$ (*m/z* = 1313.2) in LC-MS/MS confirmed the sequence of **73**.

Ac-Met-Lys-Tyr-Leu-Gly-Ser(PO_3H_2)-Ψ[(*E*)C=CH]-Pro-Ile-Thr-Thr-Val-NH_2, 74. The solid phase peptide synthesis of **74** was performed in a manner similar to that for **72** except that the reaction was conducted on a smaller scale (60 mg Rink amide MBHA resin, 0.04 mmol, 0.66 mmol/g). Fmoc-Ser(PO(OBn)OCH_2CH_2CN)-Ψ[(*E*)C=CH]-Pro-OH (0.040 mmol, 25 mg), **77**, was coupled with HOAt (0.12 mmol, 16 mg), HATU (0.12 mmol, 46 mg), and 2, 4, 6-collidine (0.24 mmol, 32 μL) for 2.5 h at 30 °C. The coupling reaction was monitored by analytical C18 HPLC (conditions as below) for the disappearance of **77**. The resin was capped with 10% Ac_2O and 10% DIEA in CH_2Cl_2 (2.5 mL) for 30 min immediately after the coupling of **77**. After the Kaiser test gave yellow color, 20% piperidine was used to remove the β-cyanoethyl group and deprotect the Fmoc simultaneously in 3.5 h. The crude phosphopeptidomimetic was purified using a preparative reverse phase Vydac C4 column at 15 mL/min, 10% B to 40% B over 9 min, 40% B to 38% B over 5 min and 38% B to 90% B over 2 min. No TFA was added to the HPLC mobile phases for the purification of **74**. Purified **74** (1.1 mg, 2.1% yield) eluted at 12.74 min as a white solid. Analytical HPLC on an Xbridge C18 analytical column (1.0 mL/min, 10% B for 2 min, 10% B to 90% B over 15 min, retention time 8.11 min) showed > 99% purity. ESI-MS (+), calculated for $C_{58}H_{97}N_{12}O_{18}PS$ $[M + H]^+$) *m/z* = 1313.50, found *m/z* = 1313.2 and *m/z* = 1235.2 for $[M + Na]^+$. The presence of b_3, b_4, b_5 and b_7 ions (*m/z* = 465.0, 578.0, 635.9 and 998.2) in a product ion scan experiment of $[M + H]^+$ (*m/z* = 1313.2) in LC-MS/MS confirmed the sequence of **74**.

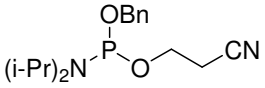

***O*-Benzyl-*O*-β-cyanoethyl-*N,N*-diisopropylphosphoramidite, 75.**

Chloro-*O*-*β*-cyanoethyl-*N,N*-diisopropylphosphoramidite (160 mg, 0.69 mmol) was dissolved in ether (1.3 mL) and cooled to 0 °C for 5 min. A solution of BnOH (75 mg, 0.69 mmol) and DIEA (177 mg, 1.37 mmol) in ether (0.9 mL) was added to the cold reaction solution. The resulting mixture was stirred for 2 h at rt. Salt was removed by filtration and the filtrate was concentrated to afford 211 mg **75** (with DIEA, 100%) as a light yellow oil, which was used in the next step without further purification. ^{1}H NMR δ 7.23-7.38 (m, 5H), 4.76-4.64 (m, 2H), 3.85 (m, 2H), 3.66 (m, 2H), 2.62 (t, *J* = 6.3, 2H), 1.20 (t, *J* = 6.5, 12H).

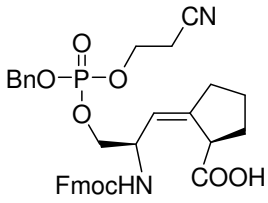

Fmoc–Ser(PO(OBn)(OCH$_2$CH$_2$CN))–Ψ[(*Z*)CH=C]–Pro–OH, 76. Fmoc–Ser–Ψ[(*Z*)CH=C]–Pro–OH, **1** (40 mg, 0.10 mmol) was dissolved in THF (0.8 mL). To the stirring reaction mixture, NMM (10 mg, 0.10 mmol) was added followed by the addition of TBSCl (15 mg, 0.10 mmol). The reaction was stirred at rt for 30 min, after which a solution of *O*-benzyl-*O*-*β*-cyanoethyl-*N,N*-diisopropylphosphoramidite, **75** (60 mg, 0.2 mmol) in THF (0.5 mL) was added dropwise, followed by the addition of 5-ethylthio-1H-tetrazole (51 mg, 0.40 mmol) in one portion. The reaction mixture was stirred for 4 h at rt, then cooled to –40 °C, and tert-butyl hydroperoxide (5 M in decane, 80 μL, 0.4 mmol) was added dropwise. The cold bath was removed and the reaction was stirred at rt for 30 min. The mixture was again cooled to 0 °C, and 5 mL of 10% aqueous $Na_2S_2O_3$ was added. The mixture was stirred at rt for 5 min and transferred for separation using ether (2 × 30 mL). The organic layer was combined, dried over $MgSO_4$, and concentrated. Chromatography on silica

gel with 5% MeOH in $CHCl_3$ eluted 28 mg (45 %) of **76** as a colorless oil. ^{1}H NMR (CD_3OD) δ 7.74 (d, *J* = 7.6, 2H), 7.59 (d, *J* = 7.1, 2H), 7.35-7.24 (m, 9H), 5.42 (d, *J* = 8.4, 1H), 5.05 (dd, *J* = 3.9, 8.2, 2H), 4.48 (m, 1H), 4.30 (m, 2H), 4.12 (m, 3H), 3.94 (m, 2H), 3.68 (t, *J* = 5.9, 1H), 2.74 (m, 2H), 2.41 (m, 1H), 2.30 (m, 1H), 1.90 (m, 3H), 1.82 (m, 1H), 1.60 (m, 1H). ^{13}C NMR (CD_3OD) δ 174.9, 154.8, 152.4, 144.0, 141.2, 128.4, 127.8, 127.3, 126.5, 124.8, 119.5, 70.0, 68.5, 66.4, 62.4, 53.4, 49.5, 29.6, 26.6, 24.3, 18.6, 13.8. ^{31}P NMR (CD_3OD) δ -2.42. ESI-MS(+) for $C_{34}H_{35}N_2O_8P$ $[M + H]^+$ = 631.21, found *m/z* = 631.2.

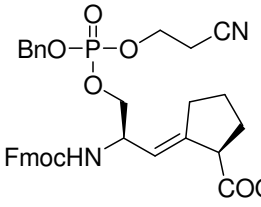

Fmoc–Ser(PO(OBn)(OCH$_2$CH$_2$CN))–Ψ[(*E*)CH=C]–Pro–OH, 77.

Compound **77** was prepared in the same manner as **76.** Chromatography on silica gel gave 50 mg (86%) of **77** as a colorless syrup. ^{1}H NMR (CD_3OD) δ7.74 (d, *J* = 7.1, 2H), 7.60 (d, *J* = 7.2, 2H), 7.33-7.25 (m, 9H), 5.36 (d, *J* = 7.1, 1H), 5.06 (dd, *J* = 3.4, 7.6, 2H), 4.62 (m, 1H), 4.24 (m, 2H), 4.13 (m, 3H), 3.97 (m, 2H), 3.46 (m, 1H), 2.75 (m, 2H), 2.40 (m, 1H), 2.29 (m, 1H), , 1.96 (m, 2H), 1.80 (m, 1H), 1.56 (m, 1H). ^{13}C NMR (DMSO-d_6) δ 174.5, 155.6, 147.0, 144.1, 135.4, 128.3, 127.7, 127.1, 126.9, 124.8, 119.4, 69.5, 68.8, 66.5, 62.6, 53.3, 33.7, 31.2, 26.5, 24.1, 18.6, 13.8. ^{31}P NMR (CD_3OD) δ -2.36. ESI-MS(+) for $C_{34}H_{35}N_2O_8P$ $[M + H]^+$ = 631.21, found *m/z* = 631.2.

LC-MS/MS analysis:

The optimized conditions for the Cdc2 kinase reaction for the detection by mass spectrometry were the following: Final concentrations of Cdc2 kinase reaction conditions:

50 mM Tris-HCl, pH 7.5, 10 mM $MgCl_2$, 1 mM EGTA, 2 mM DTT, 0.01% Brij 35, 400 μM ATP, 66.7 μM peptide substrates and 10 units of Cdc2 kinase. One unit of Cdc2 kinase is defined as the amount of enzyme required to incorporate 1 pmol of phosphate into Cdc2 kinase peptide substrate in 1 min at 30 °C. (Figure 4.16)

The following HPLC conditions were used for the LC-MS/MS analysis of phosphopeptidomimetics resulting from the Cdc2 kinase reaction: Eclipse XDB reverse phase C18 column (Agilent), 5 μM, 150 × 4.6 mm was utilized. Solvent A for the LC-MS/MS analysis was 0.1% formic acid in H_2O, and solvent B was 0.1% formic acid in CH_3CN, according to the following schedule: 10% B for 1 min, 10% B to 90% B over 9 min and 90% B for 2.50 min.

Table 4.8. Compound dependent parameters of Qtrap 3200 in an MRM experiment for AcMKYLGpSPITTVNH$_2$

Q1	Q3	Dwell (ms)	DP (V)	EP (V)	CEP (V)	CE (V)	CXP (V)
1330.4	1232.8	200	106.5	11	56	65	58
1352.20	1254.1	200	109.50	10.5	42.2	76	25.2
1352.2	551.1	200	121	10.5	46.1	96.2	25.2
1352.2	726.0	200	121	11	46.1	96.2	25.2
1352.2	1027.6	200	114	11	45	100	34.0

Instrument dependent parameters using a Qtrap 3200 in an MRM experiment for AcMKYLGpSPITTVNH$_2$ are the following: CUR (20), IS (5500 V), TEM (350°C), GS1 (50), GS2 (50).

Table 4.9. Compound dependent parameters of Qtrap 3200 for the MRM experiment to detect **73** and **74**

Q1	Q3	Dwell (ms)	DP (V)	EP (V)	CEP (V)	CE (V)	CXP (V)
1313.2	1215.1	200	100	10	33.6	66	56
1335.2	1237.3	200	96	11	43	80	56

Instrument dependent parameters using a Qtrap 3200 for the MRM experiment to **73** and **74** are the following: CUR (20), IS (5500 V), TEM (350°C), GS1 (50), GS2 (30).

Instrument dependent parameters of Qtrap 3200 in the MRM experiment to detect the phosphorylation position of **72** in Cdc2 kinase reaction arew the following: CUR (20), IS (5500 V), TEM (350°C), GS1 (50), GS2 (30).

Table 4.10. Compound dependent parameters of Qtrap 3200 in the MRM experiment to detect the phosphorylation position of **72** in Cdc2 kinase reaction

Q1	Q3	Dwell (ms)	DP (V)	EP (V)	CEP (V)	CE (V)	CXP (V)
1313.2	1215.1	200	100	10	33.6	66	56
1313.2	578.0	200	92	10	40	82	27
1313.2	465.0	200	95	10	45.3	90	21
1313.2	998.2	200	100	10	40	70	45

References

1. Pauling, L., *The Nature of the Chemical Bond, Cornell University Press, Cornell* **1948**.
2. Stein, R. L., *In Advances in Protein Chemistry Ed, Lorimer, G., Academic Press, Inc.: San Diego* **1993,** *44*, 1-24.
3. Fischer, G., Chemical aspects of peptide bond isomerisation. *Chem. Soc. Rev.* **2000,** *29*, (*2*), 119-127.
4. Hinderaker, M. P.; Raines, R. T., An electronic effect on protein structure. *Protein Sci.* **2003,** *12*, (*6*), 1188-1194.
5. Stewart, D. E.; Sarkar, A.; Wampler, J. E., Occurrence and Role of Cis Peptide-Bonds in Protein Structures. *J. Mol. Biol.* **1990,** *214*, (*1*), 253-260.
6. Brandts, J. F.; Halvorson, H. R.; Brennan, M., Consideration of the Possibility that the slow step in protein denaturation reactions is due to cis-trans isomerism of proline residues. *Biochemistry* **1975,** *14*, (*22*), 4953-4963.
7. Levitt, M., Effect of proline residues on protein folding. *J. Mol. Biol.* **1981,** *145*, (*1*), 251-263.
8. Schmid, F. X.; Mayr, L. M.; Mucke, M.; Schonbrunner, E. R., Prolyl isomerases: role in protein folding. *Adv. Protein Chem.* **1993,** *44*, 25-66.
9. Kiefhaber, T.; Grunert, H. P.; Hahn, U.; Schmid, F. X., Replacement of a cis proline simplifies the mechanism of ribonuclease T1 folding. *Biochemistry* **1990,** *29*, (*27*), 6475-6480.
10. Baldwin, R. L., Pathway of Protein Folding. *Trends Biochem. Sci.* **1978** *3*, (*3*), 66-68.
11. Lang, K.; Schmid, F. X.; Fischer, G., Catalysis of protein folding by prolyl isomerase. *Nature* **1987,** *329*, (*6136*), 268-270.
12. Lummis, S. C.; Beene, D. L.; Lee, L. W.; Lester, H. A.; Broadhurst, R. W.; Dougherty, D. A., Cis-trans isomerization at a proline opens the pore of a neurotransmitter-gated ion channel. *Nature* **2005,** *438*, (*7065*), 248-252.
13. Lu, K. P.; Finn, G.; Lee, T. H.; Nicholson, L. K., Prolyl cis-trans isomerization as a molecular timer. *Nat. Chem. Biol.* **2007,** *3*, (*10*), 619-629.
14. Fischer, G.; Tradler, T.; Zarnt, T., The mode of action of peptidyl prolyl cis/trans isomerases in vivo: binding vs. catalysis. *FEBS Lett.* **1998,** *426*, (*1*), 17-20.
15. Scholz, C.; Scherer, G.; Mayr, L. M.; Schindler, T.; Fischer, G.; Schmid, F. X., Prolyl isomerases do not catalyze isomerization of non-prolyl peptide bonds. *Biol. Chem.* **1998,** *379*, (*3*), 361-365.
16. Fanghanel, J.; Fischer, G., Insights into the catalytic mechanism of peptidyl prolyl cis/trans isomerases. *Front. Biosci.* **2004,** *9*, 3453-3478.
17. Weiwad, M.; Werner, A.; Rucknagel, P.; Schierhorn, A.; Kullertz, G.; Fischer, G., Catalysis of proline-directed protein phosphorylation by peptidyl-prolyl cis/trans isomerases. *J. Mol. Biol.* **2004,** *339*, (*3*), 635-646.
18. Leulliot, N.; Vicentini, G.; Jordens, J.; Quevillon-Cheruel, S.; Schiltz, M.; Barford, D.; van Tilbeurgh, H.; Goris, J., Crystal structure of the PP2A phosphatase activator: implications for its PP2A-specific PPIase activity. *Mol. Cell.* **2006,** *23*, (*3*), 413-424.
19. Pielak, G. J., Woes of proline: a cautionary kinetic tale. *Protein Sci.* **2006,** *15*, (*3*),

393-394.
20. Janowski, B.; Wollner, S.; Schutkowski, M.; Fischer, G., A protease-free assay for peptidyl prolyl cis/trans isomerases using standard peptide substrates. *Anal. Biochem.* **1997,** *252*, (*2*), 299-307.
21. Hennig, L.; Christner, C.; Kipping, M.; Schelbert, B.; Rucknagel, K. P.; Grabley, S.; Kullertz, G.; Fischer, G., Selective inactivation of parvulin-like peptidyl-prolyl cis/trans isomerases by juglone. *Biochemistry* **1998,** *37*, (*17*), 5953-5960.
22. Schiene, C.; Reimer, U.; Schutkowski, M.; Fischer, G., Mapping the stereospecificity of peptidyl prolyl cis/trans isomerases. *FEBS Lett.* **1998,** *432*, (*3*), 202-206.
23. Gothel, S. F.; Marahiel, M. A., Peptidyl-prolyl cis-trans isomerases, a superfamily of ubiquitous folding catalysts. *Cell. Mol. Life Sci.* **1999,** *55*, (*3*), 423-436.
24. Pliyev, B. K.; Gurvits, B. Y., Peptidyl-prolyl cis-trans isomerases: Structure and functions. *Biochemistry-Moscow* **1999,** *64*, (*7*), 738-751.
25. Wiederrecht, G.; Etzkorn, F. A., The immunophilins. *Perspect. Drug Discovery Des.* **1994,** *2*, (*1*), 57-84.
26. Fischer, G.; Wittmann-Liebold, B.; Lang, K.; Kiefhaber, T.; Schmid, F. X., Cyclophilin and peptidyl-prolyl cis-trans isomerase are probably identical proteins. *Nature* **1989,** *337*, (*6206*), 476-478.
27. Schreiber, S. L.; Crabtree, G. R., The mechanism of action of cyclosporin A and FK506. *Immunol. Today* **1992,** *13*, (*4*), 136-142.
28. Freskgard, P. O.; Bergenhem, N.; Jonsson, B. H.; Svensson, M.; Carlsson, U., Isomerase and chaperone activity of prolyl isomerase in the folding of carbonic anhydrase. *Science* **1992,** *258*, (*5081*), 466-468.
29. Luban, J.; Bossolt, K. L.; Franke, E. K.; Kalpana, G. V.; Goff, S. P., Human immunodeficiency virus type 1 Gag protein binds to cyclophilins A and B. *Cell* **1993,** *73*, (*6*), 1067-1078.
30. Etzkorn, F. A., Pin1 flips Alzheimer's switch. *ACS Chem. Biol.* **2006,** *1*, (*4*), 214-216.
31. Corey, R. B.; Pauling, L., Fundamental dimensions of polypeptide chains. *Proc. R. Soc. Lond B Biol. Sci.* **1953,** *141*, (*902*), 10-20.
32. Pauling, L.; Corey, R. B., Stable configurations of polypeptide chains. *Proc. R. Soc. Lond B Biol. Sci.* **1953,** *141*, (*902*), 21-33.
33. Scheiner, S.; Kern, C. W., Theoretical Studies of Environmental Effects on Protein Conformation .1. Flexibility of Peptide-Bond. *J. Am. Chem. Soc.* **1977,** *99*, (*21*), 7042-7050.
34. Eberhardt, E. S.; Loh, S. N.; Hinck, A. P.; Raines, R. T., Solvent Effects on the Energetics of Prolyl Peptide-Bond Isomerization. *J. Am. Chem. Soc.* **1992** *114*, (*13*), 5437-5439.
35. Park, S. T.; Aldape, R. A.; Futer, O.; DeCenzo, M. T.; Livingston, D. J., PPIase catalysis by human FK506-binding protein proceeds through a conformational twist mechanism. *J. Biol. Chem.* **1992,** *267*, (*5*), 3316-3324.
36. Fischer, S.; Michnick, S.; Karplus, M., A Mechanism for Rotamase Catalysis by the Fk506 Binding-Protein (Fkbp). *Biochemistry* **1993,** *32*, (*50*), 13830-13837.
37. Ranganathan, R.; Lu, K. P.; Hunter, T.; Noel, J. P., Structural and functional analysis of the mitotic rotamase Pin1 suggests substrate recognition is phosphorylation dependent. *Cell* **1997,** *89*, (*6*), 875-886.
38. Lu, K. P.; Hanes, S. D.; Hunter, T., A human peptidyl-prolyl isomerase essential for

regulation of mitosis. *Nature* **1996,** *380*, (*6574*), 544-547.
39. Yaffe, M. B.; Schutkowski, M.; Shen, M.; Zhou, X. Z.; Stukenberg, P. T.; Rahfeld, J. U.; Xu, J.; Kuang, J.; Kirschner, M. W.; Fischer, G.; Cantley, L. C.; Lu, K. P., Sequence-specific and phosphorylation-dependent proline isomerization: a potential mitotic regulatory mechanism. *Science* **1997,** *278*, (*5345*), 1957-1960.
40. Shen, M.; Stukenberg, P. T.; Kirschner, M. W.; Lu, K. P., The essential mitotic peptidyl-prolyl isomerase Pin1 binds and regulates mitosis-specific phosphoproteins. *Genes Dev.* **1998,** *12*, (*5*), 706-720.
41. Zhou, X. Z.; Lu, P. J.; Wulf, G.; Lu, K. P., Phosphorylation-dependent prolyl isomerization: a novel signaling regulatory mechanism. *Cell. Mol. Life. Sci.* **1999,** *56*, (9-10), 788-806.
42. Lippens, G.; Landrieu, I.; Smet, C., Molecular mechanisms of the phospho-dependent prolyl cis/trans isomerase Pin1. *FEBS J.* **2007,** *274*, (*20*), 5211-5222.
43. Lu, K. P.; Zhou, X. Z., The prolyl isomerase PIN1: a pivotal new twist in phosphorylation signalling and disease. *Nat. Rev. Mol. Cell. Biol.* **2007**.
44. Schutkowski, M.; Bernhardt, A.; Zhou, X. Z.; Shen, M.; Reimer, U.; Rahfeld, J. U.; Lu, K. P.; Fischer, G., Role of phosphorylation in determining the backbone dynamics of the serine/threonine-proline motif and Pin1 substrate recognition. *Biochemistry* **1998,** *37*, (*16*), 5566-5575.
45. Canagarajah, B. J.; Khokhlatchev, A.; Cobb, M. H.; Goldsmith, E. J., Activation mechanism of the MAP kinase ERK2 by dual phosphorylation. *Cell* **1997,** *90*, (*5*), 859-869.
46. Brown, N. R.; Noble, M. E.; Endicott, J. A.; Johnson, L. N., The structural basis for specificity of substrate and recruitment peptides for cyclin-dependent kinases. *Nat. Cell. Biol.* **1999,** *1*, (*7*), 438-443.
47. Weiwad, M.; Kullertz, G.; Schutkowski, M.; Fischer, G., Evidence that the substrate backbone conformation is critical to phosphorylation by p42 MAP kinase. *FEBS Lett.* **2000,** *478*, (*1-2*), 39-42.
48. Zhou, X. Z.; Kops, O.; Werner, A.; Lu, P. J.; Shen, M.; Stoller, G.; Kullertz, G.; Stark, M.; Fischer, G.; Lu, K. P., Pin1-dependent prolyl isomerization regulates dephosphorylation of Cdc25C and tau proteins. *Mol. Cell.* **2000,** *6*, (*4*), 873-883.
49. Lu, P. J.; Zhou, X. Z.; Shen, M.; Lu, K. P., Function of WW domains as phosphoserine- or phosphothreonine-binding modules. *Science* **1999,** *283*, (*5406*), 1325-1328.
50. King, R. W.; Jackson, P. K.; Kirschner, M. W., Mitosis in transition. *Cell* **1994,** *79*, (*4*), 563-571.
51. Murray, A. W., Cyclin-dependent Kinases: Regulators of the Cell Cycle and More. *Chem. Biol.* **1994,** *1*, (*4*), 191-195.
52. Pines, J., Protein Kinases and Cell Cycle Control. *Semin. Cell Biol.* **1994,** *5*, (*6*), 399-408.
53. Clarke, P. R.; Karsenti, E., Regulation of p34cdc2 Protein Kinase: New Insights into Protein Phosphorylation and the Cell Cycle. *J. Cell. Sci.* **1991,** *100*, 409-414.
54. Lu, K. P., Prolyl isomerase Pin1 as a molecular target for cancer diagnostics and therapeutics. *Cancer Cell* **2003,** *4*, (*3*), 175-180.
55. Wulf, G. M.; Liou, Y. C.; Ryo, A.; Lee, S. W.; Lu, K. P., Role of Pin1 in the regulation of p53 stability and p21 transactivation, and cell cycle checkpoints in response to DNA damage.

J. Biol. Chem. **2002,** *277*, (*50*), 47976-47979.
56. Zacchi, P.; Gostissa, M.; Uchida, T.; Salvagno, C.; Avolio, F.; Volinia, S.; Ronai, Z.; Blandino, G.; Schneider, C.; Del Sal, G., The prolyl isomerase Pin1 reveals a mechanism to control p53 functions after genotoxic insults. *Nature* **2002,** *419*, (*6909*), 853-857.
57. Zheng, H.; You, H.; Zhou, X. Z.; Murray, S. A.; Uchida, T.; Wulf, G.; Gu, L.; Tang, X.; Lu, K. P.; Xiao, Z. X., The prolyl isomerase Pin1 is a regulator of p53 in genotoxic response. *Nature* **2002,** *419*, (*6909*), 849-853.
58. Yeh, E.; Cunningham, M.; Arnold, H.; Chasse, D.; Monteith, T.; Ivaldi, G.; Hahn, W. C.; Stukenberg, P. T.; Shenolikar, S.; Uchida, T.; Counter, C. M.; Nevins, J. R.; Means, A. R.; Sears, R., A signalling pathway controlling c-Myc degradation that impacts oncogenic transformation of human cells. *Nat. Cell. Biol.* **2004,** *6*, (*4*), 308-318.
59. Bayer, E.; Thutewohl, M.; Christner, C.; Tradler, T.; Osterkamp, F.; Waldmann, H.; Bayer, P., Identification of hPin1 inhibitors that induce apoptosis in a mammalian Ras transformed cell line. *Chem. Commun.* **2005**, (*4*), 516-518.
60. Wulf, G.; Finn, G.; Suizu, F.; Lu, K. P., Phosphorylation-specific prolyl isomerization: is there an underlying theme? *Nat. Cell. Biol.* **2005,** *7*, (*5*), 435-441.
61. Wulf, G. M.; Ryo, A.; Wulf, G. G.; Lee, S. W.; Niu, T.; Petkova, V.; Lu, K. P., Pin1 is overexpressed in breast cancer and cooperates with Ras signaling in increasing the transcriptional activity of c-Jun towards cyclin D1. *EMBO J.* **2001,** *20*, (*13*), 3459-3472.
62. Liou, Y. C.; Ryo, A.; Huang, H. K.; Lu, P. J.; Bronson, R.; Fujimori, F.; Uchida, T.; Hunter, T.; Lu, K. P., Loss of Pin1 function in the mouse causes phenotypes resembling cyclin D1-null phenotypes. *Proc. Natl. Acad. Sci. USA* **2002,** *99*, (*3*), 1335-1340.
63. Ryo, A.; Liou, Y. C.; Wulf, G.; Nakamura, M.; Lee, S. W.; Lu, K. P., PIN1 is an E2F target gene essential for Neu/Ras-induced transformation of mammary epithelial cells. *Mol. Cell. Biol.* **2002,** *22*, (*15*), 5281-5295.
64. Dougherty, M. K.; Muller, J.; Ritt, D. A.; Zhou, M.; Zhou, X. Z.; Copeland, T. D.; Conrads, T. P.; Veenstra, T. D.; Lu, K. P.; Morrison, D. K., Regulation of Raf-1 by direct feedback phosphorylation. *Mol. Cell.* **2005,** *17*, (*2*), 215-224.
65. Monje, P.; Hernandez-Losa, J.; Lyons, R. J.; Castellone, M. D.; Gutkind, J. S., Regulation of the transcriptional activity of c-Fos by ERK. A novel role for the prolyl isomerase PIN1. *J. Biol. Chem.* **2005,** *280*, (*42*), 35081-35084.
66. Wulf, G.; Garg, P.; Liou, Y. C.; Iglehart, D.; Lu, K. P., Modeling breast cancer in vivo and ex vivo reveals an essential role of Pin1 in tumorigenesis. *EMBO J.* **2004,** *23*, (*16*), 3397-3407.
67. Yeh, E. S.; Means, A. R., PIN1, the cell cycle and cancer. *Nat. Rev. Cancer* **2007,** *7*, (*5*), 381-388.
68. Bao, L.; Kimzey, A.; Sauter, G.; Sowadski, J. M.; Lu, K. P.; Wang, D. G., Prevalent overexpression of prolyl isomerase Pin1 in human cancers. *Am. J. Pathol.* **2004,** *164*, (*5*), 1727-1737.
69. Lu, K. P.; Suizu, F.; Zhou, X. Z.; Finn, G.; Lam, P.; Wulf, G., Targeting carcinogenesis: a role for the prolyl isomerase Pin1? *Mol. Carcinog.* **2006,** *45*, (*6*), 397-402.
70. Lamb, J.; Ramaswamy, S.; Ford, H. L.; Contreras, B.; Martinez, R. V.; Kittrell, F. S.; Zahnow, C. A.; Patterson, N.; Golub, T. R.; Ewen, M. E., A mechanism of cyclin D1 action encoded in the patterns of gene expression in human cancer. *Cell* **2003,** *114*, (*3*), 323-334.

71. Fujimori, F.; Takahashi, K.; Uchida, C.; Uchida, T., Mice lacking Pin1 develop normally, but are defective in entering cell cycle from G(0) arrest. *Biochem. Biophys. Res. Commun.* **1999,** *265*, (*3*), 658-663.
72. Ryo, A.; Uemura, H.; Ishiguro, H.; Saitoh, T.; Yamaguchi, A.; Perrem, K.; Kubota, Y.; Lu, K. P.; Aoki, I., Stable suppression of tumorigenicity by Pin1-targeted RNA interference in prostate cancer. *Clin. Cancer Res.* **2005,** *11*, (*20*), 7523-7531.
73. Lu, P. J.; Wulf, G.; Zhou, X. Z.; Davies, P.; Lu, K. P., The prolyl isomerase Pin1 restores the function of Alzheimer-associated phosphorylated tau protein. *Nature* **1999,** *399*, (*6738*), 784-788.
74. Hamdane, M.; Dourlen, P.; Bretteville, A.; Sambo, A. V.; Ferreira, S.; Ando, K.; Kerdraon, O.; Begard, S.; Geay, L.; Lippens, G.; Sergeant, N.; Delacourte, A.; Maurage, C. A.; Galas, M. C.; Buee, L., Pin1 allows for differential Tau dephosphorylation in neuronal cells. *Mol. Cell. Neurosci.* **2006,** *32*, (*1-2*), 155-160.
75. Pastorino, L.; Sun, A.; Lu, P. J.; Zhou, X. Z.; Balastik, M.; Finn, G.; Wulf, G.; Lim, J.; Li, S. H.; Li, X.; Xia, W.; Nicholson, L. K.; Lu, K. P., The prolyl isomerase Pin1 regulates amyloid precursor protein processing and amyloid-beta production. *Nature* **2006,** *440*, (*7083*), 528-534.
76. Fischer, E. H.; Krebs, E. G., Conversion of Phosphorylase b to Phosphorylase a in Muscle Extracts. *J. Biol. Chem.* **1955,** *216*, 121-132.
77. Johnson, L. N.; Lowe, E. D.; Noble, M. E. M.; Owen, D. J.; , The Structural Basis for Substrate Recognition and Control by Protein Kinases. *FEBS Lett.* **1998,** 430, (*1*), 1-11.
78. Friedrich, M., Protein Phosphorylation. Edited by Friedrich, M. **1996**, 1-31.
79. Davies, S. P.; Reddy, H.; Caivano, M.; Cohen, P., Specificity and Mechanism of Action of Some Commonly Used Protein Kinase Inhibitors. *Biochem. J.* **2000,** *351*, (*1*), 95-105.
80. Adams, J. A., Kinetic and Catalytic Mechanisms of Protein Kinases. *Chem. Rev.* **2001,** *101*, (*8*), 2271-2290.
81. Cohen, P., The Role of Protein Phosphorylation in Neutral and Hormonal Control of Cellular Activity. *Nature* **1982,** *296*, 613-620.
82. Hunter, T., 1001 Protein Kinases Redux--Towards 2000. *Semin. Cell Biol.* **1994,** *5*, (*6*), 367-376.
83. Taylor, S. S.; Adams, J. A., Protein Kinases: Coming of Age. *Curr. Opin. Struct. Biol.* **1992,** *2*, (*5*), 743-748.
84. Ullrich, A.; Schlessinger, Signal Transduction by Receptors with Tyrosine Kinase Activity. *Cell* **1990,** *61*, 203-212.
85. Draetta, G., Cell Cycle Control in Eukaryotes: Molecular Mechanisms of Cdc2 Activation. *Trends Biochem. Sci.* **1990,** *15*, 378-383.
86. Hanks, S. K.; Hunter, T., Protein kinases 6. The Eukaryotic Protein Kinase Superfamily: Kinase (Catalytic) Domain Structure and Classification. *FASEB J.* **1995,** *9*, (*576-596*).
87. Hanks, S. K., Eukaryotic Protein Kinases. *Curr. Opin. Struct. Biol.* **1991,** *1*, 369-383.
88. Kennelly, P. J., Protein Kinases and Protein Phosphatases in Prokaryotes: A Genomic Perspective. *FEMS Microbiol. Lett.* **2001,** *206*, 1-8.
89. Kennelly, P. J., Protein Phosphatases: A Phylogenetic Perspective. *Chem. Rev.* **2001,** *101*, 2291-2312.
90. Hunter, T., Protein Kinase Classification. *Methods Enzymol.* **1991,** *200*, 3-37.

91. Lindberg, R. A.; Quinn, A. M.; Hunter, T., Dual-Specificity Protein Kinases: Will any Hydroxyl Do? *Trends Biochem. Sci.* **1992,** *17*, 114-119.
92. Nishida, E.; Gotoh, Y., The MAP Kinase Cascade is Essential for Diverse Signal Transduction Pathways. *Trends Biochem. Sci.* **1993,** *18*, 128-131.
93. Avruch, J.; Zhang, X.; Kyriakis, J. M., Raf Meets Ras: Completing the Framework of a Signal Transduction Pathway. *Trends Biochem. Sci.* **1994,** *19*, 279-283.
94. Seger, R.; Krebs, E. G., The MAPK Signaling Cascade. *FASEB J.* **1995,** *9*, 726-735.
95. Marks, F., Protein phosphorylation, VCH. **1996**.
96. Hepler, J. R.; Gilman, A. G., G Proteins. *Trends Biochem. Sci.* **1992,** *17*, 323-327.
97. Meyerson, M.; Enders, G. H.; Wu, C. L.; Su, L. K.; Gorka, C.; Nelson, C.; Harlow, E.; Tsai, L. H., A Family of Human Cdc-2-related Protein Kinases. *EMBO J.* **1992,** *11*, 2909-2917.
98. Stukenberg, P. T.; Kirschner, M. W., Pin1 acts catalytically to promote a conformational change in Cdc25. *Mol. Cell.* **2001,** *7*, (*5*), 1071-1083.
99. Lu, K. P.; Osmani, S. A.; Osmani, A. H.; Means, A. R., Essential Roles for Calcium and Calmodulin in G2/M Progression in Aspergillus Nidulans. *J. Cell. Biol.* **1993,** *121*, 621-630.
100. Osmani, S. A.; Ye, X. S., Cell Cycle Regulation in Aspergillus by Two Protein Kinases. *Biochem. J.* **1996,** *317*, (*3*), 633-641.
101. Livneh, E.; Fishman, D. D., Linking Protein Kinase C to Cell-Cycle Control. *Eur. J. Biochem.* **1997,** *248*, 1-9.
102. Kuang, J.; Ashorn, C. L., At least Two Kinases Phosphorylate the MPM-2 Epitope During Xenopus oocyte Maturation. *J. Cell. Biol.* **1993,** *123*, 859-868.
103. Knighton, D. R.; Zheng, J.; Ten Eyck, L. F.; Ashford, V. A.; Xuong, N. H.; Taylor, S. S.; Sowadski, J. M., Crystal Structure of the Catalytic Subunit of Cyclic Adenosine Monophosphate-dependent Protein Kinase *Science* **1991,** *253*, 407-414.
104. Knighton, D. R.; Zheng, J.; Ten Eyck, L. F.; Ashford, V. A.; Xuong, N. H.; Taylor, S. S.; Sowadski, J. M., Structure of a Peptide Inhibitor Bound to the Catalytic Subunit of Cyclic Adenosine Monophosphate-dependent Protein Kinase. *Science* **1991,** *253*, 414-420.
105. Hanks, S. K.; Quinn, A. M.; Hunter, T., The Protein Kinase Family: Conserved Features and Deduced Phylogeny of the Catalytic Domains. *Science* **1988,** *241*, 42-52.
106. Rasmussen, H., The Cycling of Calcium as an Intracellular Messenger *Sci. Am.* **1989,** *261*, (*4*), 66-73.
107. Lucas, K. A.; Pitari, G. M.; Kazerounian, S.; Ruiz-Stewart, I.; Park, J.; Schulz, S.; Chepenik, K. P.; Waldman, S. A., Guanylyl Cyclases and Signaling by Cyclic GMP. *Pharmacol. Rev.* **2000,** *52*, (*3*), 375-414.
108. Blenis, J.; Resh, M. D., Subcellular Localization Specified by Protein Acylation and Phosphorylation. *Curr. Opin. Cell. Biol.* **1993,** *5*, (*6*), 984-989.
109. Johnson, J. E.; Cornell, R. B., Amphitropic Proteins: Regulation by Reversible Membrane Interactions. *Mol. Membr. Biol.* **1999,** *16*, (*3*), 217-235.
110. Inglese, J.; Premont, R. T., Lipid Modifications of G-protein-coupled Receptor Kinases. *Biochem. Soc. Tran.* **1996,** *24*, (*3*), 714-717.
111. Pitcher, J. A.; Freedman, N. J.; Lefkowitz, R. J., G Protein-coupled Receptor Kinases *Annu. Rev. Biochem.* **1998,** *67*, 653-692.
112. Kemp, B. E.; Pearson, R. B., Intrasteric Regulation of Protein Kinases and Phosphatases.

Biochim. Biophys. Acta. **1991,** *1094*, (*1*), 67-76.
113.Kemp, B. E.; Pearson, R. B.; House, C.; Robinson, P. J.; Means, A. R., Regulation of Protein Kinases by Pseudosubstrate Prototopes *Cell. Signal.* **1989,** *1*, 303-311.
114.Xu, W.; Doshi, A.; Lei, M.; Eck, M. J.; Harrison, S. C., Crystal Structures of c-Src Reveal Features of its Autoinhibitory Mechanism. *Mol. Cell.* **1999,** *3*, 629-638.
115.Canagarajah, B. J.; Khokhlatchev, A.; Cobb, M. H.; Goldsmith, E. J., Activation Mechanism of the MAP Kinase ERK2 by Dual Phosphorylation. . *Cell* **1997,** 90, (5), 859-869.
116.Hubbard, S. R., Crystal Structure of the Activated Insulin Receptor Tyrosine Kinase in Complex with Peptide Substrate and ATP Analog. *EMBO J.* **1997,** *16*, 5572-5581.
117.Lowe, E. D.; Noble, M. E. M.; Skamnaki, V. T.; Oikonomakos, N. G.; Owen, D. J.; Johnson, L. N., The Crystal Structure of a Phosphorylase Kinase Peptide Substrate Complex: Kinase Substrate Recognition. *EMBO J.* **1997,** *16*, 6646-6658.
118.Gibbs, C. S.; Zoller, M. J., Rational Scanning Mutagenesis of a Protein Kinase Identifies Functional Regions Involved in Catalysis and Substrate Interactions. *J. Biol. Chem.* **1991,** *266*, (*14*), 8923-8931.
119.Carrera, A. C.; Alexandrov, K.; Roberts, T. M., The Conserved Lysine of the Catalytic Domain of Protein Kinases is Actively Involved in the Phosphotransfer Reaction and not Required for Anchoring ATP. *Proc. Natl. Acad. Sci.* **1993,** *90*, (*2*), 442-446.
120. Zheng, J.; Knighton, D. R.; Ten Eyck, L. F.; Karlsson, R.; Xuong, N. H.; Taylor, S. S.; Sowadski, J. M., Crystal Structure of the Catalytic Subunit of cAMP-Dependent Protein Kinase Complexed with MgATP and Peptide Inhibitor. *Biochemistry* **1993,** *32*, (*9*), 2154-2161.
121. Madhusudan; Trafny, E. A.; Xuong, N. H.; Adams, J. A.; Ten Eyck, L. F.; Taylor, S. S.; Sowadski, J. M., cAMP-dependent Protein Kinase: Crystallographic Insights into Substrate Recognition and Phosphotransfer. *Protein Sci.* **1994,** *3*, (*2*), 176-187.
122. Robinson, M. J.; Harkins, P. C.; Zhang, J.; Baer, R.; Haycock, J. W.; Cobb, M. H.; Goldsmith, E. J., Mutation of Position 52 in ERK2 Creates a Nonproductive Binding Mode for Adenosine 5'-triphosphate *Biochemistry* **1996,** *35*, (*18*), 5641-5646.
123. Vulliet, P. R.; Hall, F. L.; Mitchell, J. P.; Hardie, D. G., Identification of a Novel Proline-directed Serine/Threonine Protein Kinase in Rat Pheochromocytoma *J. Biol. Chem.* **1989,** *264*, (*27*), 16292-16298.
124. Sharrocks, A. D.; Yang, S. H.; Galanis, A., Docking Domains and Substrate-Specificity Determination for MAP Kinases. *Trends Biochem. Sci.* **2000,** *25*, (*9*), 448-453.
125. Erneux, C.; Cohen, S.; Garbers, D. L., Tyrosine Protein Kinase Activity of Rat Spleen and Other Tissues. *J. Biol. Chem.* **1983,** *258*, (*17*), 4137-4177.
126. Cook, P. F.; Neville, M. E.; Vrana, K. E.; Hartl, F. T.; Roskoski, J. R., Adenosine Cyclic 3',5'-Monophosphate Dependent Protein Kinase: Kinetic Mechanism for the Bovine Skeletal Muscle Catalytic Subunit. *Biochemistry* **1982,** *21*, (*23*), 5794-5799.
127. Kong, C. T.; Cook, P. F., Isotope Partitioning in the Adenosine 3',5'-Monophosphate Dependent Protein Kinase Reaction Indicates a Steady-State Random Kinetic Mechanism. *Biochemistry* **1988,** *27*, (*13*), 4795-4799.
128. Grant, B.; Adams, J. A., Pre-steady-state Kinetic Analysis of cAMP-dependent

Protein Kinase Using Rapid Quench Flow Techniques. *Biochemistry* **1996,** *35*, (*6*), 2022-2029.
129. Ho, M. F.; Bramson, H. N.; Hansen, D. E.; Knowles, J. R.; Kaiser, E. T., Stereochemical Course of the Phospho Group Transfer Catalyzed by cAMP-dependent Protein Kinase. *J. Am. Chem. Soc.* **1988,** *110*, (*8*), 2680-2681.
130. Kim, K.; Cole, P. A., Kinetic Analysis of a Protein Tyrosine Kinase Reaction Transition State in the Forward and Reverse Directions. *J. Am. Chem. Soc.* **1998,** *120*, 6851-6858.
131. Williams, D. M.; Cole, P. A., Proton Demand Inversion in a Mutant Protein Tyrosine Kinase Reaction. *J. Am. Chem. Soc.* **2002,** *124*, 5956-5957.
132. Parang, K.; Cole, P. A., Designing Bisubstrate Analog Inhibitors for Protein Kinases. *Pharmacol. Ther.* **2002,** *93*, 145-157.
133. Kim, K.; Cole, P. A., Measurement of a Bronsted Nucleophile Coefficient and Insights into the Transtion State for a Protein Tyrosine Kinase *J. Am. Chem. Soc.* **1997,** *119*, (*45*), 11096-11097.
134. Herschlag, D.; Jencks, W. P., The Effect of Divalent Metal Ions on the Rate and Transition-state Structure of Phosphoryl-transfer Reactions. *J. Am. Chem. Soc.* **1987,** *109*, (*15*), 4665-4674.
135. Mildvan, A. S., Mechanisms of Signaling and Related Enzymes. *Proteins* **1997,** *29*, 401-406.
136. Granot, J.; Mildvan, A. S.; Bramson, H. N.; Kaiser, E. T., Magnetic Resonance Measurements of Intersubstrate Distances at the Active Site of Protein Kinase Using Substitution-inert Cobalt(III) and Chromium(III) Complexes of Adenosine 5'-(beta, gamma-methylenetriphosphate) *Biochemistry* **1980,** *19*, (*15*), 3537-3543.
137. Kirby, A. J.; Varvoglis, A. G., The Reactivity of Phosphate Esters. Monoester Hydrolysis. *J. Am. Chem. Soc.* **1967,** *89*, (*2*), 415-423.
138. Bossemeyer, D.; Engh, R. A.; Kinzel, V.; Ponstingl, H.; Huber, R., Phosphotransferase and Substrate Binding Mechanism of the cAMP-dependent Protein Kinase Catalytic Subunit from Porcine Heart as Deduced from the 2.0 .ANG. Structure of the Complex with Manganese(2+) Adenylyl Imidodiphosphate and Inhibitor Peptide PKI(5-24). *EMBO J.* **1993,** *12*, 849-859.
139. Florian, J.; Aqvist, J.; Warshel, A., On the Reactivity of Phosphate Monoester Dianions in Aqueous Solution: Bronsted Linear Free-Energy Relationships Do Not Have an Unique Mechanistic Interpretation *J. Am. Chem. Soc.* **1998,** *120*, 11524-11525.
140. Shaffer, J.; Adams, J. A., Detection of Conformational Changes along the Kinetic Pathway of Protein Kinase A Using a Catalytic Trapping Technique *Biochemistry* **1999,** *38*, (*37*), 12072-12079.
141. Sun, G.; Budde, R. J. A., Requirement for an Additional Divalent Metal Cation to Activate Protein Tyrosine Kinases. *Biochemistry* **1997,** *36*, (*8*), 2139-2146.
142. Adams, J. A.; Taylor, S. S., Phosphorylation of Peptide Substrates for the Catalytic Subunit of cAMP- dependent Protein Kinase. *J. Biol. Chem.* **1993,** *268*, 7747-7752.
143. Huang, C. Y.; Yuan, C. J.; Luo, S.; Graves, D. J., Mutational Analyses of the Metal Ion and Substrate Binding Sites of Phosphorylase Kinase. *Biochemistry* **1994,** *33*, (*19*), 5877-5883.

144. Adams, J. A.; Taylor, S. S., Energetic Limits of Phosphotransfer in the Catalytic Subunit of cAMP-dependent Protein Kinase as Measured by Viscosity Experiments. *Biochemistry* **1992,** *31*, (*36*), 8516-8522.
145. Sun, G.; Budde, R. J. A., Substitution Studies of the Second Divalent Metal Cation Requirement of Protein Tyrosine Kinase CSK. *Biochemistry* **1999,** *38*, (*17*), 5659-5665.
146. Brouwer, A. C.; Kirsch, J. F., Investigation of Diffusion-limited Rates of Chymotrypsin Reactions by Viscosity Variation *Biochemistry* **1982,** *21*, (*6*), 1302-1307.
147. Stone, S. R.; Morrison, J. F., Dihydrofolate Reductase from Escherichia Coli: the Kinetic Mechanism with NADPH and Reduced Acetylpyridine Adenine Dinucleotide Phosphate as Substrates. *Biochemistry* **1988,** *27*, (*15*), 5493-5499.
148. Prowse, C. N.; Hagopian, J. C.; Cobb, M. H.; Ahn, N. G.; Lew, J., Catalytic Reaction Pathway for the Mitogen-Activated Protein Kinase ERK2. *Biochemistry* **2000,** *39*, (*20*), 6258-6266.
149. Lew, J.; Taylor, S. S.; Adams, J. A., Identification of a Partially Rate-determining Step in the Catalytic Mechanism of cAMP-dependent Protein Kinase: a Transient Kinetic Study Using Stopped-Flow Fluorescence Spectroscopy *Biochemistry* **1997,** *36*, (*22*), 6717-6724.
150. Zhou, J.; Adams, J. A., Participation of ADP Dissociation in the Rate-Determining Step in cAMP-Dependent Protein Kinase. *Biochemistry* **1997,** *36*, (*50*), 15733-15738.
151. Barshop, B. A.; Wrenn, R. F.; Frieden, C., Analysis of Numerical Methods for Computer Simulation of Kinetic Processes: Development of KINSIM--a Flexible, Portable System. *Anal. Biochem.* **1983,** *130*, (*1*), 134-145.
152. Hann, M. M.; Sammes, P. G.; Kennewell, P. D.; Taylor, J. B., Double-Bond Isosteres of the Peptide-Bond - Enkephalin Analog. *J. Chem. Soc. Chem. Comm.* **1980**, (*5*), 234-235.
153. Cox, M. T.; Gormley, J. J.; Hayward, C. F.; Petter, N. N., Incorporation of Trans-Olefinic Dipeptide Isosteres into Enkephalin and Substance-P Analogs. *J. Chem. Soc. Chem. Comm.* **1980** (*17*), 800-802.
154. Andres, C. J.; Macdonald, T. L.; Ocain, T. D.; Longhi, D., Conformationally Defined Analogs of Prolylamides - Trans-Prolyl Peptidomimetics. *J. Org. Chem.* **1993,** *58*, (*24*), 6609-6613.
155. Cox, M. T.; Heaton, D. W.; Horbury, J., Preparation of Protected Trans-Olefinic Dipeptide Isosteres. *J. Chem. Soc. Chem. Comm.* **1980**, (*17*), 799-800.
156. Hann, M. M.; Sammes, P. G.; Kennewell, P. D.; Taylor, J. B., On the Double-Bond Isostere of the Peptide-Bond - Preparation of an Enkephalin Analog. *J. Chem. Soc. Perkins Trans.* **1982**, (*1*), 307-314.
157. Whitesell, J. K.; Lawrence, R. M., Stereocontrolled Synthesis of Peptide-Bond Isosteres. *Chirality* **1989,** *1*, (*1*), 89-91.
158. Bohnstedt, A. C.; Prasad, J. V. N. V.; Rich, D. H., Synthesis of *E*-Alkene and *Z*-Alkene Dipeptide Isosteres. *Tetrahedron Lett.* **1993,** *34*, (*33*), 5217-5220.
159. Welch, J. T.; Lin, J., Fluoroolefin containing dipeptide isosteres as inhibitors of dipeptidyl peptidase IV (CD26). *Tetrahedron* **1996,** *52*, (*1*), 291-304.
160. Lin, J.; Toscano, P. J.; Welch, J. T., Inhibition of dipeptidyl peptidase IV by fluoroolefin-containing *N*-peptidyl-*O*-hydroxylamine peptidomimetics. *Proc. Natl. Acad. Sci. USA* **1998,** *95*, (*24*), 14020-14024.

161. Hart, S. A.; Sabat, M.; Etzkorn, F. A., Enantio- and regioselective synthesis of a (*Z*)-alkene *cis*-proline mimic. *J. Org. Chem.* **1998,** *63*, (*22*), 7580-7581.
162. Hart, S. A.; Etzkorn, F. A., Cyclophilin inhibition by a (*Z*)-alkene *cis*-proline mimic. *J. Org. Chem.* **1999,** *64*, (*9*), 2998-2999.
163. Hart, S. A.; Trindle, C. O.; Etzkorn, F. A., Solvent-dependent stereoselectivity in a Still-Wittig rearrangement: An experimental and ab initio study. *Org. Lett.* **2001,** *3*, (*12*), 1789-1791.
164. Wang, X. D. J.; Hart, S. A.; Xu, B. L.; Mason, M. D.; Goodell, J. R.; Etzkorn, F. A., Serine-*cis*-proline and serine-*trans*-proline isosteres: Stereoselective synthesis of (*Z*)- and (*E*)-alkene mimics by Still-Wittig and Ireland-Claisen rearrangements. *J. Org. Chem.* **2003,** *68*, (*6*), 2343-2349.
165. Wang, X. J.; Xu, B.; Mullins, A. B.; Neiler, F. K.; Etzkorn, F. A., Conformationally locked isostere of phosphoSer-*cis*-Pro inhibits Pin1 23-fold better than phosphoSer-*trans*-Pro isostere. *J. Am. Chem. Soc.* **2004,** *126*, (*47*), 15533-15542.
166. Nahm, S.; Weinreb, S. M., *N*-Methoxy-*N*-Methylamides as Effective Acylating Agents. *Tetrahedron Lett.* **1981,** *22*, (*39*), 3815-3818.
167. Barton, D. H. R.; Bashiardes, G.; Fourrey, J. L., An Improved Preparation of Vinyl Iodides. *Tetrahedron Lett.* **1983,** *24*, (*15*), 1605-1608.
168. Bischofberger, N.; Waldmann, H.; Saito, T.; Simon, E. S.; Lees, W.; Bednarski, M. D.; Whitesides, G. M., Synthesis of Analogs of 1,3-Dihydroxyacetone Phosphate and Glyceraldehyde-3-Phosphate for Use in Studies of Fructose-1,6-Diphosphate Aldolase. *J. Org. Chem.* **1988,** *53*, (*15*), 3457-3465.
169. Seitz, D. E.; Ferreira, L., Efficient Preparation of Hexamethyldisilane. *Synthetic Commun.* **1979,** *9*, (*5*), 451-456.
170. Hunter, T., Signalling-2000 and beyond. *Cell* **2000,** *100*, 113-127.
171. Wagner, C. R.; Iyer, V. V.; McIntee, E. J., Pronucleotides: toward the in vivo delivery of antiviral and anticancer nucleotides. *Med. Res. Rev.* **2000,** *20*, (*6*), 417-451.
172. Zemlicka, J., Lipophilic phosphoramidates as antiviral pronucleotides. *Biochim. Biophys. Acta* **2002,** *1587*, (*2-3*), 276-286.
173. Krise, J. P.; Stella, V. J., Prodrugs of phosphates, phosphonates, and phosphinates. *Adv. Drug Delivery Rev.* **1996,** *19*, (*2*), 287-310.
174. Friis, G. J.; Bundgaard, H., Prodrugs of phosphates and phosphonates: Novel lipophilic .alpha.-acyloxyalkyl ester derivatives of phosphate- or phosphonate containing drugs masking the negative charges of these groups. *Eur. J. Pharm. Sci.* **1996,** *4*, (*1*), 49-60.
175. Azema, L.; Lherbet, C.; Baudoin, C.; Blonski, C., Cell permeation of a Trypanosoma brucei aldolase inhibitor: evaluation of different enzyme-labile phosphate protecting groups. *Bioorg. Med. Chem. Lett.* **2006,** *16*, (*13*), 3440-3443.
176. Fleisher, D.; Bong, R.; Stewart, B. H., Improved oral drug delivery: Solubility limitations overcome by the use of prodrugs. *Adv. Drug Delivery Rev.* **1996,** *19*, (*2*), 115-130.
177. Taylor, M. D., Improved passive oral drug delivery via prodrugs. *Adv. Drug Delivery Rev.* **1996,** *19*, (*2*), 131-148.
178. Cundy, K. C.; Fishback, J. A.; Shaw, J. P.; Lee, M. L.; Soike, K. F.; Visor, G. C.; Lee, W. A., Oral bioavailability of the antiretroviral agent 9-(2-phosphonylmethoxyethyl)adenine (PMEA) from three formulations of the prodrug bis(pivaloyloxymethyl)-PMEA in fasted

male cynomolgus monkeys. *Pharm. Res.* **1994,** *11*, (*6*), 839-843.
179. Farquhar, D.; Khan, S.; Srivastva, D. N.; Saunders, P. P., Synthesis and Antitumor Evaluation of Bis[(Pivaloyloxy)Methyl] 2'-Deoxy-5-Fluorouridine 5'-Monophosphate (Fdump) - a Strategy to Introduce Nucleotides into Cells. *J. Med. Chem.* **1994,** 37, (23), 3902-3909.
180. Farquhar, D.; Khan, S.; Wilkerson, M. C.; Andersson, B. S., Biologically-cleavable phosphate protective groups: 4-acyloxy-1,3,2-dioxaphosphorinanes as neutral latent precursors of dianionic phosphates. *Tetrahedron Lett.* **1995,** *36*, (*5*), 655-658.
181. Zhu, Z.; Chen, H. G.; Goel, O. P.; Chan, O. H.; Stilgenbauer, L. A.; Stewart, B. H., Phosphate prodrugs of PD154075. *Bioorg. Med. Chem. Lett.* **2000,** *10*, (*10*), 1121-1124.
182. Sinhababu, A. K.; Thakker, D. R., Prodrugs of anticancer agents. *Adv. Drug Delivery Rev.* **1996,** *19*, (*2*), 241-273.
183. Kearney, A. S., Prodrugs and targeted drug delivery. *Adv. Drug Delivery Rev.* **1996,** *19*, (*2*), 225-239.
184. Oliyai, R., Prodrugs of peptides and peptidomimetics for improved formulation and delivery. *Adv. Drug Delivery Rev.* **1996,** *19*, (*2*), 275-286.
185. Perigaud, C.; Gosselin, G.; Lefebvre, I.; Girardet, J. L.; Benzaria, S.; Barber, I.; Imbach, J. L., Rational design for cytosolic delivery of nucleoside monophosphates: "SATE" and "DTE" as enzyme-labile transient phosphate protecting groups. *Bioorg. Med. Chem. Lett.* **1993,** *3*, (*12*), 2521-2516.
186. Puech, F.; Gosselin, G.; Lefebvre, I.; Pompon, A.; Aubertin, A. M.; Kirn, A.; Imbach, J. L., Intracellular delivery of nucleoside monophosphates through a reductase-mediated activation process. *Antiviral Res.* **1993,** *22*, (*2-3*), 155-174.
187. Lefebvre, I.; Perigaud, C.; Pompon, A.; Aubertin, A. M.; Girardet, J. L.; Kirn, A.; Gosselin, G.; Imbach, J. L., Mononucleoside phosphotriester derivatives with S-acyl-2-thioethyl bioreversible phosphate-protecting groups: intracellular delivery of 3'-azido-2',3'-dideoxythymidine 5'-monophosphate. *J. Med. Chem.* **1995,** *38*, (*20*), 3941-3950.
188. Daehne, W. V.; Frederiksen, E.; Gundersen, E.; Lund, F.; Moerch, P.; Petersen, H. J.; Roholt, K.; Tybring, L.; Godtfredsen, W. O., Acyloxymethyl esters of ampicillin. *J. Med. Chem.* **1970,** *13*, (*4*), 607-612.
189. Saari, W. S.; Freedman, M. B.; Hartman, R. D.; King, S. W.; Raab, A. W.; Randall, W. C.; Engelhardt, E. L.; Hirschmann, R.; Rosegay, A., Synthesis and antihypertensive activity of some ester progenitors of methyldopa. *J. Med. Chem.* **1978,** *21*, (*8*), 746-753.
190. Perigaud, C.; Gosselin, G.; Imbach, J. L., Nucleoside Analogs as Chemotherapeutic-Agents. *Nucleosides & Nucleotides* **1992,** *11*, (*2-4*), 903-945.
191. Mitsuya, H.; Weinhold, K. J.; Furman, P. A.; St Clair, M. H.; Lehrman, S. N.; Gallo, R. C.; Bolognesi, D.; Barry, D. W.; Broder, S., 3'-Azido-3'-deoxythymidine (BW A509U): an antiviral agent that inhibits the infectivity and cytopathic effect of human T-lymphotropic virus type III/lymphadenopathy-associated virus in vitro. *Proc. Natl. Acad. Sci. USA* **1985,** *82*, (*20*), 7096-7100.
192. Sidtis, J. J.; Gatsonis, C.; Price, R. W.; Singer, E. J.; Collier, A. C.; Richman, D. D.; Hirsch, M. S.; Schaerf, F. W.; Fischl, M. A.; Kieburtz, K.; et al., Zidovudine treatment of the AIDS dementia complex: results of a placebo-controlled trial. AIDS Clinical Trials Group.

Ann. Neurol. **1993,** *33*, (*4*), 343-349.
193. Wilde, M. I.; Langtry, H. D., Zidovudine. An update of its pharmacodynamic and pharmacokinetic properties, and therapeutic efficacy. *Drugs* **1993,** *46*, (*3*), 515-578.
194. Connor, E. M.; Sperling, R. S.; Gelber, R.; Kiselev, P.; Scott, G.; O'Sullivan, M. J.; VanDyke, R.; Bey, M.; Shearer, W.; Jacobson, R. L., Reduction of maternal-infant transmission of human immunodeficiency virus type 1 with zidovudine treatment. Pediatric AIDS Clinical Trials Group Protocol 076 Study Group. *N. Engl. J. Med.* **1994,** *331*, (*18*), 1173-1180.
195. Parang, K.; Wiebe, L. I.; Knaus, E. E., Novel approaches for designing 5'-O-ester prodrugs of 3'-azido-2', 3'-dideoxythymidine (AZT). *Curr. Med. Chem.* **2000,** *7*, (*10*), 995-1039.
196. Rosowsky, A.; Kim, S. H.; Ross, J.; Wick, M. M., Lipophilic 5'-(alkyl phosphate) esters of 1-beta-D-arabinofuranosylcytosine and its N4-acyl and 2,2'-anhydro-3'-*O*-acyl derivatives as potential prodrugs. *J. Med. Chem.* **1982,** *25*, (*2*), 171-178.
197. Mullah, K. B.; Rao, T. S.; Balzarini, J.; De Clercq, E.; Bentrude, W. G., Potential prodrug derivatives of 2',3'-didehydro-2',3'-dideoxynucleosides. Preparations and antiviral activities. *J. Med. Chem.* **1992,** *35*, (*15*), 2728-2735.
198. McGuigan, C.; Wang, Y.; Riley, P. A., Synthesis and biological evaluation of phosphate triester alkyl lysophospholipids (ALPs) as novel potential anti-neoplastic agents. *Anticancer Drug Des.* **1994,** *9*, (*6*), 539-548.
199. Mcguigan, C.; Bellevergue, P.; Jones, B. C. N. M.; Mahmood, N.; Hay, A. J.; Petrik, J.; Karpas, A., Alkyl Hydrogen Phosphonate Derivatives of the Anti-Hiv Agent Azt May Be Less Toxic Than the Parent Nucleoside Analog. *Antiviral Chem. Chemother.* **1994,** *5*, (*4*), 271-277.
200. Montgomery, J. A.; Schabel, F. M., Jr.; Skipper, H. E., Experimental evaluation of potential anticancer agents. IX. Ribonucleosides and ribonucleotides of two purine antagonists. *Cancer Res.* **1962,** *22*, 504-509.
201. Pauletti, G. M.; Gangwar, S.; Okumu, F. W.; Siahaan, T. J.; Stella, V. J.; Borchardt, R. T., Esterase-sensitive cyclic prodrugs of peptides: evaluation of an acyloxyalkoxy promoiety in a model hexapeptide. *Pharm. Res.* **1996,** *13*, (*11*), 1615-1623.
202. Colin, B.; Jones, N. M.; Mcguigan, C.; Riley, P. A., Synthesis and Biological Evaluation of Some Phosphate Triester Derivatives of the Anti-Cancer Drug Arac. *Nucleic Acids Res.* **1989,** *17*, (*18*), 7195-7201.
203. Jones, B. C.; McGuigan, C.; Riley, P. A., Synthesis and biological evaluation of some phosphate triester derivatives of the anti-cancer drug araC. *Nucleic Acids Res.* **1989,** *17*, (*18*), 7195-7201.
204. Serafinowska, H. T.; Ashton, R. J.; Bailey, S.; Harnden, M. R.; Jackson, S. M.; Sutton, D., Synthesis and in-Vivo Evaluation of Prodrugs of 9-[2-(Phosphonomethoxy)Ethoxy]Adenine. *J. Med. Chem.* **1995,** *38*, (*8*), 1372-1379.
205. Starrett, J. E.; Tortolani, D. R.; Russell, J.; Hitchcock, M. J. M.; Whiterock, V.; Martin, J. C.; Mansuri, M. M., Synthesis, Oral Bioavailability Determination, and in-Vitro Evaluation of Prodrugs of the Antiviral Agent 9-[2-(Phosphonomethoxy)Ethyl]Adenine (PMEA). *J. Med. Chem.* **1994,** *37*, (*12*), 1857-1864.
206. Curley, D.; McGuigan, C.; Devine, K. G.; O'Connor, T. J.; Jeffries, D. J.;

Kinchington, D., Synthesis and anti-HIV evaluation of some phosphoramidate derivatives of AZT: studies on the effect of chain elongation on biological activity. *Antiviral Res.* **1990,** *14*, (*6*), 345-356.
207. McGuigan, C.; Nickson, C.; O'Connor, T. J.; Kinchington, D., Synthesis and anti-HIV activity of some novel lactyl and glycolyl phosphate derivatives. *Antiviral Res.* **1992,** *17*, (*3*), 197-212.
208. McGuigan, C.; Davies, M.; Pathirana, R.; Mahmood, N.; Hay, A. J., Synthesis and anti-HIV activity of some novel diaryl phosphate derivatives of AZT. *Antiviral Res.* **1994,** *24*, (*1*), 69-77.
209. Mcguigan, C.; Turner, S.; Nicholls, S. R.; Oconnor, T. J.; Kinchington, D., Haloalkyl Phosphate Derivatives of Azt as Inhibitors of Hiv - Studies in the Phosphate Region. *Antiviral Chem. Chemother.* **1994,** *5*, (*3*), 162-168.
210. McGuigan, C.; Nickson, C.; Petrik, J.; Karpas, A., Phosphate derivatives of AZT display enhanced selectivity of action against HIV 1 by comparison to the parent nucleoside. *FEBS Lett.* **1992,** *310*, (*2*), 171-174.
211.Sastry, J. K.; Nehete, P. N.; Khan, S.; Nowak, B. J.; Plunkett, W.; Arlinghaus, R. B.; Farquhar, D., Membrane-Permeable Dideoxyuridine 5'-Monophosphate Analog Inhibits Human-Immunodeficiency-Virus Infection. *Mol. Pharmacol.* **1992,** *41*, (*3*), 441-445.
212. Starrett, J. E., Jr.; Tortolani, D. R.; Hitchcock, M. J.; Martin, J. C.; Mansuri, M. M., Synthesis and in vitro evaluation of a phosphonate prodrug: bis(pivaloyloxymethyl) 9-(2-phosphonylmethoxyethyl)adenine. *Antiviral Res.* **1992,** *19*, (*3*), 267-273.
213. Rutschow, S.; Thiem, J.; Kranz, C.; Marquardt, T., Membrane-permeant derivatives of mannose-1-phosphate. *Bioorg. Med. Chem.* **2002,** *10*, (*12*), 4043-4049.
214. Shaw, J. P.; Louie, M. S.; Krishnamurthy, V. V.; Arimilli, M. N.; Jones, R. J.; Bidgood, A. M.; Lee, W. A.; Cundy, K. C., Pharmacokinetics and metabolism of selected prodrugs of PMEA in rats. *Drug Metab. Dispos.* **1997,** *25*, (*3*), 362-366.
215. Shaw, J. P.; Rekik, M.; Schwager, F.; Harayama, S., Kinetic studies on benzyl alcohol dehydrogenase encoded by TOL plasmid pWWO. A member of the zinc-containing long chain alcohol dehydrogenase family. *J. Biol. Chem.* **1993,** *268*, (*15*), 10842-10850.
216. Mitchell, A. G.; Thomson, W.; Nicholls, D.; Irwin, W. J.; Freeman, S., Bioreversible protection for the phospho group: bioactivation of the di(4-acyloxybenzyl) and mono(4-acyloxybenzyl) phosphoesters of methylphosphonate and phosphonoacetate. *J. Chem. Soc., Perkin Trans. 1* **1992,** *18*, (*1*), 2345-2353.
217. Thomson, W.; Nicholls, D.; Irwin, W. J.; Al-Mushadani, J. S.; Freeman, S.; Karpas, A.; Petrik, J.; Mahmood, N.; Hay, A. J., Synthesis, bioactivation and anti-HIV activity of the bis(4-acyloxybenzyl) and mono(4-acyloxybenzyl) esters of the 5'-monophosphate of AZT. *J. Chem. Soc., Perkin Trans* **1993,** *11*, 1239-1245.
218. Steim, J. M.; Camaioni Neto, C.; Sarin, P. S.; Sun, D. K.; Sehgal, R. K.; Turcotte, J. G., Lipid conjugates of antiretroviral agents. I. Azidothymidine-monophosphate-diglyceride: anti-HIV activity, physical properties, and interaction with plasma proteins. *Biochem. Biophys. Res. Commun.* **1990** *171*, (*1*), 451-457.
219. Van Wijk, G. M.; Hostetler, K. Y.; Suurmeijer, C. N.; van den Bosch, H., Synthesis, characterization and some properties of dideoxynucleoside analogs of cytidine diphosphate diacylglycerol. *Biochim. Biophys. Acta* **1992,** *1165*, (*1*), 45-52.

220. Hostetler, K. Y.; Parker, S.; Sridhar, C. N.; Martin, M. J.; Li, J. L.; Stuhmiller, L. M.; van Wijk, G. M.; van den Bosch, H.; Gardner, M. F.; Aldern, K. A.; et al., Acyclovir diphosphate dimyristoylglycerol: a phospholipid prodrug with activity against acyclovir-resistant herpes simplex virus. *Proc. Natl. Acad. Sci. USA* **1993,** *90*, (*24*), 11835-11839.
221. Mathe, C.; Perigaud, C.; Gosselin, G.; Imbach, J. L., Phosphopeptide Prodrug Bearing an S-Acyl-2-thioethyl Enzyme-Labile Phosphate Protection. *J. Org. Chem.* **1998,** *63*, (*23*), 8547-8550.
222. Namane, A.; Gouyette, C.; Fillion, M. P.; Fillion, G.; Huynh-Dinh, T., Improved brain delivery of AZT using a glycosyl phosphotriester prodrug. *J. Med. Chem.* **1992,** *35*, (*16*), 3039-3044.
223. Farquhar, D.; Chen, R.; Khan, S., 5'-[4-(Pivaloyloxy)-1,3,2-Dioxaphosphorinan-2-Yl]-2'-Deoxy-5-Fluorouridine - a Membrane-Permeating Prodrug of 5-Fluoro-2'-Deoxyuridylic Acid (Fdump). *J. Med. Chem.* **1995,** *38*, (*3*), 488-495.
224. Henin, Y.; Gouyette, C.; Schwartz, O.; Debouzy, J. C.; Neumann, J. M.; Huynh-Dinh, T., Lipophilic glycosyl phosphotriester derivatives of AZT: synthesis, NMR transmembrane transport study, and antiviral activity. *J. Med. Chem.* **1991,** *34*, (*6*), 1830-1837.
225. Le Bec, C.; Huynh Dinh, T., Synthesis of lipophilic phosphate triester derivatives of 5-fluorouridine and arabinocytidine as anticancer prodrugs. *Tetrahedron Lett.* **1991,** *32*, (*45*), 6553-6556.
226. Wu, W.; Sigmond, J.; Peters, G. J.; Borch, R. F., Synthesis and biological activity of a gemcitabine phosphoramidate prodrug. *J. Med. Chem.* **2007,** *50*, (*15*), 3743-3746.
227. Farquhar, D.; Srivastva, D. N.; Kuttesch, N. J.; Saunders, P. P., Biologically Reversible Phosphate-Protective Groups. *J. Pharm. Sci.* **1983,** *72*, (*3*), 324-325.
228. Kang, S. H.; Sinhababu, A. K.; Cory, J. G.; Mitchell, B. S.; Thakker, D. R.; Cho, M. J., Cellular delivery of nucleoside diphosphates: A prodrug approach. *Pharm. Res.* **1997,** *14*, (*6*), 706-712.
229. Benzaria, S.; Pelicano, H.; Johnson, R.; Maury, G.; Imbach, J. L.; Aubertin, A. M.; Obert, G.; Gosselin, G., Synthesis, in vitro antiviral evaluation, and stability studies of bis(S-acyl-2-thioethyl) ester derivatives of 9-[2-(phosphonomethoxy)ethyl] adenine (PMEA) as potential PMEA prodrugs with improved oral bioavailability. *J. Med. Chem.* **1996,** *39*, (*25*), 4958-4965.
230. Hwang, Y.; Ganguly, S.; Ho, A. K.; Klein, D. C.; Cole, P. A., Enzymatic and cellular study of a serotonin N-acetyltransferase phosphopantetheine-based prodrug. *Bioorg. Med. Chem.* **2007,** *15*, (*5*), 2147-2155.
231. Cebrat, M.; Kim, C. M.; Thompson, P. R.; Daugherty, M.; Cole, P. A., Synthesis and analysis of potential prodrugs of coenzyme A analogues for the inhibition of the histone acetyltransferase p300. *Bioorg. Med. Chem.* **2003,** *11*, (*15*), 3307-3313.
232. Hwang, Y. S.; Cole, P. A., Efficient synthesis of phosphorylated prodrugs with bis(POM)-phosphoryl chloride. *Org. Lett.* **2004,** *6*, (*10*), 1555-1556.
233. Josephson, S.; Lagerholm, E.; Palm, G., Automatic Synthesis of Oligodeoxynucleotides and Mixed Oligodeoxynucleotides Using the Phosphoamidite Method. *Acta Chem. Scand. B* **1984,** *38*, (*7*), 539-545.

234. Kang, S. H.; Sinhababu, A. K.; Cho, M. J., Synthesis and biological activity of bis(pivaloyloxymethyl) ester of 2 '-azido-2 '-deoxyuridine 5 '-monophosphate. *Nucleosides & Nucleotides* **1998,** *17*, (*6*), 1089-1098.
235. Rose, J. D.; Parker, W. B.; Someya, H.; Shaddix, S. C.; Montgomery, J. A.; Secrist, J. A., 3rd, Enhancement of nucleoside cytotoxicity through nucleotide prodrugs. *J. Med. Chem.* **2002,** *45*, (20), 4505-4512.
236. Fischer, G., Peptidyl-Prolyl Cis/Trans Isomerases and Their Effectors. *Angew. Chem. Int. Ed. Engl.* **1994,** *33*, (*14*), 1415-1436.
237. Wiederrecht, G.; Lam, E.; Hung, S.; Martin, M.; Sigal, N., The Mechanism of Action of Fk-506 and Cyclosporine-A. *Ann. N. Y. Acad. Sci.* **1993,** *696*, 9-19.
238. Rippmann, J. F.; Hobbie, S.; Daiber, C.; Guilliard, B.; Bauer, M.; Birk, J.; Nar, H.; Garin-Chesa, P.; Rettig, W. J.; Schnapp, A., Phosphorylation-dependent proline isomerization catalyzed by Pin1 is essential for tumor cell survival and entry into mitosis. *Cell Growth Differ.* **2000,** *11*, (*7*), 409-416.
239. Wang, X. J.; Etzkorn, F. A., Peptidyl-prolyl isomerase inhibitors. *Biopolymers* **2006,** *84*, (*2*), 125-146.
240. Wildemann, D.; Erdmann, F.; Alvarez, B. H.; Stoller, G.; Zhou, X. Z.; Fanghanel, J.; Schutkowski, M.; Lu, K. P.; Fischer, G., Nanomolar inhibitors of the peptidyl prolyl cis/trans isomerase Pin1 from combinatorial peptide libraries. *J. Med. Chem.* **2006,** *49*, (*7*), 2147-2150.
241. Zhang, Y.; Daum, S.; Wildemann, D.; Zhou, X. Z.; Verdecia, M. A.; Bowman, M. E.; Lucke, C.; Hunter, T.; Lu, K. P.; Fischer, G.; Noel, J. P., Structural basis for high-affinity peptide inhibition of human Pin1. *ACS Chem. Biol.* **2007,** *2*, (*5*), 320-328.
242. Vepsalainen, J. J., Bisphosphonate prodrugs: a new synthetic strategy to tetraacyloxymethyl esters of methylenebisphosphonates. *Tetrahedron Lett.* **1999,** *40*, (*48*), 8491-8493.
243. Vepsalainen, J. J.; Kivikoski, J.; Ahlgren, M.; Nupponen, H. E.; Pohjala, E. K., An Improved Synthetic Method and the First Crystal-Structures for (Dihalomethylene)Bisphosphonate Partial Esters. *Tetrahedron* **1995,** *51*, (*24*), 6805-6818.
244. Niemi, R.; Vepsalainen, J.; Taipale, H. a.; Jarvinen, T., Bisphosphonate prodrugs: synthesis and in vitro evaluation of novel acyloxyalkyl esters of clodronic acid. *J. Med. Chem.* **1999,** *42*, (*24*), 5053-5058.
245. Zhao, S.; Etzkorn, F. A., A phosphorylated prodrug for the inhibition of Pin1. *Bioorg. Med. Chem. Lett.* **2007,** *17*, (*23*), 6615-6618.
246. Xu, Y. P.; Miller, M. J., Total syntheses of mycobactin analogues as potent antimycobacterial agents using a minimal protecting group strategy. *J. Org. Chem.* **1998,** *63*, (*13*), 4314-4322.
247. Hayashi, Y.; Kinoshita, Y.; Hidaka, K.; Kiso, A.; Uchibori, H.; Kimura, T.; Kiso, Y., Analysis of amide bond formation with an alpha-hydroxy-beta-amino acid derivative, 3-amino-2-hydroxy-4-phenylbutanoic acid, as an acyl component: Byproduction of homobislactone. *J. Org. Chem.* **2001,** *66*, (*16*), 5537-5544.
248. Zhang, Y.; Fussel, S.; Reimer, U.; Schutkowski, M.; Fischer, G., Substrate-based design of reversible Pin1 inhibitors. *Biochemistry* **2002,** *41*, (*39*), 11868-11877.
249. Kofron, J. L.; Kuzmic, P.; Kishore, V.; Colon-Bonilla, E.; Rich, D. H., Determination of kinetic constants for peptidyl prolyl cis-trans isomerases by an improved

spectrophotometric assay. *Biochemistry* **1991,** *30*, (*25*), 6127-6134.
250. Fischer, G.; Bang, H.; Berger, E.; Schellenberger, A., Conformational specificity of chymotrypsin toward proline-containing substrates. *Biochim. Biophys. Acta* **1984,** *791*, (*1*), 87-97.
251. Kofron, J. L.; Kuzmic, P.; Kishore, V.; Gemmecker, G.; Fesik, S. W.; Rich, D. H., Lithium-Chloride Perturbation of Cis-Trans Peptide-Bond Equilibria - Effect on Conformational Equilibria in Cyclosporine-a and on Time-Dependent Inhibition of Cyclophilin. *J. Am. Chem. Soc.* **1992,** *114*, (*7*), 2670-2675.
252. Abdel-Kader, M.; Berger, J. M.; Slebodnick, C.; Hoch, J.; Malone, S.; Wisse, J. H.; Werkhoven, M. C.; Mamber, S.; Kingston, D. G., Isolation and absolute configuration of ent-Halimane diterpenoids from Hymenaea courbaril from the Suriname rain forest. *J. Nat. Prod.* **2002,** *65*, (*1*), 11-15.
253. Kapustin, G. V.; Fejer, G.; Gronlund, J. L.; McCafferty, D. G.; Seto, E.; Etzkorn, F. A., Phosphorus-based SAHA analogues as histone deacetylase inhibitors. *Org. Lett.* **2003,** *5*, (*17*), 3053-3056.
254. Fischer, G.; Heins, J.; Barth, A., The conformation around the peptide bond between the P1- and P2-positions is important for catalytic activity of some proline-specific proteases. *Biochim. Biophys. Acta* **1983,** *742*, (*3*), 452-462.
255. Hoffmann, I.; Clarke, P. R.; Marcote, M. J.; Karsenti, E.; Draetta, G., Phosphorylation and activation of human cdc25-C by cdc2--cyclin B and its involvement in the self-amplification of MPF at mitosis. *EMBO J.* **1993,** *12*, (*1*), 53-63.
256. Izumi, T.; Maller, J. L., Phosphorylation and activation of the Xenopus Cdc25 phosphatase in the absence of Cdc2 and Cdk2 kinase activity. *Mol. Biol. Cell.* **1995,** *6*, (*2*), 215-226.
257. Crenshaw, D. G.; Yang, J.; Means, A. R.; Kornbluth, S., The mitotic peptidyl-prolyl isomerase, Pin1, interacts with Cdc25 and Plx1. *EMBO J.* **1998,** *17*, (*5*), 1315-1327.
258. Izumi, T.; Maller, J. L., Elimination of cdc2 phosphorylation sites in the cdc25 phosphatase blocks initiation of M-phase. *Mol. Biol. Cell.* **1993,** *4*, (*12*), 1337-1350.
259. Strausfeld, U.; Fernandez, A.; Capony, J. P.; Girard, F.; Lautredou, N.; Derancourt, J.; Labbe, J. C.; Lamb, N. J., Activation of p34cdc2 protein kinase by microinjection of human cdc25C into mammalian cells. Requirement for prior phosphorylation of cdc25C by p34cdc2 on sites phosphorylated at mitosis. *J. Biol. Chem.* **1994,** *269*, (*8*), 5989-6000.
260. Peng, C. Y.; Graves, P. R.; Thoma, R. S.; Wu, Z.; Shaw, A. S.; Piwnica-Worms, H., Mitotic and G2 checkpoint control: regulation of 14-3-3 protein binding by phosphorylation of Cdc25C on serine-216. *Science* **1997,** *277*, (*5331*), 1501-1505.
261. Goss, V. L.; Cross, J. V.; Ma, K.; Qian, Y.; Mola, P. W.; Templeton, D. J., SAPK/JNK regulates cdc2/cyclin B kinase through phosphorylation and inhibition of cdc25c. *Cell. Signal.* **2003,** *15*, (*7*), 709-718.
262. Schwindling, S. L.; Noll, A.; Montenarh, M.; Gotz, C., Mutation of a CK2 phosphorylation site in cdc25C impairs importin alpha/beta binding and results in cytoplasmic retention. *Oncogene* **2004,** *23*, (*23*), 4155-4165.
263. Zhao, S.; Etzkorn, F. A., Study of the potential substrate sites of Cdc25c for Pin1 rotamase activity. *Poster paper in 230th ACS National Meeting, Washington, DC, United States* **2005**.

264. Sickmann, A.; Meyer, H. E., Phosphoamino acid analysis. *Proteomics* **2001,** *1*, (*2*), 200-206.
265. Yan, J. X.; Packer, N. H.; Gooley, A. A.; Williams, K. L., Protein phosphorylation: technologies for the identification of phosphoamino acids. *J. Chromatogr. A* **1998,** *808*, (*1-2*), 23-41.
266. McLachlin, D. T.; Chait, B. T., Analysis of phosphorylated proteins and peptides by mass spectrometry. *Curr. Opin. Chem. Biol.* **2001,** *5*, (*5*), 591-602.
267. Quadroni, M.; James, P., Phosphopeptide analysis. *EXS* **2000,** *88*, 199-213.
268. Mann, M.; Ong, S. E.; Gronborg, M.; Steen, H.; Jensen, O. N.; Pandey, A., Analysis of protein phosphorylation using mass spectrometry: deciphering the phosphoproteome. *Trends Biotechnol.* **2002,** *20*, (*6*), 261-268.
269. Jaffe, H.; Pant, H. C., Characterization of Serine and Threonine phosphorylation sites in β-elimination/ethanethiol addition-modified proteins by electrospray tandem mass spectrometry and database searching. *Biochemistry* **1998,** *37*, 16211-16224.
270. Hunt, D. F.; Yates, J. R., 3rd; Shabanowitz, J.; Winston, S.; Hauer, C. R., Protein sequencing by tandem mass spectrometry. *Proc. Natl. Acad. Sci. USA* **1986,** *83*, (*17*), 6233-6237.
271. Hoffmann, R.; Metzger, S.; Spengler, B.; Otvos, L. J., Sequencing of peptides phosphorylated on serines and threonines by post-source decay in matrix-asistanted laser desorption/ionization time-of-flight mass spectrometry. *J. Mass. Spectrum.* **1999,** *34*, 1195-1204.
272. Jensen, O. N., Modification-specific proteomics: characterization of post-translational modifications by mass spectrometry. *Curr. Opin. Chem. Biol.* **2004,** *8*, (*1*), 33-41.
273. Meng, F. Y.; Forbes, A. J.; Miller, L. M.; Kelleher, N. L., Detection and localization of protein modifications by high resolution tandem mass spectrometry. *Mass Spectrom. Rev.* **2005,** *24*, (*2*), 126-134.
274. Salih, E., Phosphoproteomics by mass spectrometry and classical protein chemistry approaches. *Mass Spectrom. Rev.* **2005,** *24*, (*6*), 828-846.
275. Chi, A.; Huttenhower, C.; Geer, L. Y.; Coon, J. J.; Syka, J. E.; Bai, D. L.; Shabanowitz, J.; Burke, D. J.; Troyanskaya, O. G.; Hunt, D. F., Analysis of phosphorylation sites on proteins from Saccharomyces cerevisiae by electron transfer dissociation (ETD) mass spectrometry. *Proc. Natl. Acad. Sci. USA* **2007,** *104*, (*7*), 2193-2198.
276. Goshe, M. B.; Conrads, T. P.; Panisko, E. A.; Angell, N. H.; Veenstra, T. D.; Smith, R. D., Phosphoprotein isotope-coded affinity tag approach for isolating and quantitating phosphopeptides in proteome-wide analyses. *Anal. Chem.* **2001,** *73*, 2578-2586.
277. Zhu, X. G.; Desiderio, D. M., Peptide quantification by tandem mass spectrometry. *Mass Spectrom. Rev.* **1996,** *15*, (*4*), 213-240.
278. Resing, K. A.; Ahn, N. G., Protein phosphorylation analysis by electrospray ionization-mass spectrometry. *Methods Enzymol.* **1997,** *283*, 29-44.
279. Syka, J. E.; Coon, J. J.; Schroeder, M. J.; Shabanowitz, J.; Hunt, D. F., Peptide and protein sequence analysis by electron transfer dissociation mass spectrometry. *Proc. Natl. Acad. Sci. USA* **2004,** *101*, (*26*), 9528-9533.
280. Zubarev, R. A.; Kelleher, N. L.; McLafferty, F. W., Electron capture dissociation of

multiply charged protein cations. A nonergodic process. *J. Am. Chem. Soc.* **1998,** *120*, (*13*), 3265-3266.
281. Zubarev, R. A., Reactions of polypeptide ions with electrons in the gas phase. *Mass Spectrom. Rev.* **2003,** *22*, (*1*), 57-77.
282. Hardouin, J., Protein sequence information by matrix-assisted laser desorption/ionization in-source decay mass spectrometry. *Mass Spectrom. Rev.* **2007,** *26*, (*5*), 672-682.
283. Paizs, B.; Suhai, S., Fragmentation pathways of protonated peptides. *Mass Spectrom. Rev.* **2005,** *24*, (*4*), 508-548.
284. Cheng, C. F.; Gross, M. L., Applications and mechanisms of charge-remote fragmentation. *Mass Spectrom. Rev.* **2000,** *19*, (*6*), 398-420.
285. Roth, S. Y.; Collini, M. P.; Draetta, G.; Beach, D.; Allis, C. D., A cdc2-like kinase phosphorylates histone H1 in the amitotic macronucleus of Tetrahymena. *EMBO J.* **1991,** *10*, (*8*), 2069-2075.
286. Parker, L. L.; Atherton-Fessler, S.; Piwnica-Worms, H., p107wee1 is a dual-specificity kinase that phosphorylates p34cdc2 on tyrosine 15. *Proc. Natl. Acad. Sci. USA* **1992,** *89*, (*7*), 2917-2921.
287. Srinivasan, J.; Koszelak, M.; Mendelow, M.; Kwon, Y. G.; Lawrence, D. S., The design of peptide-based substrates for the cdc2 protein kinase. *Biochem. J.* **1995,** *309*, 927-931.
288. Harvey, K. J.; Lukovic, D.; Ucker, D. S., Caspase-dependent Cdk activity is a requisite effector of apoptotic death events. *J. Cell. Biol.* **2000,** *148*, (*1*), 59-72.
289. Nguyen, D. L.; Seyer, K. O., Use of HBTU in coupling of amino acids with minimal side-chain protection. *Peptides (ESCOM Science Publishers)* **1990**.
290. Wakamiya, T.; Togashi, R.; Nishida, T.; Saruta, K.; Yasuoka, J.; Kusumoto, S.; Aimoto, S.; Kumagaye, K. Y.; Nakajima, K.; Nagata, K., Synthetic study of phosphopeptides related to heat shock protein HSP27. *Bioorg. Med. Chem.* **1997,** *5*, (*1*), 135-145.